SCIENTIA SINICA

Vol. V Nos. 1–4

1956

PUBLISHED BY ACADEMIA SINICA
PEKING, CHINA

CLASSIFIED CONTENTS OF VOLUME V (1956)

PHYSICS

CHEMISTRY

BOTANY

ZOOLOGY

BIOCHEMISTRY

ANATOMY

MICROBIOLOGY

GEOLOGY

METEOROLOGY

PALÆONTOLOGY

ANTHROPOLOGY

AUTHOR INDEX

SCIENTIA SINICA

Vol. V No. 1

March, 1956

PUBLISHED BY ACADEMIA SINICA
PEKING, CHINA.

CONTENTS

ON THE EQUILIBRIUM AND VIBRATION OF A TRANSVERSELY ISOTROPIC ELASTIC BODY*

Hu Hai-Chang (胡海昌)

(*Institute of Mathematics, Academia Sinica*)

I. Introduction

In the year 1940, S. G. Lehnitzky[1] obtained a stress function for the axisymmetric deformation of a transversely isotropic elastic body. His result has been generalized by A. Moisil[3, 4], W. Nowacki[5] and the author[6, 7] independently. In papers [6] and [7], the general solutions of the equations of equilibrium without body forces are expressed in terms of two stress functions. This method is applied later to the equilibrium of a spherically isotropic body[8, 9]. In this paper, we shall apply the same method to the investigations of the equilibrium under body forces, the thermal stresses, and the vibration of a transversely isotropic elastic body.

II. General Equations

Consider a transversely isotropic body. Take rectangular coordinate axes x, y, and z, such that the xy-plane is parallel to planes of isotropy of the body. Let u, v, and w be the components of displacement, $\sigma_x, \sigma_y, \cdots, \tau_{xy}$ be the components of stress and T be the temperature. In this system of coordinates, the generalized Hooke's law including thermal expansion may be written in the following form:

$$\begin{aligned}
\sigma_x &= A_{11}\frac{\partial u}{\partial x} + A_{12}\frac{\partial v}{\partial y} + A_{13}\frac{\partial w}{\partial z} - \alpha_1 T, & \tau_{yz} &= A_{44}\left(\frac{\partial w}{\partial y} + \frac{\partial v}{\partial z}\right),\\
\sigma_y &= A_{12}\frac{\partial u}{\partial x} + A_{11}\frac{\partial v}{\partial y} + A_{13}\frac{\partial w}{\partial z} - \alpha_1 T, & \tau_{xy} &= A_{44}\left(\frac{\partial w}{\partial x} + \frac{\partial u}{\partial z}\right), \qquad (1)\\
\sigma_z &= A_{13}\frac{\partial u}{\partial x} + A_{13}\frac{\partial v}{\partial y} + A_{33}\frac{\partial w}{\partial z} - \alpha_3 T, & \tau_{xy} &= A_{66}\left(\frac{\partial v}{\partial x} + \frac{\partial u}{\partial y}\right),
\end{aligned}$$

---

*First published in Chinese in *Acta Physica Sinica*, Vol. XI, No. 3, pp. 219—238, 1955.

where $A_{11}, A_{12}, \cdots A_{66}, \alpha_1, \alpha_3$ are constants, and

$$A_{11} - A_{12} = 2A_{66}. \tag{2}$$

The equations of motion are

$$\frac{\partial \sigma_x}{\partial x} + \frac{\partial \tau_{xy}}{\partial y} + \frac{\partial \tau_{xz}}{\partial z} + X = \rho \frac{\partial^2 u}{\partial t^2},$$

$$\frac{\partial \tau_{xy}}{\partial x} + \frac{\partial \sigma_y}{\partial y} + \frac{\partial \tau_{yz}}{\partial z} + Y = \rho \frac{\partial^2 v}{\partial t^2}, \tag{3}$$

$$\frac{\partial \tau_{xz}}{\partial x} + \frac{\partial \tau_{yz}}{\partial y} + \frac{\partial \sigma_z}{\partial z} + Z = \rho \frac{\partial^2 w}{\partial t^2},$$

where X, Y, and Z are the components of body forces and ρ is the specific mass of the body. Substituting expressions (1) into equations (3), we obtain equations of motion expressed in terms of displacement as follows:

$$B_{11}\frac{\partial^2 u}{\partial x^2} + B_{66}\frac{\partial^2 u}{\partial y^2} + B_{44}\frac{\partial^2 u}{\partial z^2} + B_{12}\frac{\partial^2 v}{\partial x\,\partial y} + B_{13}\frac{\partial^2 w}{\partial x\,\partial z} + X = \alpha_1\frac{\partial T}{\partial x} + \rho\frac{\partial^2 u}{\partial t^2},$$

$$B_{12}\frac{\partial^2 u}{\partial x\,\partial y} + B_{66}\frac{\partial^2 v}{\partial x^2} + B_{11}\frac{\partial^2 v}{\partial y^2} + B_{44}\frac{\partial^2 v}{\partial z^2} + B_{13}\frac{\partial^2 w}{\partial y\,\partial z} + Y = \alpha_1\frac{\partial T}{\partial y} + \rho\frac{\partial^2 v}{\partial t^2}, \tag{4}$$

$$B_{13}\frac{\partial^2 u}{\partial x\,\partial z} + B_{13}\frac{\partial^2 v}{\partial y\,\partial z} + B_{44}\frac{\partial^2 w}{\partial x^2} + B_{44}\frac{\partial^2 w}{\partial y^2} + B_{33}\frac{\partial^2 w}{\partial z^2} + Z = \alpha_3\frac{\partial T}{\partial z} + \rho\frac{\partial^2 w}{\partial t^2},$$

where

$$B_{11} = A_{11}, \quad B_{33} = A_{33}, \quad B_{44} = A_{44}, \quad B_{66} = A_{66},$$
$$B_{12} = A_{12} + A_{66}, \qquad B_{13} = A_{13} + A_{44}, \tag{5}$$

and

$$B_{11} = B_{12} + B_{66}. \tag{6}$$

In the following we shall simplify the fundamental system (4) by introducing suitable stress functions.

III. Equilibrium Under Body Forces Perpendicular to Planes of Isotropy

Let us consider first the case of equilibrium under body forces perpendicular to planes of isotropy. In this case, system (4) is simplified to the following:

$$\begin{aligned}
&B_{11}\frac{\partial^2 u}{\partial x^2}+B_{66}\frac{\partial^2 u}{\partial y^2}+B_{44}\frac{\partial^2 u}{\partial z^2}+B_{12}\frac{\partial^2 v}{\partial x\,\partial y}+B_{13}\frac{\partial^2 w}{\partial x\,\partial z}=0\,,\\
&B_{12}\frac{\partial^2 u}{\partial x\,\partial y}+B_{66}\frac{\partial^2 v}{\partial x^2}+B_{11}\frac{\partial^2 v}{\partial y^2}+B_{44}\frac{\partial^2 v}{\partial z^2}+B_{13}\frac{\partial^2 w}{\partial y\,\partial z}=0\,,\\
&B_{13}\frac{\partial^2 u}{\partial x\,\partial z}+B_{13}\frac{\partial^2 v}{\partial y\,\partial z}+B_{44}\frac{\partial^2 w}{\partial x^2}+B_{44}\frac{\partial^2 w}{\partial y^2}+B_{33}\frac{\partial^2 w}{\partial z^2}+Z=0\,.
\end{aligned}\tag{7}$$

The solution of this system consists of two parts, namely an arbitrary special solution corresponding to Z, and a general solution of the homogeneous system. The latter may be expressed in terms of two stress functions as shown in [6, 7]. Therefore in this paper we shall consider only the special solutions of system (7).

In order to satisfy the first two equations of (7), we may express u, v, w in terms of a function F as follows:

$$u=-\frac{\partial^2 F}{\partial x\,\partial z}\,,\quad v=-\frac{\partial^2 F}{\partial y\,\partial z}\,,\quad w=\frac{B_{11}}{B_{13}}\nabla_1^2 F+\frac{B_{44}}{B_{13}}\frac{\partial^2 F}{\partial z^2}\,,\tag{8}$$

where

$$\nabla_1^2=\frac{\partial^2}{\partial x^2}+\frac{\partial^2}{\partial y^2}\,.\tag{9}$$

Substituting expressions (8) into the last of the equations (7), we obtain

$$\left(\nabla_1^2+\frac{1}{s_1^2}\frac{\partial^2}{\partial z^2}\right)\left(\nabla_1^2+\frac{1}{s_2^2}\frac{\partial^2}{\partial z^2}\right)F+\frac{B_{13}}{B_{11}B_{44}}Z=0\,,\tag{10}$$

where

$$\begin{aligned}
s_1^2&=\frac{B_{44}^2+B_{11}B_{33}-B_{13}^2+\sqrt{(B_{44}^2+B_{11}B_{33}-B_{13}^2)^2-4B_{11}B_{33}B_{44}^2}}{2B_{33}B_{44}}\,,\\
s_2^2&=\frac{B_{44}^2+B_{11}B_{33}-B_{13}^2-\sqrt{(B_{44}^2+B_{11}B_{33}-B_{13}^2)^2-4B_{11}B_{33}B_{44}^2}}{2B_{33}B_{44}}\,.
\end{aligned}\tag{11}$$

Consequently our problem is reduced to the finding of a special solution of equation (10).

When Z is a polynomial in x, y, and z, a special solution of F can be easily obtained, since it may be taken as a polynomial. When

$$Z = A \cos \alpha x \cos \beta y \cos \gamma z \,, \tag{12}$$

a special solution of F may be taken as

$$F = -\frac{B_{13}}{B_{11}\,B_{44}} \cdot \frac{A \cos \alpha x \cos \beta y \cos \gamma z}{(\alpha^2+\beta^2+\nu_1 \gamma^2)(\alpha^2+\beta^2+\nu_2 \gamma^2)} \,, \tag{13}$$

where

$$\nu_1 = \frac{1}{s_1^2} \,, \qquad \nu_2 = \frac{1}{s_2^2} \,. \tag{14}$$

In general, a special solution of F may be obtained by Fourier series or integral. This method has been used by G. F. Carrier[10]. However, triple Fourier integrals are usually not convenient for calculation.

In his paper [11], the author has proposed a simple method for obtaining a special solution. Let

$$\nabla_1^2 F + \frac{1}{s_2^2}\frac{\partial^2 F}{\partial z^2} = G_1(x, y, z) \,, \qquad \nabla_1^2 F + \frac{1}{s_1^2}\frac{\partial^2 F}{\partial z^2} = G_2(x, y, z) \,. \tag{15}$$

Substituting these expressions into equations (10), we get

$$\frac{\partial^2 G_i}{\partial x^2} + \frac{\partial^2 G_i}{\partial y^2} + \frac{1}{s_i^2}\frac{\partial^2 G_i}{\partial z^2} = -\frac{B_{13}}{B_{11}\,B_{44}} Z(x, y, z) \,, \qquad (i = 1, 2) \,. \tag{16}$$

Since we are interested in a special solution, we may consider the body to be an infinite space. In this case, the solution of equation (16) is

$$G_i(x, y, z) = \frac{B_{13}}{B_{11}\,B_{44}} \cdot \frac{s_i}{4\pi} \iiint \frac{Z(\xi, \eta, \zeta)\, d\xi\, d\eta\, d\zeta}{\sqrt{(\xi-x)^2+(\eta-y)^2+s_i^2(\zeta-z)^2}} \,, \quad (i=1, 2) \,. \tag{17}$$

After having determined G_i, F may be obtained by integrating equations (15). Regarding $\nabla_1^2 F$ and $\frac{\partial^2 F}{\partial z^2}$ as two independent algebraic unknowns and solving system (15), we get

$$\begin{aligned} \nabla_1^2 F &= \frac{1}{\nu_1 - \nu_2}(\nu_1 G_1 - \nu_2 G_2) \,, \\ \frac{\partial^2 F}{\partial z^2} &= -\frac{1}{\nu_1 - \nu_2}(G_1 - G_2) \,. \end{aligned} \tag{18}$$

This system is simpler than (15) in form.

Consider, as an example, an infinite space under a concentrated force P_z. By taking the point of application of the force as the origin of the coordinate axes, we have

$$G_i(x, y, z) = \frac{B_{13}}{B_{11} B_{44}} \cdot \frac{P_z}{4\pi} \cdot \frac{s_i}{\sqrt{x^2+y^2+s_i^2 z^2}}, \qquad (i = 1, 2). \tag{19}$$

For the sake of simplicity, let us write

$$r = \sqrt{x^2 + y^2}, \qquad z_1 = s_1 z, \qquad z_2 = s_2 z. \tag{20}$$

Then expression (19) can be written in the form

$$G_i(x, y, z) = \frac{B_{13}}{B_{11} B_{44}} \cdot \frac{P_z}{4\pi} \cdot \frac{s_i}{\sqrt{r^2+z_i^2}}, \qquad (i = 1, 2). \tag{21}$$

Substituting this expression into equations (18), we have

$$\nabla_1^2 F = \frac{B_{13}}{B_{11} B_{44}} \cdot \frac{P_z}{4\pi} \cdot \frac{1}{\nu_1 - \nu_2} \left\{ \frac{1}{s_1 \sqrt{r^2+z_1^2}} - \frac{1}{s_2 \sqrt{r^2+z_2^2}} \right\}, \tag{22a}$$

$$\frac{\partial^2 F}{\partial z^2} = -\frac{B_{13}}{B_{11} B_{44}} \cdot \frac{P_z}{4\pi} \cdot \frac{1}{\nu_1 - \nu_2} \left\{ \frac{s_1}{\sqrt{r^2+z_1^2}} - \frac{s_2}{\sqrt{r^2+z_2^2}} \right\}. \tag{22b}$$

Integrating equation (22b) twice with respect to z, we have

$$F = -\frac{B_{13}}{B_{11} B_{44}} \cdot \frac{P_z}{4\pi} \cdot \frac{1}{\nu_1 - \nu_2} \left\{ z \log \frac{\sqrt{r^2+z_1^2}+z_1}{\sqrt{r^2+z_2^2}+z_2} - \right.$$
$$\left. - \frac{\sqrt{r^2+z_1^2}}{s_1} + \frac{\sqrt{r^2+z_2^2}}{s_2} \right\}. \tag{23}$$

It may be verified that this expression satisfies equation (22a). Therefore it is the required solution. Substituting expression (23) into formula (8), we obtain

$$u = -\frac{B_{13}}{B_{11} B_{44}} \cdot \frac{P_z}{4\pi} \cdot \frac{1}{\nu_1 - \nu_2} \left\{ \frac{z_1}{\sqrt{r^2+z_1^2}} - \frac{z_2}{\sqrt{r^2+z_2^2}} \right\} \frac{x}{r^2},$$

$$v = -\frac{B_{13}}{B_{11} B_{44}} \cdot \frac{P_z}{4\pi} \cdot \frac{1}{\nu_1 - \nu_2} \left\{ \frac{z_1}{\sqrt{r^2+z_1^2}} - \frac{z_2}{\sqrt{r^2+z_2^2}} \right\} \frac{y}{r^2}, \tag{24}$$

$$w = -\frac{1}{B_{11} B_{44}} \cdot \frac{P_z}{4\pi} \cdot \frac{1}{\nu_1 - \nu_2} \left\{ \frac{s_1^2 B_{44} - B_{11}}{s_1 \sqrt{r^2+z_1^2}} - \frac{s_2^2 B_{44} - B_{11}}{s_2 \sqrt{r^2+z_2^2}} \right\}.$$

These expressions coinside with that obtained by H. A. Elliot[12].

IV. Equilibrium Under Body Forces Parallel to Planes of Isotropy

Consider now the case of equilibrium under body forces parallel to planes of isotropy. Since the effects of body forces X and Y may be counted separately, we assume $Y=0$ temporarily. Under these restrictions, system (4) is reduced to the form

$$\begin{aligned}
&B_{11}\frac{\partial^2 u}{\partial x^2}+B_{66}\frac{\partial^2 u}{\partial y^2}+B_{44}\frac{\partial^2 u}{\partial z^2}+B_{12}\frac{\partial^2 v}{\partial x\,\partial y}+B_{13}\frac{\partial^2 w}{\partial x\,\partial z}+X=0\,,\\
&B_{12}\frac{\partial^2 u}{\partial x\,\partial y}+B_{66}\frac{\partial^2 v}{\partial x^2}+B_{11}\frac{\partial^2 v}{\partial y^2}+B_{44}\frac{\partial^2 v}{\partial z^2}+B_{13}\frac{\partial^2 w}{\partial y\,\partial z}=0\,, \qquad (25)\\
&B_{13}\frac{\partial^2 u}{\partial x\,\partial z}+B_{13}\frac{\partial^2 v}{\partial y\,\partial z}+B_{44}\frac{\partial^2 w}{\partial x^2}+B_{44}\frac{\partial^2 w}{\partial y^2}+B_{33}\frac{\partial^2 w}{\partial z^2}=0\,.
\end{aligned}$$

In order to satisfy the last two equations of system (25), we may put

$$\begin{aligned}
u&=\left(\frac{B_{66}}{B_{13}}\frac{\partial^2}{\partial x^2}+\frac{B_{11}}{B_{13}}\frac{\partial^2}{\partial y^2}+\frac{B_{44}}{B_{13}}\frac{\partial^2}{\partial z^2}\right)\left[\frac{B_{44}}{B_{13}}\nabla_1^2 H+\frac{B_{33}}{B_{11}}\frac{\partial^2 H}{\partial z^2}\right]-\frac{\partial^4 H}{\partial y^2\,\partial z^2}\,,\\
v&=-\left[\frac{B_{12}B_{44}}{B_{13}^2}\nabla_1^2+\left(\frac{B_{12}B_{33}}{B_{13}^2}-1\right)\frac{\partial^2}{\partial z^2}\right]\frac{\partial^2 H}{\partial x\,\partial y}\,, \qquad (26)\\
w&=-\left[\frac{B_{66}}{B_{13}}\nabla_1^2+\frac{B_{44}}{B_{13}}\frac{\partial^2}{\partial z^2}\right]\frac{\partial^2 H}{\partial x\,\partial z}\,.
\end{aligned}$$

The stress function H satisfies the equation

$$\left(\nabla_1^2+\frac{1}{s_0^2}\frac{\partial^2}{\partial z^2}\right)\left(\nabla_1^2+\frac{1}{s_1^2}\frac{\partial^2}{\partial z^2}\right)\left(\nabla_1^2+\frac{1}{s_2^2}\frac{\partial^2}{\partial z^2}\right)H+\frac{B_{13}^2}{B_{11}B_{44}B_{66}}X=0\,, \qquad (27)$$

where s_1^2 and s_2^2 are defined by (11) and

$$s_0^2=\frac{B_{66}}{B_{44}}\,. \qquad (28)$$

Consequently the problem is reduced to the finding of a special solution of equation (27).

When X is a polynomial, a special solution of H may also be a polynomial. In the case

$$X=A\cos\alpha x\cos\beta y\cos\gamma z\,, \qquad (29)$$

a special solution may be taken as

$$H=\frac{B_{13}^2}{B_{11}B_{44}B_{66}}\cdot\frac{A\cos\alpha x\cos\beta y\cos\gamma z}{(\alpha^2+\beta^2+\nu_0\gamma^2)(\alpha^2+\beta^2+\nu_1\gamma^2)(\alpha^2+\beta^2+\nu_2\gamma^2)}\,, \qquad (30)$$

where

$$\nu_0 = \frac{1}{s_0^2}, \qquad \nu_1 = \frac{1}{s_1^2}, \qquad \nu_2 = \frac{1}{s_2^2}. \tag{31}$$

In general, a special solution may be obtained in the following manner. Let

$$\begin{aligned}
&\left(\nabla_1^2 + \frac{1}{s_1^2}\frac{\partial^2}{\partial z^2}\right)\left(\nabla_1^2 + \frac{1}{s_2^2}\frac{\partial^2}{\partial z^2}\right) H = J_0(x, y, z), \\
&\left(\nabla_1^2 + \frac{1}{s_2^2}\frac{\partial^2}{\partial z^2}\right)\left(\nabla_1^2 + \frac{1}{s_0^2}\frac{\partial^2}{\partial z^2}\right) H = J_1(x, y, z), \\
&\left(\nabla_1^2 + \frac{1}{s_0^2}\frac{\partial^2}{\partial z^2}\right)\left(\nabla_1^2 + \frac{1}{s_1^2}\frac{\partial^2}{\partial z^2}\right) H = J_2(x, y, z).
\end{aligned} \tag{32}$$

Equation (27) is reduced to the form

$$\frac{\partial^2 J_i}{\partial x^2} + \frac{\partial^2 J_i}{\partial y^2} + \frac{1}{s_i^2}\frac{\partial^2 J_i}{\partial z^2} = -\frac{B_{13}^2}{B_{11} B_{44} B_{66}} X, \qquad (i = 0, 1, 2). \tag{33}$$

As in the last section, in order to obtain a special solution, we may consider the body to be an infinite space. Then from equation (33) we have

$$J_i(x, y, z) = \frac{B_{13}^2}{B_{11} B_{44} B_{66}} \cdot \frac{s_i}{4\pi} \iiint \frac{X(\xi, \eta, \zeta)\, d\xi\, d\eta\, d\zeta}{\sqrt{(\xi - x)^2 + (\eta - y)^2 + s_i^2 (\zeta - z)^2}}, \qquad (i = 0, 1, 2), \tag{34}$$

After having determined J_i, we may obtain H by integrating (32). System (32) may be written in the form

$$\begin{aligned}
&\nabla_1^4 H + (\nu_1 + \nu_2)\nabla_1^2 \frac{\partial^2 H}{\partial z^2} + \nu_1 \nu_2 \frac{\partial^4 H}{\partial z^4} = J_0, \\
&\nabla_1^4 H + (\nu_2 + \nu_0)\nabla_1^2 \frac{\partial^2 H}{\partial z^2} + \nu_2 \nu_0 \frac{\partial^4 H}{\partial z^4} = J_1, \\
&\nabla_1^4 H + (\nu_0 + \nu_1)\nabla_1^2 \frac{\partial^2 H}{\partial z^2} + \nu_0 \nu_1 \frac{\partial^4 H}{\partial z^4} = J_2.
\end{aligned} \tag{35}$$

Regarding $\nabla_1^4 H$, $\nabla_1^2 \frac{\partial^2 H}{\partial z^2}$, $\frac{\partial^4 H}{\partial z^4}$ as three algebraic unknowns and solving these unknowns from system (35), we get

$$\nabla_1^4 H = -\frac{\nu_0^2(\nu_1 - \nu_2) J_0 + \nu_1^2(\nu_2 - \nu_0) J_1 + \nu_2^2(\nu_0 - \nu_1) J_2}{(\nu_0 - \nu_1)(\nu_1 - \nu_2)(\nu_2 - \nu_0)}, \tag{36a}$$

$$\nabla_1^2 \frac{\partial^2 H}{\partial z^2} = \frac{\nu_0(\nu_1 - \nu_2) J_0 + \nu_1(\nu_2 - \nu_0) J_1 + \nu_2(\nu_0 - \nu_1) J_2}{(\nu_0 - \nu_1)(\nu_1 - \nu_2)(\nu_2 - \nu_0)}, \tag{36b}$$

$$\frac{\partial^4 H}{\partial z^4} = -\frac{(\nu_1-\nu_2)\,J_0+(\nu_2-\nu_0)\,J_1+(\nu_0-\nu_1)\,J_2}{(\nu_0-\nu_1)(\nu_1-\nu_2)(\nu_2-\nu_0)}\,. \tag{36c}$$

This system of equations is simpler than (35) in form.

Since the xy-plane is parallel to planes of isotropy, the special solution corresponding to the body forces Y may be found in the same manner.

Consider, as an example, an infinite space under a concentrate force P_x at the origin. According to formula (34), we have

$$J_i(x,y,z) = \frac{B_{13}^2}{B_{11}B_{44}B_{66}}\cdot\frac{P_x}{4\pi}\frac{s_i}{\sqrt{r^2+z_i^2}}, \qquad (i=0,1,2), \tag{37}$$

where

$$r=\sqrt{z^2+y^2}\,, \qquad z_0=s_0 z\,, \qquad z_1=s_1 z\,, \qquad z_2=s_2 z\,. \tag{38}$$

Substituting (37) into (36c), we obtain $\frac{\partial^4 H}{\partial z^4}$. Then integrating with respect to z four times, we get

$$H=-\frac{B_{13}^2}{B_{11}B_{44}B_{66}}\cdot\frac{P_x}{4\pi}\cdot\frac{(\nu_1-\nu_2)\,H_0+(\nu_2-\nu_0)\,H_1+(\nu_0-\nu_1)\,H_2}{(\nu_0-\nu_1)(\nu_1-\nu_2)(\nu_2-\nu_0)}, \tag{39}$$

where

$$H_i=\frac{1}{s_i^3}\left\{\frac{z_i}{4}(2z_i^2-3r^2)\log\frac{\sqrt{r^2+z_i^2}+z_i}{\sqrt{r^2+z_i^2}-z_i}-\left(\frac{11}{6}z_i^2-\frac{2}{3}r^2\right)\sqrt{r^2+z_i^2}\right\}. \tag{40}$$

It may be verified that expression (39) satisfies equations (36a, b). Therefore it is the required solution.

If the body forces parallel to planes of isotropy have a potential, then the calculation may be simplified greatly. In this case

$$X=-\frac{\partial U}{\partial x}\,, \qquad \mathrm{Y}=-\frac{\partial U}{\partial y}\,, \qquad Z=0\,, \tag{41}$$

and system (4) is reduced to the form

$$\begin{aligned}
&B_{11}\frac{\partial^2 u}{\partial x^2}+B_{66}\frac{\partial^2 u}{\partial y^2}+B_{44}\frac{\partial^2 u}{\partial z^2}+B_{12}\frac{\partial^2 v}{\partial x\,\partial y}+B_{13}\frac{\partial^2 w}{\partial x\,\partial z}-\frac{\partial U}{\partial x}=0\,,\\
&B_{12}\frac{\partial^2 u}{\partial x\,\partial y}+B_{66}\frac{\partial^2 v}{\partial x^2}+B_{11}\frac{\partial^2 v}{\partial y^2}+B_{44}\frac{\partial^2 v}{\partial z^2}+B_{13}\frac{\partial^2 w}{\partial y\,\partial z}-\frac{\partial U}{\partial y}=0\,,\\
&B_{13}\frac{\partial^2 u}{\partial x\,\partial z}+B_{13}\frac{\partial^2 v}{\partial y\,\partial z}+B_{44}\frac{\partial^2 w}{\partial x^2}+B_{44}\frac{\partial^2 w}{\partial y^2}+B_{33}\frac{\partial^2 w}{\partial z^2}=0\,.
\end{aligned} \tag{42}$$

By letting

$$W = \frac{1}{B_{13}} \int U \, dz \,, \tag{43}$$

the first two equations of (42) can be written in the forms

$$B_{11} \frac{\partial^2 u}{\partial x^2} + B_{66} \frac{\partial^2 u}{\partial y^2} + B_{44} \frac{\partial^2 u}{\partial z^2} + B_{12} \frac{\partial^2 v}{\partial x \, \partial y} + B_{13} \frac{\partial^2}{\partial x \, \partial z} (w - W) = 0 \,,$$

$$B_{12} \frac{\partial^2 u}{\partial x \, \partial y} + B_{66} \frac{\partial^2 v}{\partial x^2} + B_{11} \frac{\partial^2 v}{\partial y^2} + B_{44} \frac{\partial^2 v}{\partial z^2} + B_{13} \frac{\partial^2}{\partial y \, \partial z} (w - W) = 0 \,. \tag{44}$$

In order to satisfy these two equations, we may put

$$u = - \frac{\partial^2 F}{\partial x \, \partial z} \,, \qquad v = - \frac{\partial^2 F}{\partial y \, \partial z} \,,$$

$$w = W + \frac{B_{11}}{B_{13}} \nabla_1^2 F + \frac{B_{44}}{B_{13}} \frac{\partial^2 F}{\partial z^2} \,. \tag{45}$$

The stress function F in this case satisfies the equation

$$\left(\nabla_1^2 + \frac{1}{s_1^2} \frac{\partial^2}{\partial z^2} \right) \left(\nabla_1^2 + \frac{1}{s_2^2} \frac{\partial^2}{\partial z^2} \right) F + \frac{B_{13}}{B_{11} B_{44}} \left(B_{44} \nabla_1^2 W + B_{33} \frac{\partial^2 W}{\partial z^2} \right) = 0 \,. \tag{46}$$

This equation has the same form as (10). Therefore its special solution may be obtained by the same method.

V. Thermal Stresses

The temperature distribution T may depend on the time t. But we shall assume as usual that the inertial terms may be neglected. Under this assumption, the problem becomes a quasi-static problem, and system (4) is simplified to the form

$$B_{11} \frac{\partial^2 u}{\partial x^2} + B_{66} \frac{\partial^2 u}{\partial y^2} + B_{44} \frac{\partial^2 u}{\partial z^2} + B_{12} \frac{\partial^2 v}{\partial x \, \partial y} + B_{13} \frac{\partial^2 w}{\partial x \, \partial z} - \alpha_1 \frac{\partial T}{\partial x} = 0,$$

$$B_{12} \frac{\partial^2 u}{\partial x \, \partial y} + B_{66} \frac{\partial^2 v}{\partial x^2} + B_{11} \frac{\partial^2 v}{\partial y^2} + B_{44} \frac{\partial^2 v}{\partial z^2} + B_{13} \frac{\partial^2 w}{\partial y \, \partial z} - \alpha_1 \frac{\partial T}{\partial y} = 0, \tag{47}$$

$$B_{13} \frac{\partial^2 u}{\partial x \, \partial z} + B_{13} \frac{\partial^2 v}{\partial y \, \partial z} + B_{44} \frac{\partial^2 w}{\partial x^2} + B_{44} \frac{\partial^2 w}{\partial y^2} + B_{33} \frac{\partial^2 w}{\partial z^2} - \alpha_3 \frac{\partial T}{\partial z} = 0.$$

By letting

$$\tau\,(x, y, z, t) = \int T\,(x, y, z, t)\,dz\,, \tag{48}$$

the first two equations of (47) may be rewritten in the forms

$$B_{11}\frac{\partial^2 u}{\partial x^2} + B_{66}\frac{\partial^2 u}{\partial y^2} + B_{44}\frac{\partial^2 u}{\partial z^2} + B_{12}\frac{\partial^2 v}{\partial x\,\partial y} + B_{13}\frac{\partial^2}{\partial x\,\partial z}\left(w - \frac{\alpha_1}{B_{13}}\tau\right) = 0\,,$$

$$B_{12}\frac{\partial^2 u}{\partial x\,\partial y} + B_{66}\frac{\partial^2 v}{\partial x^2} + B_{11}\frac{\partial^2 v}{\partial y^2} + B_{44}\frac{\partial^2 v}{\partial z^2} + B_{13}\frac{\partial^2}{\partial y\,\partial z}\left(w - \frac{\alpha_1}{B_{13}}\tau\right) = 0\,. \tag{49}$$

In order to satisfy these two equations, we may put

$$u = -\frac{\partial^2 F}{\partial x\,\partial z}\,, \qquad v = -\frac{\partial^2 F}{\partial y\,\partial z}$$

$$w = \frac{\alpha_1}{B_{13}}\tau + \frac{B_{11}}{B_{13}}\nabla_1^2 F + \frac{B_{44}}{B_{13}}\frac{\partial^2 F}{\partial z^2}\,. \tag{50}$$

The last equation of (47) is reduced to the equation satisfied by the stress function F:

$$\left(\nabla_1^2 + \frac{1}{s_1^2}\frac{\partial^2}{\partial z^2}\right)\left(\nabla_1^2 + \frac{1}{s_2^2}\frac{\partial^2}{\partial z^2}\right)F + \frac{B_{13}}{B_{11}\,B_{44}}\left[\frac{B_{44}}{B_{13}}\alpha_1\nabla_1^2\tau + \right.$$
$$\left. + \left(\frac{B_{33}}{B_{13}}\alpha_1 - \alpha_3\right)\frac{\partial^2\tau}{\partial z^2}\right] = 0\,. \tag{51}$$

This equation has the same form as equation (10). Hence its solution can be obtained by the method described in §III.

When the temperature distribution is steady, and when there is no thermal source inside the body, the problem may be simplified greatly. In this case, the temperature T satisfies the equation

$$\frac{\partial^2 T}{\partial x^2} + \frac{\partial^2 T}{\partial y^2} + \frac{1}{s^2}\frac{\partial^2 T}{\partial z^2} = 0\,, \tag{52}$$

where s is a constant depending on the ratio of the coefficients of thermal conductivity of the body. A special solution of system (47) may be put in the form

$$u = \lambda_1\frac{\partial\varphi}{\partial x}\,, \qquad v = \lambda_1\frac{\partial\varphi}{\partial y}\,, \qquad w = \lambda_3\frac{\partial\varphi}{\partial z}\,, \tag{53}$$

where λ_1 and λ_3 are constants to be adjusted. Substituting these expressions

into equations (47), and then integrating with respect to x, y, and z respectively, we obtain

$$\begin{aligned}
&\lambda_1 B_{11}\left(\frac{\partial^2\varphi}{\partial x^2}+\frac{\partial^2\varphi}{\partial y^2}\right)+(\lambda_1 B_{44}+\lambda_3 B_{13})\frac{\partial^2\varphi}{\partial z^2}-\alpha_1 T=0\,,\\
&\lambda_1 B_{11}\left(\frac{\partial^2\varphi}{\partial x^2}+\frac{\partial^2\varphi}{\partial y^2}\right)+(\lambda_1 B_{44}+\lambda_3 B_{13})\frac{\partial^2\varphi}{\partial z^2}-\alpha_1 T=0\,,\\
&(\lambda_1 B_{13}+\lambda_3 B_{44})\left(\frac{\partial^2\varphi}{\partial x^2}+\frac{\partial^2\varphi}{\partial y^2}\right)+\lambda_3 B_{33}\frac{\partial^2\varphi}{\partial z^2}-\alpha_3 T=0\,.
\end{aligned}\tag{54}$$

This system of equations can be satisfied by taking

$$\frac{\partial^2\varphi}{\partial x^2}+\frac{\partial^2\varphi}{\partial y^2}+\frac{1}{s^2}\frac{\partial^2\varphi}{\partial z^2}=0\,,\qquad \frac{1}{s^2}\frac{\partial^2\varphi}{\partial z^2}=T\,,\tag{55}$$

$$\begin{aligned}
&\lambda_1(s^2 B_{44}-B_{11})+\lambda_3 s^2 B_{33}=s^4\alpha_1\,,\\
&-\lambda_1 B_{13}+\lambda_3(s^2 B_{33}-B_{44})=s^4\alpha_3\,.
\end{aligned}\tag{56}$$

Since T satisfies equation (52), the two equations of (55) have a common solution. Solving system (56), we get

$$\begin{aligned}
\lambda_1&=\frac{s^4[\alpha_1(s^2 B_{33}-B_{44})-\alpha_3 s^2 B_{13}]}{B_{11}B_{44}+s^2(B_{13}^2-B_{11}B_{33}-B_{44}^2)+s^4 B_{33}B_{44}}\,,\\
\lambda_3&=\frac{s^4[\alpha_1 B_{13}+\alpha_3(s^2 B_{44}-B_{11})]}{B_{11}B_{44}+s^2(B_{13}^2-B_{11}B_{33}-B_{44}^2)+s^4 B_{33}B_{44}}\,.
\end{aligned}\tag{57}$$

VI. Stress Functions for the Vibration of a Transversely Isotropic Elastic Body

Consider now the vibration of a transversely isotropic elastic body under surface tractions. For this problem the fundamental system (4) is reduced to the form

$$\begin{aligned}
&B_{11}\frac{\partial^2 u}{\partial x^2}+B_{66}\frac{\partial^2 u}{\partial y^2}+B_{44}\frac{\partial^2 u}{\partial z^2}+B_{12}\frac{\partial^2 v}{\partial x\,\partial y}+B_{13}\frac{\partial^2 w}{\partial x\,\partial z}=\rho\frac{\partial^2 u}{\partial t^2}\,,\\
&B_{12}\frac{\partial^2 u}{\partial x\,\partial y}+B_{66}\frac{\partial^2 v}{\partial x^2}+B_{11}\frac{\partial^2 v}{\partial y^2}+B_{44}\frac{\partial^2 v}{\partial z^2}+B_{13}\frac{\partial^2 w}{\partial y\,\partial z}=\rho\frac{\partial^2 v}{\partial t^2}\,,\\
&B_{13}\frac{\partial^2 u}{\partial x\,\partial z}+B_{13}\frac{\partial^2 v}{\partial y\,\partial z}+B_{44}\frac{\partial^2 w}{\partial x^2}+B_{44}\frac{\partial^2 w}{\partial y^2}+B_{33}\frac{\partial^2 w}{\partial z^2}=\rho\frac{\partial^2 w}{\partial t^2}\,.
\end{aligned}\tag{58}$$

We shall simplify this system of equations by the method proposed in paper [13]. As before, we first express u and v in terms of two stress functions F and φ as follows:

$$u = -\frac{\partial^2 F}{\partial x\,\partial z} - \frac{\partial \varphi}{\partial y}, \quad v = -\frac{\partial^2 F}{\partial y\,\partial z} + \frac{\partial \varphi}{\partial x}. \tag{59}$$

This presentation is not unique, since the homogeneous equations corresponding to (59)

$$\frac{\partial^2 F_0}{\partial x\,\partial z} + \frac{\partial \varphi_0}{\partial y} = 0, \quad \frac{\partial^2 F_0}{\partial y\,\partial z} - \frac{\partial \varphi_0}{\partial x} = 0 \tag{60}$$

have non-zero solutions. Actually, the solution of (60) is

$$\varphi_0 + i\frac{\partial F_0}{\partial z} = f(x+iy, z, t), \tag{61}$$

where f is an arbitrary function of $(x+iy)$, z and t. Consequently the displacement components u and v will not be altered by adding F_0 and φ_0 to F and φ.

Substituting expressions (59) into the first two equations of (58), we have

$$\begin{aligned}
&\frac{\partial}{\partial x}\frac{\partial}{\partial z}\left\{-B_{11}\frac{\partial^2 F}{\partial x^2} - B_{11}\frac{\partial^2 F}{\partial y^2} - B_{44}\frac{\partial^2 F}{\partial z^2} + \rho\frac{\partial^2 F}{\partial t^2} + B_{13}\,w\right\} - \\
&\qquad -\frac{\partial}{\partial y}\left(B_{66}\frac{\partial^2 \varphi}{\partial x^2} + B_{66}\frac{\partial^2 \varphi}{\partial y^2} + B_{44}\frac{\partial^2 \varphi}{\partial z^2} - \rho\frac{\partial^2 \varphi}{\partial t^2}\right) = 0, \\
&\frac{\partial}{\partial y}\frac{\partial}{\partial z}\left\{-B_{11}\frac{\partial^2 F}{\partial x^2} - B_{11}\frac{\partial^2 F}{\partial y^2} - B_{44}\frac{\partial^2 F}{\partial z^2} + \rho\frac{\partial^2 F}{\partial t^2} + B_{13}\,w\right\} + \\
&\qquad +\frac{\partial}{\partial x}\left(B_{66}\frac{\partial^2 \varphi}{\partial x^2} + B_{66}\frac{\partial^2 \varphi}{\partial y^2} + B_{44}\frac{\partial^2 \varphi}{\partial z^2} - \rho\frac{\partial^2 \varphi}{\partial t^2}\right) = 0,
\end{aligned} \tag{62}$$

From this it follows that

$$\begin{aligned}
&\frac{\partial}{\partial z}\left\{-B_{11}\frac{\partial^2 F}{\partial x^2} - B_{11}\frac{\partial^2 F}{\partial y^2} - B_{44}\frac{\partial^2 F}{\partial z^2} + \rho\frac{\partial^2 F}{\partial t^2} + B_{13}\,w\right\} + \\
&\qquad +i\left(B_{66}\frac{\partial^2 \varphi}{\partial x^2} + B_{66}\frac{\partial^2 \varphi}{\partial y^2} + B_{44}\frac{\partial^2 \varphi}{\partial z^2} - \rho\frac{\partial^2 \varphi}{\partial t^2}\right) = g(x+iy, z, t),
\end{aligned} \tag{63}$$

where g is an arbitrary function of $(x+iy)$, z and t. But if the function f in formula (61) is so chosen that

$$iB_{44}\frac{\partial^2 f}{\partial z^2} - i\rho\frac{\partial^2 f}{\partial t^2} = g(x+iy, z, t), \tag{64}$$

then by adding F_0 and φ_0 to F and φ, the right hand side of equation (63) may be brought to zero. Therefore we may put $g=0$ without loss of generality. Thus from (63) we have

$$\frac{\partial}{\partial z}\left\{-B_{11}\frac{\partial^2 F}{\partial x^2}-B_{11}\frac{\partial^2 F}{\partial y^2}-B_{44}\frac{\partial^2 F}{\partial x^2}+\rho\frac{\partial^2 F}{\partial t^2}+B_{13}\,w\right\}=0\,, \tag{65}$$

$$\frac{\partial^2\varphi}{\partial x^2}+\frac{\partial^2\varphi}{\partial y^2}+\frac{B_{44}}{B_{66}}\frac{\partial^2\varphi}{\partial z^2}-\frac{\rho}{B_{66}}\frac{\partial^2\varphi}{\partial t^2}=0\,. \tag{66}$$

(66) is the equation satisfied by the function φ. From (65), we get

$$-B_{11}\frac{\partial^2 F}{\partial x^2}-B_{11}\frac{\partial^2 F}{\partial y^2}-B_{44}\frac{\partial^2 F}{\partial z^2}+\rho\frac{\partial^2 F}{\partial t^2}+B_{13}\,w=h(x,y)\,, \tag{67}$$

where h is an arbitrary function of x and y. It is evident that u, v will not be altered by adding an arbitrary function of x, y to F. Therefore we may put $h=0$. Thus we obtain

$$w=\frac{B_{11}}{B_{13}}\nabla_1^2 F+\frac{B_{44}}{B_{13}}\frac{\partial^2 F}{\partial z^2}-\frac{\rho}{B_{13}}\frac{\partial^2 F}{\partial t^2}\,. \tag{68}$$

This is the expression for the displacement component w. Substituting expressions (59) and (68) into the last equation of (58), we finally obtain the equation satisfied by F as follows:

$$\begin{aligned}&\frac{B_{11}B_{44}}{B_{13}^2}\nabla_1^4 F+\frac{B_{44}^2+B_{11}B_{33}-B_{13}^2}{B_{13}^2}\nabla_1^2\frac{\partial^2 F}{\partial z^2}+\frac{B_{33}B_{44}}{B_{13}^2}\frac{\partial^4 F}{\partial z^4}-\\&-\frac{\rho}{B_{13}}\left\{\frac{B_{11}+B_{44}}{B_{13}}\nabla_1^2+\frac{B_{33}+B_{44}}{B_{13}}\frac{\partial^2}{\partial z^2}\right\}\frac{\partial^2 F}{\partial t^2}+\frac{\rho^2}{B_{13}^2}\frac{\partial^4 F}{\partial t^4}=0\,.\end{aligned} \tag{69}$$

For the sake of simple writing, let us denote

$$\begin{aligned}&\frac{B_{11}}{B_{13}}=\alpha\,,\quad \frac{B_{33}}{B_{13}}=\beta\,,\quad \frac{B_{44}}{B_{13}}=\gamma\,,\quad \frac{B_{66}}{B_{44}}=s_0^2\,,\\&\frac{B_{12}}{B_{13}}=\frac{B_{11}-B_{66}}{B_{13}}=\alpha-\gamma s_0^2\,,\quad \frac{\rho}{B_{13}}=\kappa\,.\end{aligned} \tag{70}$$

The results obtained above can be stated as follows. The solution of the system of equations (58) can be expressed in terms of two stress functions as follows:

$$\begin{aligned}&u=-\frac{\partial^2 F}{\partial x\,\partial z}-\frac{\partial\varphi}{\partial y}\,,\quad v=-\frac{\partial^2 F}{\partial y\,\partial z}+\frac{\partial\varphi}{\partial x}\,,\\&w=\alpha\nabla_1^2 F+\gamma\frac{\partial^2 F}{\partial z^2}-\kappa\frac{\partial^2 F}{\partial t^2}\,,\end{aligned} \tag{71}$$

where F and φ satisfy respectively the following equations:

$$\alpha\gamma\nabla_1^4 F + (\gamma^2+\alpha\beta-1)\nabla_1^2\frac{\partial^2 F}{\partial x^2} + \beta\gamma\frac{\partial^4 F}{\partial x^4} -$$

$$-\kappa\left[(\alpha+\gamma)\nabla_1^2 + (\beta+\gamma)\frac{\partial^2}{\partial z^2}\right]\frac{\partial^2 F}{\partial t^2} + \kappa^2\frac{\partial^4 F}{\partial t^4} = 0\,, \tag{72}$$

$$\nabla_1^2\varphi + \frac{1}{s_0^2}\frac{\partial^2\varphi}{\partial z^2} - \frac{\kappa}{\gamma s_0^2}\frac{\partial^2\varphi}{\partial t^2} = 0\,. \tag{73}$$

From these two equations it can be seen that φ is a wave function, but F, in general, cannot be expressed in terms of wave functions.

VII. Propagation of Waves in Cylinder

Consider a transversely isotropic cylinder with planes of isotropy perpendicular to generators. A nondispersive wave is propagated along the cylinder with constant velocity c. In this case, the displacement components have the forms

$$u = u(x, y, \zeta)\,, \qquad v = v(x, y, \zeta)\,, \qquad w = w(x, y, \zeta)\,, \tag{74}$$

where

$$\zeta = z - ct\,. \tag{75}$$

Stress functions have the forms

$$F = F(x, y, \zeta)\,, \qquad \varphi = \varphi(x, y, \zeta)\,. \tag{76}$$

Consequently equations (72) and (73) are reduced to

$$\alpha\gamma\nabla_1^4 F + [\gamma^2+\alpha\beta-1-\kappa c^2(\alpha+\gamma)]\nabla_1^2\frac{\partial^2 F}{\partial\zeta^2} +$$

$$+ [\beta\gamma-\kappa c^2(\beta+\gamma) + \kappa^2 c^4]\frac{\partial^4 F}{\partial\zeta^4} = 0\,, \tag{77}$$

$$\nabla_1^2\varphi + \frac{\gamma-\kappa c^2}{\gamma s_0^2}\frac{\partial^2\varphi}{\partial\zeta^2} = 0\,. \tag{78}$$

Let $\pm s_1$, $\pm s_2$ be the four roots of the equation

$$\alpha\gamma - [\gamma^2+\alpha\beta-1-\kappa c^2(\alpha+\gamma)]s^2 + [\beta\gamma-\kappa c^2(\beta+\gamma) + \kappa^2 c^4]s^4 = 0\,. \tag{79}$$

Then equation (77) can be written in the form

$$\left(\nabla_1^2 + \frac{1}{s_1^2}\frac{\partial^2}{\partial\zeta^2}\right)\left(\nabla_1^2 + \frac{1}{s_2^2}\frac{\partial^2}{\partial\zeta^2}\right)F = 0\,. \tag{80}$$

Let F_1 and F_2 be the solutions of the equations

$$\nabla_1^2 F_i + \frac{1}{s_i^2} \frac{\partial^2 F_i}{\partial \zeta^2} = 0 , \qquad (i=1, 2) . \tag{81}$$

It is evident that

$$F = F_1 + F_2 \tag{82}$$

is a solution of equation (80). Substituting (82) into (71), and putting

$$\frac{\partial F_1}{\partial \zeta} = \varphi_1 , \qquad \frac{\partial F_2}{\partial \zeta} = \varphi_2 , \qquad \varphi = \varphi_0 , \tag{83}$$

we finally obtain the following expressions:

$$\begin{aligned} u &= -\frac{\partial \varphi_1}{\partial x} - \frac{\partial \varphi_2}{\partial x} - \frac{\partial \varphi_0}{\partial y} \\ v &= -\frac{\partial \varphi_1}{\partial y} - \frac{\partial \varphi_2}{\partial y} + \frac{\partial \varphi_0}{\partial x} , \\ w &= -\sum_{i=1, 2} \frac{\alpha - s_i^2 (\gamma - \kappa c^2)}{s_i^2} \frac{\partial \varphi_i}{\partial \zeta} . \end{aligned} \tag{84}$$

It is clear that φ_1 and φ_2 satisfy the same equations as F_1 and F_2.

The propagation of axisymmetric waves in transversely isotropic circular cylinder has been investigated by C. Chree[14] and R. W. Morse[15].

VIII. Vibrations of Bodies of Revolution

Consider a transversely isotropic elastic body of revolution with planes of isotropy perpendicular to the axis of revolution. Take as cylindrical coordinates r, θ, and z, such that the z-axis coinsides with the axis of revolution. In cylindrical coordinates we have the following formulas:

$$\begin{aligned} u_r &= -\frac{\partial^2 F}{\partial r \, \partial z} - \frac{1}{r} \frac{\partial \varphi}{\partial \theta} , \\ u_\theta &= -\frac{1}{r} \frac{\partial^2 F}{\partial \theta \, \partial z} + \frac{\partial \varphi}{\partial r} , \\ w &= \alpha \nabla_1^2 F + \gamma \frac{\partial^2 F}{\partial z^2} - \kappa \frac{\partial^2 F}{\partial t^2} . \end{aligned} \tag{85}$$

The stress functions F and φ satisfy equations (72) and (73) respectively, in which the differential operator ∇_1^2 takes the form

$$\nabla_1^2 = \frac{1}{r}\frac{\partial}{\partial r} r \frac{\partial}{\partial r} + \frac{1}{r^2}\frac{\partial^2}{\partial \theta^2} . \tag{86}$$

There are three important modes of vibration of bodies of revolution. Let us examine these modes individually.

1. *Torsional vibration.* In the case of torsional vibration, we may put

$$F = 0 , \qquad \varphi = \varphi\,(r, z, t) . \tag{87}$$

Consequently we obtain

$$u_r = 0 , \quad w = 0 , \quad u_\theta = \frac{\partial \varphi}{\partial r} , \tag{88}$$

$$\frac{1}{r}\frac{\partial}{\partial r} r \frac{\partial \varphi}{\partial r} + \frac{1}{s_0^2}\frac{\partial^2 \varphi}{\partial z^2} - \frac{\kappa}{\gamma s_0^2}\frac{\partial^2 \varphi}{\partial t^2} = 0 . \tag{89}$$

Among the six stress components in cylindrical coordinate, four equal zero and the remaining two are related to φ by the relation

$$\tau_{\theta z} = B_{44}\frac{\partial^2 \varphi}{\partial r\, \partial z} , \qquad \tau_{r\theta} = B_{66}\left(\frac{\partial^2 \varphi}{\partial r^2} - \frac{1}{r}\frac{\partial \varphi}{\partial r}\right). \tag{90}$$

For isotropic bodies, $B_{44} = B_{66} = \mu$ we have

$$u_\theta = \frac{\partial \varphi}{\partial r} , \quad \tau_{\theta z} = \mu \frac{\partial^2 \varphi}{\partial r\, \partial z} , \quad \tau_{r\theta} = \mu\left(\frac{\partial^2 \varphi}{\partial r^2} - \frac{1}{r}\frac{\partial \varphi}{\partial r}\right), \tag{91}$$

$$\frac{1}{r}\frac{\partial}{\partial r} r \frac{\partial \varphi}{\partial r} + \frac{\partial^2 \varphi}{\partial z^2} - \frac{\rho}{\mu}\frac{\partial^2 \varphi}{\partial t^2} = 0 . \tag{92}$$

For transversely isotropic bodies, by substituting

$$s_0 z = \zeta , \qquad s_0 \tau_{\theta z} = \tau_{\theta \zeta} , \tag{93}$$

we have

$$u_\theta = \frac{\partial \varphi}{\partial r} , \quad \tau_{\theta \zeta} = B_{66}\frac{\partial^2 \varphi}{\partial r\, \partial \zeta} , \quad \tau_{r\theta} = B_{66}\left(\frac{\partial^2 \varphi}{\partial r^2} - \frac{1}{r}\frac{\partial \varphi}{\partial r}\right), \tag{94}$$

$$\frac{1}{r}\frac{\partial}{\partial r} r \frac{\partial \varphi}{\partial r} + \frac{\partial^2 \varphi}{\partial \zeta^2} - \frac{\rho}{B_{66}}\frac{\partial^2 \varphi}{\partial t^2} = 0 . \tag{95}$$

These two sets of equations are identical with (91) and (92). This fact indicates that the problem of torsional vibration of transversely isotropic bodies of revolution can be reduced to that of isotropic bodies of revolution.

2. *Axially symmetrical vibration.* In the case of axially symmetrical vibration, we may put

$$\varphi = 0\,, \qquad F = F\,(r, z, t)\,. \tag{96}$$

Consequently we have

$$u_\theta = \theta\,, \quad u_r = -\frac{\partial^2 F}{\partial r\,\partial z}\,, \quad w = \alpha\,\nabla_1^2 F + \gamma\,\frac{\partial^2 F}{\partial z^2} - \kappa\,\frac{\partial^2 F}{\partial t^2}\,. \tag{97}$$

The stress function F satisfies equation (72), where the differential operator ∇_1^2 is reduced to

$$\nabla_1^2 = \frac{1}{r}\,\frac{\partial}{\partial r}\,r\,\frac{\partial}{\partial r}\,. \tag{98}$$

In general F is not expressible in terms of wave functions.

3. *Flexural vibration.* In the case of flexural vibration, we can put neither F nor φ equal to zero. But as for the static problem, here we may assume that F and φ have the following forms

$$F = f\,(r, z, t)\,\cos\theta\,, \qquad \varphi = \psi\,(r, z, t)\,\sin\theta\,. \tag{99}$$

Consequently in this case u_r, w, σ_r, σ_θ, σ_z, τ_{rz} are proportional to $\cos\theta$ and u_θ, $\tau_{\theta z}$, $\tau_{r\theta}$ are proportional to $\sin\theta$.

References

[1] Лехницкий, С. Г., 1940. Симметричная деформация и кручение тела вращения с анизотропией частного вида. *Прикл. Мат. Мех.*, **4**.

[2] Лехницкий, С. Г., 1950. *Теория упругости анизотропного тела.* Гостехиздат.

[3] Moisil, A., 1950. Asupra unui vetor analog vectorului lui Galerkin pentru erhilibrul corporilor elastice ar isotropie tranversa. *Bull. Stiint.,* Ser. Mat. Fiz., Acad. Repub. Pop. Române, **2**, 207.

[4] Moisil, A., 1951. Les relation entre les tensions pour les corps élastiques à isotropic transverse. Acad. Repub. Pop. Române, *Bul. Sti.* Sect. Sti. Mat. Fiz., **3**, 473—480.

[5] Nowacki, W., 1953. The Determining of Stresses and Deformations in Transversely Isotropic Elastic Bodies. *Arch. Mech. Stos.,* **5**, 545—556.

[6] Hu, Hai-Chang, 1953. On the Three Dimensional Problems of the Theory of Elasticity of a Transversely Isotropic Body. *Acta Physica Sinica,* **9**, 130—144 (in Chinese with English summary).

[7] Hu, Hai-Chang, 1953. On the Three Dimensional Problems of the Theory of Elasticity of a Transversely Isotropic Body. *Acta Scientia Sinica,* **2**, 145—151.

[8] Hu, Hai-Chang, 1954. On the General Theory of Elasticity for a Spherically Isotropic Medium. *Acta Physica Sinica,* **10**, 57—69 (in Chinese with English summary).

[9] Hu, Hai-Chang, 1954. On the General Theory of Elasticity for a Spherically Isotropic Medium. *Acta Scientia Sinica,* **3**, 247—260.

[10] Carrier, G. F., 1944. The Thermal Stress and Body-force Problems of the Infinite Orthotropic Solid. *Quart. Appl. Math.,* **2**, 31—36.

[11] Hu, Hai-Chang, 1955. On the Equlibrium of a Transversely Isotropic Elastic Body under Body Forces. *Acta Physica Sinica,* **11**, 219—230 (in Chinese with English summary).

[12] Elliot, H. A., 1948. Three-dimensional Stress Distribution in Hexagonal Crystals. *Proc. Cambridge Phil. Soc.,* **44**, 552—533.

[13] Hu, Hai-Chang, 1955. On the Vibration of a Transversely Isotropic Elastic Body. *Acta Physica Sinica,* **11**, 231—238 (in Chinese with English summary).

[14] Chree, C., 1890. On the Longitudinal Vibrations of Aeolotropic Bar with One Axis of Material Symmetry. *Quart. J. Math.,* **24**, 340—358.

[15] Morse, R. W., 1954. Compressional Waves along an Anisotropic Circular Cylinder Having Hexagonal Symmetry. *J. Acoust. Soc. Amer.,* **26** 1018—1021.

[16] Jaerisch, P., 1889. Allgemeine Integration der Elasticitätsgleichungen für die Schwingungen und das Gleichgewicht Isotroper Rotationsköper, *J. f. Math.* (Crelle), **104**, 177—210.

INTERNAL FRICTION PEAKS ASSOCIATED WITH THE TEMPERING OF MARTENSITE IN STEELS*

Kê T'ing-Sui (T. S. Kê, 葛庭燧) and Ma Ying-Liang (馬應良)

(Institute of Metal Research, Academia Sinica)

Abstract

Internal friction in hardened carbon steels was measured with a torsion pendulum and an internal friction peak was observed around 130°C when measurements were taken from room temperature upwards. This peak disappeared completely after the temperature of the specimen once reached 170°C. This phenomenon was observed in carbon steels containing carbon ranging from 0.29% to 1.4%, and also in an alloy steel. The appearance of this internal friction peak seems to indicate that the transformation product (ϵ-carbide) formed in the first-stage tempering of martensite is coherent with its parent phase, and the origin of internal friction is the stress-induced movement of the plane of coherence.

The above-mentioned internal friction peak was not observed in 0.25% carbon steel specimens having a martensitic structure. However, after such a specimen had been tempered at a temperature around 300°C, an internal friction peak was observed around 150°C. This indicates that the transformation product formed in martensite containing 0.25% carbon in the third-stage tempering is coherent with its parent phase. Since the internal friction peak associated with this transformation product behaves differently from that associated with ϵ-carbide, it is concluded that the third-stage transformation product is not ϵ-carbide.

I. Introduction

In the tempering of hardened carbon steels, the first-stage transformation occurs in the temperature range of 80—160°C. Important information as to the nature of the transformation product formed during this stage was given by Kurjumov and Lysak based on the results of X-ray study on single crystal martensite. They found that a low-carbon martensite containing 0.25%C was formed as an intermediate phase during the first-stage of tempering[1]. This shows that the change of tetragonality (axis ratio) of martensite is not continuous in the process of decomposition, but changes abruptly to a low-carbon martensite with a definite lower axis ratio corresponding to a carbon content of 0.25% C. This experimental observation was later confirmed by other workers[2].

The first stage of tempering consists, thus, of the formation of a low carbon martensite containing about 0.25% C and a transitional phase of carbide

---

*First published in Chinese in *Acta Physica Sinica,* Vol. XI, No. 6, pp. 479—492, 1955.

having a hexagonal close-packed structure, and is called ϵ-carbide because its resemblance in structure with the ϵ-phase in Fe-N system[3]. On the basis of X-ray observations, Jack considered that this ϵ-carbide was coherent with the primary martensite, with the (101) plane parallel to and coherent with the (101) plane of martensite. According to him, the interplanar spacing of the (101) planes of ϵ-carbide is almost identical with that of the (101) planes of tetragonal martensite, so that periodicity is maintained along the (101) direction. Although Jack's suggestion on the existence of ϵ-carbide was confirmed later by many workers, yet the evidence he pointed out as to the coherency has been considered to be inconclusive.

We observed recently an internal friction peak associated with the tempering of martensite in steels. This observation leads to the belief that internal friction measurements may be applicable to the study of mechanism of transformation in the tempering of martensite.

In a two-phase structure having a coherency relationship, the application of a stress (no matter how small it is) often gives rise to a stress-induced movement of the coherency plane and leads to the appearance of internal friction. Worrell has observed an internal friction peak associated with the stress-induced movement of the twin-boundaries in a Cu-Mn alloy (containing about 90% Mn)[4]. Internal friction measurements may thus be utilized as a useful tool for judging the existence of a state of coherency.

In the following is described the occurrence of the internal friction peaks in the tempering of martensite in steels. Further experimental results will be reported later.

II. Experimental Arrangement and Specimens

A torsion pendulum[5] with a frequency of vibration of about 2 cycles per second was used for internal friction measurements. Specimens were prepared mostly from low carbon steel and III X15 steel.

The low carbon steel contains 0.22% C, 0.44% Mn, 0.018% Si, 0.015% P and 0.04% S. Steel rods were swaged to a final diameter of about 1.5 mm with several times of intermediate vacuum annealing. Specimens thus obtained were annealed at 650°C in vacuum and then furnace-cooled.

Carburizing treatment of the specimens was proceeded inside a high temperature furnace (920°C) in an atmosphere of circulating dry hydrogen and benzene vapour. After carburizing, the specimen was homogenized by heating in vacuum for 2–4 hours at a temperature 20—30°C higher than the carburizing temperature.

Steel III X15 contains 0.96% C, 1.5% Cr, 0.29% Mn, 0.1% Ni, 0.27% P and 0.01% S. Specimens of this steel were also prepared by swaging to a final

diameter of 2 mm with several times of intermediate annealing. The final annealing temperature was 870°C.

The carbon content in all specimens was determined by combustion method after the final treatment.

III. Experimental Results

1. *Discovery of the internal friction peak*

A specimen from low carbon steel was carburized at 920°C for about two hours. It was then homogenized at 950°C for four hours and quenched into cold water. Carbon analysis showed that the specimen contains 1.36% C. Metallographic examination revealed a structure of martensite and retained austenite. Internal friction measurements were made on the specimen immediately after quenching with a frequency of vibration of 2 cycles per second. As the temperature was raised, a pronounced internal friction peak appeared around 130°C. This peak rose again beginning at about 160°C as shown by curve I of Fig. 1. The specimen was cooled in the measuring furnace to room temperature from 220°C.

Internal friction measurements were again taken by raising the temperature. Curve II of Fig. 1 shows that the internal friction peak around 130°C observed in the first experiment now disappeared completely. It is seen from curve II that when the temperature was raised above 220°C, another internal friction peak appeared near 235°C. This peak was shown to be associated with the interaction of carbon atoms with the quenching stress from the results of previous experiments[6].

Attention was drawn toward the appearance of the 130°C peak, which was observed for the first time. In order to remove the interference effect of the 235°C peak, internal friction values of curve II were subtracted from those of curve I. The dotted curve III thus obtained shows that this new internal friction peak extends from 70°C to 170°C which coincides with the temperature range of the first stage tempering of martensite. This suggests that the observed internal friction peak may be connected with the transformation of martensite in the first-stage tempering. With this in mind, another specimen was similarly treated as the first one only that the specimen was refrigerated at −78°C immediately after it was quenched from 950°C. Internal friction measurements were taken with this refrigerated specimen beginning at room temperature and curve IV was obtained as shown in Fig. 1. The 130°C peak is seen to be higher after this low-temperature treatment. It is well known that no structural change could occur in the specimen after the refrigeration except the transformation of part of the retained austenite into martensite. Accordingly, the increase in height of the internal friction peak is related to the increase of the amount of martensite in the specimen.

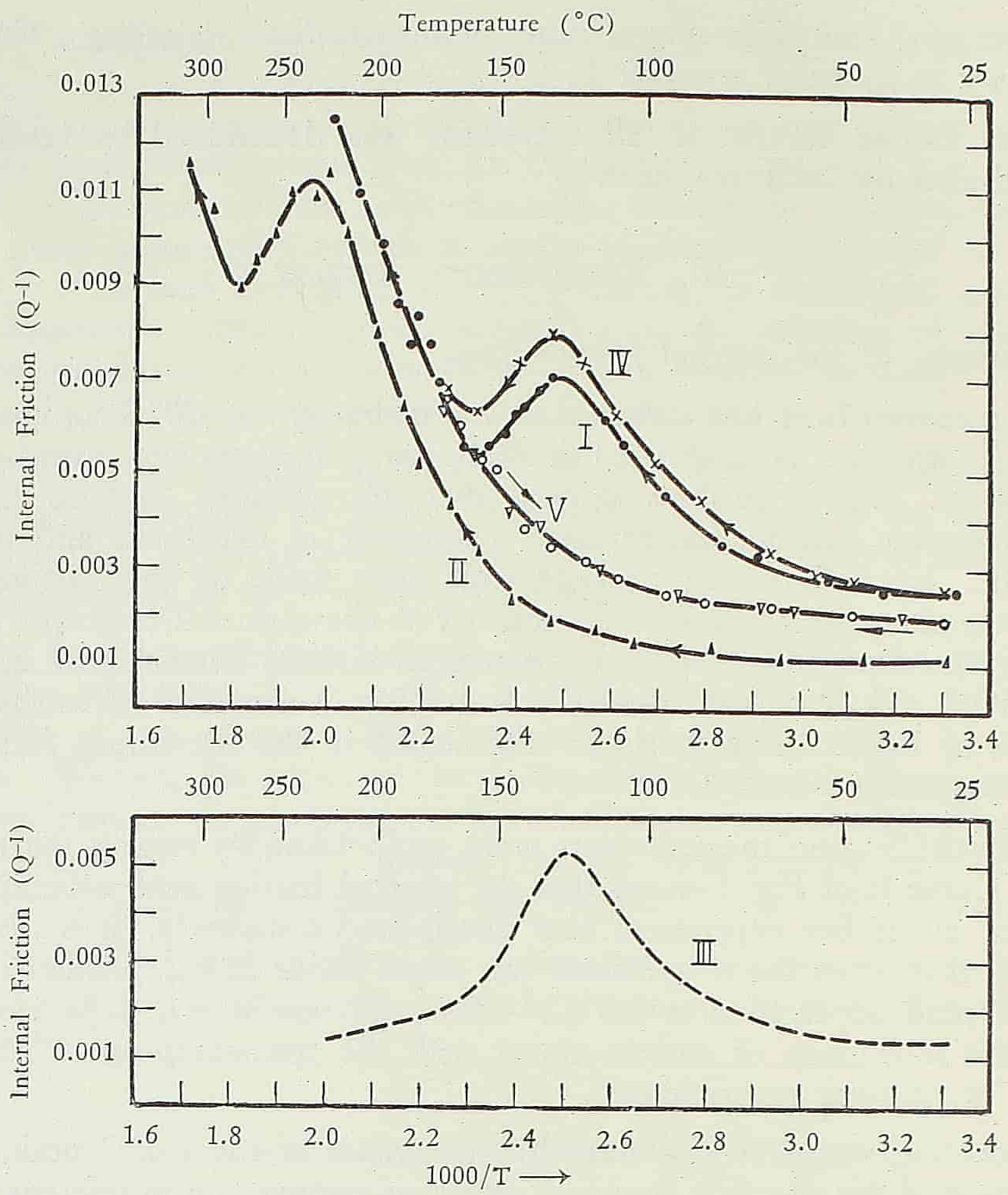

Fig. 1. Variation of internal friction with temperature of quench-hardened steel containing 1.36% C. Curve I, measurements begin at room temperature after quenching from 950°C; curve II, measurements again taken from room temperature after the completion of curve I up to 220°C; curve III, internal friction peak obtained by subtracting curve II from curve I; curve IV, specimen refrigerated at –78°C after quenching from 950°C; curve V, measurements taken with lowering temperature from 175°C.

When internal friction measurements were taken by lowering the temperature from 170°C, the originally observed 130°C peak disappeared completely as shown by curve V. As the temperature was again raised from room temperature, the internal friction values followed precisely along curve V.

The phenomenon described above is highly reproducible. When the specimen of which the 130°C peak disappeared was again subjected to austenitizing and quenching treatments, the 130°C peak re-appeared as before.

2. *Effect of carbon content*

Specimens of low-carbon steel were carburized to have a carbon content of 1.3%, 1.2%, 1.1%, 0.72%, 0.52% and 0.29%. Internal friction measurements with these specimens showed that an internal friction peak was observed around 130°C when the specimen contained martensite, and no 130°C peak was observed when the specimen contained no martensite or when a martensite-containing specimen was tempered at a temperature above 170°C.

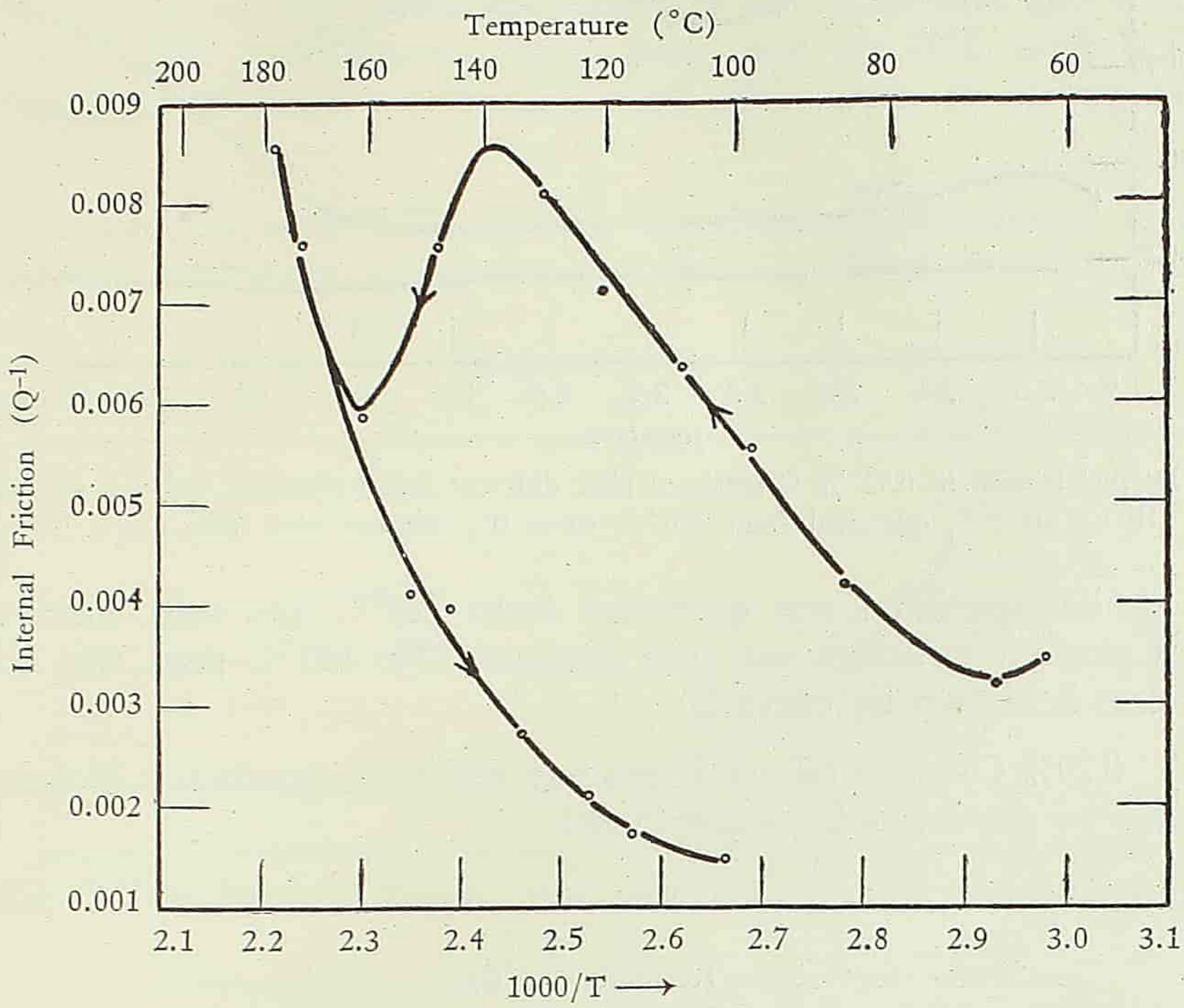

Fig. 2. Internal friction peak associated with the first-stage tempering of the quench-hardened steel containing 0.72% C (quenched from 910°C). Peak disappeared completely when measurements taken with lowering temperature from 170–180°C.

(1) 0.72% C.—A specimen containing 0.72% carbon was quenched into cold water from 910°C. Metallographic examinations showed that the specimen has a martensitic structure. The internal friction curve for this specimen is shown in Fig. 2, in which a pronounced peak occurs at 130–140°C. As measurements were taken up to 170–180°C and then the temperature was lowered, the internal friction peak disappeared completely as shown in the same figure.

(2) 0.52% C.—When a specimen containing 0.52% C was quenched from 910°C so as to have a martensitic structure, the internal friction peak observed was shown by curve I in Fig. 3. The peak is seen to increase again at higher temperatures. When a similar specimen was furnace-cooled from 910°C so as to have a pearlitic structure, curve III was observed without the 130°C peak. This curve remains flat up to 240°C.

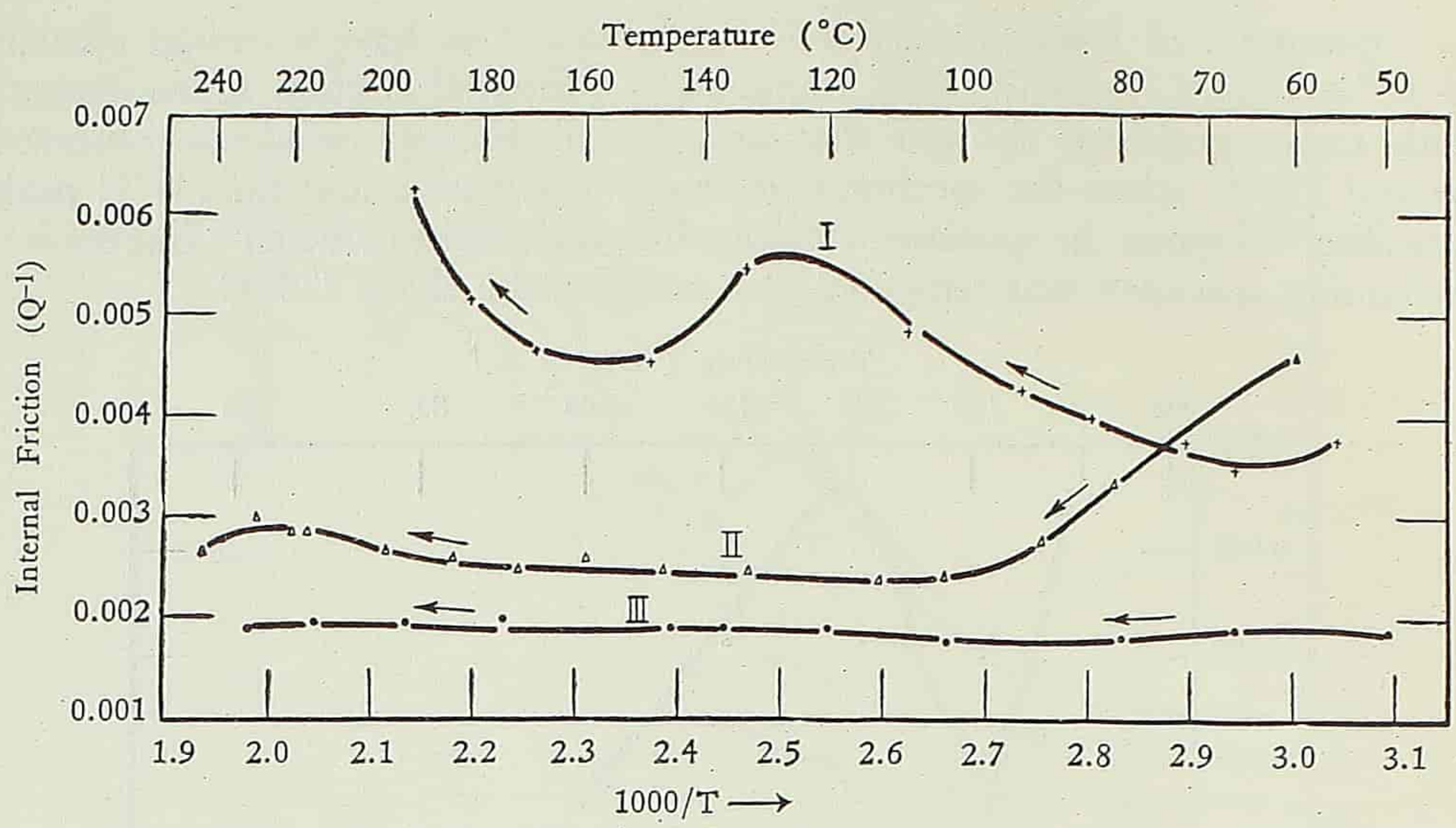

Fig. 3. Internal friction in 0.52 % C specimen after different heat treatments. Curve I, quenched from 910°C; curve II, quenched from 720°C; curve III, furnace-cooled from 910°C.

A similar specimen was quenched from 720°C into cold water during which a pearlitic structure was also obtained. No 130°C peak was observed in this case as shown by curve II.

(3) 0.29% C.—The effects of the rate and the temperature of quenching are shown by the following experiments.

When a 0.29% carbon specimen was quenched from 950°C into 10%

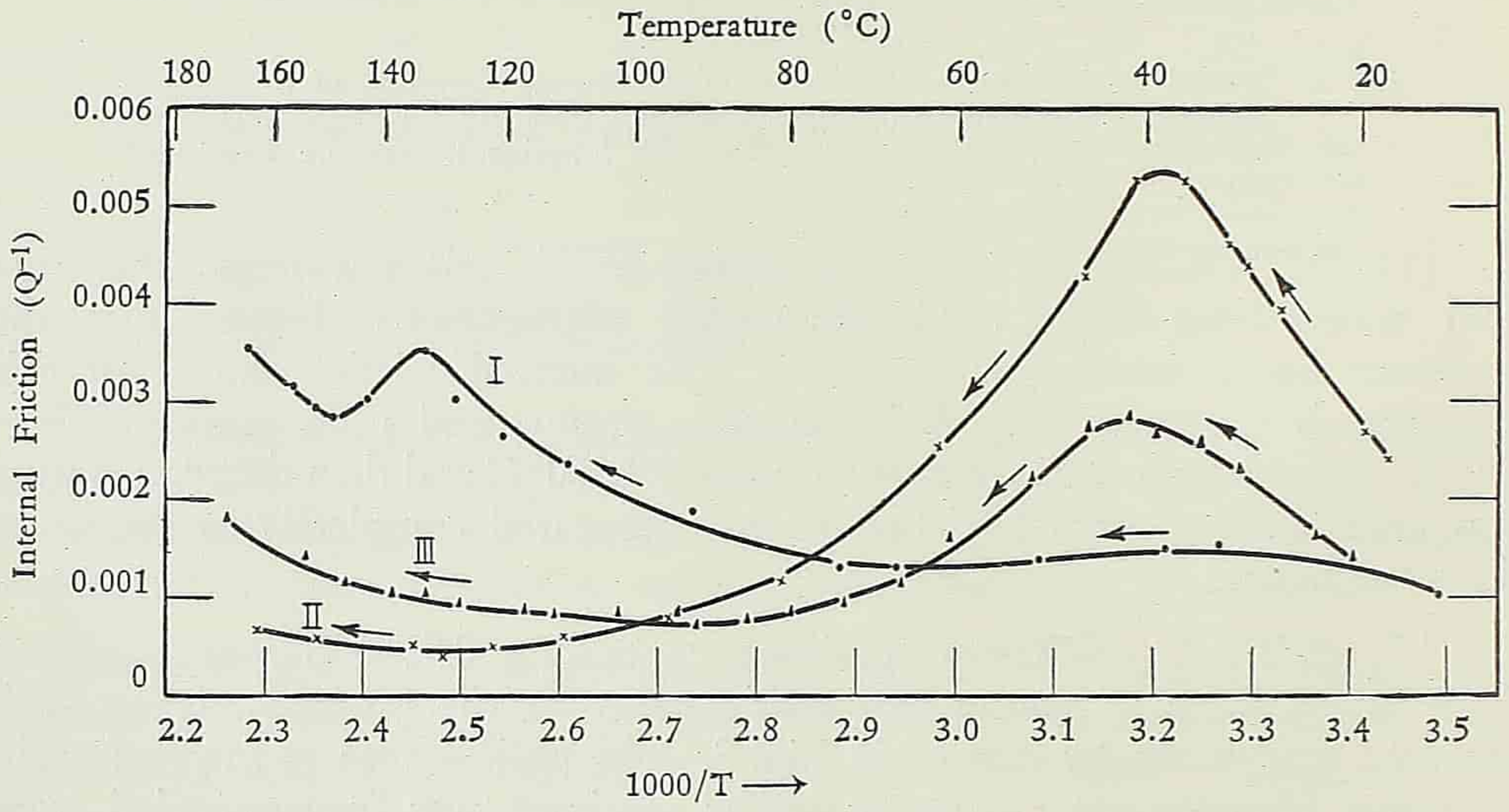

Fig. 4. Internal friction in 0.29% C specimen after different heat treatments. Curve I, quenched into 10% brine from 950°C; curve II, quenched into 10% brine from 700°C; curve III, quenched into oil from 950°C.

brine, the 130°C peak was observed as shown by curve I of Fig. 4. If it was quenched into mineral oil from the same temperature, the 130°C peak was not observed as shown by curve III. It is to be noticed that in the latter case an internal friction peak was observed around 40°C, a peak known to be associated with the stress-induced micro-diffusion of carbon in α-iron. The appearance of this 40°C peak shows that the specimen contains ferrite. Curve II of Fig. 4 was observed when the specimen was quenched into 10% brine from 700°C. The curve has no 130°C peak, and the 40°C peak is higher, indicating that the ferrite in the specimen dissolves more carbon in solid solution.

In experiments with 0.25% carbon specimen vacuum-treated at 950°C and quenched into water, a troostite structure was obtained and the internal

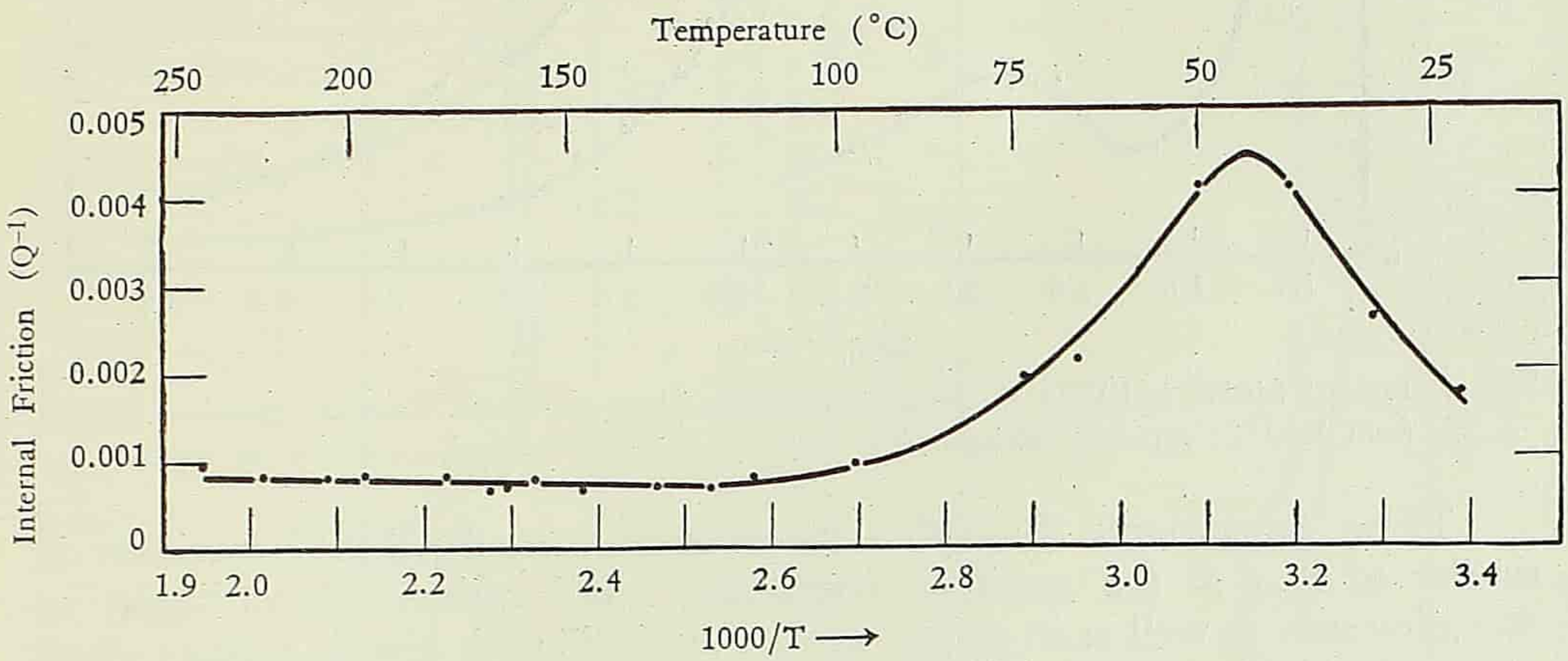

Fig. 5. Internal friction in 0.25% C specimen (with a troostite structure).

friction curve observed is shown in Fig. 5. The shape of the curve is similar to that of curve II of Fig. 4. Further experiments on 0.25% carbon specimen will be described in § IV.

3. *Experiments on alloy-steel.*

A ШX15 specimen (0.96% C) was oil-quenched from 1100°C and internal friction measured starting at room temperature. Curve I of Fig. 6 was obtained with a frequency of vibration of 1.5 cycles per second. This curve appears to be broadened around 130°C. Another similarly heat-treated specimen was refrigerated at −78°C immediately after the quenching in order to allow the retained austenite in the specimen to transform partly into martensite. The 130°C peak is much more pronounced for this specimen as is shown by curve II of Fig. 6. After the temperature reached somewhere around 170°C, measurements were taken by lowering the temperature. The 130°C peak completely disappeared.

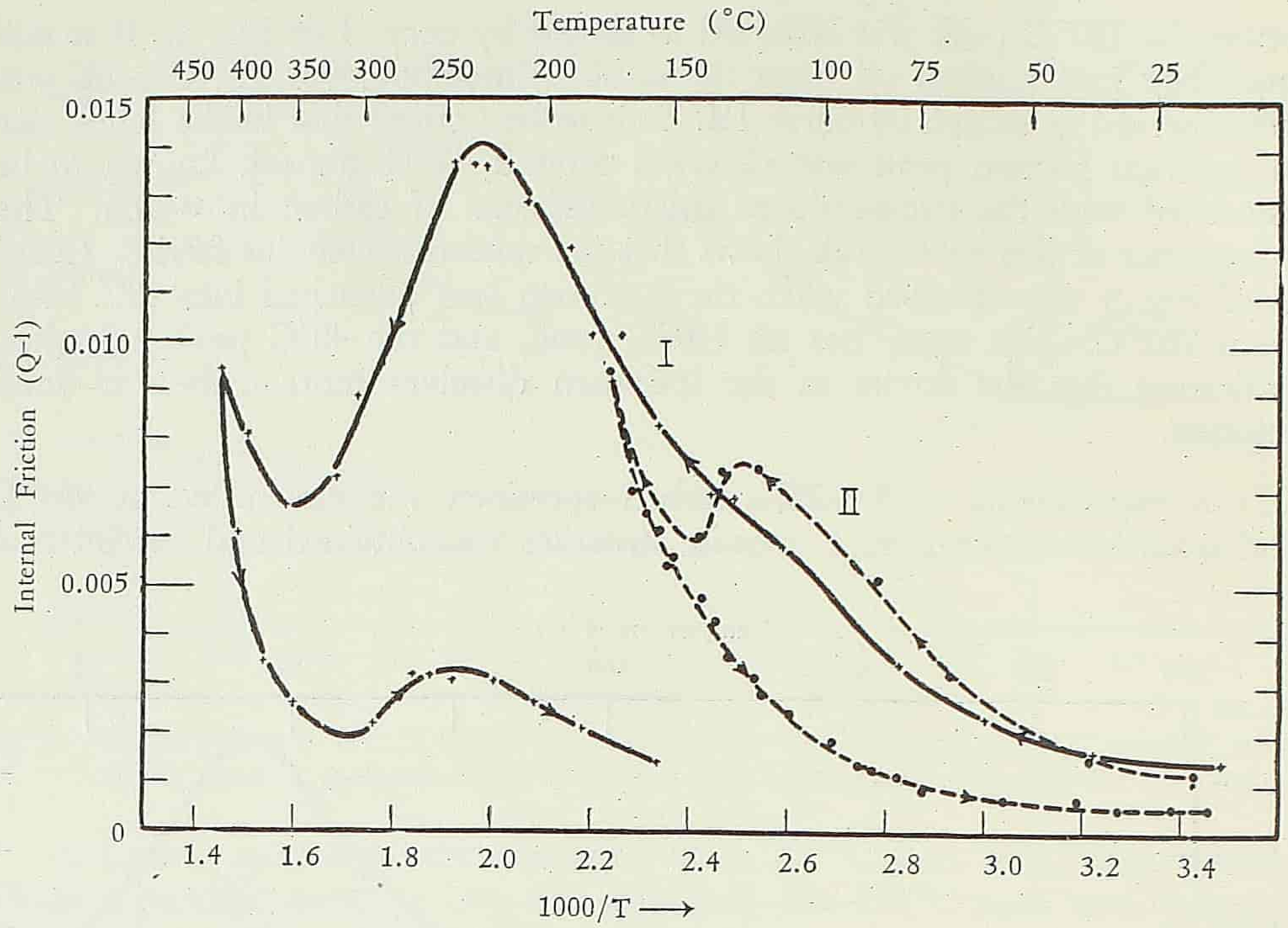

Fig. 6. Internal friction in ШX15 specimen after different heat treatments. Curve I, quenched into oil from 1100°C; curve II, refrigerated at –78°C immediately after the treatment in curve I.

These experiments show that the behaviour of the ШX15 specimen is similar to that of the specimen containing 1.36% carbon. Accordingly, in this alloy steel as well as in carbon steels, the 130°C peak always appears when martensite is present in the specimen and always disappears when the specimen consisting of martensite is tempered at a temperature corresponding to the first-stage tempering. These facts lead to the belief that the 130°C internal friction peak is associated with the transformation of martensite in the first-stage tempering of hardened steels.

4. *Some experiments on low-carbon martensite* (0.25% C).

Ordinary welding-rods containing 0.25% C (determined by carbon analysis) were used as specimens in the experiment. The diameter of the rod is 2 mm. It was treated at 930°C for half an hour and then quenched into 10% brine. Metallographic examinations revealed a martensitic structure in the specimen. The internal friction for this specimen measured with a frequency of vibration of 2 cycles per second is shown by curve I of Fig. 7. The curve remains to be flat up to the temperature of 160°C. The occurrence of the 235°C peak indicates the existence of a state of stress in the specimen induced by quenching. The absence of the 40°C peak indicates the absence of ferrite (α-Fe) in the specimen.

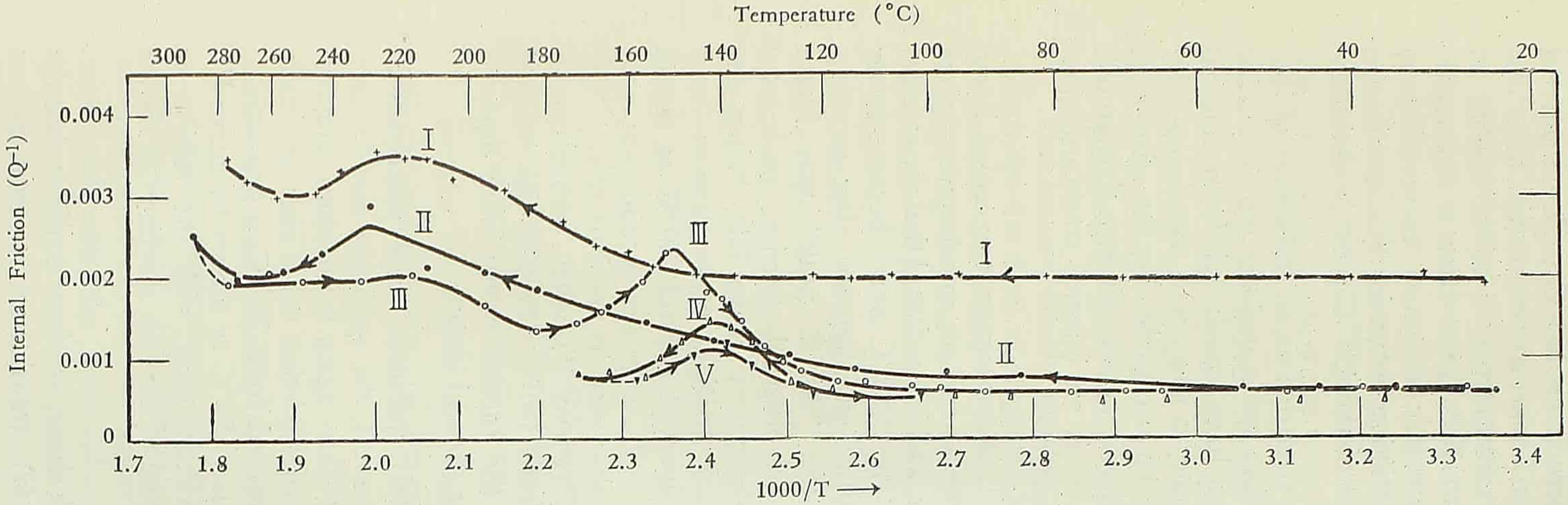

Fig. 7. Internal friction in a welding-rod specimen containing 0.25% C after different heat treatments. Curve I, quenched into 10% brine from 930°C (martensitic structure); curve II, after tempering at 280°C; curve III, measurements with lowering temperature after the completion of curve II; curve IV, measurements taken by raising the temperature after the completion of curve III; curve V, measurements taken by lowering the temperature after the completion of curve IV. Frequency of vibration: Curves I-II-III, 2 cycles per second; curves IV-V, 0.46 cycle per second.

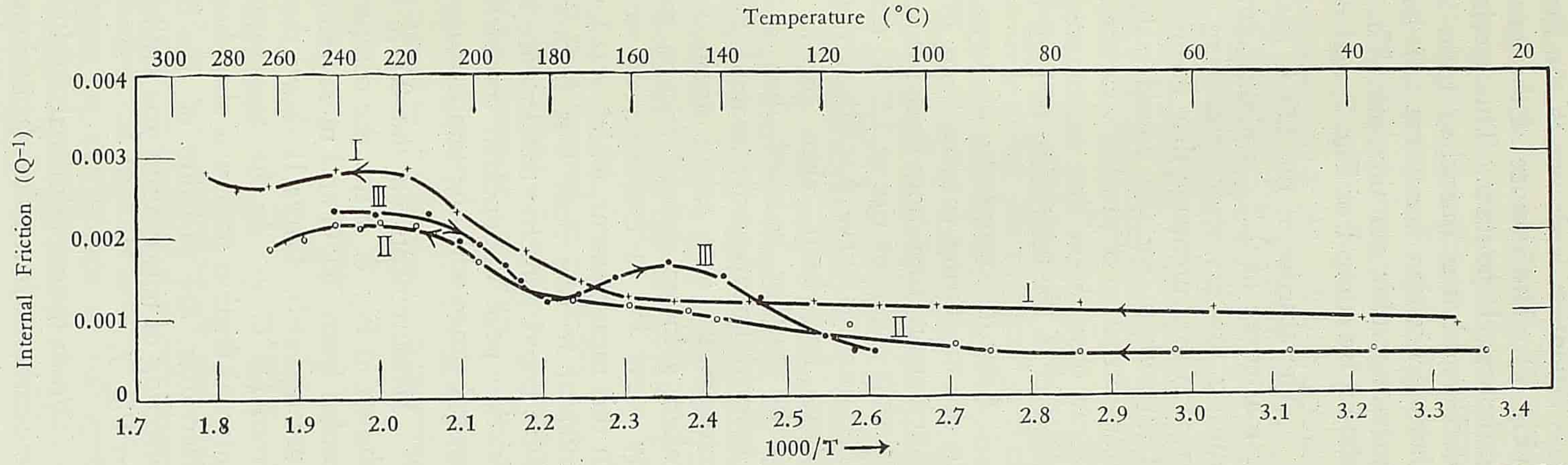

Fig. 8. Internal friction in a carbon steel specimen containing 0.25% C after different heat treatments. Curve I, quenched into 10% brine from 930°C (martensitic structure); curve II, after tempering at 280°C; curve III, measurements with lowering temperature after the completion of curve II.

Attention is drawn to the fact that there is no 130°C peak on curve I (Fig. 7). The absence of this peak was also found to be the case in a low-carbon steel specimen. This specimen was carburized to a carbon content of 0.25% and was quenched from 930°C into 10% brine after a thoroughly homogenization treatment. It has a martensitic structure as revealed by metallographic examinations. The internal friction curve for this specimen is shown by curve I of Fig. 8, and the absence of the 130°C peak is obvious.

The absence of the 130°C peak can be regarded as an indication of that a martensite of 0.25% carbon composition does not transform into ϵ-carbide during the first-stage tempering. Since we have concluded from internal friction measurements that ϵ-carbide is formed in specimens containing 0.29–1.4% carbon, we can consider the absence of ϵ-carbide in the first-stage transformation of the 0.25% carbon specimens as in agreement with Kurjumov's X-ray observation that martensite of 0.25% C is an integral transformation-product in the tempering of high carbon martensite.

After the completion of curve I of Fig. 7, the specimen was cooled down in the measuring furnace from 280°C. Internal friction measurements were taken again from room temperature upwards, and it was found that the internal friction began to rise at 120°C (cure II). The "235°C peak" became lower than that of curve I. When the temperature was lowered after measurements had been taken up to 300°C, the "235°C peak" was found to be further reduced, but a pronounced internal friction peak was observed unexpectedly around 150°C as shown by curve III. When the temperature was raised again and internal friction measurements were taken, a lower internal friction peak was observed around 140°C as shown by curve IV (a frequency of vibration of 0.46 cycle per second was used in this measurement, which was lower than that used in previous runs). The internal friction peak was further lowered (curve V) when measurements were taken with the temperature lowered from 180°C. Finally, this internal friction peak disappeared completely after the measurements were repeated several times with the temperature changing up and down.

Measurements on the 0.25% carbon steel specimen were proceeded as shown in Fig. 8. After the completion of curve I, the specimen was furnace-cooled from 280°C and measurements were taken again from room temperature upwards. Curve II shows that the internal friction value rises gradually from 120°C up. As the temperature was lowered from 260°C, a pronounced internal friction peak was also observed around 150°C as shown by curve III. Hereafter, the variation of this internal friction peak with the raising or lowering of temperature was similar to the case of the first specimen as shown in Fig. 7.

From the experimental results described above, we may consider that the low-carbon martensite (containing 0.25% C) transforms at temperatures

around 300°C into a product which is coherent with its parent phase and thus gives rise to internal friction. This corresponds to the transformation occurred in the third-stage tempering. To obtain a pronounced internal friction peak, specimens should be tempered at a sufficiently high temperature for a sufficient length of time so that an appreciable amount of the transformation product was formed. In completing curve I of Fig. 7 or Fig. 8, the specimen reached a temperature of 280°C only for a brief period and therefore the internal friction showed only a gradual rise from 120°C upwards (curve II). Only when the specimen was tempered again at a higher temperature for a longer period of time that a pronounced internal friction peak was observed around 150°C (curve III). But, on the other hand, the internal friction became lower when the tempering temperature was too high or the tempering time was too long. This is probably because of that the coherency of the transformation product was destroyed by these treatments.

The transformation product of the third-stage tempering of low-carbon martensite has been investigated by electron microscopic observations[7]. With a specimen containing 0.15% C, the formation of carbide was observed after a tempering for one hour at 205–315°C. According to the internal friction experiments described above, we can consider that the transformation product is coherent with its parent phase, but this product is not ϵ-carbide. The 130°C internal friction peak associated with ϵ-carbide disappeared completely after a tempering at 170°C. This indicates that the coherency which gives rise to the internal friction peak was completely destroyed by tempering at 170°C. However, the internal friction peak associated with the transformation product of the low-carbon martensite was observed with temperature lowered from 300°C. This indicates that the coherency was not destroyed by a tempering at 300°C.

One may also conclude that no ferrite was formed when 0.25% carbon martensite was tempered around 300°C, as the carbon-diffusion peak around 40°C was not observed after such a tempering treatment (see Figs. 7, 8).

Further research is in progress on the internal friction peak associated with the transformation of low-carbon martensite in the third-stage tempering.

IV. Discussions

1. *On the mechanism of the internal friction peak.*

Further experiments are necessary for an understanding of the exact mechanism of the 130°C internal friction peak. Following is a preliminary account based on the assumption that the observed internal friction peak is associated with the stress-induced movement of the surface of coherency between the ϵ-carbide and its parent phase. While internal friction measurements are taken from room temperature upwards to about 80°C, the

martensite in the specimen begins to decompose to form low-carbon martensite (containing 0.25% C) and ϵ-carbide. When the temperature continues to rise, more ϵ-carbide is formed in the specimen, so the internal friction increases with the rise of temperature. However, as the temperature becomes too high, the coherency between ϵ-carbide and its parent phase will be easily destroyed. The optimum temperature of the peak is seen to be about 130°C. This may be due to that around this temperature, the ϵ-carbide formed is plentiful and at the same time its coherency with its parent phase has not been destroyed much. In fact, the position of this internal friction peak changes with the speed at which the internal friction measurements were taken.

The stress-induced movement of a surface of coherency is associated with a definite time of relaxation, and should give rise to a stable internal friction peak. The constant changing of the observed 130°C peak is evidently due to the two opposing tendencies described above.

Work is in progress in utilizing the 130°C peak in studying the kinetics of the formation of ϵ-carbide and the destruction of its coherency with its parent phase.

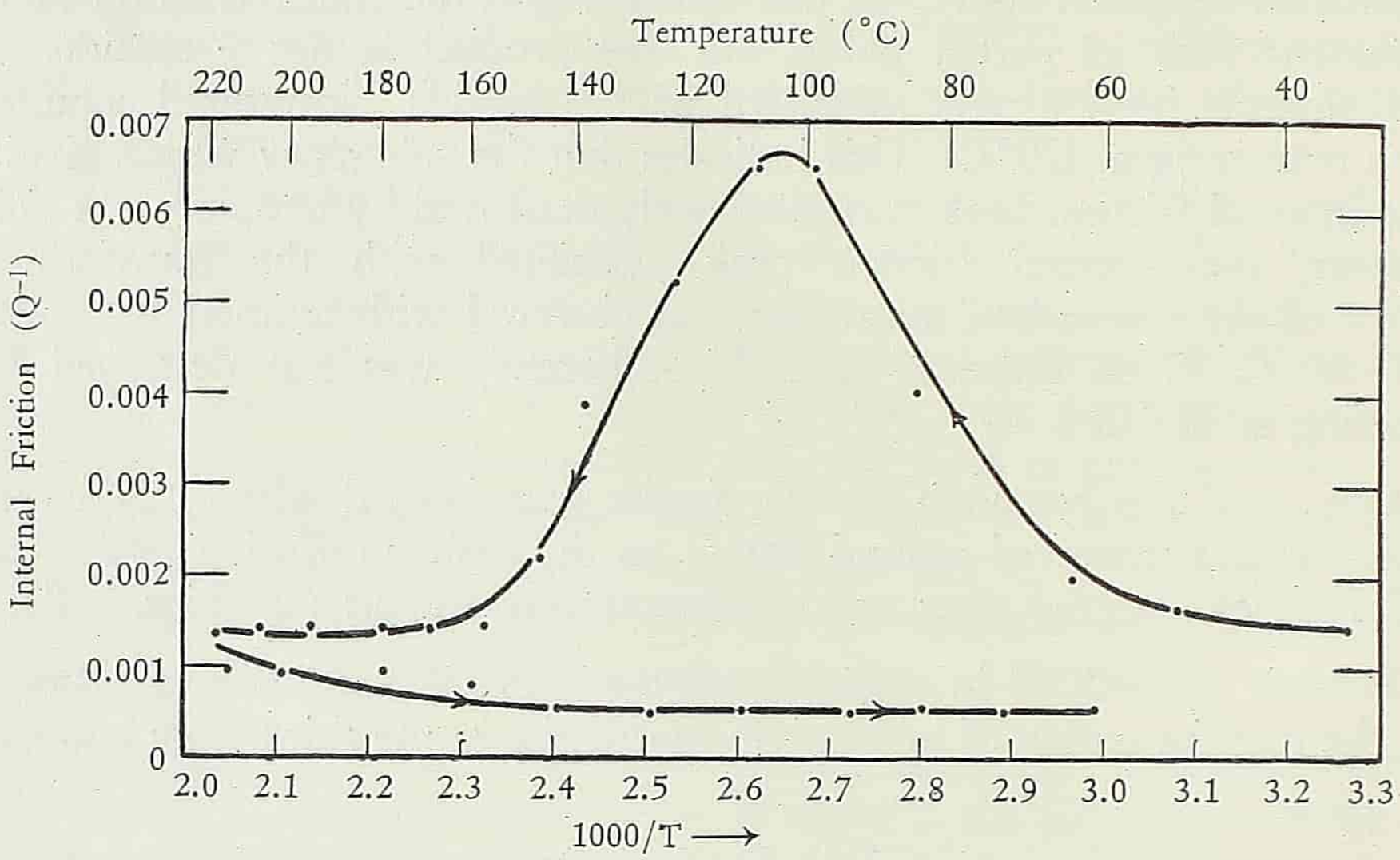

Fig. 9. Internal friction peak in a 0.72% C specimen air-cooled from 910°C and its disappearance with lowering temperature.

2. *Some additional internal friction peaks*

A specimen containing 0.72% C was air-cooled from 910°C. The internal friction measurement on this specimen gave some inexplicable results. A pronounced internal friction peak was observed around 110°C (the frequency of vibration used remained to be 2 cycles per second as before) as shown in Fig. 9. This peak is characterized by the fact that it does not rise again at

high temperatures, that is, the 235°C peak (see Fig. 1) does not exist. If the 235°C peak is associated with a certain state of stress existing in the specimen[6], then it is difficult to see why the existence of martensite in the specimen does not create a state of stress in the specimen.

Another internal friction peak having a peculiar shape as shown in Fig. 10 was observed with a specimen carburized at 910°C for one hour and

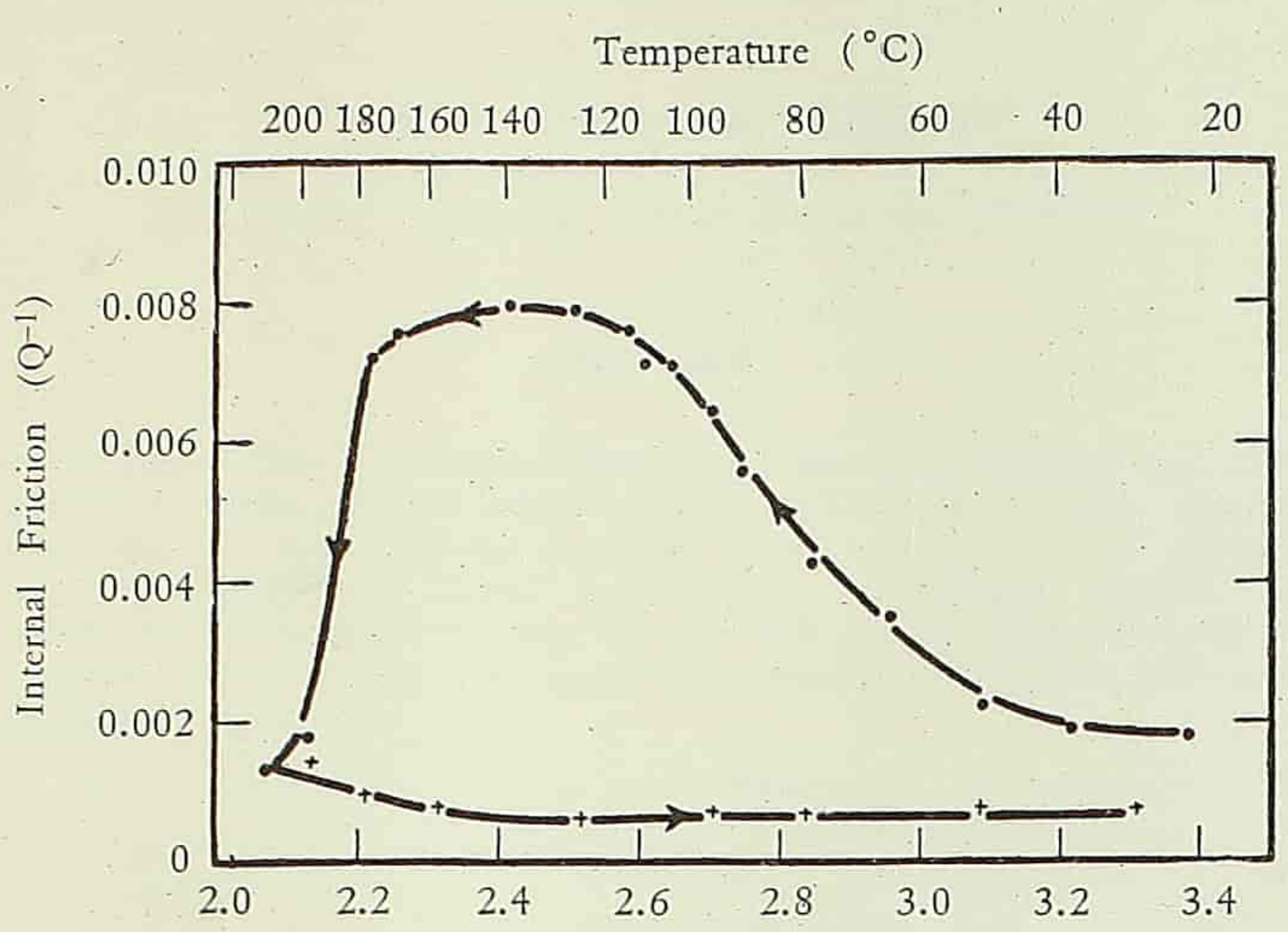

Fig. 10. Internal friction peak in a 0.72–1.0% C specimen air-cooled from 910°C and its disappearance with lowering temperature.

then air-cooled. This internal friction peak also does not rise again at higher temperatures. The carbon content of this specimen is estimated at 0.72–1.0% from the carburizing temperature and time.

References

[1] Курдюмов, Г. В., и Лысак, Л., 1949. *ЖТФ*, **19**, 525.

[2] Roberts, C. S., Averbach, B. L., and Cohen, M., 1953. *Trans. ASM*, **45**, 576.

[3] Jack, K. H., 1951. *J. Iron Steel Inst.*, **169**, 26.

[4] Worrell, F. T., in Zener, C., 1948. Elasticity and Anelasticity of Metals (University of Chicago Press), pp. 159—163.

Siefert, A. V., and Worrell, F. T., 1951. *J. App. Phys.* **22**, 1257.

[5] Kê, T. S., 1947. *Phys. Rev.*, **71**, 533.

[6] Kê, T. S., Yung, P. T., and Wang, Y. N., 1955. *Acta Physica Sinica*, **11**, 91; *Scientia Sinica*, **4**, 263.

[7] Lement, B. S., Averbach, B. L., and Cohen, M., 1954. *Trans. ASM*, **46**, 851.

ON VOLUME VISCO-ELASTIC THEORY OF FLUIDS AND ITS APPLICATON TO SOUND DISPERSION PHENOMENA*

Lu Ho-Fu (Hoff Lu, 盧鶴紱)**

(Department of Physics, Futan University, Shanghai)

Abstract

In this paper is shown that our volume visco-elastic theory of fluids is not merely applicable to the case of structural relaxation (as is liable to be regarded), but equally applicable to all three kinds of relaxations—thermal, structural and chemical. From our equation of irreversibility of volume change is inferred the equation of thermal irreversibility as originally assumed by Herzfeld and Rice for the case of thermal relaxation. Also, in the case of chemical relaxation, our equation of irreversibility of volume change is shown to imply the equation of chemical irreversibility as obtained from kinetic considerations by Liebermann.

Regarding the application of this theory to sound absorption and dispersion phenomena, Bourgin-Kneser equations for the case of thermal relaxation and Liebermann equation for the case of chemical relaxation are shown to follow directly from the results of our theory of compressibilities when appropriate thermodynamic considerations have been made. This derivation reveals that Liebermann equation of sound absorption can be a good approximation only for the case of liquids.

In the case of gases, illustrations are given in which the existing sound absorption and dispersion measurements are already accurate enough as to make it possible to determine from them the static and instantaneous compressibilities β_0 and β_∞ and hence the two ratios of heat capacities γ_0 and γ_∞ as well as the external and internal heat capacities $C^{(e)}$ and $C^{(i)}$, thus subsequently enabling us to draw directly from them certain conclusions regarding the structure of the molecule and the processes of energy exchanges upon collision.

Finally, the appropriateness of our definition of volume viscosity is discussed.

I. On the Volume Visco-Elastic Equation

The volume visco-elastic theory of fluids formulated phenomenologically by the author[1, 2, 3, 4] started out with the assumption that the relative compression $s=-\Delta V/V$ of a fluid element ultimately produced by a suddenly applied constant pressure is composed of two parts, one instantaneous and the other relaxational, viz.,

$$s_0 = s_\infty + s_r\,. \tag{1}$$

The instantaneous part s_∞ is the usual elastic strain and, when present alone,

---

*First published in Chinese in *Acta Physica Sinica*, Vol. XII, No. 1, pp. 5—19, 1956.

**Now at Peking University.

is the result of a reversible process. This part is considered to be instantaneous since the suddenly applied pressure is transmitted almost instantaneously (by the molecular motion and intermolecular interactions) throughout the fluid element. The presence of the relaxational part s_r makes the overall process of compression irreversible; upon sudden release of the applied pressure, the expansion will not retrace the original path of compression in the P—S diagram and, as is shown in a paper[4] of the author (equations (5)—(9)), there will, in general, be a dissipation of mechanical energy turned into heat. Thus, the relaxational part constitutes a dilatational viscous flow. In any dilatational process, the rate of compression at any instant was written as

$$\frac{ds}{dt} = \frac{ds_\infty}{dt} + \left(\frac{ds}{dt}\right)_{\text{vis}}, \tag{2}$$

where $\left(\frac{ds}{dt}\right)_{\text{vis}}$ represents the contribution to $\frac{ds}{dt}$ from relaxational molecular processes. Since, when $\frac{dp}{dt} = 0$, we have $\frac{ds_\infty}{dt} = 0$, and further in addition, when $s = s_0$, we have $\frac{ds}{dt} = \left(\frac{ds}{dt}\right)_{\text{vis}} = 0$, we see that to a first approximation we may, in the case of a single relaxation time, τ_2, expect to have

$$\left(\frac{ds}{dt}\right)_{\text{vis}} = \frac{s_0 - s}{\tau_2}; \tag{3}$$

or, using(2), this may be written as

$$\frac{d(s - s_\infty)}{dt} = -\frac{s - s_0}{\tau_2}. \tag{4}$$

The phenomenological theory formulated by the author leads to just such an equation, viz.,

$$\left(\frac{ds}{dt}\right)_{\text{vis}} = \frac{s_0 - s}{\beta_0 \eta_2}, \tag{5}$$

i.e.,

$$\tau_2 = \beta_0 \eta_2, \tag{6}$$

where β_0 is the static (total) compressibility under given thermodynamical condition and η_2 a coefficient of volume viscosity (see § VI).

Since $\frac{ds_\infty}{dt} = \beta_\infty \frac{dp}{dt}$ where β_∞ is the instantaneous compressibility, equation (2) gives for the volume visco-elastic equation,

$$\frac{ds}{dt} = \beta_\infty \frac{dp}{dt} + \frac{s_0 - s}{\tau_2}, \tag{7}$$

or

$$\frac{ds}{dt} = \beta_\infty \frac{dp}{dt} + \frac{s_0 - s}{\beta_0 \eta_2} . \tag{8}$$

Since $s_0 = \beta_0(p-p_0)$, equation (7) may also be written in the form

$$s + \tau_2 \frac{ds}{dt} = \beta_0(p - p_0) + \beta_\infty \tau_2 \frac{dp}{dt} . \tag{9}$$

Since the values of the compressibilities β_0 and β_∞ depend on the thermodynamical condition under which the compression takes place, we may talk about, for instance, isothermal or adiabatic visco-elastic equations when isothermal or adiabatic compressibilities are used respectively. However, since, strictly speaking, a process can be isothermal only when it is carried out quasistatically or infinitely slowly, the visco-elastic equation becomes trivial (reduces to $s=\beta_0(p-p_0)$) unless τ_2 is much larger than the time required to establish thermal equilibium, as is the case considered in § V).

II. On the Equivalence of Different Molecular Mechanisms of Volume Relaxation

Volume relaxation may arise from different molecular processes, including:

(1) Thermal relaxation (Herzfeld and Rice[5], Bourgin[6], Kneser[7]), arising from the finite rate of conversion of external energy of translation and rotation into internal energy of vibrations of molecules, or, vice versa.

(2) Structural relaxation (Frenkel[8], Hall[9]), arising from the finite rate of molecular rearrangement from a relatively loose structure into a more compact structure, or, vice versa.

(3) Chemical relaxation (Einstein[10], Luck[11], Liebermann[12, 13]), arising from the finite rate of reaction of the chemical components.

When any of these processes exists, the compressibility will depend upon the rate of compression. Our phenomenological theory makes no discrimination of these processes; they all give rise to a relaxational compressibility, $\beta_r=\beta_0-\beta_\infty$.

In the case of thermal relaxation, the relaxational compressibility arises from the relatively slow transfer of thermal energy from external degrees of freedom into internal ones, either from translational into rotational or from translational and rotational into vibrational, as the case may be. In this case, when thermodynamic equilibrium is not attained, it has nevertheless been found fruitful to assume separately states of partial equilibrium of the external

and internal degrees of freedom (hereafter referred to as external state and internal state respectively), and thus talk about external temperature $T^{(e)}$ and internal temperature $T^{(i)}$ and also external heat capacity $C^{(e)}$, internal heat capacity $C^{(i)}$, and total heat capacity $C=C^{(e)}+C^{(i)}$. During compression by the application of a constant pressure, the mechanical energy will first turn into thermal energy associated with the external degrees of freedom, so that obviously we shall have $T^{(e)}>T^{(i)}$, and $T^{(e)}$ tends to decrease while $T^{(i)}$ tends to increase so that $s<s_0$, inasmuch as the volume depends solely on the external degrees of freedom. When thermodynamic equilibrium is attained, $T^{(e)}=T^{(i)}$ and $s=s_0$. When the applied pressure is withdrawn, $s_0=0$, the thermal energy associated with the external degrees of freedom will first turn into mechanical energy so that $T^{(e)}<T^{(i)}$, $T^{(e)}$ tends to increase while $T^{(i)}$ tends to decrease, and therefore $s>s_0$. Hence, to a first approximation, one may expect to have s_0-s proportional to $T^{(e)}-T^{(i)}$. Furthermore, since upon compression $s-s_\infty$ is caused by the transfer of the thermal energy from external into internal degrees of freedom, we may likewise expect to have $d(s-s_\infty)$ proportional to $dT^{(i)}$, i.e., we may have

$$\frac{s_0-s}{\tau_2}\sim\frac{T^{(e)}-T^{(i)}}{\tau_2}\quad\text{and}\quad\frac{d(s-s_\infty)}{dt}\sim\frac{dT^{(i)}}{dt}.$$

Thus, our equation of volume irreversibility (4) is seen to imply in this case

$$\frac{dT^{(i)}}{dt}=-\frac{T^{(i)}-T^{(e)}}{\tau_{th}},\tag{10}$$

with $\tau_{th}=$ constant $\times\tau_2$. Equation (10) is just the equation of thermal irreversibility that was assumed by Herzfeld and Rice. Starting with this equation and noting that pressure is due to translational motion alone so that $T^{(e)}$ and V determine the pressure, $p=p(T^{(e)},V)$, of the non-equilibrium state in exactly the same way as T and V determine the pressure of the state of thermodynamic equilibrium, one can, by means of thermodynamic relations, arrive at an equation for the change of non-equilibrium states that is formally identical with our visco-elastic equation (9). For instance, this derivation has been comprehensively given in the review article by Markham, Beyer and Lindsay[14] (equation (6.14)). Comparing the two equations, the thermal relaxation time is seen to be

$$\tau_{th}=\frac{C_p}{C_p^{(e)}}\tau_2.\tag{11}$$

In molecular theories, τ_{th} is, for a gas almost completely unexcited, the mean lifetime of the excited internal state responsible for the relaxation, being the reciprocal of the probability per molecule per unit time of the transition in question[15].

The fact that equation (10) may be inferred from equation (4) supports the author's viewpoint that our visco-elastic theory of sound absorption phenomena should be applicable to both gases and liquids. This is not merely an assumption as is liable to be understood[14], since one can obtain Kneser-Bourgin equations for sound absorption and dispersion directly from the corresponding equations in terms of compressibilities previously derived by the author[2,3] from our visco-elastic equations. This will be shown in § III.

Next, consider the case of chemical relaxation supposed to exist alone, that is caused by a single chemical reaction. Let ΔN be the increase in number of moles, N, of a certain chemical component in the fluid element due to the chemical reaction in question. Since $V=V(p,T,N)$ for the chemically non-equilibrium states, this increase gives rise to a partial change of volume, which to a first approximation is

$$s-s_\infty=-\frac{1}{V}\left(\frac{\partial V}{\partial N}\right)_p \Delta N\,, \tag{12}$$

where ΔN is considered to be small. When thermodynamic equilibrium is attained, $s=s_0$ with

$$s_0-s_\infty=-\frac{1}{V}\left(\frac{\partial V}{\partial N}\right)_p (\Delta N)_0\,, \tag{13}$$

where $(\Delta N)_0$ is the ultimate increase of N caused by a constant pressure applied under the given thermodynamic condition. Supposing that $\frac{1}{V}\left(\frac{\partial V}{\partial N}\right)_p$ under the given thermodynamic condition (e.g., constant temperature or constant entropy) be insensitive to the existing change of chemical composition, the substitution of (13) and the difference between (13) and (12), viz.,

$$s_0-s=-\frac{1}{V}\left(\frac{\partial V}{\partial N}\right)_p\left[(\Delta N)_0-\Delta N\right], \tag{14}$$

into our equation of irreversibility (4) will yield the following equation of chemical irreversibility:

$$\frac{d(\Delta N)}{dt}=-\frac{\Delta N-(\Delta N)_0}{\tau_2}\,. \tag{15}$$

This equation appears to have been first given by Liebermann[12]. Since τ_2 is then the relaxation time of the chemical reaction in the neighbourhood of equilibrium, $1/\tau_2$ may be defined, as done by Liebermann, as the rate of the equilibrium reaction. As shown by Liebermann from simple kinetic considerations, $1/\tau_2$ differs from the conventional reaction rate constant by a constant of proportionality depending on the equilibrium constant of the reaction and the molar fractions of the reacting components.

The fact that equation (15) may be derived from equation (4) suggests that Liebermann's equation for sound absorption due to chemical relaxation may also be obtained directly from the result of our visco-elastic theory. This will be shown in § V.

Thus, our visco-elastic theory is seen to include all three mechanisms. Thermal relaxation is expected to exist in the case of polyatomic gases and possibly in certain gas-like organic liquids. Structural relaxation can only occur with liquids. Chemical relaxation may exist in gas mixtures and solutions. Of course, either because more than one relaxation times may be present for a single relaxation mechanism or because two or all three kinds of relaxational mechanisms referred to above may exist simultaneously, the multi-relaxational visco-elastic theory given in reference [3] may be needed.

Since all the three relaxations are phenomenologically equivalent, it is necessary to rely on molecular theories for their identification. It seems that there exists but one convincing type of calculations leading to this identification, viz., when the energy levels of the various modes of vibrations of the molecules have been found from spectrum analysis, $C^{(i)}$ may be calculated by statistical mechanics and the identification with the thermal mechanism may be made by calculating sound absorption or dispersion with it by means of Kneser-Bourgin formula. Furthermore, the temperature dependence of absorption coefficient is different for different mechanisms, and although much remains to be studied regarding the details of these relations it seems that their qualitative indications have promised to serve as a possible aid for deciding the correct mechanism (see Markham *et al*[14], pp. 379—398).

III. Derivation of Kneser-Bourgin Equations of Sound Absorption from Volume Visco-Elastic Theory

Confined to the case of a single relaxation time τ_2 for a pure gas or a gas-like liquid, equation (7) or (8) gives for the sound absorption coefficient per wave length due to volume viscosity (see equation (24) of reference [2], being denoted there by γ_2)

$$\mu = 2\pi \frac{\beta_r \omega \tau_2}{\beta_0 + \beta_\infty \omega^2 \tau_2^2} = 2\pi \frac{\beta_r \omega \eta_2}{1 + \beta_0 \beta_\infty \omega^2 \eta_2^2}, \tag{16}$$

whose maximum value occurs at the frequency

$$\omega_m = \frac{v_\infty}{v_0 \tau_2} = \frac{1}{\tau_2} \sqrt{\frac{\beta_0}{\beta_\infty}}. \tag{17}$$

In terms of ω_m (16) takes the form

$$\mu = 2\pi \frac{\beta_0 - \beta_\infty}{\sqrt{\beta_0\,\beta_\infty}} \frac{\omega_m\,\omega}{\omega_m^2 + \omega^2}\,.$$

The velocity dispersion caused by the relaxational compression is (see equation (18) of reference [2]) given by

$$v^2 = \frac{\beta_0 + \beta_\infty\,\omega^2\,\tau_2^2}{\rho(\beta_0^2 + \beta_\infty^2\,\omega^2\,\tau_2^2)} = \frac{1}{\rho\,\beta_0} \frac{1 + \beta_0\,\beta_\infty\,\omega^2\,\eta_2^2}{1 + \beta_\infty^2\,\omega^2\,\eta_2^2}\,, \tag{18}$$

whose inflectional point with respect to log ω occurs at

$$\omega_i = v_\infty^2 / v_0^2\,\tau_2 = \beta_0/\beta_\infty\,\tau_2\,. \tag{19}$$

In these equations, the β's are adiabatic compressibilities. Let β_T be the isothermal compressibility. Then, we have from thermodynamics

$$\beta_0 = \beta_T/\gamma_0 = \beta_T\,C_v/C_p\,, \tag{20}$$

and, since for the present case of thermal relaxation $V = V(T^{(e)}, P)$ we see at once for non-equilibrium states with the internal state remaining unchanged

$$\beta_\infty = \beta_T/\gamma_\infty = \beta_T\,C_v^{(e)}/C_p^{(e)}\,, \tag{21}$$

where obviously $C_v^{(e)} = C_v - C^{(i)}$, $C_p^{(e)} = C_p - C^{(i)}$.

Substituting (20) and (21) into (16), we get

$$\mu = 2\pi \frac{(C_p^{(e)}\,C_v - C_p\,C_v^{(e)})\,\omega\,\tau_2}{C_p^{(e)}\,C_v + C_p\,C_v^{(e)}\,\omega^2\,\tau_2^2}\,. \tag{22}$$

But, since from thermodynamics

$$C_p = C_v + T\,V\,\alpha^2/\beta_T\,, \tag{23}$$

where $\alpha = \frac{1}{V}\left(\frac{\partial V}{\partial T}\right)_p$, and, noting that α and β_T both involve adjustment of translational but not of rotational and vibrational motions, i.e., they depend only on the external state,

$$C_p^{(e)} = C_v^{(e)} + T^{(e)}\,V\,\alpha^2/\beta_T\,, \tag{24}$$

we have, since in (23) $T = T^{(e)}$,

$$\begin{aligned} C_p^{(e)}\,C_v - C_p\,C_v^{(e)} &= (T^{(e)}\,V\,\alpha^2/\beta_T)\,(C_v - C_v^{(e)}) \\ &= (C_p - C_v)\,C^{(i)}\,. \end{aligned} \tag{25}$$

Substituting this into (22), we get for the absorption coefficient per wave length

$$\mu = 2\pi \frac{(C_p - C_v)\, C^{(i)}\, \omega\, \tau_2}{C_p^{(e)}\, C_v + C_p\, C_v^{(e)}\, \omega^2\, \tau_2^2} . \tag{26}$$

Substituting (20) and (21) into (17), we get

$$\omega_m = \frac{1}{\tau_2} \sqrt{\frac{C_p^{(e)}\, C_v}{C_v^{(e)}\, C_p}} . \tag{27}$$

Combining (27) with (26), we get

$$\mu = 2\pi \frac{(C_p - C_v)\, C^{(i)}}{\sqrt{C_v\, C_p\, C_v^{(e)}\, C_p^{(e)}}} \frac{\omega_m\, \omega}{\omega_m^2 + \omega^2} . \tag{28}$$

Disregarding intermolecular forces, we obviously have per mole,

$$C_p - C_v = R, \text{ and } C_p^{(e)} - C_v^{(e)} = R,$$

and (28) becomes simplified to

$$\mu = 2\pi \frac{RC^{(i)}}{\sqrt{C_v(C_v+R)\, C_v^{(i)}\, (C_v^{(i)}+R)}} \frac{\omega_m\, \omega}{\omega_m^2 - \omega^2} . \tag{29}$$

This agrees with the well-known Kneser-Bourgin equation (see equation for $\tan \psi$ in reference [7] and equation (9.4) of reference [6]). Denoting C_v by C, $C_v^{(e)}$ by C_∞, and $C^{(i)}$ by C_i, we may write this equation in the form given by Fricke[16]:

$$\mu = \frac{2\pi R\, C_i}{\sqrt{C(C+R)\, C_\infty(C_\infty+R)}} \frac{\omega_m\, \omega}{\omega_m^2 + \omega^2} , \tag{29a}$$

where $C_i = C - C_\infty$.

Substituting (11) into (27), we get for the thermal relaxation time, i.e., the average lifetime of the energy quanta in the excited internal state of the molecule,

$$\tau_{th} = \frac{1}{\omega_m} \sqrt{\frac{C_v\, C_p}{C_v^{(e)}\, C_p^{(e)}}} , \tag{30}$$

or, when the intermolecular forces are disregarded,

$$\tau_{th} = \frac{1}{\omega_m} \sqrt{\frac{C(C+R)}{C_\infty(C_\infty+R)}} , \tag{31}$$

which is also in agreement with that given by Fricke.

Substituting (20), (21), and (27) into (18), we get

$$v^2 = \frac{1}{\rho \beta_T} \frac{C_p C_p^{(e)} (\omega^2 + \omega_m^2)}{C_v^{(e)} C_p \omega^2 + C_v C_p^{(e)} \omega_m^2}, \tag{32}$$

giving

$$v_0 = \sqrt{\gamma_0 / \rho \beta_T} = 1 / \sqrt{\rho \beta_0} \text{ and } v_\infty = \sqrt{\gamma_\infty / \rho \beta_T} = 1 / \sqrt{\rho \beta_\infty},$$

as they should. Disregarding intermolecular forces, we have $\beta_T = 1/p$, and (32) becomes

$$v^2 = \frac{p}{\rho} \left[1 + R \frac{(C+R)\omega^2 + (C_\infty + R)\omega_m^2}{C_\infty (C+R)\omega^2 + C(C_\infty + R)\omega_m^2} \right], \tag{33}$$

which agrees with the corresponding Kneser-Bourgin equation (see equation (19) in reference [7] and equation (12.1) in reference [6]). Using equation (31), we may express this in a still neater form:

$$v^2 = \frac{p}{\rho} \left(1 + R \frac{C + C_\infty \omega^2 \tau_{th}^2}{C^2 + C_\infty^2 \omega^2 \tau_{th}^2} \right). \tag{34}$$

IV. Molecular Structure and Collision Processes from Gaseous Compressibilities

When either two of the following four quantities:

(1) Sound velocity at very low frequencies: v_0,
(2) Sound velocity at very high frequencies: v_∞,
(3) Maximum absorption: $\mu_m = \mu(\omega_m)$,
(4) Dispersion velocity: $v_i = v(\omega_i)$.

have been determined, β_0 and β_∞, the two limiting compressibilities, can readily be calculated. Furthermore, if, in addition, either ω_m or ω_i is determined, τ_2 and hence η_2 can then be calculated. In case the dispersion region is inaccessible, these quantities will have to be determined by accurate fitting to the observed part of the absorption or dispersion curve.

In the case of pure gases, only thermal relaxation can exist, and the knowledge of these quantities permits calculation of the heat capacities of the gas and also may provide us certain more definite information regarding the structure of the molecule and the characterities of the collision processes. Since it seems that these have not been fully recognized, they will be reviewed from the viewpoint of our theory in order to bring out how our theory may be directly applied to such investigations.

If the equation of state or the second virial coefficient of the gas is known, β_T is known and γ_0 and γ_∞ can be calculated from β_0 and β_∞ by using (20) and (21). We shall then find that in addition to the well-known dependence of γ_0 on molecular structure, the difference between γ_0 and γ_∞ allows more definite conclusions to be made at once as will be illustrated below. Knowing γ_0 and γ_∞, one can calculate the heat capacities C_p, C_v, and $C^{(i)}$ from

$$C_p = \frac{\gamma_0}{\gamma_0 - 1} T V \alpha^2 / \beta_T , \qquad C_v = C_p / \gamma_0 ,$$

$$C^{(i)} = C_v(\gamma_\infty - \gamma_0)/(\gamma_\infty - 1) . \tag{35}$$

From the value of $C^{(i)}$ thus calculated together with available spectroscopic data one can make judgment as to what internal states of excitation effectively participate in the relaxation, e.g., what modes of vibration are sonically activated. $C^{(i)}$ having been obtained, the thermal relaxation time can be computed from (11), viz.,

$$\tau_{th} = \frac{C_p}{C_p - C^{(i)}} \tau_2 . \tag{36}$$

Since, when the energy of excitation E in question is, as actually the case, much larger than kT so that the concentration of excited molecules is much less than that of unexcited ones, τ_{th} is the mean lifetime of the excited state of the molecule responsible for the relaxation process, and the average number of molecular collisions necessary for a molecule to lose its energy of excitation will be $Z \tau_{th}$, where Z is the average number of collisions a molecule encounters per unit time, being equal to the average molecular speed divided by mean free path. From kinetic theory, this may be calculated from the coefficient of shearing viscosity and Sutherland's constant[17]. Thus, the effective probability, $P = 1 / Z \tau_{th}$ of de-excitation per collision may be calculated. Since under normal conditions Z is of the order of 10^{10}, $P \approx \tau_{th}^{-1} \times 10^{-10}$.

These calculations have been made from available sound absorption and dispersion data for various gases and vapours which appear to be sufficiently accurate and the results are given in Tables I and II respectively. In these illustrations we have for the sake of simplicity disregarded the effect of the intermolecular forces by putting $\beta_T = 1/p$ and $C_p - C_v = R$.

In Table I are tabulated the results of calculations from ultrasonic absorption data. The values of ρ and v_0 are taken from the Handbook of Chemistry and Physics, and from the International Critical Tables, corrections having been made for differences in temperature. In the case of hydrogen, data for 25°C and 25.63°C, both under atmospheric pressure, are those of Stewart[19] and Zartmen[20] respectively. They both give $\gamma_0 \approx 7/5$ and $\gamma_\infty \approx 5/3$. These

results are also obtained from the dispersion data as given in Table II. These two values permit us to say that there is relaxation of the two rotational degrees of freedom and that while rotational states are excited there is practically no transition in the vibrational state. This is reasonable since we know that the transition energy between the two lowest rotational states of H_2 corresponds to a temperature as low as 171° K whereas the excitation energy of its vibrational level corresponds to a temperature as high as 6140°K[21]. The absorption data for the triatomic gases are those obtained by Fricks[16] under the atmospheric pressure. CO_2, N_2O, and CS_2 all give $\gamma_\infty \approx 7/5$, indicating that the three translational and apparently only two rotational degrees of freedom respond to changes of pressure immediately while the vibrational degrees of freedom give rise to relaxation. This shows a linear structure for these molecules. In the case of SO_2, $\gamma_\infty \approx 4/3$, indicating that all six degrees of freedom, translational and rotational, respond to the pressure change immediately. This shows that SO_2 is a non-linear molecule. All these conclusions regarding molecular structure are in agreement with those established from the infra-red and Raman spectroscopic and electron diffraction data.

In Table II are tabulated the results of calculations from the ultrasonic dispersion data. In this table only the value of ρ is taken from the Handbook

Table I*

Gas or vapour	H_2		CO_2	N_2O	CS_2	SO_2
Temp. °C	25	25.63	23	23	23	23
Exp'tal μ_m	0.50	0.75	0.230	0.296	0.406	0.149
Calc'd v_∞/v_0	1.08	1.12	1.038	1.048	1.066	1.024
Exp'tal ρ (10^{-3} gm/cm^3)	0.083	0.080	1.81	1.81	(3.13)**	2.68
Exp'tal v_0 (m/sec)	1310	1336	269.7	270.9	202.8	217.6
Calc'd β_0 (10^{-7} cm^2/dyne)	6.9	7.0	7.59	7.53	7.77	7.88
Calc'd β_∞ (10^{-7} cm^2/dyne)	5.9	5.6	7.05	6.86	6.84	7.51
Calc'd γ_0	1.4	1.4	1.30	1.32	1.28	1.26
Cald'd γ_∞	1.7	1.8	1.40	1.44	1.44	1.32
Exp'tal $\omega_m/2\pi$(kc/sec)	10×10^3	10×10^3	20	153	379	1040
Calc'd τ_2 (10^{-6} sec)	0.017	0.017	8.26	1.09	0.450	0.157
Calc'd C_p (cal/mole)	7.0	7.0	8.62	8.21	9.10	9.26
Calc'd C_i (cal/mole)	2.1	2.5	1.7	1.7	2.7	1.4
Calc'd τ_{th} (10^{-6} sec)	0.02	0.03	9.9	1.4	0.63	0.2

*Formulas used in calculations:

$$\frac{v_\infty}{u_0} = \frac{\mu_m}{2\pi} + \sqrt{1+\left(\frac{\mu_m}{2\pi}\right)^2}, \qquad \beta_0 = 1/\rho v_0^2, \qquad \beta\infty = \beta_0 \Big/ \left(\frac{v\infty}{v_0}\right)^2,$$

$$\gamma_0 = 1/\beta_0 p, \qquad \gamma\infty = 1/\beta p, \qquad \tau_2 = \frac{1}{\omega_m}\sqrt{\frac{\gamma_\infty}{\gamma_0}},$$

$$C_p = \frac{\gamma_0 R}{\gamma_0 - 1}, \qquad C_i = \frac{(\gamma_\infty - \gamma_0) R}{(\gamma_\infty - 1)(\gamma_0 - 1)}, \qquad \tau_{th} = \frac{C_p}{C_p - C_i}\tau_2 .$$

**Calculated from the molecular weight.

Table II*

Gas or vapour		H_2	SF_6	CS_2	C_6H_6
Temp. °C		36.5	36.10	45	90
Exp'tal	ρ (10^{-3} gm/cm^3)	0.080	5.74	(2.91)	2.75
	v_0 (m/sce)	1336	138.5	202.0	200.0
	v_∞ (m/sec)	1460	153.4	$\geqslant$216.0	$\geqslant$208.0
Calc'd	β_0 (10^{-7} cm^2/dyne)	7.00	9.08	8.43	9.09
	β_∞ (10^{-7} cm^2/dyne)	5.87	7.41	$\leqslant$7.36	$\leqslant$8.40
	γ_0	1.41	1.09	1.17	1.09
	γ_∞	1.68	1.34	$\geqslant$1.35	$\geqslant$1.18
Exp'tal	$\omega_i/2\pi$ (10^6c/sec)	~8	0.89	~0.45	~0.45
Calc'd	τ_2 (10^{-7} sec)	~0.15	4.4	~8.2	~3.8
	C_p (cal/mole)	6.85	24.1	13.7	24.1
	C_i (cal/mole)	2.7	16	6.0	11
	τ_{th} (10^{-7} sec)	~0.25	10	~15	~7

of Chemistry and Physics (the one in parathesis is calculated from the molecular weight). The dispersion data for hydrogen are those of Zartman[20], yielding results in agreement with those of Table I. The data for SF_6 are those of O'Connor[22]; they yield $\gamma_\infty=4/3$ indicating also that all six degrees of freedom, translational and rotational, respond to pressure change immediately. The data for CS_2 and C_6H_6 are those of Railston[23]. The value of γ_∞ for C_6H_6 indicates that only a portion of the vibrational degrees of freedom is responsible for the observed relaxation, the remaining portion being also able to respond to pressure change immediately[1]. The latter type of result has never been reported and consequently it is desirable to check Railston's data by further experiments.

V. Derivation of Liebermann's Equation of Sound Absorption in Solutions from Volume Visco-Elastic Theory

In the case of chemical relaxation, on account of the slow rate of chemical reaction, the time required to establish chemical equilibrium may be and often is larger than that required to establish thermal equilibrium. Hence, as mentioned in § I, in such a case we have to distinguish the instantaneous and static isothermal compressibilities, β_T^∞ and β_T^0. Here, β_T^∞ refers to compression at a rate that is very fast relative to the slow chemical change although

*Formulas used same as in Table I except $\beta_\infty=1/\rho v_\infty^2$ and $\tau_2=\gamma_\infty/\gamma_0\omega_i$.

1) In the case of C_6H_6 we have also used van der Waals and Berthelot equations of state to calculate β_T. The results make γ larger than that given in Table II by about 2 and 3 per cent respectively. Thus, consideration of deviation of the vapour from being ideal does not make this result disappear.

still sufficiently slow relative to thermal adjustment. Thus, the adiabatic compressibilities become now

$$\beta_0 = \beta_T^0/\gamma_0 \quad \text{and} \quad \beta_\infty = \beta_T^\infty/\gamma_\infty \,. \tag{37}$$

Let C' be the partial heat capacity resulting from the chemical reaction. Denote $C_p^0 - C_v^0$ by Δ, which will be a small quantity in the case of liquids. Then, we have

$$\left.\begin{aligned} C_p^\infty &= C_p - C' \,, \\ C_v^\infty &= C_p - \Delta - C' \,, \end{aligned}\right\} \tag{38}$$

where we have neglected the small difference between C_p' and C_v', this being obviously justified in the case of liquids. Substituting these in (37), we have

$$\beta_0 = \beta_T^0 \,(C_p - \Delta)\,/\,C_p \,, \tag{39}$$

$$\beta_\infty = \beta_T^\infty \,(C_p - \Delta - C')\,/\,(C_p - C') \,. \tag{40}$$

Substituting (39) and (40) into that part of equation (23) of reference [2] which expresses that part of amplitude coefficient of absorption due to volume viscosity alone, viz.,

$$\begin{aligned} \alpha &= \frac{\omega^2 \tau_2}{2\rho v^3} \; \frac{\beta_0 - \beta_\infty}{\beta_0^2 + \beta_\infty^2 \, \omega^2 \tau_2^2} \\ &= \frac{\omega^2 \tau_2}{2v} \; \frac{\beta_0 - \beta_\infty}{\beta_0 + \beta_\infty \, \omega^2 \tau_2^2} \,, \end{aligned} \tag{41}$$

we get

$$\alpha = \frac{\omega^2 \tau_2}{2v} \; \frac{\beta_T^0 (C_p - \Delta)\,(C_p - C') - \beta_T^\infty \, C_p (C_p - \Delta - C')}{\beta_T^0 (C_p - \Delta)\,(C_p - C') + \beta_T^\infty \, C_p (C_p - \Delta - C') \, \omega^2 \tau_2^2} \tag{42}$$

for the amplitude absorption coefficient due to volume viscosity arising from chemical reaction. The numberator of the last fraction may be written

$$(\beta_T^0 - \beta_T^\infty) \, C_p \Big[C_p - (\Delta + C') \Big] + \beta_T^0 \, C' \, \Delta \,.$$

Since in the case of a liquid, it is expected that

$$C_p \gg \Delta + C' \,,$$

this is approximately

$$(\beta_T^0 - \beta_T^\infty) \, C_p^2 + \beta_T^0 \, C' \, \Delta \,.$$

The denominator is a sum of two terms and here we may disregard the small difference between β_T^0 and β_T^∞, noting that the isothermal partial compressibility $\beta_T^0 - \beta_T^\infty$ is due to volume change in chemical reaction alone. This approximation reduces equation (42) to

$$\alpha = \frac{1}{2v}\left(\frac{C'\Delta}{C_p^2} + \frac{\beta_T^0 - \beta_T^\infty}{\beta_T^0}\right)\frac{\omega^2\tau_2}{1+\omega^2\tau_2^2}, \tag{43}$$

which is just Liebermann's equation, equation (14) of reference [12]. From this derivation it becomes apparent that Lieberman's equation can be a good approximation only for the case of liquids.

In any case in which chemical reaction takes place so fast that τ_2 is smaller than the time taken to establish thermal equilibrium, i.e., when τ_2 due to chemical change is less than τ_{th}, we have to put $\beta_T^0 = \beta_T^\infty$ and only the heat capacity term remains. In this case, equation (43) reduces to[1)]

$$\alpha = \frac{C'\Delta}{2v\,C_p^2}\,\frac{\omega^2\tau_2}{1+\omega^2\tau_2^2}. \tag{44}$$

VI. Note on the Definition of the Coefficient of Volume Viscosity

Our definition for the coefficient of volume viscosity implies that the relaxational processes make the mean pressure $\bar{p}$ increase above the effective pressure $p' = p_0 + s/\beta_0$ by an amount that is assumed to be proportional to the rate of relaxational compression $\left(\frac{ds}{dt}\right)_{\text{vis}}$, viz.,

$$\begin{aligned}\bar{p} - p' &= \eta_2\left(\frac{ds}{dt}\right)_{\text{vis}} \\ &= \eta_2\left(\frac{ds}{dt} - \frac{ds_\infty}{dt}\right).\end{aligned} \tag{45}$$

It is this added stress that gives rise to the extra dissipation of energy as discussed in reference [4]. When there is no relaxational compression, the dilatational process will, as stated in § I, reduce to a reversible one, the volume

---

1) This is similar in form to the corresponding Bourgin-Kneser equation for the case of thermal relaxation, viz.,

$$\alpha = \frac{C^{(i)}(C_p - C_v)}{2v\,C_p^{(e)}\,C_v}\,\frac{\omega^2\tau_2}{1+\frac{C_v^{(e)}\,C_p}{C_p^{(e)}\,C_v}\omega^2\tau_2^2},$$

which is obtained by substituting (26) into $\alpha = \mu/2\lambda = \mu\omega/4\pi v$.

viscous flow being then absent. Therefore, the absence of relaxation should mean the absence of volume viscosity, or, in other words, η_2 should concern itself only with the viscous part of $\frac{ds}{dt}$ and not with $\frac{ds_\infty}{dt}$. With our definition of η_2 the visco-elastic equation (8) or (9) may be written in the form

$$p - p_0 = k_0 s + \eta_2 \left(\frac{ds}{dt}\right)_{\text{vis}}, \tag{46}$$

or

$$p - p_0 + \beta_\infty \eta_2 \frac{dp}{dt} = k_0 s + \eta_2 \frac{ds}{dt}, \tag{47}$$

which, when relaxation is absent, i.e., when $\tau_2 = 0$ and hence $\eta_2 = 0$, reduces to the correct limiting form

$$p - p_0 = ks, \tag{48}$$

where now $k = k_0 = k_\infty$ and $s = s_0 = s_\infty$.

Recently, Litovitz, Lyon and Peselnick[24] have criticized our definition of volume viscosity. For sinusoidal change alone, they have, instead, introduced a frequency dependent volume viscosity

$$\eta_v(\omega) = \frac{(k_\infty - k_0)\,\tau_v}{1+\omega^2 \tau_v^2}, \tag{49}$$

where

$$\tau_v = \beta_\infty \eta_2 = \tau_2 \beta_\infty / \beta_0 \tag{50}$$

is the relaxation time[1)] for pressure change at constant volume $\left(\frac{ds}{dt} = 0\right)$ as readily shown from (47). In our choice of expression, this may be written as

$$\eta_v(\omega) = \frac{(\beta_0 - \beta_\infty)\,\tau_2}{\beta_0^2 + \beta_\infty^2 \omega^2 \tau_2^2} = \frac{(\beta_0 - \beta_\infty)\,\eta_2}{\beta_0(1 + \beta_\infty^2 \eta_2^2 \omega^2)}. \tag{51}$$

In terms of this η_v the visco-elastic equation (7) or (9) yields the following stress-strain relation for harmonic changes

$$p - p_0 = \left(k_0 + \frac{\beta_\infty}{\beta_0} \omega^2 \tau_2 \eta_v\right) s + \eta_v \frac{ds}{dt}. \tag{52}$$

Since, when relaxational process is absent, $k_0 = k_\infty = k$, $\tau_2 = 0$, and (49) makes η_v vanish, we see that equation (52) also yields the correct limiting form

---

1) By setting τ_v equal to τ_1 the relaxation time for the change of shearing stress, our equations for sound absorption phenomena reduce to those used by Litovitz, Lyon and Peselnick. In fact, these equations were derived by them in identically the same manner as already done previously by the author.

$$p - p_0 = ks$$

for this case. However, as $\omega \to 0$ equation (52), in general, tends to

$$p - p_0 = k_0 s + \eta_v \frac{ds}{dt}$$

$$= k_0 s + \eta_v \left(\frac{ds}{dt}\right)_{\text{vis}} + \eta_v \frac{ds_\infty}{dt}, \tag{53}$$

where now

$$\eta_v = (k_\infty - k_0)\tau_v = \frac{\beta_0 - \beta_\infty}{\beta_0}\eta_2$$

is the coefficient of volume viscosity originally defined by Frenkel. It is seen that this definition makes volume viscosity also express the elastic part of the variation. This seems to be quite undesirable.

References

[1] Lu, Hoff, 1950. *Chinese Jour. Phys.*, **7**, 365

[2] Lu, Hoff, 1951. *Jour. Acous. Soc. Amer.*, **23**, 12.

[3] Lu, Hoff, 1951. *Chinese Jour. Phys.*, **8**, 5.

[4] Lu, Hoff, 1951. *Chinese Jour. Phys.*, **8**, 145.

[5] Herzfeld, K. F., & Rice, F. O., 1929. *Phys. Rev.*, **31**, 691.

[6] Bourgin, D. G., 1936. *Phys. Rev.*, **50**, 355.

[7] Kneser, H. O., 1931. *Ann. d. Physik*, **11**, 761.

[8] Frenkel, J., 1946. Kinetic Theory of Liquids, Oxford, 208.

[9] Hall, L., 1948. *Phys. Rev.*, **73**, 775.

[10] Einstein, A., 1920. Sitz. Berl. Akad., 380.

[11] Luck, D. G. C., 1932. *Phys. Rev.*, **40**, 440.

[12] Liebermann, L., 1949. *Phys. Rev.*, **76**, 1520.

[13] Liebermann, L., 1948. *Jour. Acoust. Soc. Amer.*, **20**, 868.

[14] Markham, Beyer Lindsay, 1951. *Rev. Mod. Phys.*, **23**, 353.

[15] See, e.g., Richards, W. T., 1939. *Rev. Mod. Phys.*, **11**, 40.

[16] Fricke, E. F., 1940. *Jour. Acoust. Soc. Amer.*, **12**, 245.

[17] Fowler, R. H., 1936. Statistical Mechanics, 2nd ed., Oxford, Ch. III.

[18] Knudsen, V. O., and Fricke, E., 1940. *Jour. Acoust. Amer.*, **12**, 255.

[19] Stewart, E. S., 1946. *Phys. Rev.*, **69**, 632.

[20] Zartman, I. F., 1949. *Jour. Acoust. Soc. Amer.*, **21**, 171.

[21] Slater, J. C., 1939. Introduction to Chemical Physics, McGraw-Hill, Ch. IX.

[22] O'Connor, C. L., 1954. *Jour. Acoust. Soc. Amer.*, **26**, 361.

[23] Railston, W., 1939. *Jour. Acoust. Soc. Amer.*, **11**, 107.

[24] Litovitz, Lyon, and Peselnick, 1954. *Jour. Acoust. Soc. Amer.*, **26**, 566.

STUDIES ON FUSED RING SYSTEMS II*

A. RESOLUTION OF γ-(6-METHOXY-2-CARBOXY-1,2,3,4-TETRAHYDRO-1-NAPHTHYL)-BUTYRIC ACID.

B. PREPARATION OF METHYL *d*– AND *l*-1-HYDROXY-2-METHYL-2-CARBOMETHOXY-7-METHOXY-1,2,3,4,9,10,11,12-OCTAHYDROPHENANTHRENE-1-ACETATE.

CHANG CHIN (張 錦)

(*Peking Petroleum Institute*)

Bachmann, Kushner and Stevenson[1] prepared γ-(6-methoxy-2-carboxy-3,4-dihydro-1-naphthyl)-butyric acid (VII) by the following series of reactions. With this dibasic acid as intermediate, Bachmann and coworkers prepared a mixture of the diastereoisomers of natural estrone. From this mixture, they obtained a crystalline compound which was named estrone A.

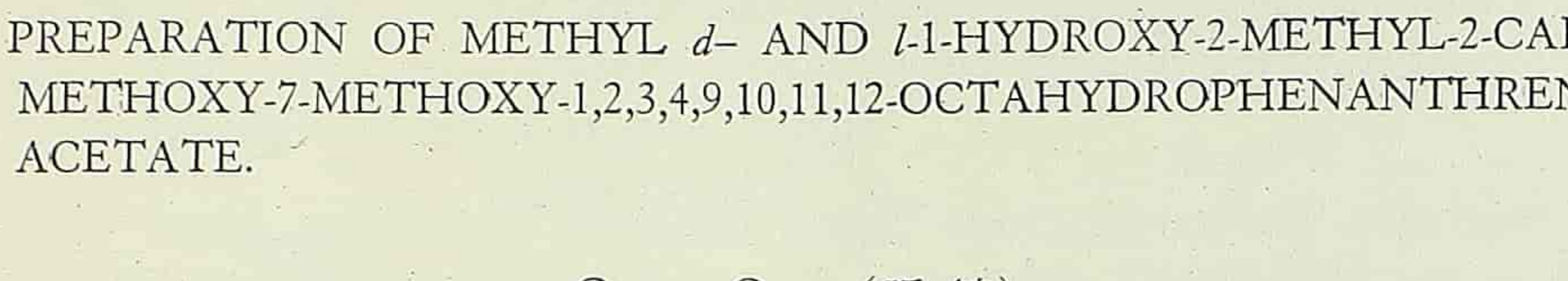

*First published in Chinese in *Acta Chimica Sinica,* Vol. XXI, No. 3, pp. 303—314, 1955.

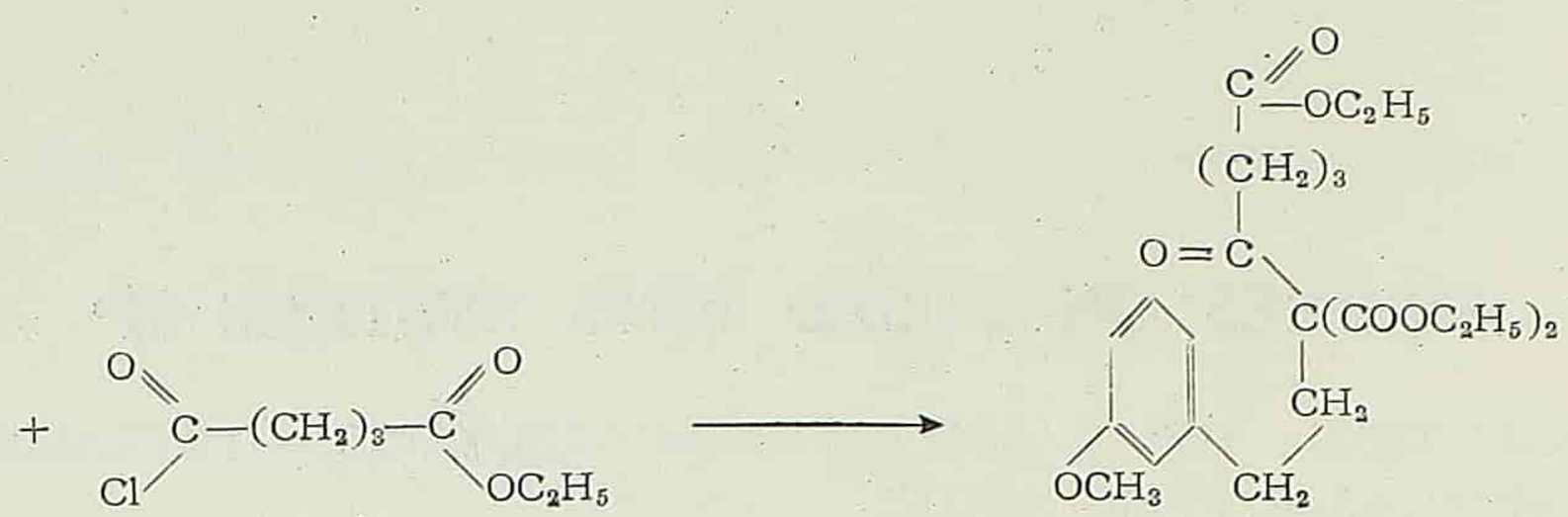

V

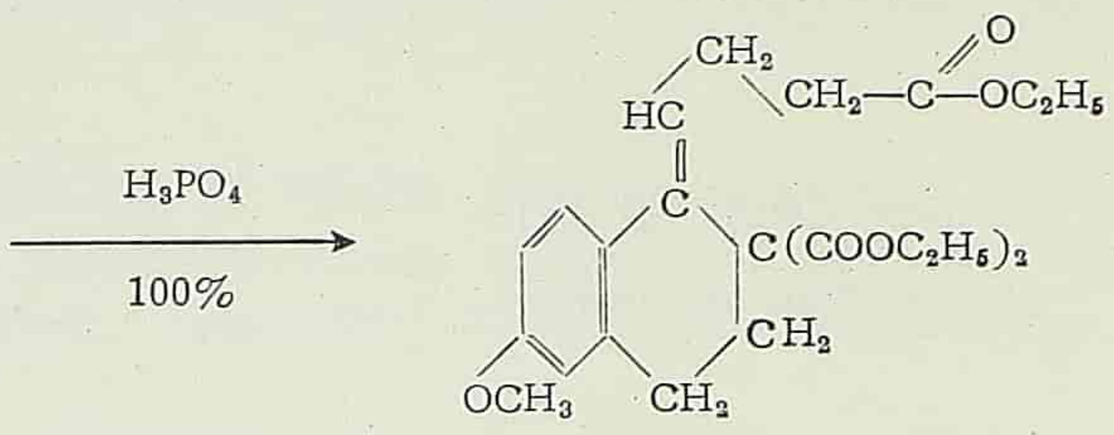

VI

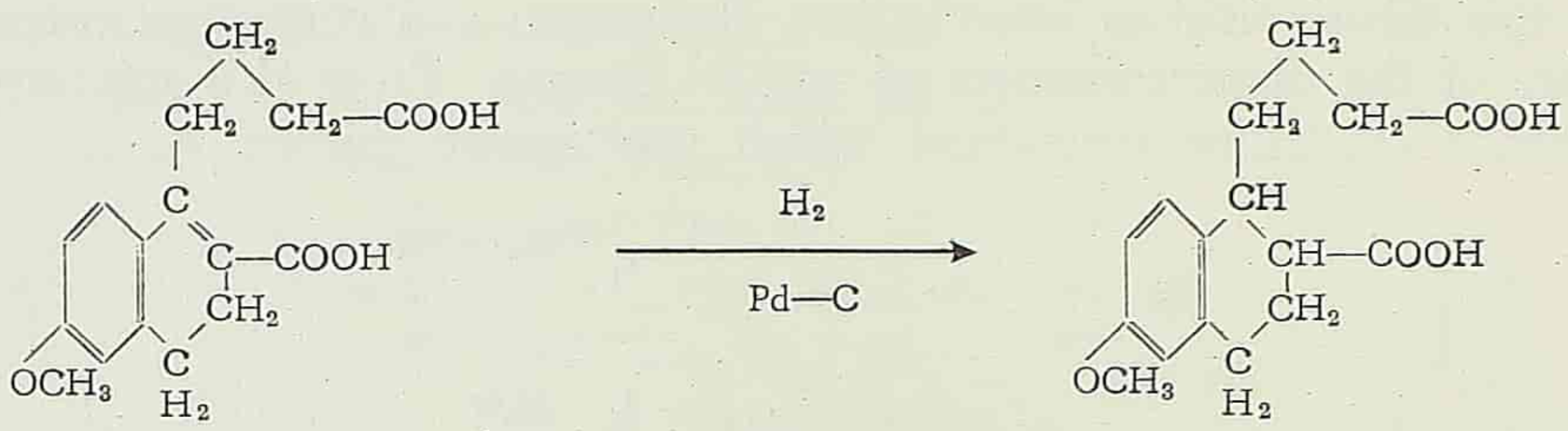

VII VIII

In continuing the work on the synthesis of estrone, the same series of reactions was employed in the preparation of the unsaturated dibasic acid (VII), except that in some steps the experimental conditions used were somewhat modified. From steps (V) to (VI), Bachmann and coworkers used 100% orthophosphoric acid as cyclization agent which was only suitable for small batches of 2.5 g of the keto malonic ester in each run. In our experiment, two other cyclization agents were used: (1) anhydrous hydrofluoric acid, and (2) concentrated sulfuric acid. Under different conditions, both of these cyclizing agents could smoothly convert the keto malonic ester (V) into the unsaturated triester (VI). By using these two cyclizing agents, not only larger runs could be made but also the yields were much higher than that obtained by Bachmann and coworkers[1].

With acetic acid purified over chromium trioxide as solvent, the unsaturated dibasic acid (VII) was hydrogenated in the presence of 5% palladium-

carbon to γ-(6-methoxy-2-carboxy-1,2,3,4-tetrahydro-1-naphthyl)-butyric acid (VIII) according to the method of Bachmann and coworkers[1]. In the course of the reduction, two diastereoisomers should be produced, but only one principal product was obtained. This crystalline acid was readily resolved with brucine in anhydrous methyl alcohol into *l*– and *d*-acid brucine salts. The former, being the less soluble, readily crystallized out, while the latter, being very soluble in methyl alcohol, was obtained as a yellow gum after the complete removal of the solvent. These two salts were separately hydrolyzed, thus *l*-γ-(6-methoxy-2-carboxy-1,2,3,4-tetrahydro-1-naphthyl)-butyric acid and *d*-γ-(6-methoxy-2-carboxy-1,2,3,4-tetrahydro-1-naphthyl)-butyric acid were obtained in pure forms.

The *l*-acid and *d*-acid obtained above were respectively esterified with diazomethane. The respective dimethyl ester, after Dieckmann reaction and methylation, produced the corresponding mixtures of the diastereoisomeric keto esters (XI) and (XV):

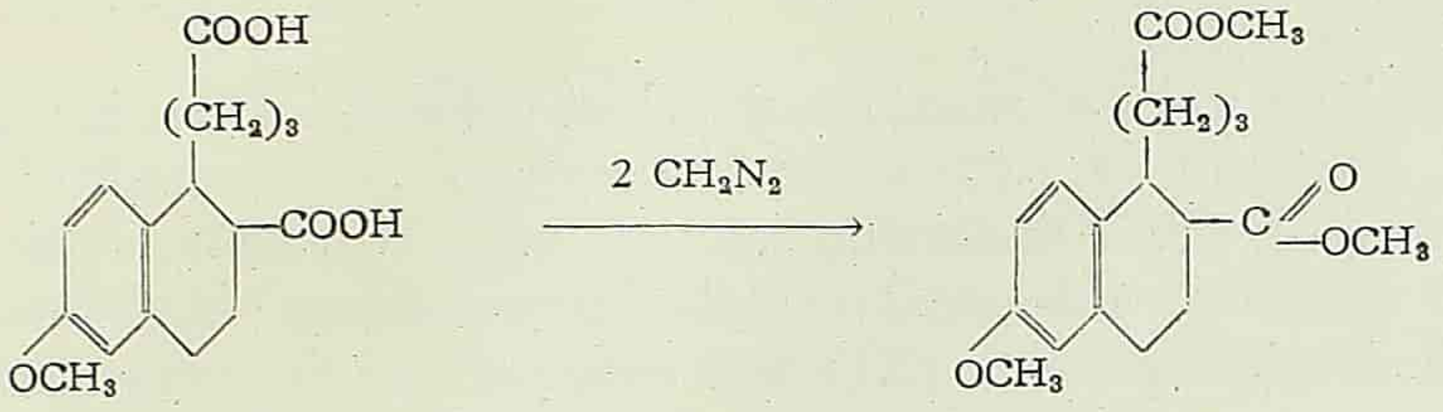

l–Acid IX

X

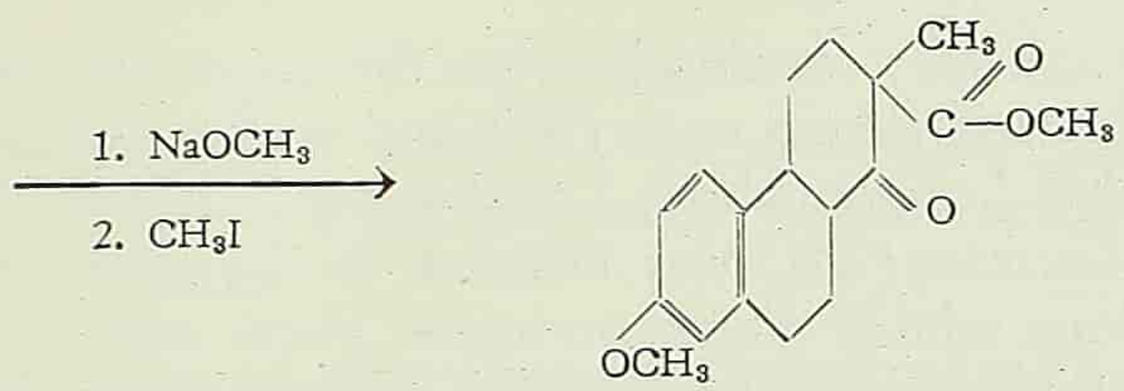

d–Keto ester XI

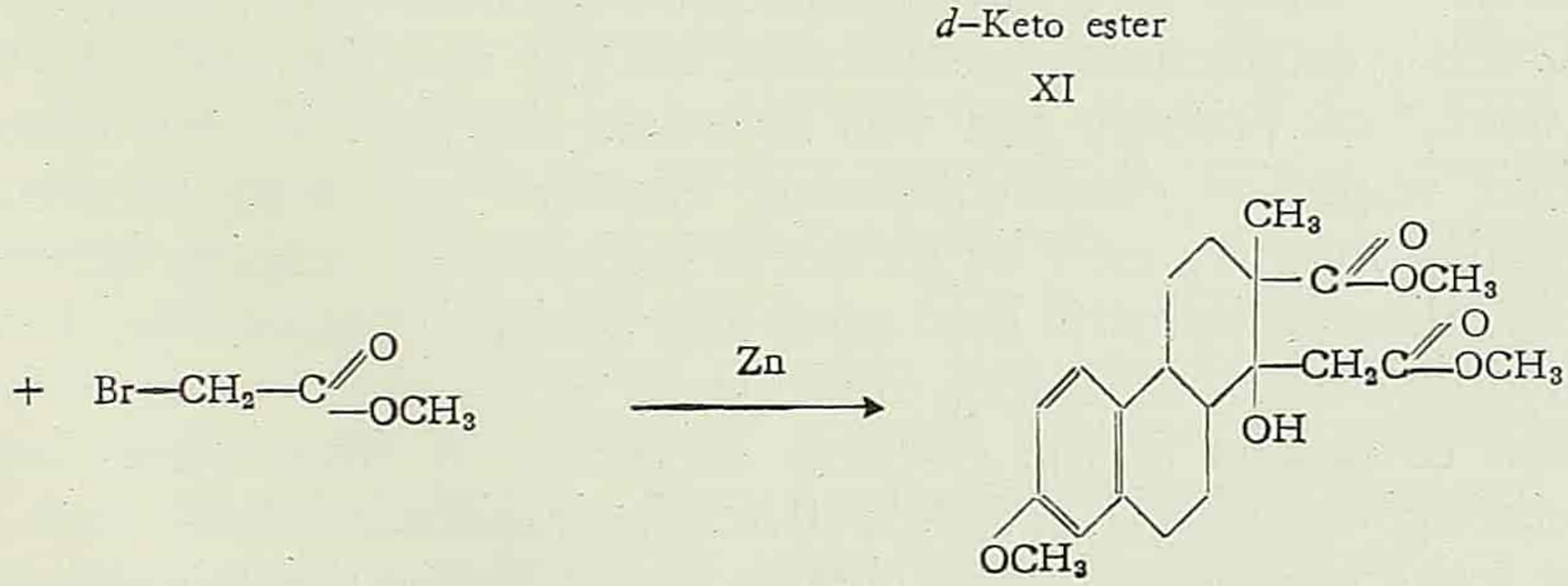

d–Hydroxy ester XII

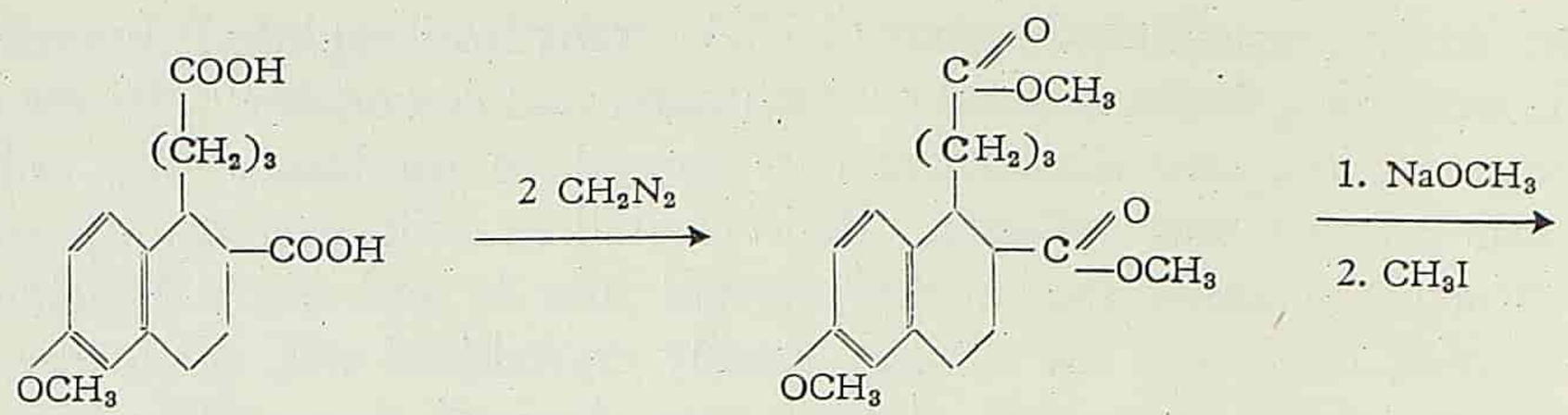

d–Acid

XIII

XIV

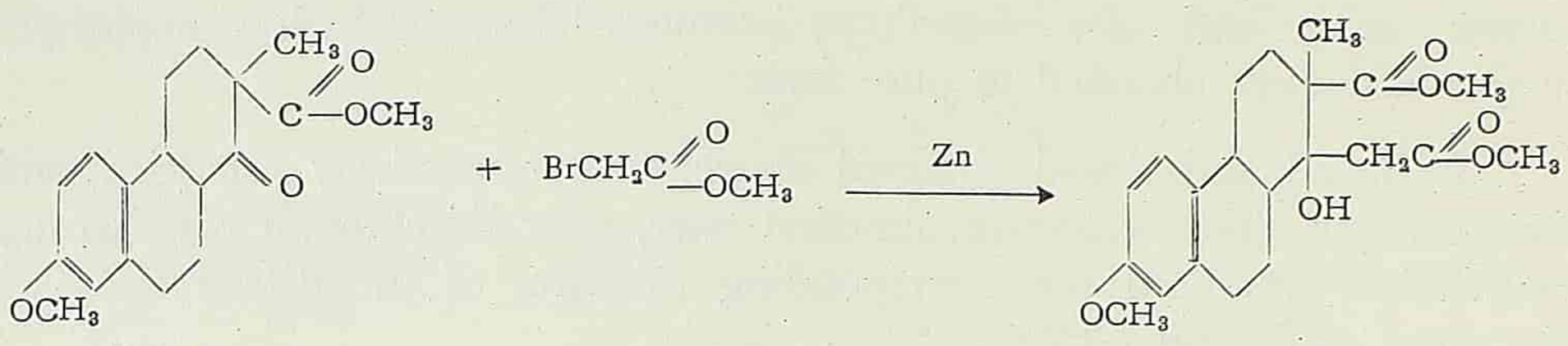

l–Keto ester

XV

l–Hydroxy ester

XVI

In the above series of reactions, the chief point of interest is that from the dimethyl ester of *l*-γ-(6-methoxy-2-carboxy-1,2,3,4-tetrahydro-1-naphthyl)-butyric acid (X), after Dieckmann reaction and methylation, a mixture of the diastereoisomers of *d*-1-keto-2-methyl-2-carbomethoxy-7-methoxy-1,2,3,4,9,10,-11,12-octahydrophenanthrene (XI) was obtained. In the same way, from the dimethyl ester of *d*-γ-(6-methoxy-2-carboxy-1,2,3,4-tetrahydro-1-naphthyl)-butyric acid (XIV), after Dieckmann reaction and methylation, a mixture of the diastereoisomeric *l*-keto esters (XV) was obtained (compare with (2)).

By use of Reformatsky reaction between the acetone-petroleum ether least soluble diastereoisomeric *d*-keto ester (XI) and methyl bromoacetate, methyl *d*-1-hydroxy-2-methyl-2-carbomethoxy-7-methoxy-1, 2, 3, 4, 9, 10, 11, 12-octahydrophenanthrene-1-acetate (XII) was obtained. In the same way, from acetone-petroleum ether least soluble diastereoisomeric *l*-keto ester (XV) and methyl bromoacetate, methyl *l*-1-hydroxy-2-methyl-2-carbomethoxy-7-methoxy-1,2,3,4,-9,10,11,12-octahydrophenanthrene-1-acetate (XVI) was obtained. At the start of our work, our primary aim was to isolate the pure *d*– and *l*-keto esters from their respective diastereoisomeric mixtures and then to prepare the corresponding hydroxy ester by means of Reformatsky reaction between each of the pure diastereoisomeric keto esters and methyl bromoacetate. From each of the hydroxy esters, according to the series of reactions employed by Bachmann and coworkers in the synthesis of estrone A from 1-keto-2-methyl-2-carbomethoxy-7-methoxy-1, 2, 3, 4, 9, 10-hexahydrophenanthrene, each of the optically active estrones could be obtained. But before the completion of our work, Miescher and coworkers[3] published their work on the synthesis of *dl*-estrone from one of the racemic 1-keto-2-methyl-2-carbomethoxy-7-methoxy-

1,2,3,4,9,10,11,12-octahydrophenanthrenes which they called keto ester A, employing the same series of reactions. From this racemic estrone, after resolution through *l*-menthoxy-acetate, natural estrone was obtained. Consequently our work stopped at this point, and we began to look for other routes for the synthesis of estrone.

Experimental*

m-Iodoanisole (I).—This compound was prepared according to the method of Votocek and Matejka[4]. A mixture of 123 g of *m*-anisidine, 500 g of ice and 240 ml of 1:1 sulfuric acid was cooled to –5°. A solution of 70 g of sodium nitrite in 200 ml of water was added slowly with stirring. After all the sodium nitrite solution had been added, the reaction mixture was poured into a solution of 200 g of potassium iodide in 400 ml of water and 100 ml of concentrated sulfuric acid with stirring. After the reaction mixture was left standing at room temperature overnight, it was steam distilled. The product was extracted with benzene and the benzene extract was first washed with sodium bisulfite solution and then with water. After being dried with anhydrous magnesium sulfate, the solvent was removed and the residue distilled; b. p. 130° (20 mm); yield, 193 g.

β-*m*-Anisylethyl Alcohol (II).—This compound was prepared according to the method of Bachmann and Thomas[5], except that a solution of ethylene oxide in anhydrous ether was used instead of gaseous form. Light yellow oil was obtained as the product, b. p. 118–123° (2 mm).

β-*m*-Anisylethyl Bromide (III).—Using the method of Bachmann and Thomas[5], this compound was obtained as light yellow oil; b. p. 158–160° (8 mm).

β-*m*-Anisylethylmalonic Ester (IV).—According to the method of Bachmann and coworkers[1], this compound was obtained as light yellow oil; b. p. 188–192° (0.4 mm).

Ethyl 5-Keto-6,6-dicarbethoxy-8-*m*-anisyloctanoate (V).—This compound was prepared according to the method of Bachmann and coworkers[1] with a few slight modifications. To a suspension of 9.2 g of powdered sodium in 300 ml of thiophene-free benzene, a solution of 118 g of the substituted malonic ester (IV) in 100 ml of pure benzene was added. The mixture was refluxed till all the sodium had reacted. The mixture was cooled with ice water and 90 g of ethyl glutaryl chloride was added slowly with stirring. After the mixture was left standing at room temperature overnight, it was poured into 400 ml of water. Then the two layers were separated and the aqueous layer was extracted once with benzene. The combined benzene

*The experimental work was carried out at the University of Michigan.

solution was washed twice with 5% sodium bicarbonate and twice with water and then it was dried over anhydrous magnesium sulfate. After the removal of the solvent at reduced pressure, the low boiling fraction was quickly distilled off at 0.2 mm in an oil bath of 150°. The yellow oily residue was directly used for the following experiment without further purification. The crude product amounted to 160 g.

γ-(6-Methoxy-2-carboxy-3, 4-dihydro-1-naphthyl)-butyric Acid (VII).— This compound was prepared according to the method of Bachmann and coworkers[1] with two major modifications: (1) The keto malonic ester (V) used by Bachmann and coworkers had been purified by flash distillation, but we have found that by cyclizing the crude substituted keto malonic ester as obtained in the above experiment better results could always be obtained. (2) We used two different cyclizing agents, both of which are suitable for making larger runs. Our methods of cyclizing the keto malonic ester (V) are as follows:

(1) With anhydrous hydrofluoric acid as cyclizing agent—One hundred grams of the crude keto malonic ester (V) was placed in a 1000-ml platinum beaker which was cooled to a temperature of –10 to –15° with ice-salt mixture. To this well-cooled keto malonic ester, about 500 ml of liquid anhydrous hydrofluoric acid was added. After the reaction mixture was kept at about (–10°) for 8 hours, the temperature was gradually raised to room temperature. The hydrofluoric acid was blown off with air. To the residue, about 400 g of cracked ice was added. After the mixture was neutralized with solid sodium carbonate, it was extracted three times with ether, 300 ml being used each time. The ether was distilled off and a solution of the residue in 400 ml of 95% ethyl alcohol and 200 ml of 45% potassium hydroxide was refluxed for 4 hours. After the major portion of the ethyl alcohol had been removed, the turbid solution was extracted once with ether to remove the small amount of oily substance. Then the clear yellow aqueous solution was slowly poured into 300 ml of concentrated hydrochloric acid and the tribasic acid was liberated as an oil. This oil was extracted three times with ether, 300 ml being used each time. After the ether was distilled off, 500 ml of water was added to the dark oily residue. Vigorous evolution of carbon dioxide took place while the mixture was heated on a steam bath during the first few hours. After the mixture had been heated on the steam bath for twelve hours, it was cooled, and the oily tribasic acid changed to semi-solid dibasic acid upon losing carbon dioxide. This was filtered and the semi-solid, after trituration with 50 ml of ether, 34 g of colourless solid was obtained; m.p. 182–188° (with decomposition). The yield was 47% based on β-*m*-anisylethylmalonate while the yield was only 27% using the method of Bachmann and coworkers)[1]. The crude acid, after recrystallization from benzene-dioxane, formed colourless needles; m.p. 188–190° (with decomposition) alone or when mixed with a sample prepared by Bachmann and coworkers.

(2) With concentrated sulfuric acid as cyclization agent—To 800 ml of concentrated sulfuric acid which was cooled with ice-salt mixture to −8°, 100 g of the crude keto malonic ester (V) was slowly added with vigorous stirring. After the addition, the temperature of the mixture was gradually raised to 0° and maintained at this temperature for about 10 hours. Then the mixture was poured into about 1 kg of ice with stirring and yellow oil was liberated which was extracted three times with ether. After the ether was distilled off, the dark oily residue was worked up according to the method described for the hydrofluoric acid cyclization in the above experiment. The yield of the dibasic acid (VII) amounted to 32 g; m.p. 179–185° (with decomposition). After recrystallization from benzene-dioxane, the acid melted at 188–190° alone or when mixed with a sample prepared by Bachmann and coworkers.

γ-(6-methoxy-2-carboxy-1,2,3,4-tetrahydro-1-naphthyl)-butyric Acid (VIII)—This acid was prepared according to the method of Bachmann and coworkers[1]. A solution of 8.7 g of the unsaturated dibasic acid (VII) (m.p. 188–190°) in 150 ml of purified acetic acid was hydrogenated in the presence of 1 g of 5% palladium-carbon at normal temperature and pressure. After three hours, the amount of hydrogen absorbed was almost complete (actual uptake 730 ml; theoretical uptake 731 ml). After the catalyst was filtered off and the solvent removed at reduced pressure, a colourless solid was recrystallized from benzene-methyl alcohol, m.p. 156–158° alone or when mixed with a sample prepared by Bachmann and coworkers[1]; yield 7.8 g (90% of the theoretical).

Resolution of γ-(6-Methoxy-2-carboxy-1, 2, 3, 4-tetrahydro-1-naphthyl)-butyric Acid.—To a solution of 79 g of brucine in 1,200 ml of anhydrous methyl alcohol heated on a steam bath, 29.2 g of γ-(6-methoxy-2-carboxy-1,2,3,4-tetrahydro-1-naphthyl)-butyric acid (m.p. 156–158°) was added slowly. After all of the acid had been added, heating was continued for about half an hour. The mixture was filtered and the clear filtrate was put in the ice box overnight. Plenty of needle-like crystals separated out. This was filtered and amounted to 49 g (first fraction of the di-brucine salt). After this fraction was recrystallized from anhydrous methyl alcohol for three times, its melting point and rotation became constant; m.p. 161–167° (began to shrink at 145°). Rotation. A solution of 0.1 g of the dibrucine salt in 10 ml of absolute ethyl alcohol gave $\alpha -0.74$, $[\alpha]_D^{25} -74.0°$

Analysis. Calcd. for $C_{62}H_{72}N_4O_{13}$:	C, 68.87;	H, 6.70;	N, 5.17.
Found:	C, 69.10;	H, 6.89;	N, 5.02.

The filtrate from the first fraction of the di-brucine salt was concentrated to about 500 ml. After being cooled with ice, needle-like crystals separated out from the solution. This was filtered, dried and amounted to 8 g (second fraction).

The filtrate from the second fraction was concentrated to 150 ml. Upon cooling with ice, nothing separated out from the solution. Then the solvent was blown off with air and yellow resinous material was obtained which amounted to 50 g (third fraction). The difference in solubility between this fraction of the di-brucine salt and that of the first fraction is so great that these two fractions can be readily separated from each other. This fraction of the salt was used for the following experiment without further purification.

Liberation of the *l*-acid (IX) and *d*-acid (XIII) from the respective salts. —A solution of 38 g of the purified first fraction of the di-brucine salt in 300 ml of chloroform was extracted with 2 *N* potassium hydroxide for 4 times, 50 ml being used each time. The potassium hydroxide extracts were combined and filtered from any insoluble material. The clear aqueous solution was poured into 100 ml of concentrated hydrochloric acid and a colourless solid separated out which was filtered and washed with water for three times. After being dried, the crude acid amounted to 10 g; m.p. 168–170°. After recrystallization from benzene-ethyl alcohol, it melted at 171–172°.

Rotation. A solution of 70 mg of the *l*-acid in 10 ml of absolute ethyl alcohol gave $\alpha -0.86$, $[\alpha]_D^{25} -123°$.

Analysis. Calcd. for $C_{16}H_{20}O_5$: C, 65.74; H, 6.87.
Found: C, 65.65; H, 7.0.

A solution of 49 g of the unpurified third fraction of the di-brucine salt in 300 ml of chloroform was extracted four times with 2 *N* potassium hydroxide, 50 ml being used each time. The potassium hydroxide extracts were combined and filtered. After the clear filtrate was poured into 100 ml of concentrated hydrochloric acid cooled with ice, a slightly yellowish solid separated out. This was filtered and washed three times with water. After being dried, it amounted to 12.4 g; m.p. 168–170°. After recrystallization from benzene-ethyl alcohol, the acid formed colourless needles; m.p. 171–172°.

Rotation. A solution of 0.12 g of the *d*-acid in 10 ml of absolute alcohol gave $\alpha +1.45$, $[\alpha]_D^{25} +121°$.

Analysis. Calcd. for $C_{16}H_{20}O_5$: C, 65.74; H, 6.87.
Found: C, 65.67; H, 6.83.

Dimethyl ester of *l*-γ-(6-methoxy-2-carboxy-1,2,3,4-tetrahydro-1-naphthyl)-butyric Acid (X).—To a suspension of 6.0 g of the *l*-acid (m.p. 168–170°) in a 20 ml of anhydrous ether, an ethereal solution of diazomethane prepared from 20 g of *N*-nitroso-β-methylaminoisobutyl methyl ketone[6] was added. After the mixture was left standing at room temperature for one hour, the ether was blown off with air and colourless oil was obtained. This was directly used for the following experiment.

d-1-Keto-2-methyl-2-carbomethoxy-7-methoxy-1, 2, 3, 4, 9, 10, 11, 12-octahydrophenanthrenes (XI).—To a solution of the dimethyl ester of the *l*-acid in 60 ml of thiophene-free benzene, powdered sodium methylate prepared from 0.94 g of metallic sodium was added. The mixture was refluxed in an atmosphere of nitrogen. Within the first hour, plenty of the precipitated sodium salt of the keto ester separated out. After 4 hours, the mixture was cooled with ice and 10 ml of methyl iodide followed by 20 ml of absolute methyl alcohol was added. After the reaction mixture was left standing at room temperature for 10 hours, the precipitated sodium salt completely dissolved and a clear solution was obtained which was warmed on a water bath for half an hour. Upon cooling, the mixture was poured into 40 ml of water and acidified with acetic acid. The benzene layer was separated and the aqueous layer was extracted once with benzene. The combined benzene solution was washed twice with water and dried with anhydrous magnesium sulfate. After the solvent was removed at reduced pressure, a yellow oil was obtained and amounted to 5.8 g which is probably a mixture of the diastereoisomeric *d*-keto esters.

By dissolving the yellow oil in a mixture of acetone-petroleum ether and placed in the ice box overnight, colourless crystals separated out. After being filtered and dried, it amounted to 1.4 g (first fraction); m.p. 110–113° (began to soften at the sides at 106°). After three recrystallizations from acetone-petroleum ether, it melted at 114–116°; yield, 0.67 g.

Rotation. A solution of 0.0655 g of the *d*-keto ester in 10 ml of absolute ethyl alcohol gave $\alpha+0.583$, $[\alpha]_D^{25}+89°$.

Analysis. Calcd. for $C_{18}H_{22}O_4$: C, 71.50; H, 7.33.
Found: C, 71.62; H, 7.43.

When the filtrate from the first fraction was concentrated to about half of its volume and left standing in the ice box, colourless crystals separated out, which, after being filtered and dried, amounted to 2.7 g; m.p. 75–89° (second fraction). The filtrate from the second fraction is the third fraction. At present, no work had been carried out on the separation of the diastereoisomers from the second and third fractions as yet. This kind of work will be carried out in the future.

Methyl *d*-1-Hydroxy-2-methyl-2-carbomethoxy-7-methoxy-1,2,3,4-9,10,11,12-octahydrophenanthrene-1-acetate (XII).—To a solution of 0.4 g of *d*-keto ester (XI) (m.p. 114–116°) in 10 ml of pure benzene and 10 ml of absolute ether, 5 g of granulated zinc (20 mesh) was added. The mixture was heated to reflux and 0.4 ml of methyl bromoacetate and 1 crystal of iodine were added with vigourous stirring. Within the first hour, colourless precipitate separated out from the reaction mixture. At every half-hour interval, 0.1 ml of methyl bromoacetate, 1 crystal of iodine and 2 g of granulated zinc were added in

turn. Altogether four additions were made and the reaction time was two hours and a half. Upon cooling, the reaction mixture was poured into 10 ml of ice water and a few drops of acetic acid were added to dissolve the addition product produced in the reaction and mixed with the zinc. The zinc was washed twice with a small amount of benzene. The ether-benzene layer was separated from the aqueous layer and washed once with *N* ammonium hydroxide and twice with water. After being dried with anhydrous magnesium sulfate, the solvent was distilled off at reduced pressure and light yellow oil was obtained; yield, 0.42 g. This oily product, upon recrystallization from methyl alcohol, formed colourless needles; m.p. 86–88° (began to soften at the sides at 83°).

Rotation. A solution of 0.022 g of the hydroxy ester in 10 ml of anhydrous ethyl alcohol gave $\alpha+0.25$, $[\alpha]_D^{25}+113.6°$.

Analysis. Calcd. for $C_{21}H_{28}O_6$: C, 67.00; H, 7.50.
Found: C, 67.14; H, 7.55.

Dimethyl Ester of *d*-γ-(6-Methoxy-2-carboxy-1,2,3,4-tetrahydro-1-naphthyl)-butyric Acid (XIV).—To a suspension of 6 g of *d*-acid (XIII) (m.p. 168–170°) in 20 ml of anhydrous ether, an ethereal solution of diazomethane prepared from 20 g of *N*-nitroso-β-methylaminoisobutyl methyl ketone[6] was added. After the mixture was left standing at room temperature for an hour, the ether was blown off with air and colourless oil was obtained as residue which was used directly for the following experiment.

l-1-Keto-2-methyl-2-carbomethoxy-7-methoxy-1, 2, 3, 4, 9, 10, 11, 12-octahydrophenanthrenes (XV).—The dimethyl ester of the *d*-acid obtained from the previous experiment was cyclized by Dieckmann reaction followed by methylation according to the method described for the preparation of the *d*-keto ester (XI). The product from this reaction amounted to 5.7 g of yellow oil which is probably a mixture of the diastereoisomers of the *l*-keto ester.

By dissolving the yellow oil in a mixture of acetone and petroleum ether and leaving the solution in the ice box overnight, colourless crystals separated out. The crystals were filtered off and dried and amounted to 1.7 g; m.p. 108–112° (began to soften at the sides at 100°; first fraction). After four recrystallizations from acetone-petroleum ether, this fraction of the keto ester melted at 114–116°; yield, 0.74 g.

Rotation. A solution of 0.047 g of the *l*-keto ester in 10 ml of absolute ethyl alcohol gave $\alpha-0.425$, $[\alpha]_D^{25}-90.4°$.

Analysis. Calcd. for $C_{18}H_{22}O_4$: C, 71.50; H, 7.33.
Found: C, 71.56; H, 7.27.

After the filtrate from the first fraction was concentrated to about half

its volume and left standing in the ice box, colourless crystals separated out. This was filtered and amounted to 2.6 g; m.p. 72–85° (second fraction). The filtrate from the second fraction is the third fraction. At present, no further work has been done on the separation of the diastereoisomers from these two fractions as yet, and this work will be continued in the future.

Methyl *l*-1-Hydroxy-2-methyl-2-carbomethoxy-7-methoxy-1,2,3,4,9,10,11,12-octahydrophenanthrene-1-acetate (XVI).—Reformatsky reaction between 0.4 g of the *l*-keto ester (m.p. 114–116°) and methyl bromoacetate was carried out according to the procedure described for the preparation of the *d*-enantiomorph (XII). The yellow oily product (0.4 g), after repeated recrystallizations from methyl alcohol, formed colourless needles; m.p. 86–88° (began to soften at 82°).

Rotation. A solution of 0.018 g of the hydroxy ester in 10 ml of absolute ethyl alcohol gave α—0.203, $[\alpha]_D^{25}$—113°.

Analysis. Calcd. for $C_{21}H_{28}O_6$: C, 67.00; H, 7.50.
Found: C, 67.20; H, 7.65.

Summary

1. By use of acetic acid purified over chromium trioxide as solvent, 5% Pd-C as catalyst, γ-(6-methoxy-2-carboxy-3,4-dihydro-1-naphthyl)-butyric acid was smoothly reduced to γ-(6-methoxy-2-carboxy-1,2,3,4-tetrahydro-1-naphthyl)-butyric acid. From this reaction, only one diastereoisomer was obtained as the principal product. This diastereoisomer could readily be resolved in absolute methyl alcohol by means of brucine into two fractions of diastereoisomeric salts with wide difference in solubility. The less soluble fraction, being the salt of *l*-γ-(6-methoxy-2-carboxy-1,2,3,4-tetrahydro-1-naphthyl)-butyric acid and brucine, separated out as a crystalline compound. From this fraction of salt, *l*-γ-(6-methoxy-2-carboxy-1, 2, 3, 4-tetrahydro-1-naphthyl)-butyric acid was obtained in pure form, while the more soluble fraction, being the salt of *d*-γ-(6-methoxy-2-carboxy-1, 2, 3, 4-tetrahydro-1-naphthyl)-butyric acid and brucine, was obtained as a resinous product after the complete removal of the solvent. From this fraction of salt, *d*-γ-(6-methoxy-2-carboxy-1,2,3,4-tetrahydro-1-naphthyl)-butyric acid was obtained in pure form.

2. From the dimethyl ester of *l*-γ-(6-methoxy-2-carboxy-1, 2, 3, 4-tetrahydro-1-naphthyl)-butyric acid, by means of Dieckmann reaction followed by methylation, a mixture of diastereoisomeric *d*-1-keto-2-methyl-2-carbomethoxy-7-methoxy-1,2,3,4,9,10,11,12-octahydrophenanthrenes was obtained. From the dimethyl ester of *d*-γ-(6-methoxy-2-carboxy-1,2,3,4-tetrahydro-1-naphthyl)-butyric acid, by means of Dieckmann reaction followed by methylation, a mixture of the diastereoisomeric *l*-1-keto-2-methyl-2-carbomethoxy-7-methoxy-

1,2,3,4,9,10,11,12-octahydrophenanthrenes was obtained. From each of these two mixtures of the diastereoisomeric keto esters, by use of acetone-petroleum ether mixed solvents, only the least soluble diastereoisomer was obtained pure.

3. By means of Reformatsky reaction between methyl bromoacetate and *d*-1-keto-2-methyl - 2 - carbomethoxy - 7 - methoxy-1, 2, 3, 4, 9, 10, 11, 12-octahydrophenanthrene, methyl *d*-1-hydroxy-2-methyl-2-carbomethoxy-7-methoxy-1,2,3,4,9,10,11,12-octahydrophenanthrene-1-acetate was obtained. In the same way, from the pure diastereoisomeric *l*-1-keto-2-methyl-2-carbomethoxy-7-methoxy-1,2,3,4,9,10,11,12-octahydrophenanthrene, methyl *l*-1-hydroxy-2-methyl-2-carbomethoxy-7-methoxy-1, 2, 3, 4, 9, 10, 11, 12-octahydrophenanthrene-1-acetate was obtained.

References

[1] Bachmann, W. E., Kushner, S., and Stevenson, A. C., 1942. *J. Am. Chem. Soc.* **64**, 974.

[2] Bachmann, W. E., Cole, W., and Wilds, A. L., 1940. *J. Am. Chem. Soc.* **62**, 824.

[3] Anner, G., and Miescher, K., 1948. *Helv.* **31**, 2173.

[4] Votocek, E., and Matejka, J., 1915. *Ber.* **46**, 1756.

[5] Bachmann, W. E., and Thomas, G. D., 1942. *J. Am. Chem. Soc.* **64**, 95.

[6] Organic Syntheses 1951. **25**, 28 (2nd ed.).

STUDIES ON THE ACTIVITY COEFFICIENTS OF NONELECTROLYTES IN AQUEOUS SALT SOLUTIONS*

I. THE EFFECT OF COBALT-AMMINES ON THE SOLUBILITIES OF *n*-VALERIC ACID IN WATER**

TZU-CHING HUANG (黃子卿) and WEN-CHEH YANG (楊文治)

(Department of Chemistry, Peking University)

INTRODUCTION

If salt is added to a saturated aqueous solution of nonelectrolyte, its solubility will change. Such phenonmenon is called salting-out or salting-in depending upon the increase or decrease of solubility of the nonelectrolyte. Although salting-out is most common, salting-in is occasionally found. Either of these effects is called salt effect in this paper.

In 1889, Setschenow[1] showed that the salt effect can be generalized by the following empirical equation,

$$\log \frac{S_0}{S} = kC_s, \tag{1}$$

where S_0 is the solubility of nonelectrolyte in pure water, S is that in aqueous salt solution and C_s is the concentration of salt. k is called the "salting-out constant". For $k>0$, $S<S_0$, i.e., salting-out; for $k<0$, $S>S_0$, i.e., salting-in. Eq. (1) holds from dilute to concentrated solution of salt, (several mols per litre). According to thermodynamics, $S_0 / S=f$, where f is the activity coefficient of nonelectrolyte. Thus Eq. (1) can be written as

$$\log f = kC_s. \tag{2}$$

If a weak base or a weak acid is used in substitution for the nonelectrolyte, Eq. (2) is still approximately correct.

---

*First published in Chinese in *Acta Chimica Sinica*, Vol. XXII, No. 1, pp. 67—77, 1956.

**Part of a thesis submitted by W. C. Yang to the Faculty of Graduate School of Chemistry, Peking University, September 1954.

Theoretical

Debye and McAulay[2] proposed an electrostatic theory to explain the salt effect. When a nonelectrolyte is added to water, its dielectric constant is changed. Their calculation shows that if the nonelectrolyte lowers the dielectric constant of water, the addition of salt will increase the activity coefficient of the nonelectrolyte and therefore decrease its solubility, since $S=S_0/f$. Conversely, if the nonelectrolyte raises the dielectric constant of water, the addition of salt will lower the value of f and salting-in results. The equation of Debye and McAulay is

$$lnf = \alpha v\, n' \frac{\sum v_i z_i^2}{v} \frac{\epsilon^2}{2D_0 b k T}, \tag{3}$$

where α and b are defined by the following equations,

$$D = D_0 (1 - \alpha n) .$$

$$\frac{1}{b} = \sum_i \frac{1}{b_i} .$$

In the above equations, n' is the number of molecules of salt per cc of solution, $v = \sum_i v_i$ is the number of ions each molecule of salt gives upon dissociation, n is the number of molecules of nonelectrolyte per cc of solution, D_0 and D are the dielectric constants of water and solution of nonelectrolyte respectively, b_i and z_i are respectively the radius and valence of ion of ith kind, α is a constant, ϵ is the elementary charge, k is the Boltzmann constant and T is the absolute temperature. For a given salt solution saturated by a nonelectrolyte at a given temperature, all the terms on the right side of Eq. (3) are constant except n', and log f is proportional to n'. Thus, Eq. (3) gives the theoretical derivation of Eq. (2). The nature of salt effect is determined by the sign of α. If $\alpha>0$, $f>1$, i.e., salting-out; if $\alpha<0$, $f<1$, i.e., salting-in.

Later, on the basis of the same electrostatic model, Debye[3] deduced a more exact formula,

$$\frac{1}{f} = 1 - \sigma C_s , \tag{4}$$

where σ is a parameter. If the nonelectrolyte lowers the dielectric constant of water, $\sigma>0$, $f>1$, i.e., salting-out; if $\sigma<0$, $f<1$, i.e., salting-in.

Attempts to improve Debye's theories were made by Scatchard[4], Butler[5], Gross[6], Belton[7], Kirkwood[8] and Шахпаранов[9], but these authors built their theories essentially on the same mechanism as that of Debye, namely, electrostatic interaction.

The chief drawback of Debye's theory is that he only considered the electrostatic force and ignored the role of forces of other types that may play in the salt effect. According to Debye's theory, any salt should produce a salting-out effect, if the nonelectrolyte lowers the dielectric constant of water. Actually for the same nonelectrolyte, some salts cause its salting-out and some, especially those with large anions, bring about salting-in.

The effect of the nature of salt was considered by some authors. Larsson[10] recognized the additivity of the effects of the positive and negative ions in the salt. Gross[11] went one step further by assuming that the cation salts-out and the anion salts-in the nonelectrolyte and that the resulting effect is due to the balance of the antagonistic action of the two ions. Actually some large cations salt-in the nonelectrolyte, although such data are extremely rare.

At present, there are two types of theories dealing with the role of ions playing in the salt effect besides mere electrostatic interaction. In the first type, it is assumed that ions break the structure of water and cause a change of its volume[12] or a change of its entropy[13]. In the second type, it is assumed that the existence of van der Waals-London's dispersion force between ion and molecule has also influence on the course of salt effect. We shall deal only with the second type here.

In 1930, London[14] worked out a general theory of intermolecular force, of which the dispersion force is an important part. According to London, the dispersion energy U between two different molecules, 1 and 2, is

$$U = -\frac{3\alpha_1\alpha_2}{2r^6}\frac{h\nu_{01}h\nu_{02}}{h\nu_{01}+h\nu_{02}}. \qquad (5)$$

In Eq. (5), r is the distance between molecules 1 and 2, h the Planck constant, α_1 and ν_{01} are the polarizability and characteristic frequency in the unperturbed state for molecule 1, α_2 and ν_{02} have similar meanings for molecule 2. U has the following properties: (1) it is the energy of attraction, (2) it increases with the increase of polarizability and therefore with the increase of the size of the molecule, and (3) it has additive property[15].

Kortum[16] pointed out that the optical properties of salt solutions cannot be explained by electrostatic effect, and hence it is necessary to consider the part played by vander Waals' force. He suggested the use of dispersion force to explain the salting-in of nonelectrolyte by large ions. From an experimental study of salt effect on the solubilities of *m*-nitrobenzoic acid in water, Huang, Chu and Han[17] pointed out that salting-out decreases and salting-in increases with the increase of the size of the ion. This apparently is the effect of London's dispersion force. Bockris, Bowler-Reed and Kitchener[18] used London's equation and deduced a salting-in formula. They said, "The effect could be treated by regarding the water in the salt solution as having a 'pseudo-tem-

perature increase' from its expanded density". For the salting-in of benzoic acid by tetraalkyl-ammonium iodides, results calculated from their formula agree rather poorly with the observed ones. Summarizing the works of our predecessors, we propose the following mechanism for the salt effect on the solubility of nonelectrolyte in water.

Let an aqueous salt solution be saturated with a nonelectrolyte. We assume that for the salt, ion of one kind of charge is much larger in size than the ion of opposite charge, and that the molecule of nonelectrolyte is much bigger than that of water. The forces giving rise to the phenomenon of salt effect are mainly two, namely, the electrostatic force and the London dispersion force. The nature of salt effect depends upon which of the two dominates the system. If the electrostatic force predominates, salting-out results; if the dispersion force predominates, salting-in results. The simplified picture how this happens seems to be as follows. Through electrostatic interaction between ion and dipole, water molecules gather around the ions (mainly around the smaller ones). This decreases the amount of "free water" serving as solvent for the nonelectrolyte and produces a salting-out effect. Between the large ion and large nonelectrolyte molecule, there exists, however, a strong dispersion force, which draws the latter around the former. This decreases the amount of nonelectrolyte in free water and makes room for more nonelectrolytes to dissolve, i.e., to produce a salting-in effect. The balance of the two antagonistic effects gives the observed salt effect.

We shall describe in more detail how ions of large size bring about salting-in of nonelectrolyte. The large ions can be divided into two kinds according to the symmetry and asymmetry of their structures. If the ion has a symmetrical structure, (for example, R_4N^+), it probably behaves like a large charged sphere. Since the distance between the centre of sphere and water molecule in closest approach is large, electrostatic interaction between them is small. On the other hand, the ion and the nonelectrolyte molecule, both being large, possess high polarizabilities, and the dispersion force between them is significant. When this force exceeds the electrostatic force between ion and water, salting-in results.

If the large ion has an asymmetrical structure, (for emample, 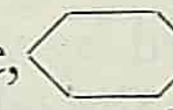), then the electrical charge is concentrated in the small polar portion, (e.g. COO^-), while the rest portion, (e.g. ) remains nonpolar. Then the water molecules will be attracted to the small polar portion by electrostatic force, while the nonelectrolyte molecules will be attracted to the large nonpolar portion by dispersion force. If the latter force is large, salting-in effect is produced.

In general, when the ionic radius is very large (e.g. iodate ion, picrate ion, or tetraalkylammonium ion), very little or no solvation occurs[19]. Provided the nonelectrolyte molecules succeed in gathering around the ion, salting-in can still take place even if there is solvation. This is evident from the fact that the ratio of nonelectrolyte to water in the "free water" amounts only to a small fraction, and the removal of some nonelectrolyte molecules affects this ratio far more than the removal of the same number of water molecules.

We have not considered the question of the breaking of water structure by the ion, since there is reason to believe that a very large ion has little effect on the structure of water[19].

Our viewpoint is that provided there is no other disturbing factor, any kind of ion, (positive or negative), with a sufficiently large size will salt-in nonelectrolyte molecules of large sizes. Hence, the belief that the cation causes salting-out, and the anion, salting-in of the nonelectrolyte is incorrect.

We plan to test the mechanism proposed above by a series of experimental studies. We report here our first experimental study, namely the effect of five cobalt-ammines on the solubilities of *n*-valeric acid in water. Since these complex salts possess large positive cations and as the molecules of *n*-valeric acid are also large, the London dispersion force between the two should be rather strong and we expect a salting-in of the acid. We choose *n*-valeric acid as a ""nonelectrolyte" for the following reasons: (1) Being a weak acid ($K_a \approx 10^{-5}$), it can be determined readily by titration with standard alkali; (2) being a liquid, it reaches equilibrium easily with salt solution; (3) its solubility in water is neither too large nor too small, (37.43 g per litre at 25°C); (4) the cobalt complex is stable in acid solution[20].

Literature reports only one work using cobalt complexes for the study of salt effect, and that is the work of two Soviet chemists, Kozakevich and Yankelevich[21]. They used phenol as the "nonelectrolyte". Their complex ions contain NH_3, H_2O, $C_2H_4(NH_2)_2$, $C_2H_5NH_2$, Cl^- or $C_2O_4^=$ as radicals.

Experimental*

Preparation of reagents: The following reagents are prepared.

Cobalt-ammines: Five cobalt-ammines are prepared from the C. P. $CoCl_2$ $6H_2O$, or $Co(NO_3)_2 \cdot 6H_2O$ of Shika Company.

(1) Hexamminecobaltic chloride, $[Co(NH_3)_6]Cl$, (luteo): This is prepared according to the method of Bjerrum and Reynold[22].

*This work began in the winter of 1949 and was interrupted by the illness of the junior author (Yang). It was resumed in the spring of 1954.

(2) Chloropentamminecobaltic chloride, $[Co(NH_3)_5Cl]Cl_2$, (purpuro): This is prepared according to the procedure described in Biltz and Biltz's Laboratory Methods of Inorganic Chemistry[23].

(3) Nitritopentamminecobaltic chloride, $[Co(NH_3)_5NO_2]Cl$, (xantho).

(4) trans-Dinitritotetramminecobaltic chloride, trans-$[Co(NH_3)_4(NO_2)_2]Cl$, (croceo).

(5) cis-Dinitritotetramminecobaltic chloride, cis-$[Co(NH_3)_4(NO_2)_2]Cl$ (flavo).

The last three salts are prepared according to Jörgenson[24]. After preparation, these five salts are purified and washed with ether and heated to dryness in an oven at 45–50°.

n-Valeric acid: This is prepared by the following steps:

$$n\text{-butyl alcohol} \xrightarrow{1} n\text{-butyl chloride} \xrightarrow{2} n\text{-butyl cyanide}$$
$$\xrightarrow{3} \text{sodium } n\text{-valerate} \xrightarrow{4} n\text{-valeric acid.}$$

n-butyl alcohol from Chi Fa Co. of Shanghai is distilled. Step 1 is KBr method[25] and the product, *n*-butyl bromide is purified once. Steps, 2, 3 and 4 are done according to Adams and Marvel[26]. The *n*-valeric acid thus obtained is distilled several times until its density at 25°C is constant. Its physical properties are: b. p., 186.2–186.6°C; D_4^{25}, 0.93445. Timmermann and Hennaut-Rolland's values[27] are: b. p., 186.35°C; D_4^{25}, 0.93465.

Standard NaOH solution: A solution of 0.1 *n* (or 0.2 *n*) NaOH is prepared according to standard procedure and stored up in pyrex flask provided with a sodalime tube and an automatic flowing device. It is standardized by benzoic acid or standard HCl solution before use.

Indicators: Phenolphthalein is used as indicator to titrate *n*-valeric acid in xantho– and flavo-cobaltic chloride solutions. Thymol blue is used as indicator to titrate the acid in the other three salts. Since its colour changes from yellow to blue, it is more suitable for use in red solution as purpuro salt.

Apparatus: Solubility bottle: This is a glass-stoppered bottle of cylindrical shape, made of Chinese Tyrex glass. Its capacity is about 80 cc. After the solution is put in and the bottle glass-stoppered, it is further closed up by a large thin rubber tube and sealed with paraffin.

Thermostat: This is a thermostat of the toluene-mercury regulator type. The rotating axle in the centre of the bath has wing-shaped plates provided with clamps which can hold up the solubility bottle at any angles.

Procedure: 60 cc of cobaltammine solution at definite concentration and 4 cc of *n*-valeric acid are put into the solubility bottle. It is continuously shaken

and heated to 45°C. Then it is sealed according to the procedure described above and put into the thermostat at 25°C. It is first clamped to the wing-plate in a position so that its axis is perpendicular to the rotating axle. This keeps the content in violent stirring. After one hour, the mixture becomes turbid. Then it is clamped so that its axis becomes parallel to the rotating axle and rotated for two hours more. Finally let it stand vertically for two or three hours in the thermostat. The last two steps make the turbid mixture separate again into two clear liquid layers.

Since *n*-valeric acid forms the upper layer of the content, direct pipetting of the salt solution in the lower layer causes some valeric acid to be carried out on the tip of the pipette and brings in error in analysis. To avoid this, the following procedure is adopted. Let the solubility bottle stand vertically in the thermostat with its neck above water. The glass stopper is replaced by a cork fitted with a glass tubing, one end of which, already blown into a thin bulb, almost touches the bottom of the solubility bottle. In the near neighbourhood of this bottle, put in a large test tube with its mouth above water. It is closed up by a rubber stopper fitted with two bent glass tubings, one of which is connected with that of the solubility bottle by a short rubber tube. When it is found by close observation that no *n*-valeric acid adheres to the glass bulb, break it by pressing it against the bottom. By sucking the other bent tubing of the large test tube, the aqueous salt solution in the solubility bottle is transferred, without contact with the *n*-valeric acid layer, to the large test tube.

20 cc of the salt solution is pipetted out, (the pipette being at the same temperature as the thermostat, i.e. 25°C), and its *n*-valeric acid content is analyzed by titration with a standard NaOH solution. For every salt solution, two or three titrations are made.

Data and Calculations

In Table 1, the first column gives the cobaltammines, the second, their concentrations, C_s, in mols per litre; the third, the solubilities of *n*-valeric acid, S, in grams per litre; the fourth, the activity coefficient of *n*-valeric acid, f, as defined by S_0/S; the fifth, $\log f$; the sixth, $1/f$. All these quantities are values at 25°C. S_0=37.43 g/litre. According to Lieben and Rossi[28], it requires 27 cc of water to dissolve 1 cc of *n*-valeric acid at 16°C. On the basis of this datum, I.C.T. gives S_0=35 g per 1,000 g of solution at 16°C. No datum at 25°C is available for comparison. We also find that for *n*-valeric acid at 25°C, D_4^{25}= 0.9979. Since *n*-valeric acid is a weak electrolyte, our f is not exactly the same as the activity coefficient of real nonelectrolyte which involves no ions. Our f is only an approximate expression, which other authors also used for treatment of solution of weak eletrolytes[29].

Table 1 Solubilities and Activity Coefficients of *n*-Valeric Acid in Aqueous Cobalt-ammine Solutions at 25°C

Cobalt-ammine	C_s	S	$S_o/S=f$	log f	$1/f$
Purpuro	0.0034	37.42	1.0003	0.0001	0.9997
	0.0068	37.34	1.0024	0.0011	0.9976
	0.0114	37.33	1.0027	0.0012	0.9973
	0.0190	37.25	1.0048	0.0021	0.9952
Croceo	0.0046	37.39	1.0011	0.0005	0.9989
	0.0077	37.29	1.0038	0.0016	0.9963
	0.0128	37.27	1.0043	0.0019	0.9957
	0.0143	37.30	1.0035	0.0015	0.9965
	0.0213	37.01	1.0114	0.0049	0.9888
	0.0239	37.19	1.0065	0.0028	0.9936
	0.0355	36.91	1.0141	0.0061	0.9861
	0.0399	36.91	1.0141	0.0061	0.9861
Xantho	0.0163	37.04	1.0105	0.0046	0.9896
	0.0325	36.63	1.0218	0.0094	0.9786
	0.0541	36.20	1.0340	0.0145	0.9671
	0.0904	35.39	1.0577	0.0243	0.9455
Luteo	0.0027	37.34	1.0024	0.0011	0.9976
	0.0054	37.25	1.0048	0.0021	0.9952
	0.0108	37.05	1.0103	0.0044	0.9899
	0.0180	36.85	1.0157	0.0068	0.9845
	0.0299	36.53	1.0246	0.0106	0.9760
	0.0499	35.99	1.0400	0.0170	0.9615
	0.0831	35.22	1.0628	0.0264	0.9410
	0.1388	33.60	1.1140	0.0469	0.8977
Flavo	0.0116	37.33	1.0027	0.0012	0.9973
	0.0199	37.19	1.0064	0.0028	0.9936
	0.0323	37.10	1.0089	0.0039	0.9912
	0.0539	36.82	1.0166	0.0071	0.9837
	0.0898	36.52	1.0249	0.0107	0.9757
	0.1495	35.87	1.0435	0.0185	0.9583

From columns 2 and 3 in Table 1, we get Fig. 1. According to Eq. (2), if log f is plotted vs. C_s, the result should be a straight line. Such plot is made in Fig. 2. According to Eq. (4), if $1/f$ is plotted vs. C_s, the result should also be a straight line. Such plot is made in Fig. 3.

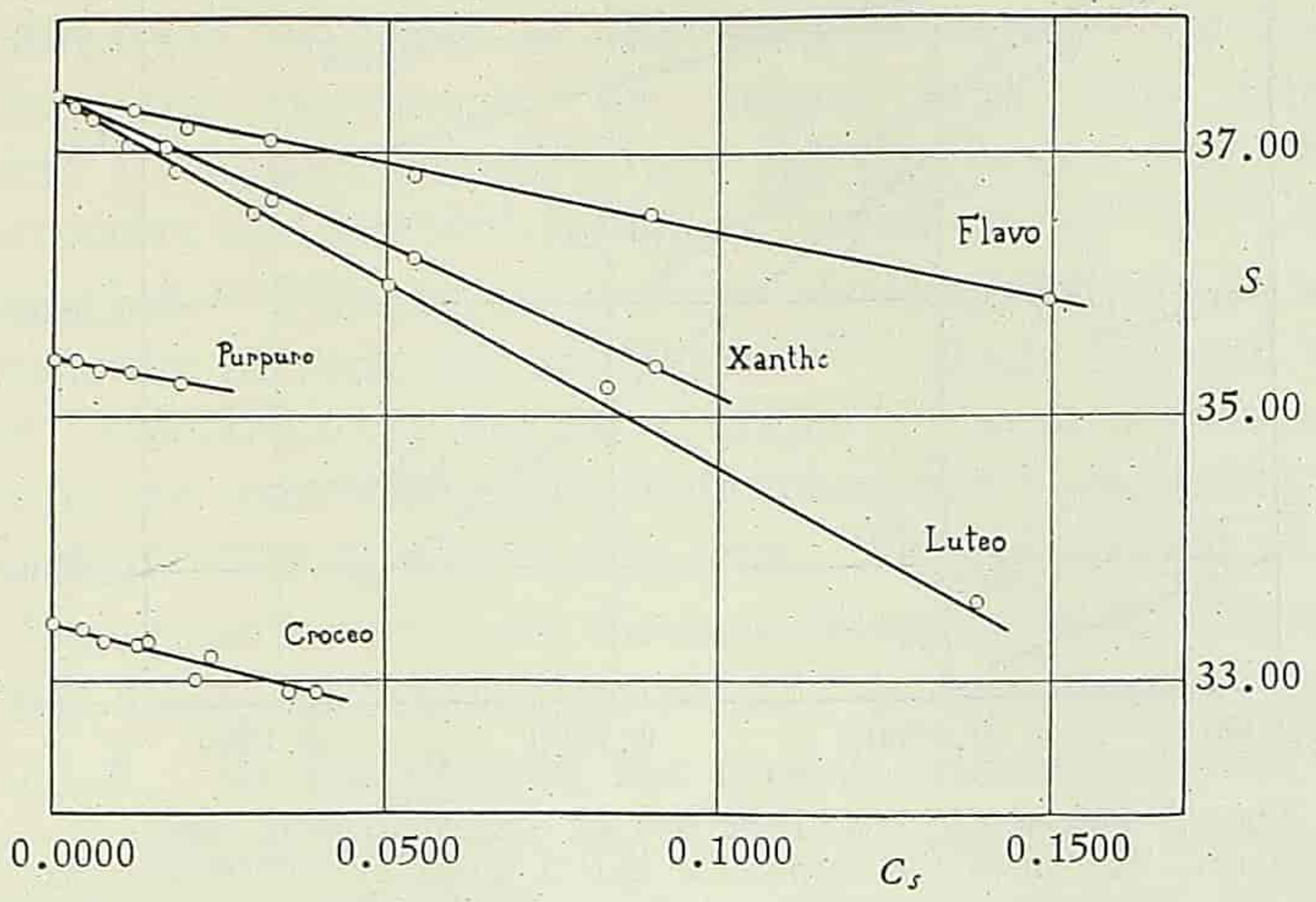

Fig. 1. Plot of solubilities of *n*-valeric acid vs. concentrations of salts.

Note: The curve for purpuro is shifted down by 2 and that for croceo by 4 units to avoid disfiguration of other three curves.

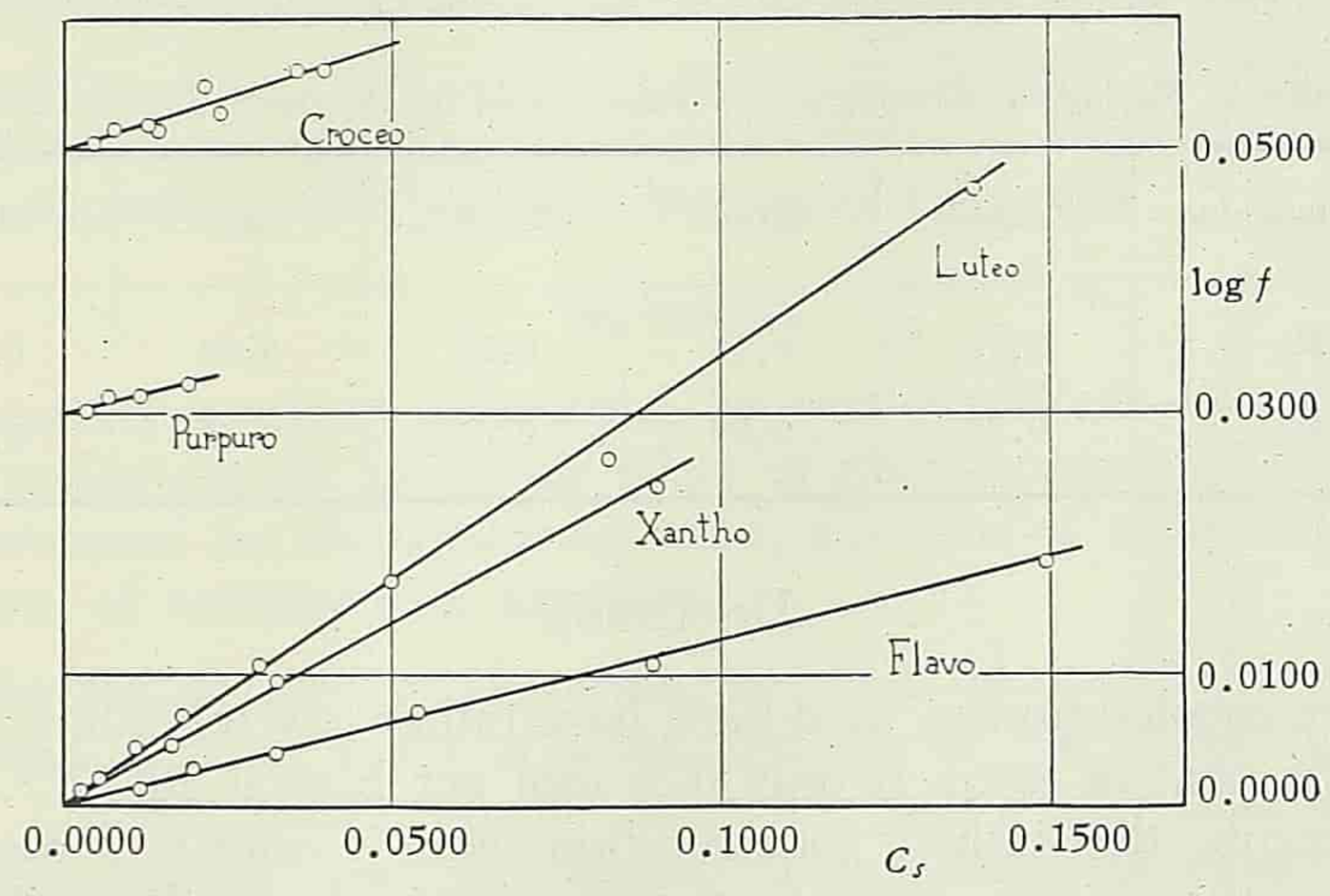

Fig. 2. Plot of log f of *n*-valeric acid vs. concentrations of salts.

Note: The curve for purpuro is shifted up by 0.0300 and that for croceo by 0.0500 units to avoid disfiguration of the other three curves.

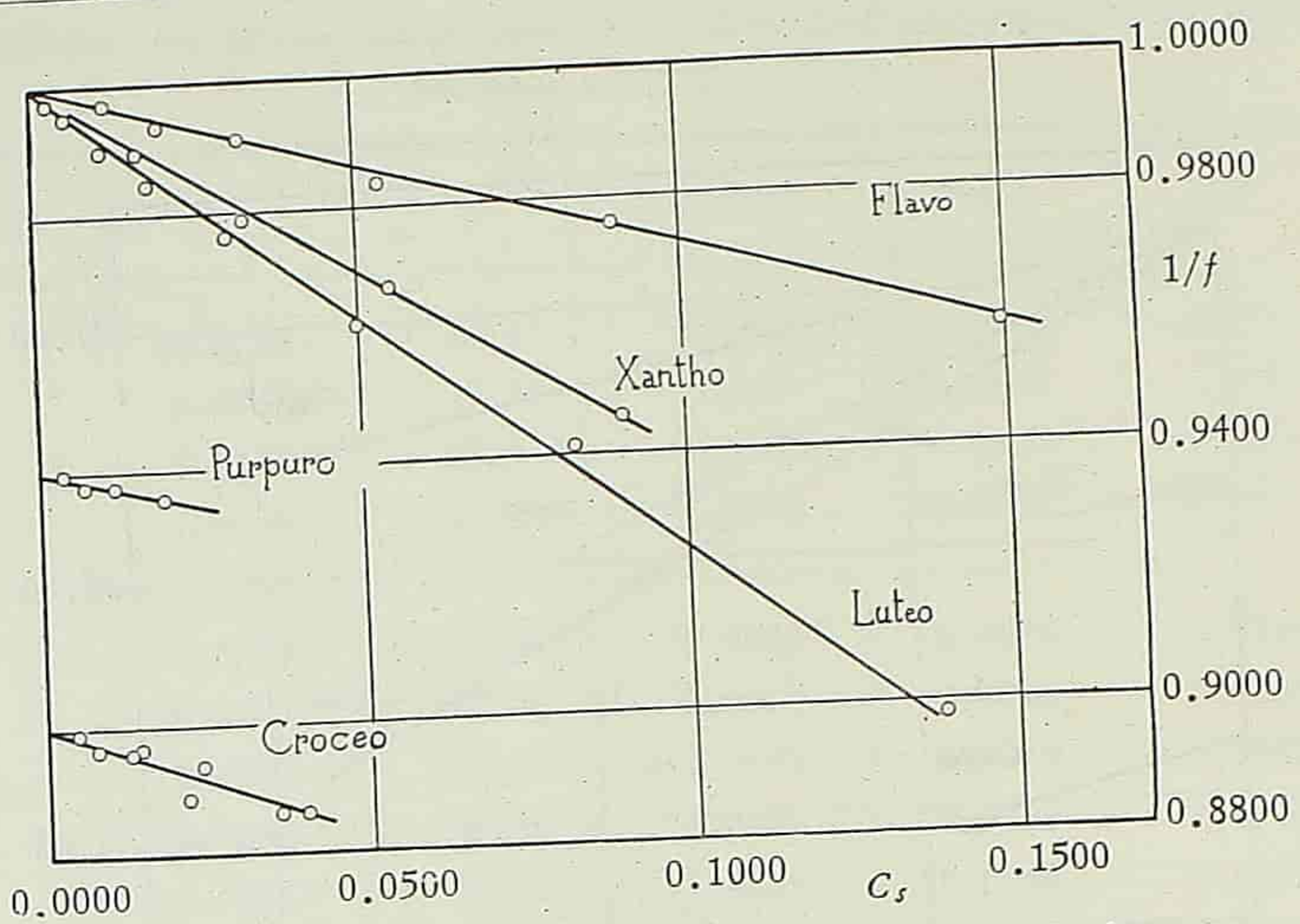

Fig. 3. Plot of $1/f$ of n-valeric acid vs. concentrations of salts.
Note: The curve for purpuro is shifted down by 0.0600 and that for croceo by 0.1000 units to avoid disfiguration of the other three curves.

From the slope of each straight line in Fig. 2, we get k_1 equal to k of Eq. (2). Similarly, we get k_2 from Fig. 3. k_2 is not identical with σ of Eq. (4), (4), since f in Eq. (4) is the activity coefficient of real nonelectrolyte containing no ions. k_1 and k_2 are called salting-out constants. Positive values of k_1 and k_2 indicate salting-out, while negative values, salting-in. Table 2 is a collection of salting-out constants of n-valeric acid by five cobaltammines.

Table 2 Salting-out Constants of n-Valeric Acid by Cobalt-ammines at 25°C

Cobaltammine	Purpuro	Croceo	Xantho	Luteo	Flavo
K_1	0.12	0.16	0.28	0.34	0.13
K_2	0.24	0.35	0.61	0.75	0.27

Discussion

The five cobaltammines, used here, have rather low solubilities, the largest of which, i.e. that of luteo, is only 0.26 mol per litre at 20°C[30]. Hence in our experiments, the highest concentration used is only 0.15 mol per litre. But the lower the concentration of cobaltammine is, the smaller will be the salt effect and the larger will be the experimental error. Moreover, the colouring of the solution by cobaltammine decreases the sensitivity of the indicator and increases the analytical error. Hence it is difficult to get accurate salting-out constants at low concentrations of these salts. Nevertheless, we get fairly good straight lines in Figs, 2 and 3, and the salting-out results are essentially in agreement with the theories of Debye-McAulay and of Debye.

The results are contrary to our expectation. The chief reason why *n*-valeric acid is salted out by cobaltammines instead of being salted in is probably that the sizes of the complex cations are not sufficiently large. Before the experiment, we judged their sizes superficially by their chemical formulas. Actually they are not large. For example, from the crystal structure of $[Co(NH_3)_6]I_3$ the "crystal radius" of $[Co(NH_3)_6]^{+++}$ is only about 2.5 Å.* The crystal structure of $[Co(NH_3)_6]I_3$ is similar to the combined structure of rock salt and fluorite[31]. Each unit cell contains four molecules of $[Co(NH_3)_6]I_3$ four $[Co(NH_3)_6]^{+++}$ form a face-centered cubic, eight I^- occupy the centres of eight small cubes, one I^- the centre of the body, and three I^- the centres of twelve side lines. The side length of the unit cell is 10.89 Å. Hence the nearest Co-I distance along the body diagonal is $10.89 \times \sqrt{3/4}$ or 4.71Å. Since the "crystal radius" of I^- is 2.2Å, that of $[Co(NH_3)_6]^{+++}$ is at most 2.5 Å. Similarly, from the crystal structure of $K_3[Co(NO_2)_6]$ and the side length of unit cell 10.44 Å[32], we find that the "crystal radius" of $[Co(NO_2)_6]^{---}$ is about 3.2 Å. Hence the crystal radii of the cations of our cobaltammines lie probably within the range of 2.5–3.2 Å, and they are not very large. It is evident that the dispersion force between the ion and *n*-valeric acid cannot compete with the electrostatic force between the ion and water and the result is salting-out. It is significant that the cation of luteocobaltic chloride, i.e. $[Co(NH_3)_6]^{+++}$ which has the smallest crystal radius, is salted out to the largest extent (see Table 2).

There is another possible factor which helps to bring about the salting-out of *n*-valeric acid. The carboxyl group of the acid is known to be an electron-attracting radical[33]. It probably repels the large cation and lowers down the dispersion effect between this ion and the acid.

Summary

Mechanisms based on interaction by van der Waals-London dispersion force for explaining the salting-in effect of nonelectrolyte in water by large ions are proposed for the following cases; (1) ions of symmetrical structure and (2) ions of asymmetrical structure.

For the test of such mechanisms, we have measured the solubilities of *n*-valeric acid at 25°C in the aqueous solutions of the following five cobaltammines: (1) hexamminecobaltic chloride (luteo), (2) chloropentamminecobaltic chloride (purpuro), (3) nitritopentamminecobaltic chloride (xantho), (4) trans-dinitritotetramminecobaltic chloride, and (5) cis-dinitritotetramminecobaltic chloride. All these salts salt out *n*-valeric acid.

The activity coefficient, f, of *n*-valeric acid as determined by the ratio of its solubility in pure water, S_0, to that in a salt solution, S, is calculated for

*We are indebted to Prof. Y. C. Tang for this information.

each salt concentration, C_s. The plots of $\log f$ and $1/f$ *vs.* C_s for five salts are all linear, in agreement with the theories of Debye and McAulay and of Debye.

We give explanations why these complex ions do not bring about the salting-in of *n*-valeric acid in water.

References

[1] Setschenow, 1889. *Z. physik. Chem.*, **4**, 117.
[2] Debye, und MeAulay, 1925. *Physik. Z.*, **26**, 22.
[3] Debye, 1927. *Z. physik. Chem.*, **130**, 55.
[4] Scatchard, 1926. *Chem. Rev.*, **3**, 383; 1927. *Trans. Faraday Soc.*, **23**, 454.
[5] Butler, 1929. *J. Phys. Chem.*, **33**, 1015.
[6] Gross, 1929. *Monatsh.*, **53**, 445.
[7] Belton, 1937. *Trans. Faraday Soc.*, **33**, 653.
[8] Kirkwood, 1939. *Chem. Rev.*, **24**, 233.
[9] Шахпаранов, 1953. Вестник Московского Университета, Серия Физико-Математических и Естественных Наук, Выпуск, **6**, 9.
[10] Larrson, 1931. *Z. physik. Chem.*, **153**, 299.
[11] Gross, 1933. *Chem. Rev.*, **13**, 91.
[12] McDevit, and Long, 1952. *J. Am. Chem. Soc.*, **74**, 1773.
[13] Frank, and Evans, 1945. *J. Chem. Phys.*, **13**, 507.
[14] London, 1930. *Z. phys. Chem.* B **11**, 222. and other papers.
[15] London, 1937. *Trans. Faraday Soc.*, **33**, 8.
[16] Kortum, 1936. *Z. Elektrochem.*, **42**, 287.
[17] Huang, Tzu-Ching, Chu, Lucy Ju-Yung, and Han, Shu-Tang, 1947. *Sci. Rept. Natl. Tsing Hua Univ., Series* **A 4**, 268.
[18] Bockris, Bowler-Reed, and Kitchener, 1951. *Trans. Faraday Soc.*, **47**, 184.
[19] Kortum, and Bockris, 1951. Textbook of Electrochemistry, Vol. 1, 135—137.
[20] Gmelin, 1930. Handbuch der anorganischen Chemie, System No. 58, Kobalts, Teil B, p. 48.
[21] Kozakevich, and Yankelevich, 1937. *J. Phys. Chem.* (U.S.S.R.), **10**, 113. From *Chem. Abst.* 1938. **32**, 444.
[22] Fernelius, 1946. *Inorganic Systhesis,* **2**, 216, McGrawhill.
[23] Biltz, and Biltz, Laboratory Methods of Inorganic Chemistry, 2nd English Edition, Section 131.
[24] Jörgenson, 1898. *Z. anorg. Chem.*, **17**, 455, 463 and 474.
[25] Gilman, 1932. *Organic Synthesis,* Vol. 1, 26. John Wiley. Joseph, Ross, and Vulliet, 1949. *J. Chem. Edu.*, **26**, 329.
[26] Adams, and Marvel, 1920. *J. Am. Chem. Soc.*, **42**, 312.
[27] Timmermann, et Hennaut-Rolland, 1932. *J. Chim. Phys.*, **29**, 551.
[28] Lieben, und Rossi, 1871. *Ann.*, **159**, 59.
[29] Randall, and Failey, 1927. *J. Am. Chem. Soc.*, **49**, 2678.
[30] Brönsted, and Petersen, 1921. *J. Am. Chem. Soc.*, **43**, 2269.
[31] Ормонт, 1950. Структуры Неорганических Веществ, ст. 703, Государственое Технико - Теоретической Литературы, Москва. Gmelin, *ibid*, pp. 57—58.
[32] Ормонт, *ibid.*, ст. 733.
[33] Fieser, and Fieser, 1950. Organic Chemistry, 2nd ed. p. 604.

STUDIES ON SUCCINIC DEHYDROGENASE

I. ISOLATION, PURIFICATION, AND PROPERTIES*

WANG TSING-YING (汪靜英), TSOU CHEN-LU (鄒承魯),
and WANG YING-LAI (王應睞)

(Institute of Physiology and Biochemistry, Academia Sinica)

The nature of succinic dehydrogenase, the enzyme specifically concerned with the activation of succinate as defined previously by one of us[2], has been a matter of controversy for a number of years. Bach, Dixon and Zerfas[3], Ball, Anfinsen and Cooper[4], and Pappenheimer and Hendee[5] were of the opinion that it was identical with cytochrome *b*. Based on a study of the cyanide inactivation of succinic dehydrogenase, one of us[2] has shown that these two are, in fact, not identical. This conclusion has since been confirmed by Chance[6], using a totally different method. Axelrod, Potter and Elvehjem[7] reported that livers of rats maintained on a riboflavin-deficient diet were low in succinic oxidase activity, suggesting the implication of the vitamin in the enzyme system, but exactly which component of the complex system was affected could not be ascertained from their experiments. A more detailed analysis of the enzyme system during riboflavin deficiency carried out in our own laboratory[8] showed that only the dehydrogenase component was involved. All of these are, however, indirect evidences and a final solution of the nature of succinic dehydrogenase must await the preparation of the enzyme in a pure state.

Succinic dehydrogenase occurs in tissues tightly bound to the particulate matter of the cell and cannot be solubilized by ordinary treatments. It has resisted all attempts at its isolation and purification by enzyme chemists for over twenty years. In a brief communication, Morton[9] claimed to have obtained the enzyme in aqueous solution by treatment with *n*-butanol, but further purification has not been reported since. Neufeld, Scott and Stotz[10] obtained a soluble succinic dehydrogenase by ammonium sulphate fractionation in the presence of bile salts, but the purification achieved was not very high. Recently, Singer and his coworkers[11–13], using phenazine methosulphate as

---

*Communicated to the 3rd International Congress of Biochemistry, Brussels, 5 August, 1955, by Wang, Tsou, and Wang[1] and to appear in Chinese in *Acta Physiologica Sinica,* Vol. XX, No. 2, 1956.

an electron carrier in the assay of the enzyme activity, claimed to have isolated the enzyme in an essentially homogeneous state when examined in the ultracentrifuge. Their enzyme preparation contained no hemin and no significant amount of any of the known water-soluble vitamins except α-lipoic acid*.

We have also been engaged in the isolation and purification of the enzyme and have succeeded in obtaining a preparation which is almost electrophoretically pure and which has a specific activity over twice that reported by Singer, Kearney and Zastrow. This preparation contains iron and a flavin prosthetic group. We are presenting in this paper the detailed method of purification together with some observations on the nature of the prosthetic group and other properties of the enzyme preparation.

Materials and Methods

Enzymes. Cytochrome *c*-deficient heart muscle preparation from fresh pig hearts was prepared as described by Tsou[14]. Cytochrome *c* of iron content 0.43% was obtained from pig hearts by the method of Tsou and Li[15]. *D*-amino acid oxidase apoenzyme was prepared from pig kidney cortex according to Negelein and Brömel[16] up to step 3 in their paper. Trypsin and chymotrypsin were crystallized from fresh ox pancreas by the method of Kunitz and Northrop[17] except that the conversion of trypsinogen to trypsin was carried out according to McDonald and Kunitz[18]. These were the same preparations used five years ago[19].

Chemicals. The sources of some of the chemicals used in the present work are as indicated below: potassium ferricyanide, from Schering Kahlbaum, zur Analyse reagent; *p*-cresol, from Hopkin & Williams, redistilled once before use; 2, 3-dimercaptopropanol, synthesized according to Stocken[20] and purified by fractionation under reduced pressure; flavin adenine dinucleotide, prepared from pig heart according to Straub[21]; calcium phosphate gel, prepared according to Keilin and Hartree[22]; phenazine methosulphate, synthesized according to Kehrmann and Havas[23]; versene (ethylene diamine tetraacetic acid), synthesized according to Smith *et al*[24].

Determination of enzyme activity. The decrease in light absorption at 420 mμ due to ferricyanide reduction by succinate was used as a measure of the enzyme activity. Unless otherwise specified, the reaction mixture contained: 0.1 M phosphate buffer, pH 7.8, 0.033 M succinate, 5 mM potassium ferricyanide and enzyme solution added at zero time with a total volume of 3.5 ml. After a 10-minute reaction at the desired temperature, 1 ml of 20% trichloroacetic acid was added, and this was followed several minutes later by

*In their recent communication to the 3rd International Congress of Biochemistry, August, 1955 Kearney and Singer have withdrawn their previous statement on the absence of water-soluble vitamins in their enzyme preparation, because of the finding of riboflavin in the purified enzyme.

the addition of 2.5 ml of water. The precipitate was removed by centrifugation and the light absorption of the supernatant was read against a blank containing 2 mM $K_3Fe(CN)_6$ in the spectrophotometer (Beckman, Model DU) using cells of 10 mm light path. An enzyme preparation causing a decrease of optical density of 0.100 per mg N at 0°C is defined as having a specific activity of 1. Within the range of concentrations used, potassium ferricyanide obeys Beer's law and its molecular extinction coefficient at 420 mμ is 1.03×10^3.

In some experiments, the rate of ferricyanide reduction was directly followed in the spectrophotometer. In such cases, the reaction mixture had the same composition except that the reaction was carried out in Beckman cells of a 5 mm light path. The blank is a 1-cm Beckman cuvette containing 2 mM ferricyanide solution. When constant temperature was desired, the apparatus previously described was employed[25].

Using this assay method, the enzyme activity was found to be directly proportional to the amount of enzyme protein present as can be seen in Fig. 1. The reaction follows a linear course for over 10 minutes as is shown in Fig. 2.

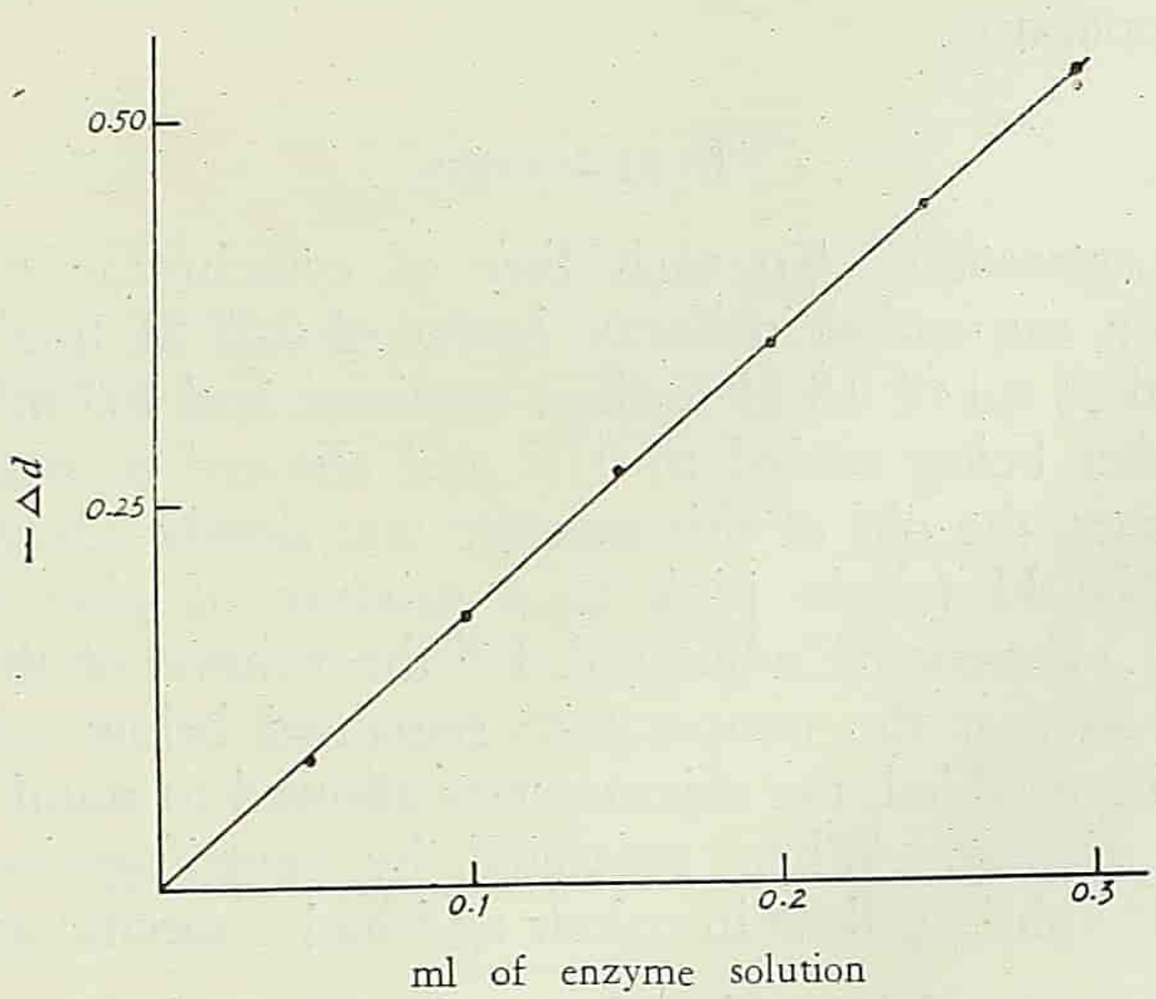

Fig. 1. Relation between enzyme concentration and rate of ferricyanide reduction. The reaction was carried out in 5 mm Beckman cells at 38°C. The decrease in optical density at 420 mμ after 2½ min. reaction is plotted against ml of a stock enzyme solution added to 3.5 ml of reaction mixture. The stock enzyme solution had a specific activity of 76 and a concentration of 0.683 mg N/ml.

Protein determinations. These were carried out either colorimetrically with the biuret reagent[26] or turbidimetrically with trichloroacetic acid[27]. Both methods were standardized against nitrogen determination by micro-Kjeldahl.

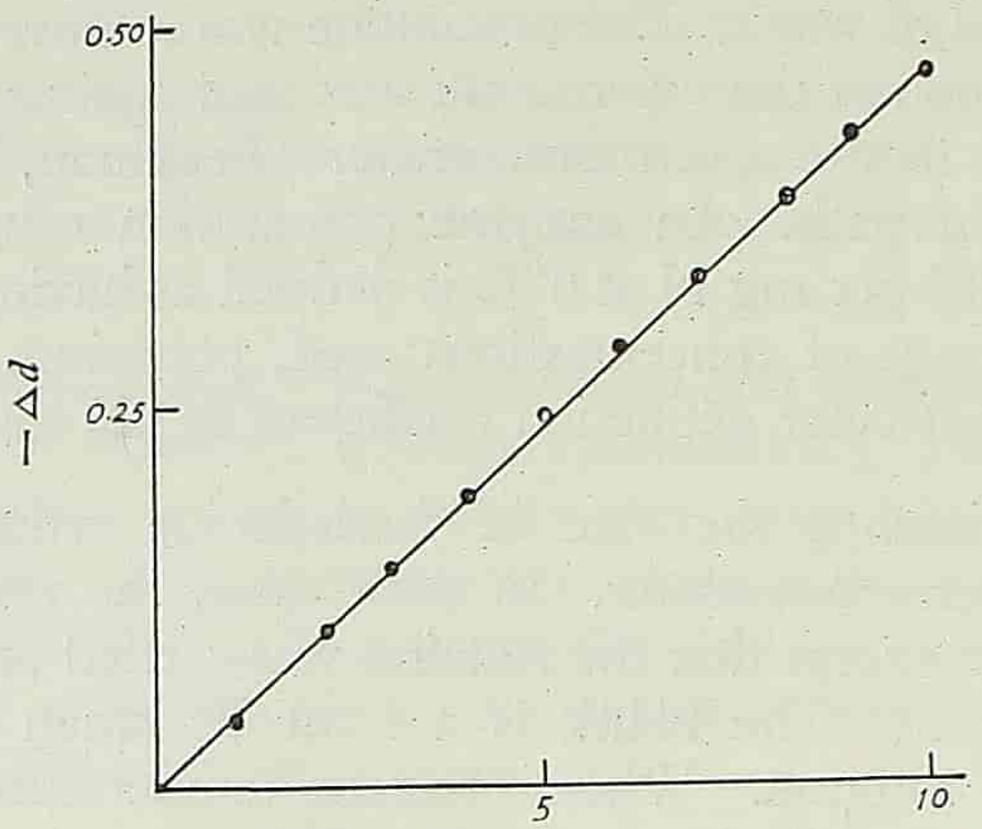

Fig. 2. Course of ferricyanide reduction. Conditions as in Fig. 1 except that the reaction was carried out at room temperature (about 32°C), and the reaction mixture contained 0.0076 mg of enzyme *N* with a specific activity of 156.

Micro-electrophoresis. This was carried out with the Antweiler micro-electrophoresis apparatus.

Purification

1. *Butanol extraction.* To each litre of cytochrome *c*-deficient heart muscle preparation suspended in borate buffer of 0.05 M final concentration, pH 8, were added 60 ml of 0.8 M sodium succinate and 100 ml of neutralized 0.1 M KCN. After being cooled to 0°C and allowed to stand at this temperature for 2 hours, the pH of this mixture was slowly adjusted to 9 by the addition of N NaOH (slight pink to a mixture of phenolphthalein and thymolphthalein). Pre-cooled *n*-butanol, 1/5 the volume of the mixture, was added gradually so that the temperature remained below 1.5°C. After all the butanol had been added, the mixture was allowed to stand for 30 minutes with occasional stirring. When separated by centrifugation, the middle aqueous layer was lightly yellow in colour and had a specific activity of 15–25.

2. *Adsorption on calcium phosphate gel.* The cold butanol extract was adjusted to pH 6 (methyl red) with *N*-acetic acid. Calcium phosphate gel was added to a final concentration of 3.6 mg/ml. The mixture was stirred for 5 minutes and centrifuged and the supernatant was discarded. The precipitate was eluated by stirring for 15 minutes with 4/5 of the volume of the extract of cold 0.075 M phosphate buffer, pH 7.8. The eluate obtained by centrifugation was yellow in colour, perfectly clear and had a specific activity of 45–70.

3. *First ammonium sulphate fractionation.* The eluate was adjusted to pH 7.2 (phenol red) by *N*-acetic acid and solid $(NH_4)_2SO_4$ added. The precipitate formed between 0.35–0.55 saturation of ammonium sulphate was

separated by centrifugation at 0–2°C. The precipitate, when dissolved in a small amount of 0.075 M phosphate buffer, pH 7.2, was amber in colour and had a specific activity of 90–120.

4. *Second ammonium sulphate fractionation.* The protein content of the solution obtained above was determined and the solution was diluted until the final protein concentration was approximately 0.6%. The pH was adjusted to 7.2 (phenol red) and the ammonium sulphate content was determined by Nessler's reagent. Neutralized ammonium sulphate solution (0.9 saturation) was slowly added in the cold and the fraction precipitated between 0.4–0.5 saturation of ammonium sulphate was collected and dissolved in a small amount of 0.04 M phosphate buffer pH 7.8. The final preparation is a clear amber-coloured solution with a specific activity of 200–250.

The main purification steps are summarized in Table 1. Table 2 shows the increase in specific activity and the recovery of enzyme activity at each step of purification.

Table 1. Scheme of Purification of Succinic Dehydrogenase.

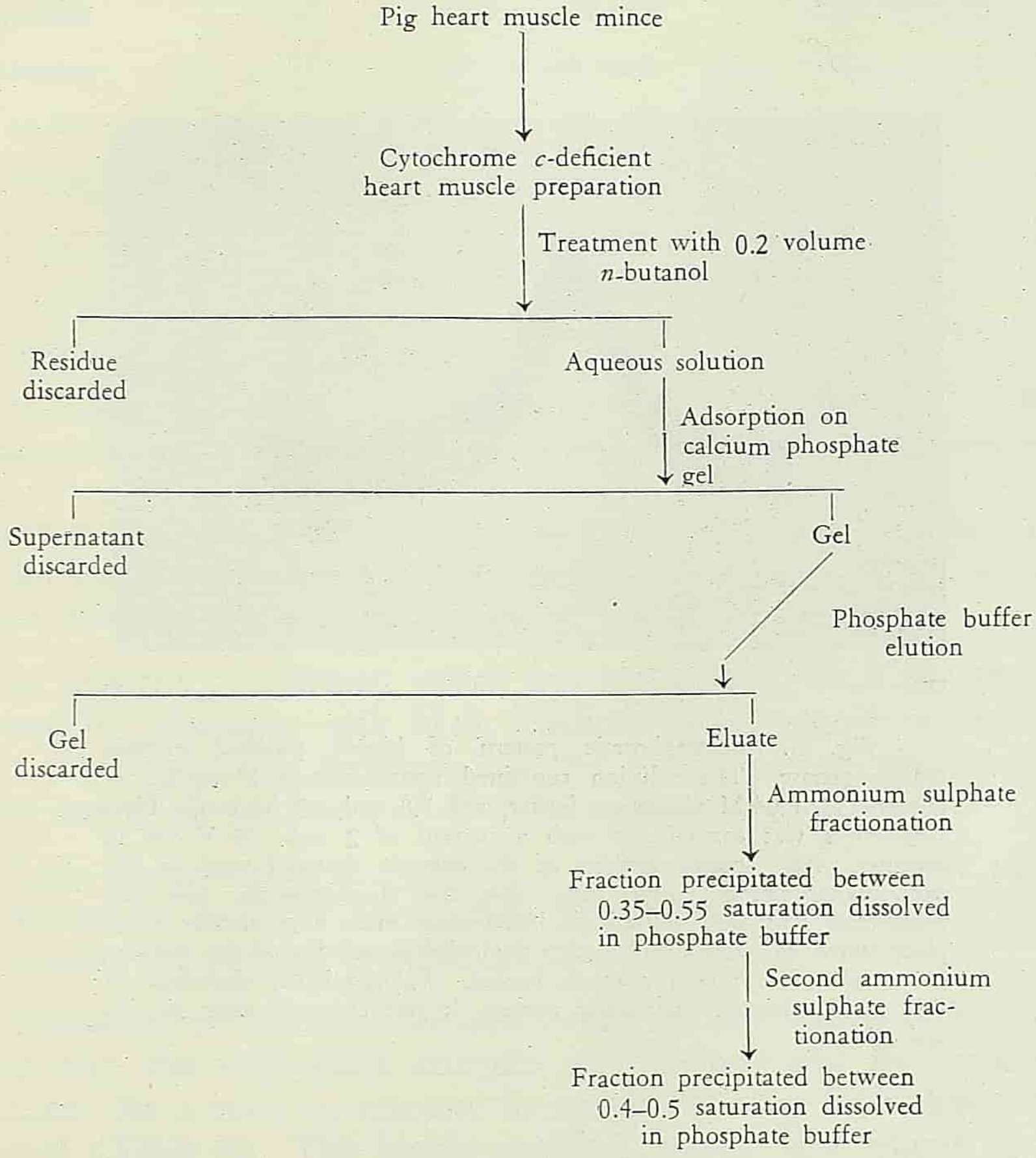

Table 2. Activities and Yields of Succinic Dehydrogenase in the Different Steps of Purification.

Purification Steps	Volume, ml	Yield, %	Specific Activity
Cytochrome *c*-deficient heart muscle preparation	2000	100	5—8
Aqueous extract after n-butanol treatment	1400	35	15—25
Eluate from Ca phosphate gel	1200	21	45—70
First ammonium sulphate fractionation	50	15	90—120
Second ammonium sulphate fractionation	5	3	200—250

The final preparation is about 40 times more active than the original cytochrome *c*-deficient heart muscle preparation and is over 200 times more active than a heart muscle homogenate.

The best preparation obtained, is nearly electrophoretically homogeneous as can be seen in Fig. 3.

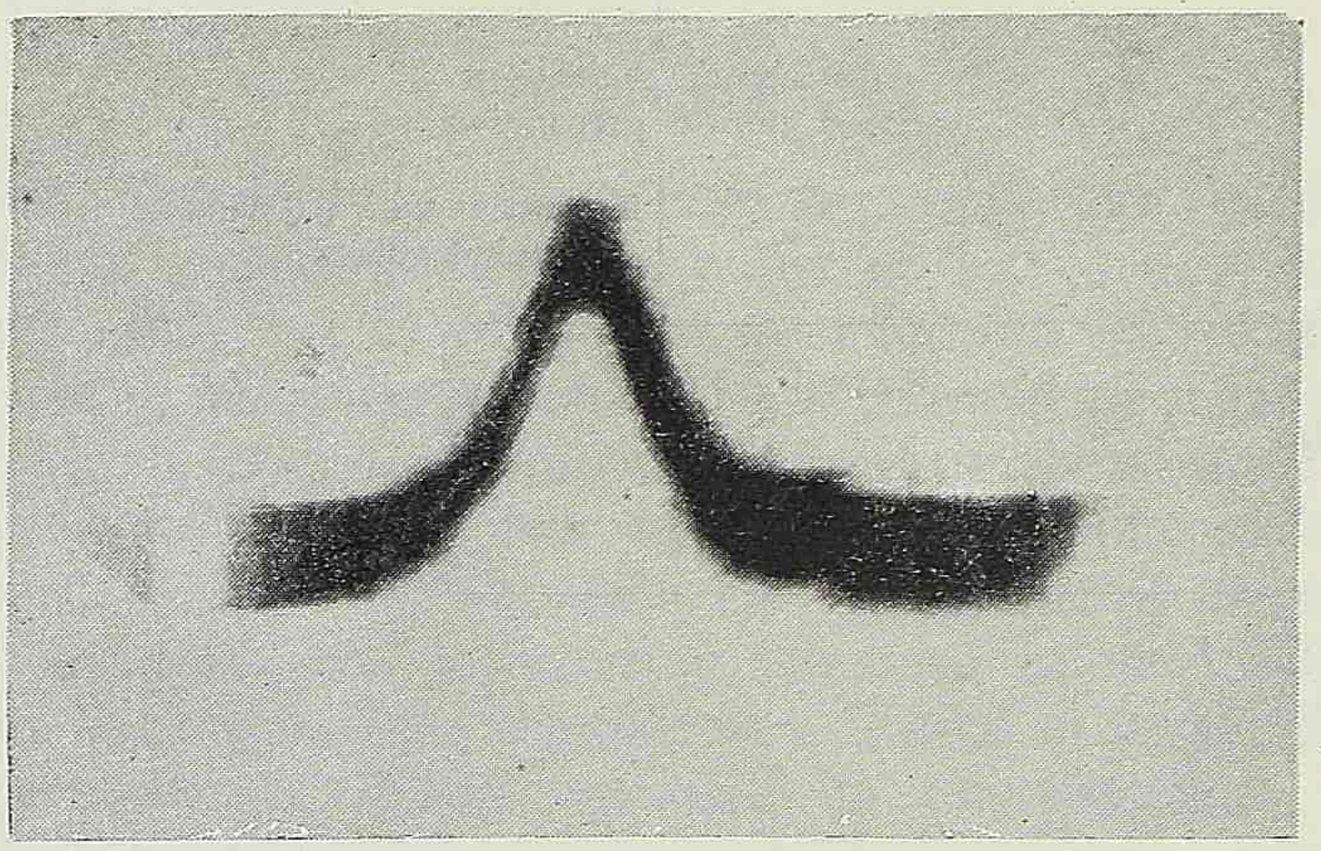

Fig. 3. Electrophoretic pattern of highly purified succinic dehydrogenase. The solution contained approximately 2 mg/ml of enzyme *N*, 0.04 M phosphate buffer, pH 7.8 and 0.2 M NaCl. Electrophoresis was carried out with a current of 2 mA, 25 V for 30 minutes. The specific activity of the enzyme material used in this experiment, assayed some time after the electrophoretic run had completed, was 163. Partial air inactivation must have already taken place when the assay was made; the original activity of the enzyme preparation was probably much higher. As mentioned elsewhere in this paper, the electrophoretic pattern is not changed after air inactivation.

Properties of the Purified Enzyme

Stability. The solubilized enzyme is unstable in the presence of air even when stored at −15°C. Versene gives no protection whereas succinate protects only to a slight extent against this spontaneous inactivation. Sucrose, glycerol, and glycine are more effective than succinate in protecting the enzyme against air inactivation. These results are summarized in Table 3. However, the

Table 3. Stability of Solubilized Succinic Dehydrogenase under Various Conditions.

Aerobic or Anaerobic	Temperature °C	Protective Agent	Time of Keeping, Days	Activity Remaining, % of Original
Aerobic	0	——	3	20—26
Aerobic	−15	——	3	20—26
Aerobic	0	Succinate, 10 mM	3	35
Aerobic	−15	Succinate, 10 mM	3	35
Aerobic	−15	Sucrose, 300 mM	3	100
Aerobic	−15	Sucrose, 300 mM	30	50
Aerobic	−15	Glycerol, 260 mM	3	90
Aerobic	−15	Glycine, 20 mM	3	70
Aerobic	0	Versene, 3.4 mM	3	17
Aerobic	0	Versene, 0.34 mM	3	17
Anaerobic	0	——	60	100

enzyme is perfectly stable when kept under vacuum or under nitrogen in the complete absence of oxygen; one sample has been kept for 2 months under vacuum without any appreciable loss in activity.

An enzyme preparation which has lost its activity in air cannot be reactivated by treatment with H_2S, 2,3-dimercaptopropanol or reduced glutathione under vacuum, showing that the inactivation of the enzyme is not simply due to air oxidation of essential sulfhydryl groups.

Table 4 shows that the enzyme is stable only in a narrow pH range in the absence of succinate even when kept under nitrogen. In the presence of succinate, the enzyme is stable between pH 5.6–9.5.

Activation of succinic dehydrogenase by succinate. Both the particle-bound and the solubilized enzyme can be activated by incubation with succinate. As a rule, an increase in activity of over 100% has usually been observed (Table 5). The highly purified enzyme still retains this property.

Table 4. Stability of Succinic Dehydrogenase under Various pH.

A partially purified enzyme preparation was kept under vacuum at 0°C for 64 hours. The pH value of the medium during incubation was as indicated below. At the end of the incubation period, the remaining activity was assayed and expressed as % of the original.

pH During Incubation	Succinate Concentration, M	Remaining Activity, % of Original
5.6	—	3
5.6	0.04	93
6.5	—	63
7.8	—	100
8.7	—	70
8.7	0.04	100
9.5	—	4
9.5	0.04	100

The activated enzyme loses some activity when succinate is removed by dialysis under vacuum and can be re-activated by succinate.

Table 5. Activation of Succinic Dehydrogenase by Succinate.

The enzyme was incubated with 0.04 M succinate at 0°C under nitrogen and at the times indicated below aliquots were withdrawn and assayed with ferricyanide. Activities are expressed as percentages of the activity before the addition of succinate.

Incubation Time	Activity	
	Heart Muscle Preparation	Purified Enzyme (specific activity=64)
0	100	100
10 min.		120
30 min.	107	151
3.5 hr.	182	
24 hr.		273

Effect of phosphate on enzyme activity. The activity of the solubilized enzyme is not significantly changed when the phosphate concentration in the reaction mixture is changed from 0.05 M to 0.15 M. If borate or imidazole buffer is used instead of phosphate buffer, the activity of the dehydrogenase is only slightly lower. The phosphate concentration during reaction in borate or imidazole buffer was, by direct determination, only 3.8×10^{-5} M. If 0.05 M phosphate is also present, the enzyme activity is the same as in phosphate

buffer alone. These results, summarized in Table 6, are in disagreement with the report of Kearney, Singer and Zastrow[28].

Table 6. Activity of Succinic Dehydrogenase in Various Buffers.

Buffers	Concentration, mM	Other Additions	Concentration, mM	Relative Activity
Phosphate	50	——	——	100
Phosphate	100	——	——	100
Phosphate	150	——	——	105
Phosphate	50	Versene	3.4	116
Phosphate	50	Versene	6.9	121
Borate	50	——	——	75
Imidazole	50	——	——	75
Imidazole	50	Phosphate	5	77
Imidazole	50	Phosphate	10	80
Imidazole	50	Phosphate	20	90
Imidazole	50	Phosphate	50	98
Imidazole	50	Phosphate	90	103
Imidazole	50	Versene	3.4	102
Imidazole	50	Versene	6.9	105
Imidazole	50	Versene	9.4	104

The specific activity of the enzyme preparation used in these experiments was 76. During enzymic assay in borate or imidazole buffer, the enzyme was first dialyzed against imidazole buffer. The dialyzed enzyme had a phosphate concentration by direct determination of 1.5 mM. As 0.1 ml enzyme was used per 4 ml reaction mixture, the final phosphate concentration was only 38 μM.

Effect of succinate concentration. Fig. 4A shows the effect of succinate concentration on enzyme activity. It can be seen that the enzyme is nearly saturated with its substrate at a succinate concentration of 2×10^{-2} M. Lineweaver and Burk[29] plots give Michaelis constants of 1.9 and 0.58 mM at 0° and 38°C respectively (Fig. 4B). The latter value is in essential agreement with the values of 0.25–0.51 mM, reported by Thorn[30] using an assay method very similar to ours.

Effect of different acceptors. With ferricyanide as acceptor, the reaction rate increases with increasing ferricyanide concentration until a concentration of 5 mM is reached, beyond which further increase in ferricyanide becomes inhibitory. Within this concentration range, a plot of the reciprocals of the reaction rates against those of ferricyanide concentrations gives a straight line (Fig. 5).

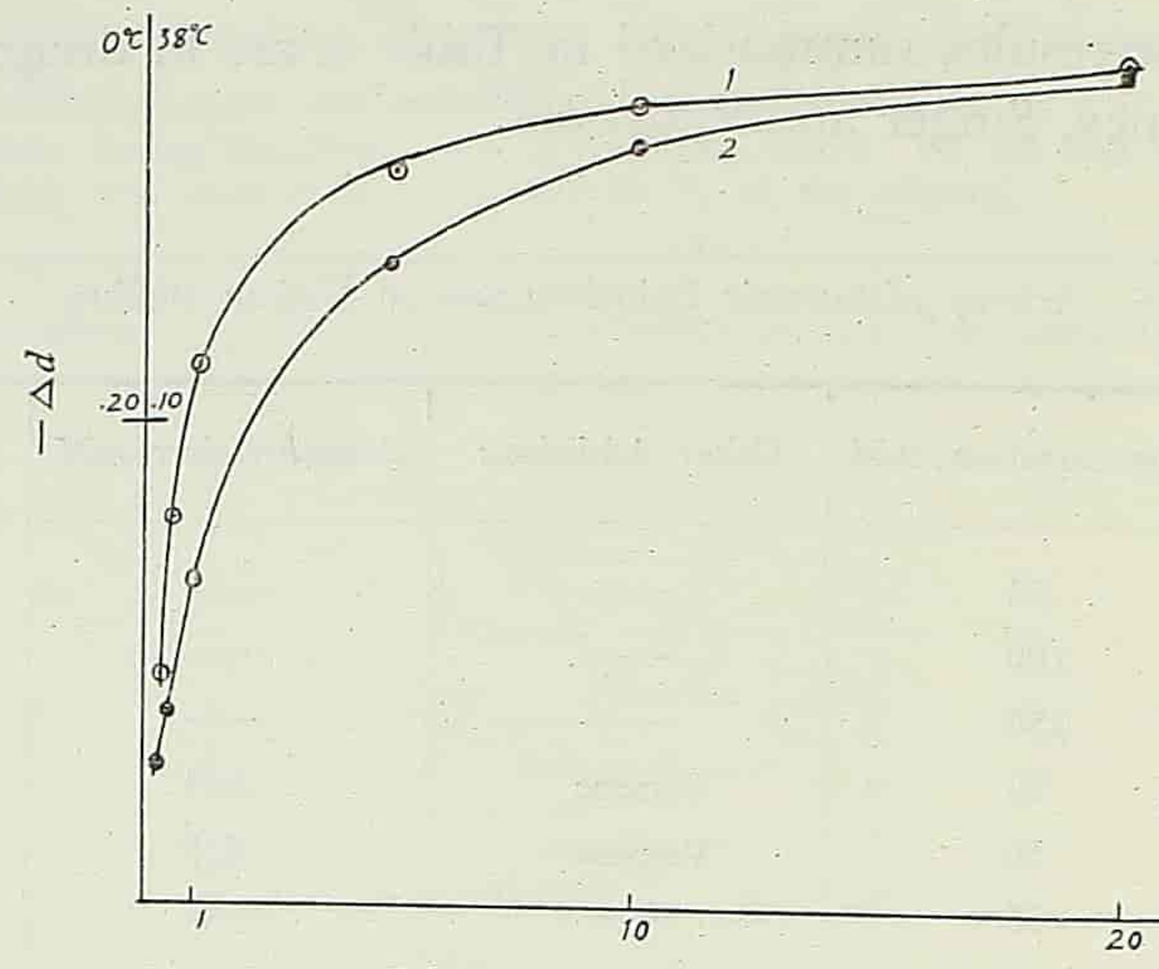

Fig. 4A. Effect of succinate concentration on the activity of succinic dehydrogenase. Curve 1: Reaction mixture contained 80 mM phosphate buffer pH 7.8, 5.2 mM potassium ferricyanide, the required concentration of succinate and 0.061 mg enzyme *N* in a total volume of 4 ml. Temperature 38°C, reaction time 2.5 min. Curve 2: The same reaction mixture except that the enzyme concentration used was 0.108 mg enzyme *N*; the temperature, 0°C, and the reaction time, 10 minutes. The enzyme preparation had a specific activity of 76.

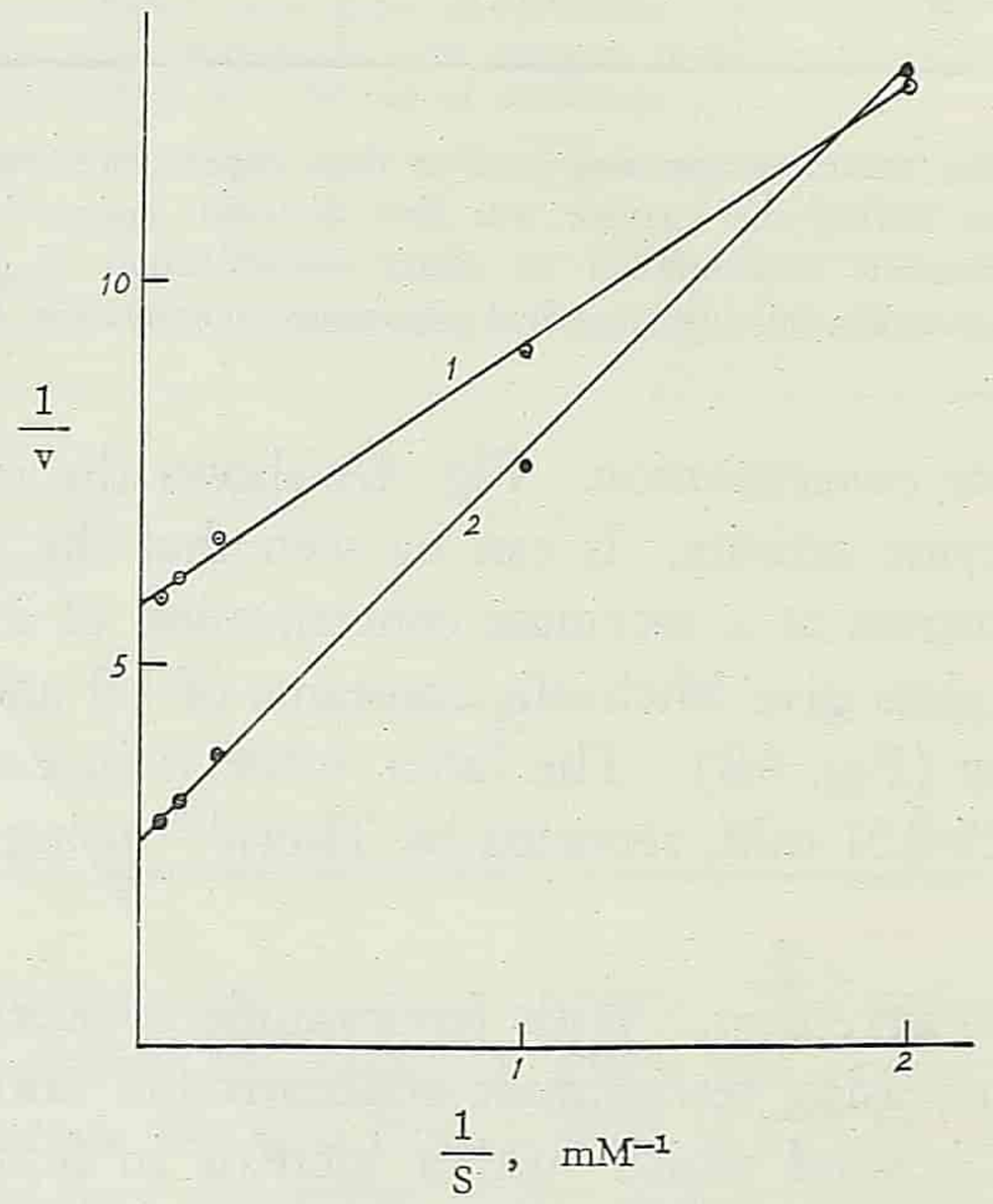

Fig. 4B. Effect of succinate concentration on the activity of succinic dehydrogenase. Data in Fig. 4A plotted according to Lineweaver and Burk. The velocity (v) of the reaction is expressed as decrease of optical density ($-\Delta d$).

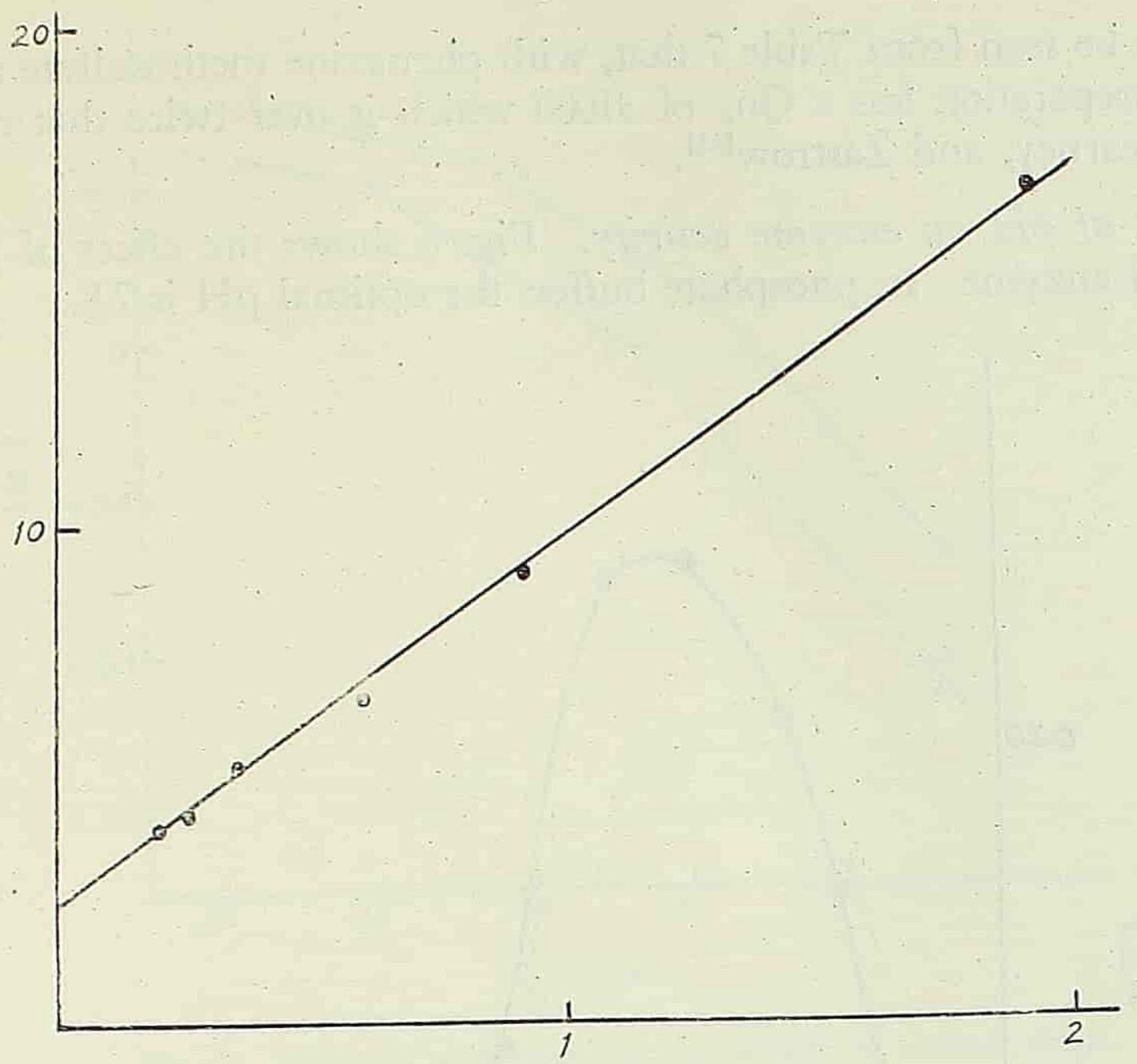

Fig. 5. Effect of ferricyanide concentration on the activity of succinic dehydrogenase. The reaction mixture contained 52 mM phosphate buffer, pH. 7.8, 30mM of succinate, the required concentration of ferricyanide and 0.0687 mg enzyme *N*. The enzyme preparation used had a specific activity of 17 and the reaction was carried out at room temperature (about 30°C). The reciprocals of the reaction velocities (optical density decrease at 420 mμ per 5 min.) are plotted against the reciprocals of initial ferricyanide concentrations according to Lineweaver and Burk.

With phenazine methosulphate as acceptor, the reaction rate, in terms of succinate oxidation, is much more rapid than with ferricyanide. Methylene blue is much less efficient as an acceptor than ferricyanide and with cytochrome *c*, the reaction rate is barely measurable. These results are summarized in Table 7.

Table 7. A Comparison of Different Acceptors.

Acceptor	Concentration, mM	Temperature, °C	Relative[3] Activity	Qo_2 (μl 0_2/hr/mg protein)
Ferricyanide	5	38	1	3600
Phenazine methosulphate[1]	25	38	8.5	31000
Methylene blue[2]	0.45	25	1/7	
Cytochrome *c*[2]	0.037	25	1/200	

(1) Measured exactly as described by Kearney *et al*[28].
(2) Measured anaerobically.
(3) Relative activities are calculated as the number of moles of succinate oxidized per minute and expressed relative to the activity with ferricyanide which is arbitrarily taken as unity.

It can be seen from Table 7 that, with phenazine methosulfate as acceptor, our best preparation has a Qo_2 of 31000 which is over twice that reported by Singer, Kearney, and Zastrow[12].

Effect of pH on enzyme activity. Fig. 6 shows the effect of pH on the solubilized enzyme. In phosphate buffer, the optimal pH is 7.8.

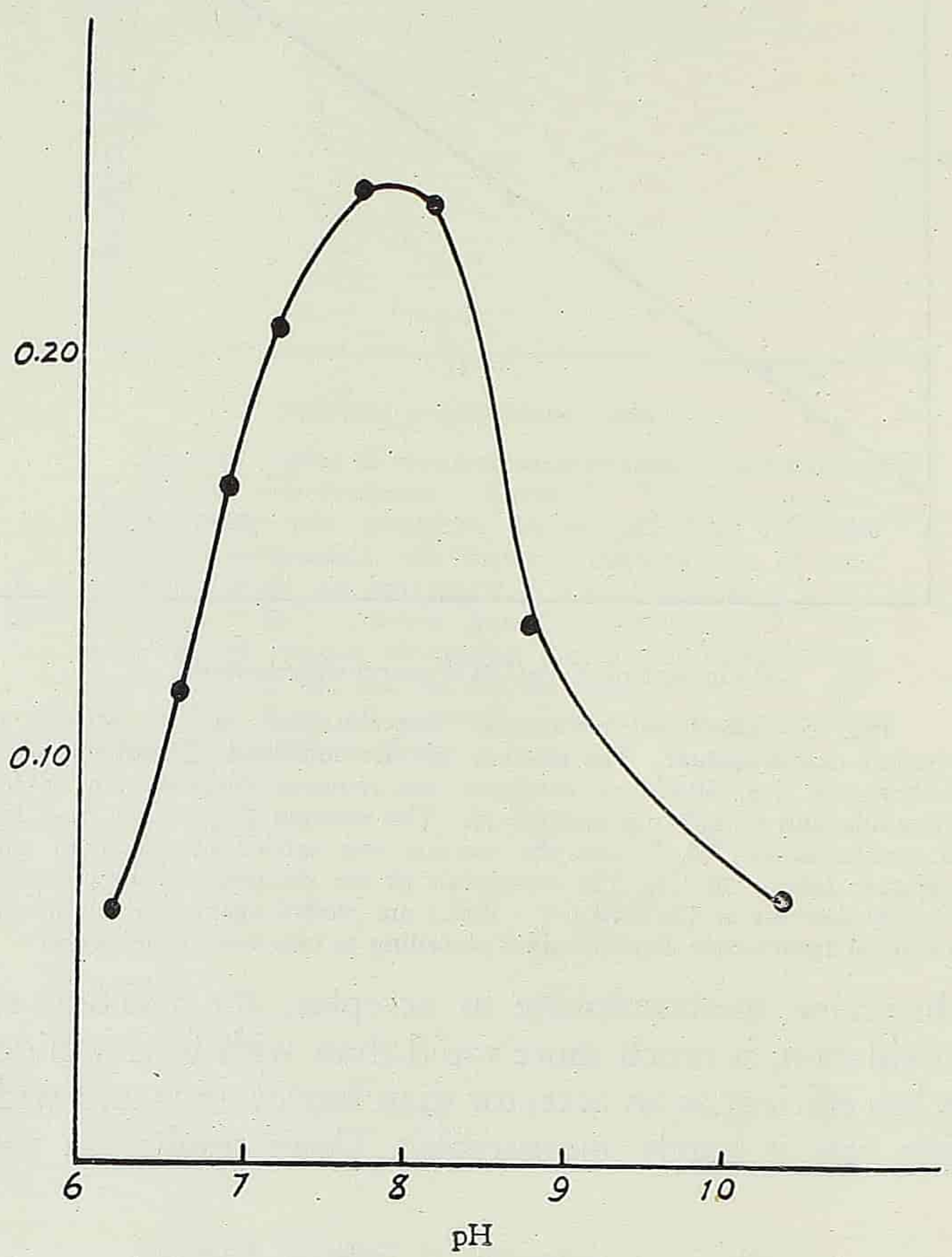

Fig. 6. Effect of pH on the activity of succinic dehydrogenase. The reaction mixture contained 30 mM succinate, 2 mM of ferricyanide, 0.079 mg of enzyme *N* (specific activity, 41) and 53 mM of phosphate at the required pH. Room temperature about 28°C. The exact pH value of each reaction mixture was determined after 10 min. reaction by the glass electrode.

Effect of temperature on enzyme activity. The effect of temperature on the enzyme activity before and after succinate activation has also been studied and the Arrhenius plots obtained are shown in Fig. 7. It can be seen that the activation energy remains constant only in a narrow temperature range and that at higher temperatures activation energy values become lower. The enzyme seems to have the same activation energy before and after succinate activation, although it appears that for the substrate activated enzyme the

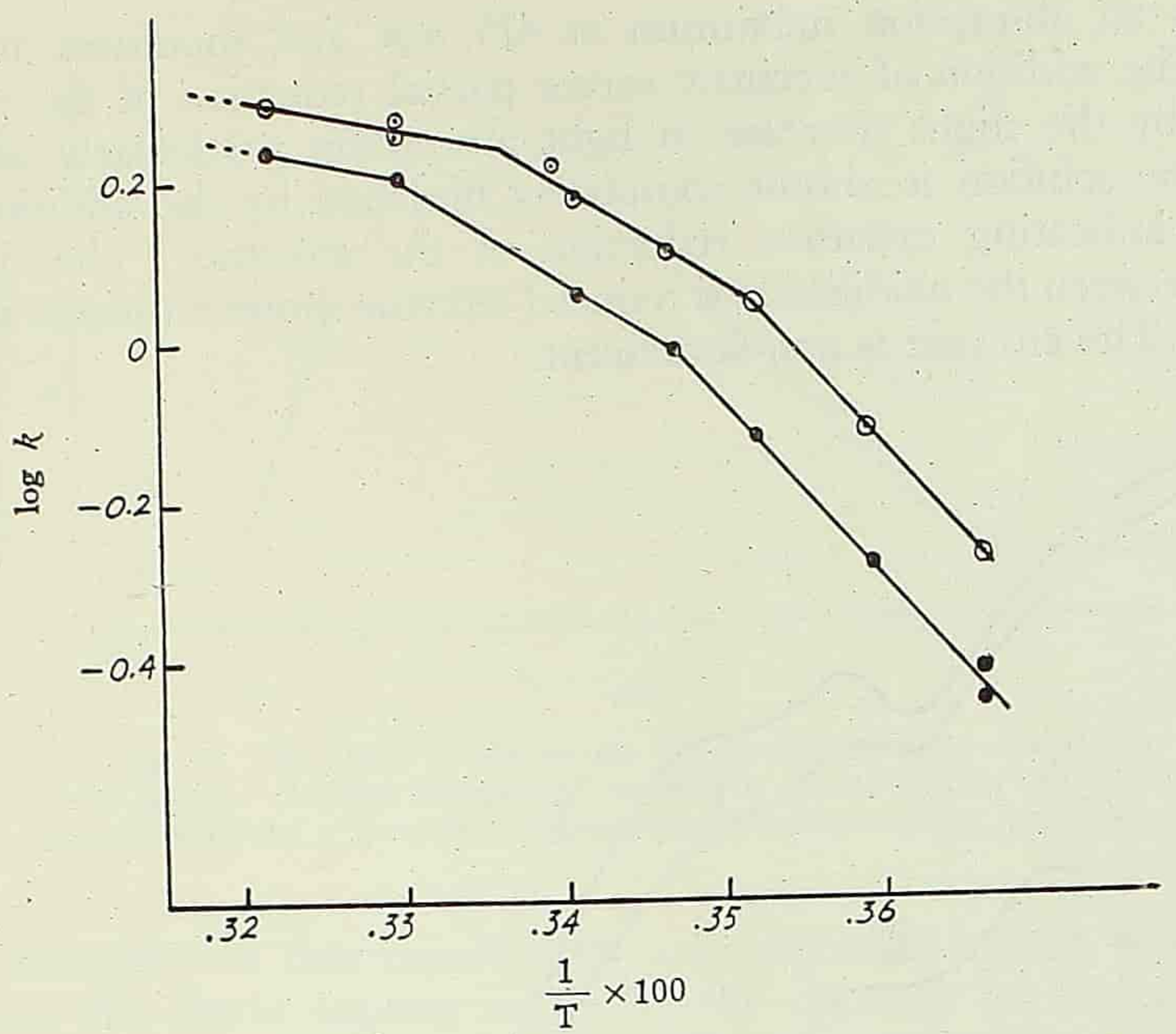

Fig. 7. Effect of temperature on the activity of succinic dehydrogenase. Reaction carried out as described in the section on methods. The logarithm values of the optical-density changes in 10 min. are plotted against the reciprocals of absolute temperatures. The upper curve is for the enzyme previously activated by incubation with succinate for 5 days at 0 °C under vacuum and the lower curve is for the enzyme without succinate activation.

critical temperatures of transition from one value of activation energy to another tend to be lower. The activation energy values obtained from the graphs are summarized in Table 8.

Table 8. Activation Energy Values for the Succinic Dehydrogenase-catalyzed Oxidation of Succinate by Ferricyanide.

Activation Energy, cal.	Temperature Range, °C	
	Before Incubation with Succinate	After Incubation with Succinate
10200	0—15	0—10
5800	15—30	10—23
2380	30—38	23—38

Some Preliminary Observations on the Prosthetic Group of the Enzyme

Colour and absorption spectra of purified enzyme. The highly purified enzyme solution is perfectly clear and is strongly amber coloured. Fig. 8 shows

that it has an absorption maximum at 415 mμ and shoulders at 460 and 360 mμ. The addition of succinate causes partial reduction of the enzyme as evidenced by the slight decrease in light absorption particularly at 460 mμ. The enzyme solution is almost completely bleached by the addition of Na-dithionite, indicating extensive reduction of the enzyme. The differential spectrum between the oxidized and reduced enzyme shows a distinct maximum at 460 mμ. The enzyme is non-fluorescent.

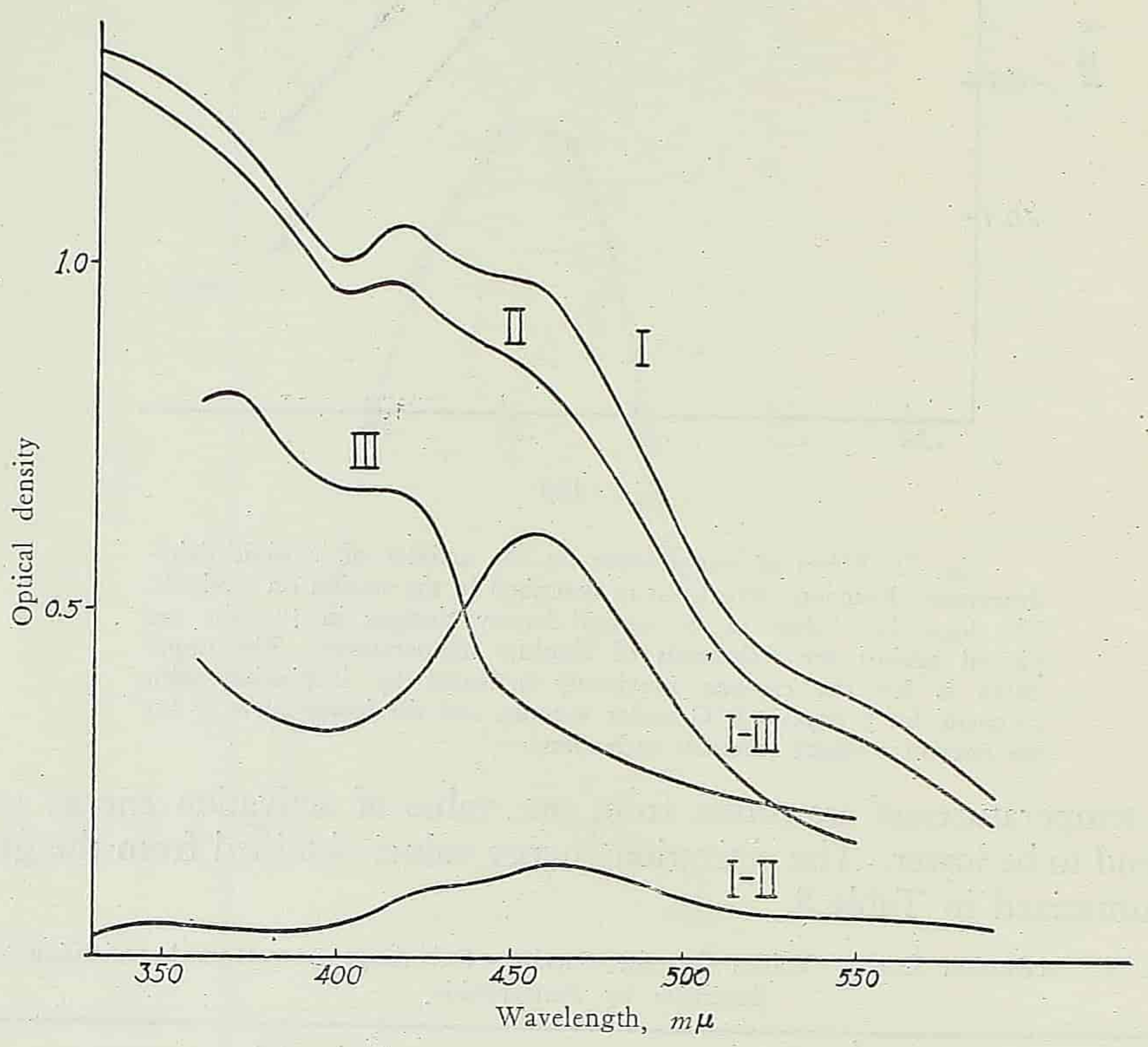

Fig. 8. Absorption spectra of succinic dehydrogenase. Light absorption measured in Beckman spectrophotometer with 5 mm cuvette. Curve I shows the absorption spectrum of a highly purified succinic dehydrogenase (same enzyme preparation as used in Fig. 3) with a concentration of 1 mg enzyme N/ml. To 1.5 ml of the above solution was added 0.02 ml of 0.8 M succinate and the resulting spectrum is shown by curve II (concentration change by dilution corrected). Curve III shows the fully reduced enzyme solution after the addition of sodium dithionite. Curves I-II and I-III are obtained by subtraction of curves II and III respectively from curve I.

Iron and flavin content. When the highly purified enzyme solution is digested with crystalline trypsin and crystalline chymotrypsin, the colour gradually changes from amber to a bright lemon yellow, the activity is lost and it now shows distinct greenish yellow fluorescence, the intensity of which varies with the pH of the medium (Fig. 9). Highly purified enzyme preparation also contains iron. Both the iron and the flavin contents increase with the specific activity of the enzyme in the later stages of purification.

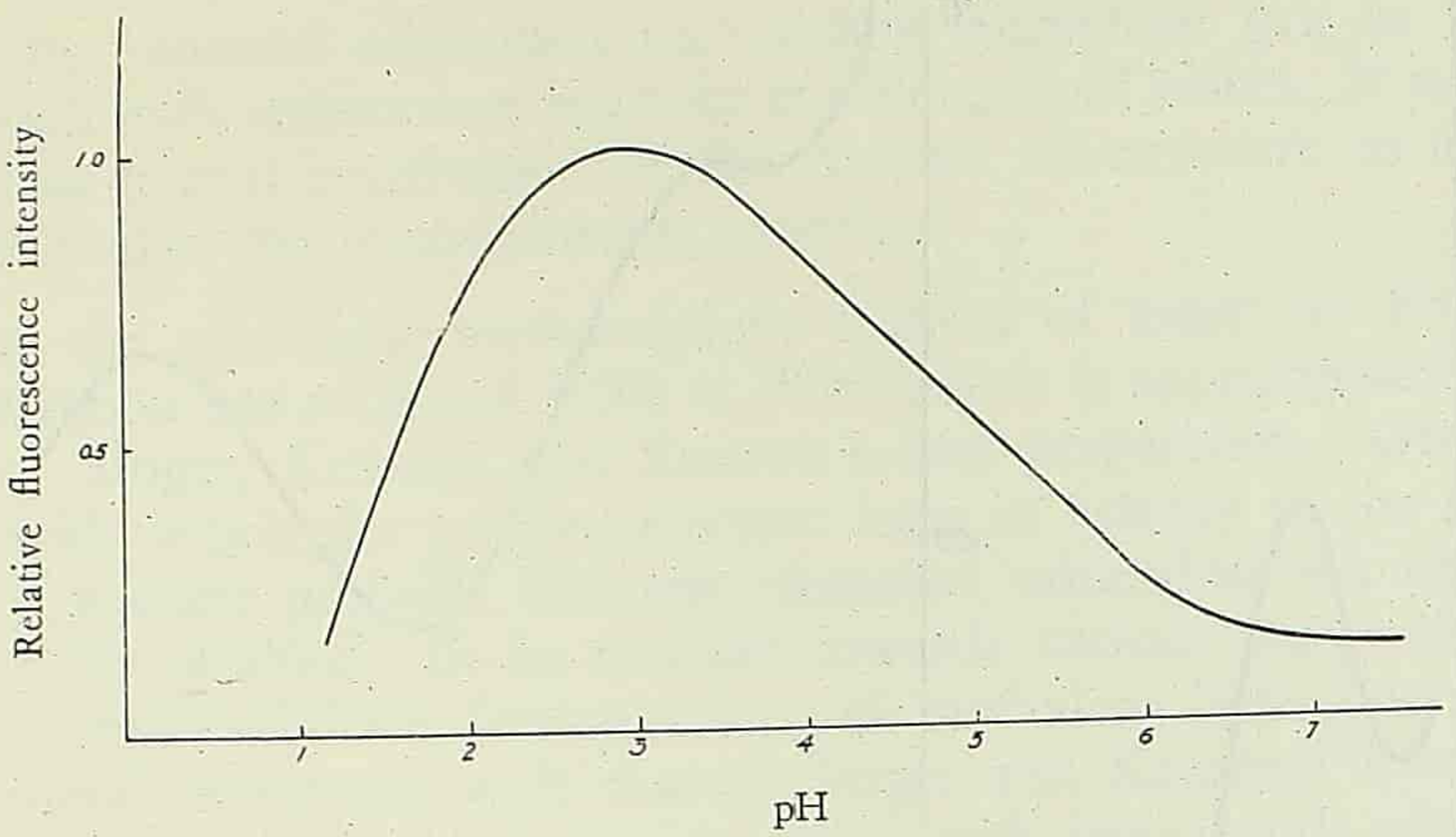

Fig. 9. The effect of pH on the fluorescence intensity of the prosthetic group. Relative fluorescence intensity is plotted against pH. The sample used was a proteolytic enzymes-digested-dehydrogense preparation.

The iron content was determined after acid digestion by the α, α'-dipyridyl method and the flavin content either by the decrease in absorption at 450 mμ after Na-dithionite reduction or from the intensity of fluorescence at pH 3 after being treated with proteolytic enzymes and calculated on the assumption that the intensity is the same as flavin-adenine dinucleotide[31]. It was found that the highly purified enzyme contained 1 gram-mole of flavin and 4 gram-atoms of iron for every 140,000–160,000 grams of the enzyme protein. Occasionally, lower iron to flavin ratio was found in certain preparations of lower specific activity. Both the iron and the flavin components are tightly bound to the protein part of the enzyme and cannot be removed by prolonged dialysis or repeated precipitation of the enzyme with ammonium sulphate. When the enzyme solution has been digested by treatment with proteolytic enzymes, the absorption spectrum of the solution is also changed, so that it no longer shows an absorption maximum at 415 mμ, and the 460 mμ shoulder is shifted to 450 mμ. All these seem to indicate that both iron and flavin are integral parts of succinic dehydrogenase. It also appears probable that the 415 mμ maximum is due to the linkage between the prosthetic group and the protein.

Separation of the flavin prosthetic group. After proteolytic digestion, the enzyme solution was acidified and made 0.7 saturated with ammonium sulphate by the addition of the solid salt. The prosthetic group* was then extracted into *p*-cresol and thoroughly washed by acid ammonium sulphate solution. It was again transferred into aqueous solution by adding ether to the *p*-cresol solution, precipitated as the mercury salt and the latter decomposed

*In what follows the word "prosthetic group" refers to the product of proteolytic action which contained the flavin prosthetic group of the enzyme.

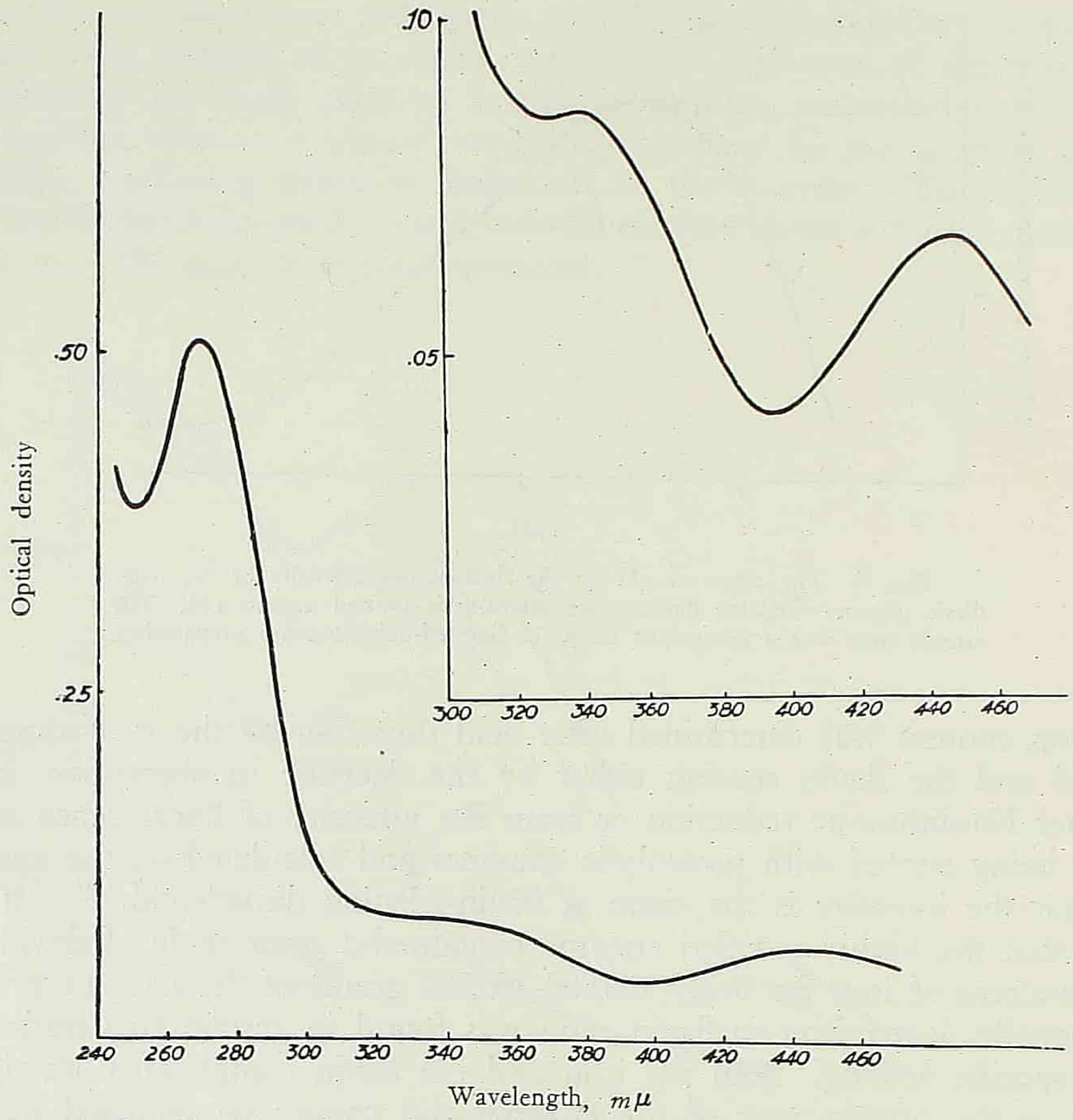

Fig. 10. Absorption spectrum of the isolated prosthetic group. The insert shows the absorption spectrum in the violet region in greater detail.

by hydrogen sulphide. This is essentially the method of Warburg and Christian[32] for the purification of flavin-adenine dinucleotide.

The prosthetic group was thus obtained as a yellow aqueous solution, showing greenish yellow fluorescence, and has an absorption spectrum as shown in Fig. 10, with maxima at 270, 340, and 450 mμ. It is bleached by reduction with Na-dithionite and the reduced solution is no longer fluorescent. The fluorescent intensity of the prosthetic group varies with pH and shows a maximum at pH 3. This property is similar to that reported in the literature for flavin-adenine dinucleotide[31, 33]. It has some flavin-adenine dinucleotide activity in the *D*-amino acid oxidase test.

Discussion

From the electrophoretic pattern it is seen that the purified preparation of succinic dehydrogenase obtained by our procedure is practically homogeneous except for a small trace of protein with higher mobility which could not be

removed by repeated adsorption on calcium phosphate gel, or by further fractionation with ammonium sulphate at different pH values. It is interesting to note that partial inactivation of the enzyme by exposure to air did not significantly alter the electrophoretic pattern.

Using the phenazine methosulphate method of assay we find that our best preparation has a Qo_2 of 31000 at 38°C which is approximately twice the activity of Singer, Kearney and Zastrow's best perparation. Owing to the rapidity with which the purified enzyme loses its activity in the presence of oxygen, it is quite probable that our estimated value does not represent the actual activity attained. In its reaction towards various acceptors, especially phenazine methosulphate, ferricyanide, and methylene blue, our preparation shows general agreement with that of Singer and Kearney[11], except for a somewhat lower activity of their preparation with ferricyanide which may be due to the use of a suboptimal concentration of the acceptor in their assay system. According to Kearney, Singer and Zastrow[28], a purified sample of the enzyme prepared in non-phosphate medium showed a specific requirement for inorganic phosphate. At its saturation requirement which occurred at or above 0.05 M of phosphate, the enzyme activity was many times higher than that at or below 0.005 M of phosphate. Our purified preparation also exhibits optimal activity at or above a phosphate concentration of 0.05 M, but in disagreement with the observations of these workers[28] it shows no spectacular drop of activity when the assay is carried out in borate or imidazole buffer without the addition of phosphate (a direct determination of phosphate in the test system gave a phosphate concentration of less than 3.8×10^{-5} M). The cause of this discrepancy is still unknown.

The results of our investigations have established the metalloflavoprotein nature of the enzyme specifically concerned with the activation of succinate. The metal involved is non-haematin iron which can be liberated from the protein by denaturation. The flavin prosthetic group is very firmly bound to the apoenzyme and cannot be dissociated from the latter by ordinary treatments, including heat denaturation in weak acid solutions. On boiling the enzyme in dilute acid solution, the iron is split off while the flavin prosthetic group remains attached to the precipitate of denatured protein imparting to it a lemon-yellow colouration. In this property the enzyme differs from the other known flavin-containing enzymes.

The chemical constitution of the flavin prosthetic group as well as the mode of function of the enzyme in the dehydrogenation of succinate is under investigation.

Summary

1. Succinic dehydrogenase has been extensively purified from an aqueous *n*-butanol extract of modified Keilin-Hartree heart muscle preparation by a

procedure which involves adsorption on calcium phosphate gel and repeated fractionation with ammonium sulphate at low temperatures. The final preparation obtained is almost electrophoretically pure and has a specific activity of about 40 times that of the heart muscle preparation and nearly 200 times that of a heart muscle homogenate.

2. The effects of temperature, substrate concentration, acceptors and other factors on the enzyme activity have been studied.

3. The purified enzyme is a metalloflavoprotein containing non-haematin iron. An analysis of the purified enzyme gives a ratio of 140,000–160,000 grams of protein to 1 gram-molecule of flavin or 4 gram-atoms of iron.

References

[1] Wang, Ying-Lai, Tsou, Chen-Lu, and Wang, Tsing-Ying. 1955. 3rd. Int. Congress of Biochem. Brussels.
[2] Tsou, Chen-Lu, 1951. *Biochem. J.*, **49**, 512.
[3] Bach, S. J., Dixon, M., and Zerfas, L. G., 1946. *Biochem. J.*, **40**, 229.
[4] Ball, E. C., Anfinson, E. B., and Cooper, C., 1947. *J. Biol. Chem.*, **168**, 257.
[5] Pappenheimer, A. M., and Hendee, E. D., 1949. *J. Biol. Chem.*, **180**, 597.
[6] Chance, B., 1952. *J. Biol. Chem.*, **197**, 567.
[7] Axelrod, A. E., Potter, V. R., and Elvehjem, C. A., 1942. *J. Biol. Chem.*, **142**, 85.
[8] Wang, Tsing-Ying, and Wang, Ying-Lai (unpublished results).
[9] Morton, R. K., 1950. *Nature*, **166**, 1092.
[10] Neufeld, H. A., Scott, C. R., and Stotz, E., 1954. *J. Biol. Chem.*, **210**, 869.
[11] Singer, T. P., and Kearney, E. B., 1954. *Biochem. Biophys. Acta*, **15**, 151.
[12] Singer, T. P., Kearney, E. B., and Zastrow, N., 1955. *Biochem. Biophys. Acta*, **17**, 154.
[13] Singer, T. P., and Kearney, E. B., 1955. *Fed. Proc.*, **14**, 282.
[14] Tsou, Chen-Lu, 1952. *Biochem. J.*, **50**, 493.
[15] Tsou, Chen-Lu and Li, Wen-Chieh, 1955. *Acta Physiologica Sinica*, **19**, 361.
[16] Negelein, E., and Brömel, H., 1939. *Biochem. Z.*, **300**, 225.
[17] Kunitz, M., and Northrop, J. H., 1936. *J. Gen. Physiol.*, **19**, 991.
[18] McDonald, M. R., and Kunitz, M., 1946. *J. Gen. Physiol.*, **29**, 155.
[19] Tsou, Chen-Lu, 1951. *Biochem. J.*, **49**, 362.
[20] Stocken, L. A., 1947. *J. Chem. Soc.*, 952.
[21] Straub, F. B., 1938. *Nature*, **141**, 603.
[22] Keilin, D., and Hartree, E. F., 1937. *Proc. Roy. Soc.* B, **124**, 397.
[23] Kehrmann, F., und Havas, E., 1913. *Ber.*, **46**, 343.
[24] Smith, R., Bullock, J. L., Bersworth, F. C., and Martell, A. E., 1949. *J. Org. Chem.*, **14**, 355.
[25] Wu, Chin-Yung, and Tsou, Chen-Lu, 1955. *Scientia Sinica*, **4**, 137.
[26] Levin, R., and Brauer, R. W., 1951. *J. Lab. Clin. Med.*, **38**, 474.
[27] Bücher, Th., 1947. *Biochem. Biophys. Acta*, **1**, 292.
[28] Kearney, E. B., Singer, T. P., and Zastrow, N., 1955. *Arch. Biochem. Biophys.*, **55**, 579.
[29] Lineweaver, H., and Burk, D., 1934. *J. Amer. Chem. Soc.*, **56**, 658.
[30] Thorn, M. B., 1953. *Biochem. J.*, **54**, 540.
[31] Bessey, O. A., Lowry, O. H., and Love, R. H., 1949. *J. Biol. Chem.* **180**, 755.
[32] Warburg, O., and Christian, W., 1938. *Biochem. Z.*, **298**, 150.
[33] Weber, G., 1950. *Biochem. J.*, **47**, 114.

A COMPARATIVE, PHYSICO-CHEMICAL STUDY OF TROPOMYOSINS FROM DIFFERENT SOURCES*

TSAO TIEN-CHIN (曹天欽), TAN PEI-HSING (譚佩幸), and PENG CHIA-MU (彭家睦)

(Institute of Physiology and Biochemistry, Academia Sinica)

I. INTRODUCTION

Our knowledge of and speculations on the possible structure and function of tropomyosin have been based, as in the case of actin and myosin, chiefly on the investigations of the rabbit or the frog skeletal muscle. Recently an increasing number of reports have appeared[1–29], which drew attention to the contractile apparatus of the smooth and the cardiac muscles as well as the striated muscle of animals other than the rabbit or the frog. Considerations were also given to the changes of protein components of muscle during drastic physiological or pathological changes such as embryonic development, enlargement of uterus during pregnancy, atrophy and dystrophy, metamorphosis, etc. These studies concerned mainly the activity of adenosine triphosphatase, the contents and properties of actin, myosin and adenosine triphosphate and the interaction of the three. They serve to establish the essential similarity of the contractile apparatus in muscles from different sources, and at the same time reveal a number of significant variations, both in quantity and quality, in their enzymic or structural make-up. These differences, no less than the similarities, should naturally be borne in mind in any attempt at the elucidation of the contractile mechanism of muscle.

There is at present no definite clue to the physiological function of another structural protein, tropomyosin. Is it the substrate for the contractile or holding function of muscle, or does it play yet other roles in muscle physiology? The structure and the physico-chemical properties of rabbit skeletal tropomyosin were already the subjects of extensive investigations and the size, shape and aggregation of this molecule[30], its amino acid composition[31, 32] and its terminal structure[33, 34] are now fairly well known. With regard to tropomyosins from other sources, Bailey[31] prepared tropomyosins from whiting, and horse and pig hearts; Hamoir[35, 36] investigated the ultracentrifugal and

---

*First published in Chinese in *Acta Physiologica Sinica,* Vol. XIX, Nos. 3-4, pp. 389—406, 1955.

electrophoretic behaviour of carp nucleotropomyosin; and quite recently Snellman and Tcnow[37] reported the isolation from human and bovine uteri the so-called contractile "actotropomyosin", the existence of which we disputed in an earlier paper. In this laboratory we have modified Bailey's classical procedures and evolved a general method[38] for the isolation of tropomyosins from the skeletal, the cardiac and the smooth muscles of cow, pig, rabbit, rat, pigeon, duck, snake, toad, carp, shell carp and crab. We have also demonstrated that during the later stages of embryonic development and throughout the course of pregnancy the tropomyosin content of the respective bovine foetus and uterus appeared to remain constant. In those investigations, the differences in crystalline form, in ribonucleic acid content, and in viscosity behaviour suggested to us that there might be significant differences in the macromolecular structure of tropomyosins from different sources. This contention has now been confirmed experimentally. The aim of this paper is to present the results with regard to the size, shape, polymerizability, solubility and electrophoretic mobility of tropomyosins from different types of muscle. The isolation and crystallization of tropomyosins from sepia mantle, from the body muscle of prawn and from the foot and adductor muscles of bivalves will also be described. The determination of the yet deeper differences in chemical structure will be the substance for a later communication.

II. Experimental

I. *Biological material.*

We selected pig heart, duck gizzard, sepia mantle and the body muscle of prawn as our experimental material for subsequent physico-chemical studies. Cold-preserved sepia (*Sepia esculenta*) and prawn (*Penaeus orientalis*) were obtained from a fishmonger, and fresh pig heart and duck gizzard from the local slaughter-house; they were kept in crushed-ice during transport. Of these we chose the pig heart and the duck gizzard to represent respectively cardiac and smooth muscles of vertebrates, and the prawn and the sepia mantle to be examples of striated and smooth muscles of invertebrates. The bivalves employed were *Anodonta pacifica Heude* and *Cristaria plicata Leach.*

2. *Extraction, purification and crystallization of tropomyosin.*

Pig heart, sepia mantle and bivalve foot tropomyosins were prepared according to Bailey's classical procedures[31, 33]. The method for the preparation of duck gizzard tropomyosin was described in a previous paper of ours[38].

The texture of the prawn muscle and the solubility behaviour of the extracted tropomyosin differ considerably from other muscle systems, thus necessitating slight alterations of the usual procedures. The body muscle of the prawn was cut into large lumps and immersed in 3 volumes of ethanol

overnight. The partially dehydrated lumps were then chopped into a finer state and again soaked in a fresh change of ethanol. This was followed by another change of ethanol and two changes of ether, and the debris was allowed to dry in air. The dehydrated muscle was extracted with neutral M KCl or NaCl, and the subsequent steps followed closely those outlined by Sheng and Tsao[38], except that the salting-out range of the prawn tropomyosin was between 15 and 30% saturation of ammonium sulphate instead of 40–70% as for all the other tropomyosins so far investigated. The ammonium sulphate paste thus prepared bears the appearance of a transparent gel.

All the above-mentioned tropomyosins were purified three or four times, and were electrophoretically homogeneous in a versonal buffer, pH 8.5, or a phosphate buffer, pH 6.5.

As the available amount of tropomyosins derived from the foot and adductor muscles of bivalves was much limited, we only carried out electrophoretic measurements and crystallization experiments with these proteins. Crystallization was effected by dialysis against 0.01 M sodium acetate pH 5.4, containing 16 g of ammonium sulphate per litre following the method initiated by Bailey[31]. Crystals of Anodonta foot muscle tropomyosin did not appear until after standing for a month in the ice-chest. The crystallization of prawn tropomyosin required a slightly higher ionic strength and a lower pH. An aqueous 2–3% solution of this tropomyosin was first dialyzed against 0.01 M sodium acetate, pH 5.8, containing 30 g of ammonium sulphate per litre. Overnight, 1 ml of M acetate buffer, pH 4.8, was added to each 100 ml of the dialysate. Crystals appeared in the course of one or two days. The various crystalline forms are given in plates I to III.

The samples of the bovine, the rat, the carp, the shell-carp, the crab, and the uterine tropomyosins used in electrophoretic experiments were those prepared by Sheng and Tsao[38].

3. *Analysis of nitrogen content and protein concentration.*

Purified samples were first dialysed against several changes of water, then against 0.1 M KCl to remove ammonium sulphate, and finally against several more changes of water to remove the last traces of all salt ions. Aliquots were taken for the determination of the dry weight of protein and the nitrogen content. Dry weight was the constant weight obtained after freeze-drying over P_2O_5. These data combined to give the total nitrogen content of each protein. The values for duck gizzard, pig heart, prawn and sepia tropomyosins were found to be respectively 15.5%, 15.0%, 17.7% and 19.0%. Bailey[31] reported a value of 16.7% for rabbit tropomyosin.

Protein concentrations were determined by the micro-Kjeldahl method[39], employing the total nitrogen values given above and expressed as g. protein 100 ml solution. Some samples were also analyzed with the aid of the Zeiss interferometer, the drum readings and concentrations for each protein having

previously been correlated in the form of a standard curve.

4. *Osmotic pressure measurements*

These were carried out at 1°C in the toluene osmometers of Adair[40]. Details were described in a previous paper (Chi and Tsao[41]). For the calculation of the particle weight, the ratio of pressure P (in mm Hg) and concentration C, P/C or log (P/C)[30], was plotted against C and the limiting value at zero concentration, obtained by the method of least squares, was employed.

5. *Viscosity measurements*

These were made in the Tsuda[42] horizontal capillary viscometer as described in another paper (Tan and Tsao[43]). The axial ratio of each tropomyosin was assessed by the use of Simha's equation[44, 45] from the value of intrinsic viscosity $[\eta]$.

6. *Flow birefringence*

This was observed with the aid of polaroid sheets.

7. *Determination of electrophoretic homogeneity and mobility*

The purity of protein preparations was examined in the Antweiler micro-electrophoresis apparatus. The electrophoretic mobility was measured at 0.5°C in a L.K.B. Tiselius-Svensson apparatus model 3021 B. The conductivity of protein and buffer solutions was measured with the aid of a Dr. Lange conductometer.

III. Results

1. *Polymerizability of tropomyosin*

In neutral, salt-free solutions, tropomyosin sols have an exceedingly high viscosity which decreases in a dramatic way as small amounts of salts are added. Simultaneously flow birefringence disappears. Physico-chemical investigations, such as electron optical observations[46] and measurements of viscosity, osmotic pressure[30] and light scattering[47], have demonstrated that rabbit tropomyosin molecules aggregate linearly to form fibrils in neutral, salt-free solutions and salt ions bring about depolymerization. We have examined the relative viscosity and the flow birefringence of solutions of duck gizzard, pig heart, prawn and sepia tropomyosins as a function of ionic strength, and have chosen the same protein concentration, 0.85%, in order to facilitate a direct comparison of the polymerizability. The results are shown in Figs. 1 and 2. The scale of the abcissa in Fig. 2 is four times that of Fig. 1 so as to make the differences in viscosity behaviour easily discernible. In both figures, the curve for rabbit tropomyosin is included for comparison; the portion <0.1 is taken from Bailey's paper[31] and the portion >0.1 com-

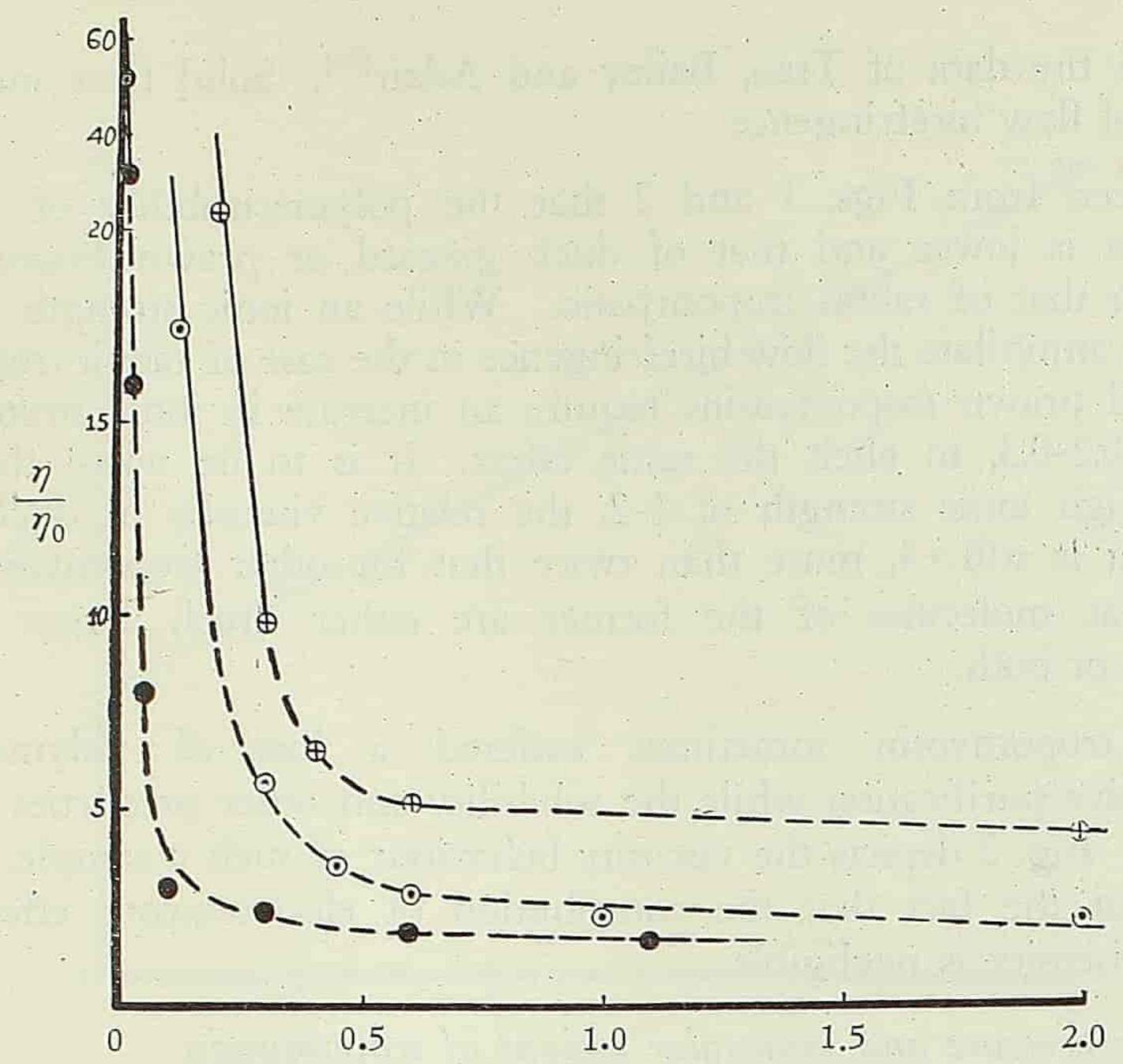

Fig. 1. Polymerization of tropomyosins as a function of ionic strength. (1) ● rabbit tropomyosin, ⊙ prawn tropomyosin, ⊕ duck gizzard tropomyosin. (solid lines signify possession of flow birefringence.)

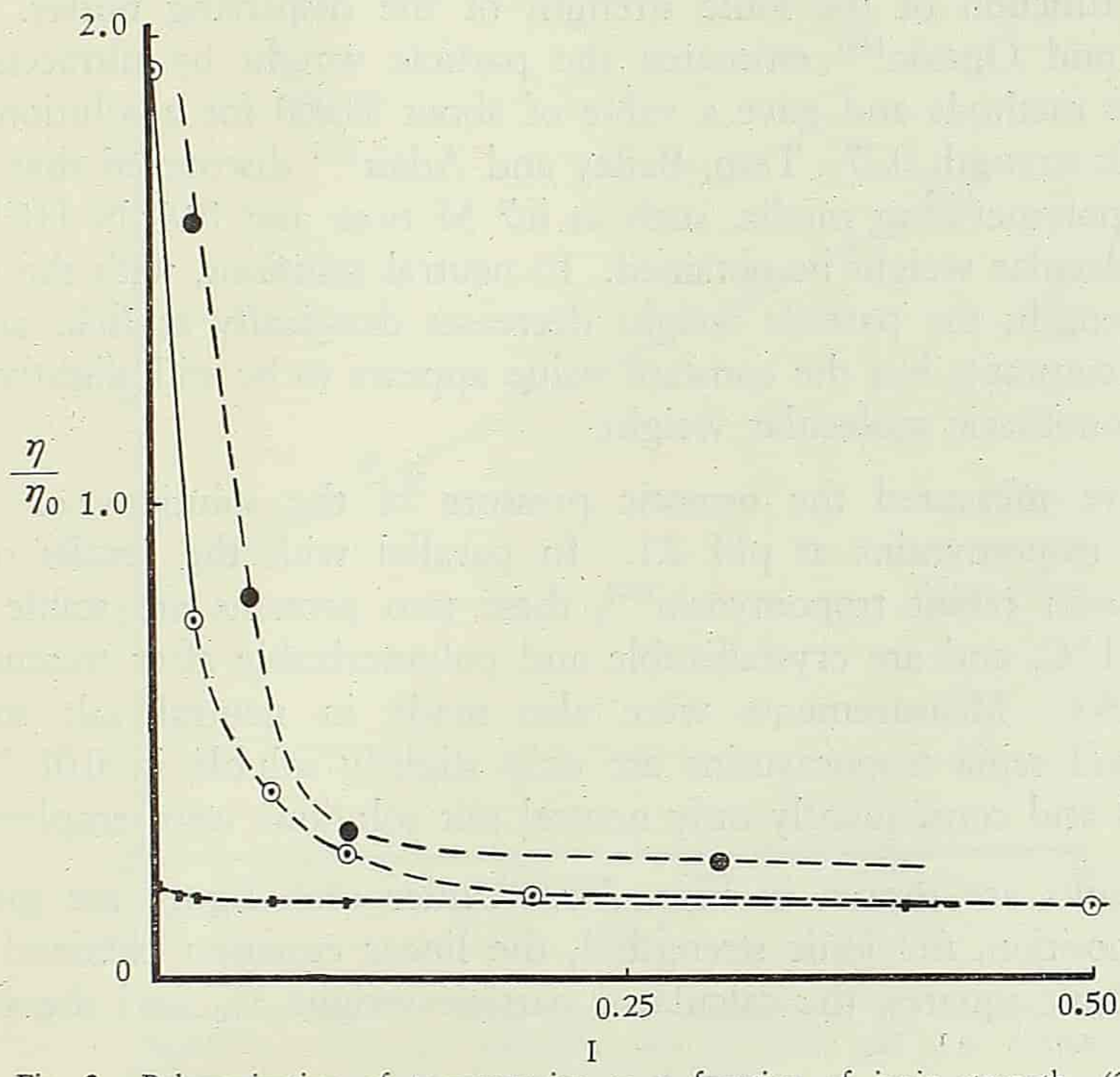

Fig. 2. Polymerization of tropomyosins as a function of ionic strength. (2) ● rabbit tropomyosin, ⊙ pig heart tropomyosin, ■ sepia tropomyosin. (solid lines signify possession of flow birefringence.)

puted from the data of Tsao, Bailey and Adair[30]. Solid lines indicate the possession of flow birefringence.

It is seen from Figs. 1 and 2 that the polymerizability of pig heart tropomyosin is lower and that of duck gizzard or prawn tropomyosin is higher than that of rabbit tropomyosin. While an ionic strength of 0.01 is sufficient to annihilate the flow birefringence in the case of rabbit tropomyosin, gizzard and prawn tropomyosins require an increase in ionic strength 20-30 times, i.e. 0.2–0.3, to elicit the same effect. It is to be noted that at the relatively high ionic strength of 1–2, the relative viscosity of duck gizzard tropomyosin is still >4, more than twice that for other tropomyosins. This signifies that molecules of the former are either much larger or more asymmetric or both.

Sepia tropomyosin sometimes suffered a loss of polymerizability upon excessive purification while the solubility and other properties remained unchanged. Fig. 2 depicts the viscosity behaviour of such a sample. It serves to bring out the fact that the contribution of electroviscous effect to the measured viscosity is negligible.

2. *Osmotic pressure and molecular weight of tropomyosin*

Previous investigations have shown that the particle weight of rabbit tropomyosin, owing to its reversible polymerizability and depolymerizability, is a sensitive function of the ionic strength of the dispersing buffer. Bailey, Gutfreund and Ogston[48] estimated the particle weight by ultracentrifugal and osmotic methods and gave a value of about 90,000 for a solution of pH 6.5 and ionic strength 0.27. Tsao, Bailey and Adair[30] discovered that only in strongly depolymerizing media, such as 6.7 M urea and 0.01 N HCl, could the true molecular weight be obtained. In neutral solutions, with the increase in ionic strength, the particle weight decreases drastically at first, and then approaches constant; but the constant value appears to be still slightly higher than the monomeric molecular weight.

We have measured the osmotic pressure of the solutions of gizzard and prawn tropomyosins at pH 2.1. In parallel with the results obtained previously with rabbit tropomyosin[30], these two proteins are stable at this low pH at 1°C, and are crystallizable and polymerizable after treatment for several weeks. Measurements were also made in neutral salt solutions. Pig heart and sepia tropomyosins are only slightly soluble in 0.01 N HCl, 0.09 M KCl and consequently only neutral salt solutions were employed.

The results are shown in Figs. 3–8. Under each figure are given the buffer composition, the ionic strength I, the linear equation obtained by the method of least squares, the calculated particle weight M_0 and the standard deviation.

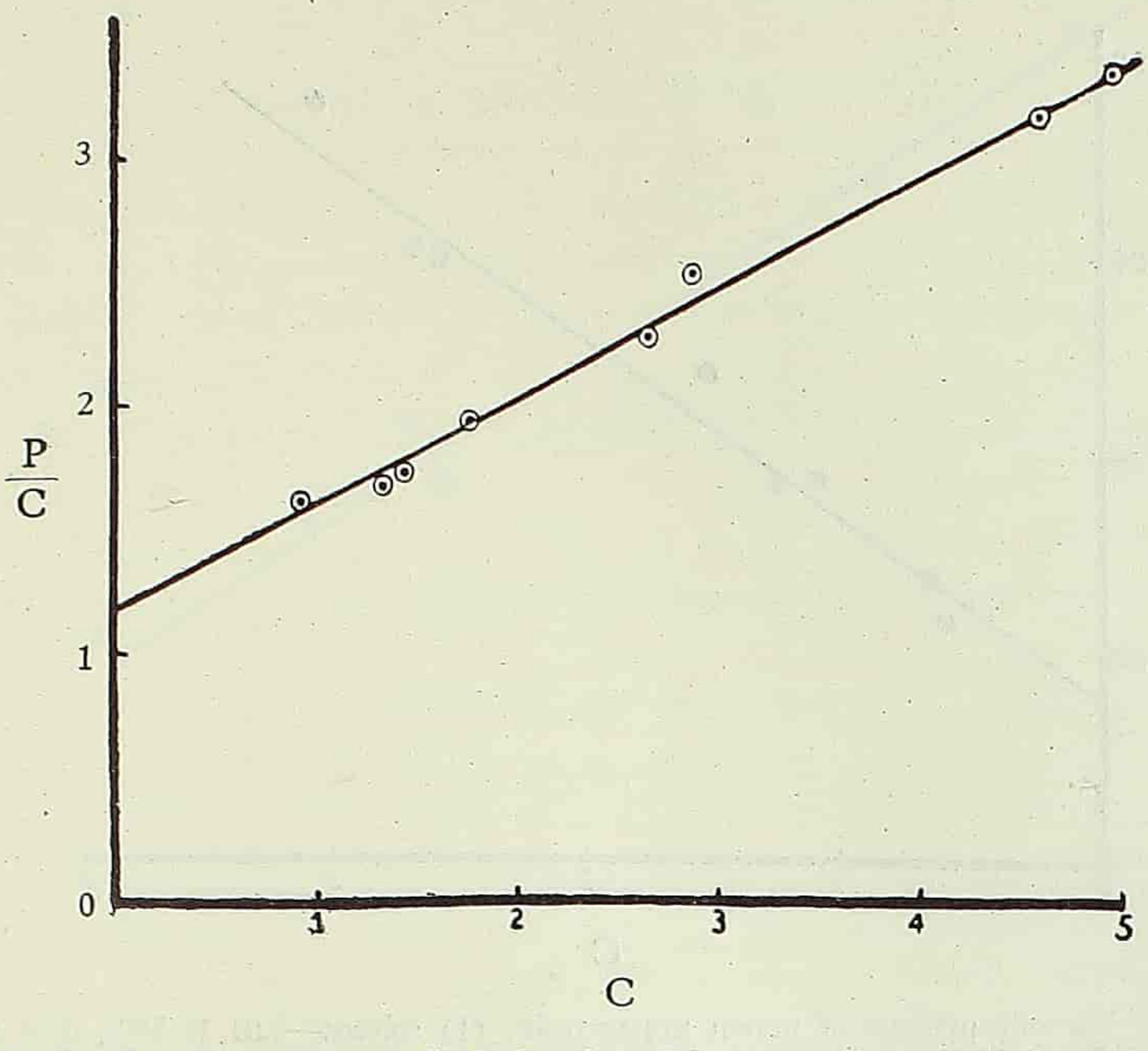

Fig. 3. Osmotic pressure of duck gizzard tropomyosin. (1) solvent—0.01 N HCl, 0.19 M KCl, pH 2.1, I=0.2. 1°C. P/C=0.450 C + 1.16, M_0=147,000±4,000.

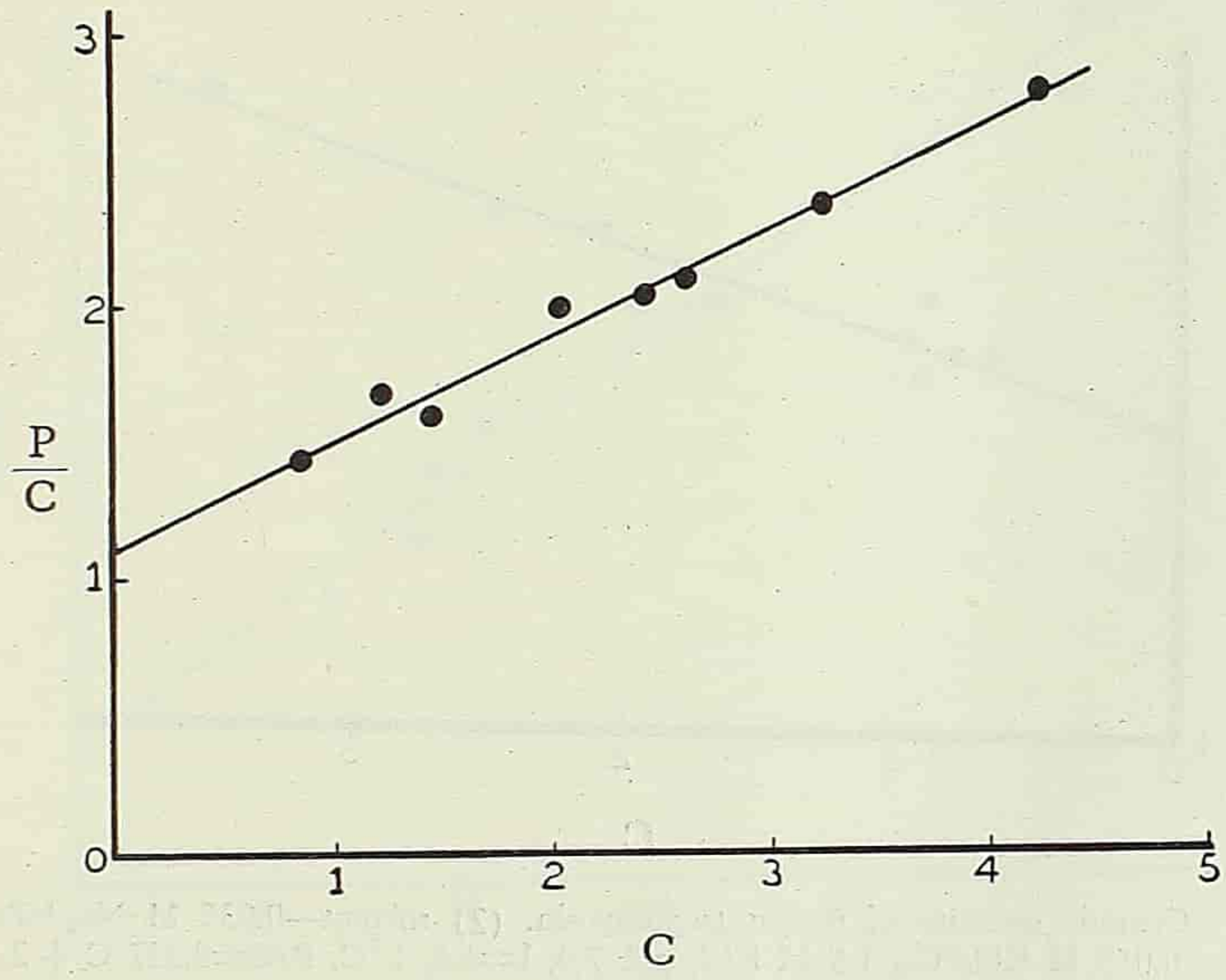

Fig. 4. Osmotic pressure of duck gizzard tropomyosin. (2) solvent—0.035 M Na_2HPO_4, 0.015 M KH_2PO_4, 0.5 M KCl, pH 7.0, I=0.6, 1°C. P/C=0.392 C + 1.11, M_0=153,000 ± 5,500.

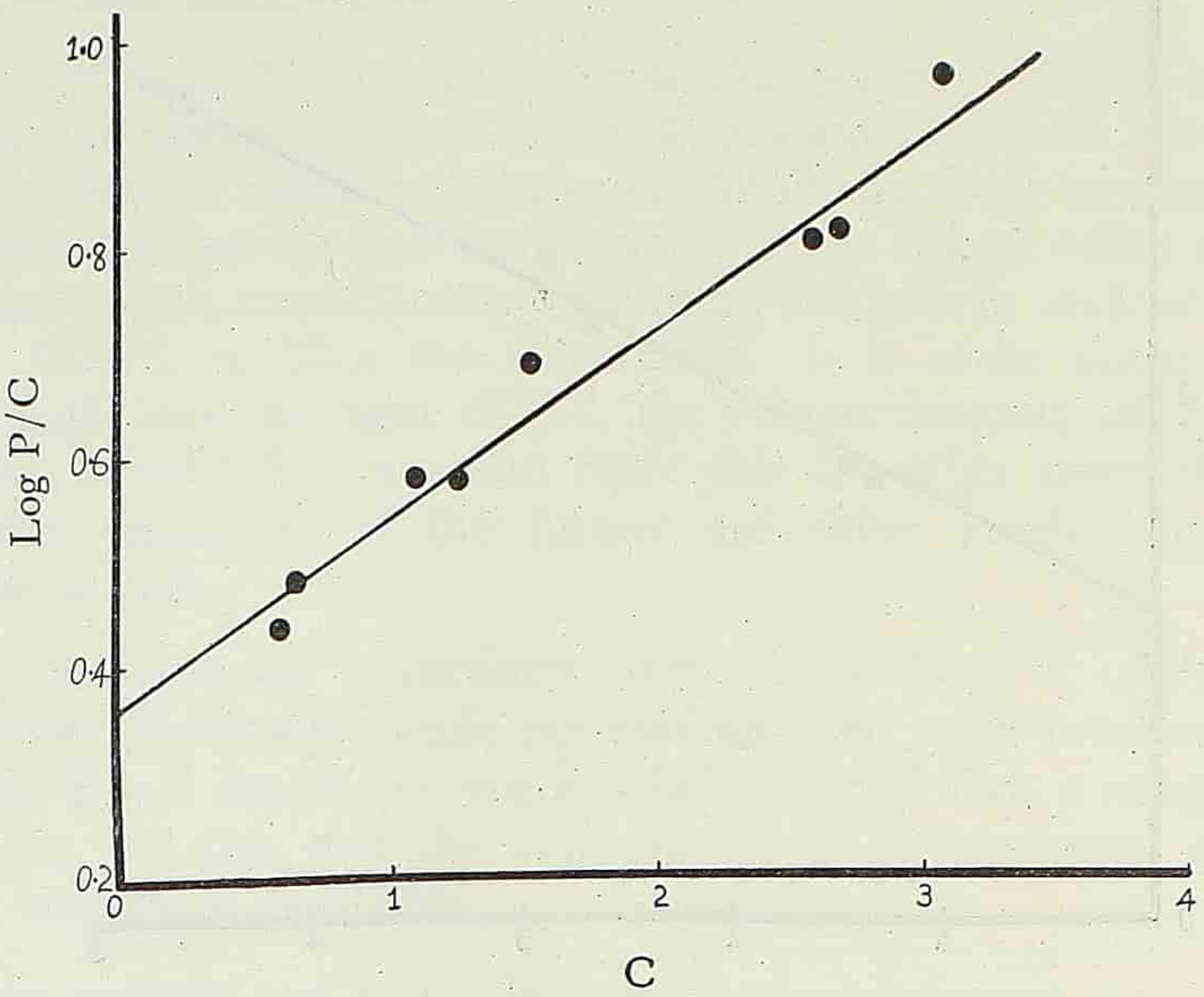

Fig. 5. Osmotic pressure of prawn tropomyosin. (1) solvent—0.01 N HCl, 0.09 M KCl, pH 2.1, I=0.1, 1°C, log (P/C)=0.185 C + 0.363, M_0 =74,000 ± 5,000.

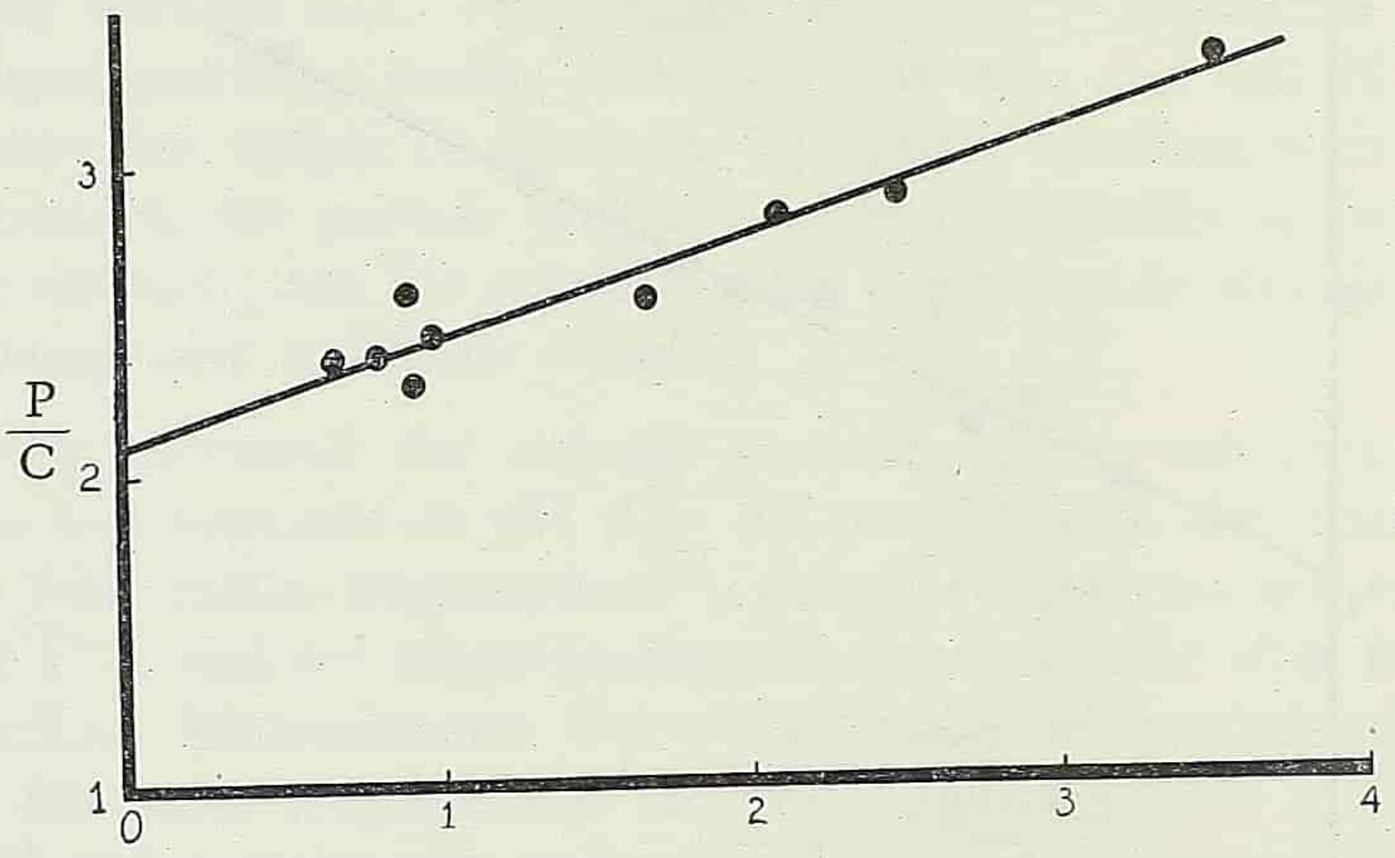

Fig. 6. Osmotic pressure of prawn tropomyosin. (2) solvent—0.035 M Na_2HPO_4 0.015 M KH_2PO_4, 1.5 M KCl, pH 7.0, I=1.6, 1°C. P/C=0.337 C + 2.12, M_0=80,000±3,000.

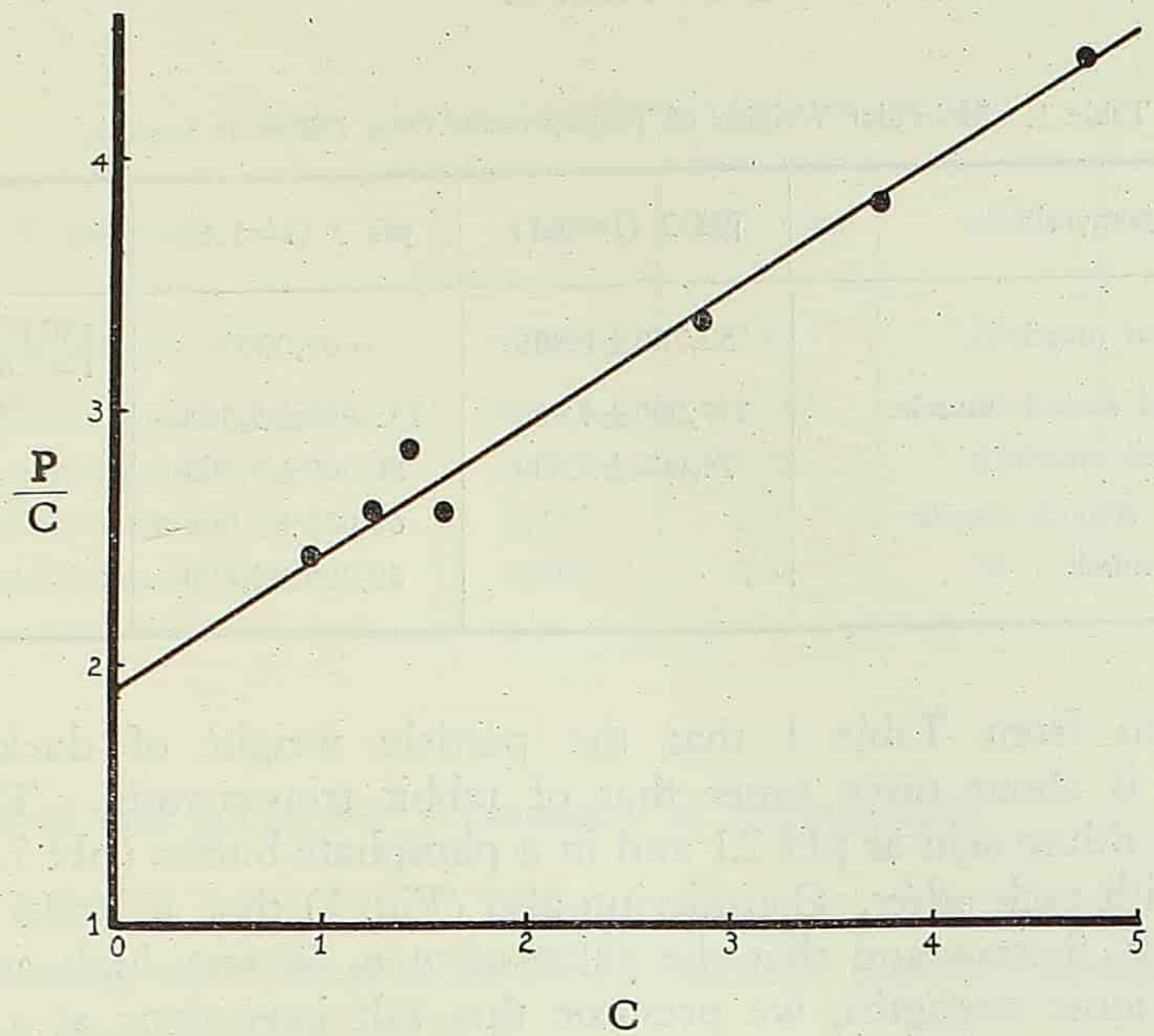

Fig. 7. Osmotic pressure of pig heart tropomyosin. solvent—same as in Fig. 6. 1°C
$P/C = 0.493\ C + 1.92$, $M_0 = 89{,}000 \pm 4{,}000$.

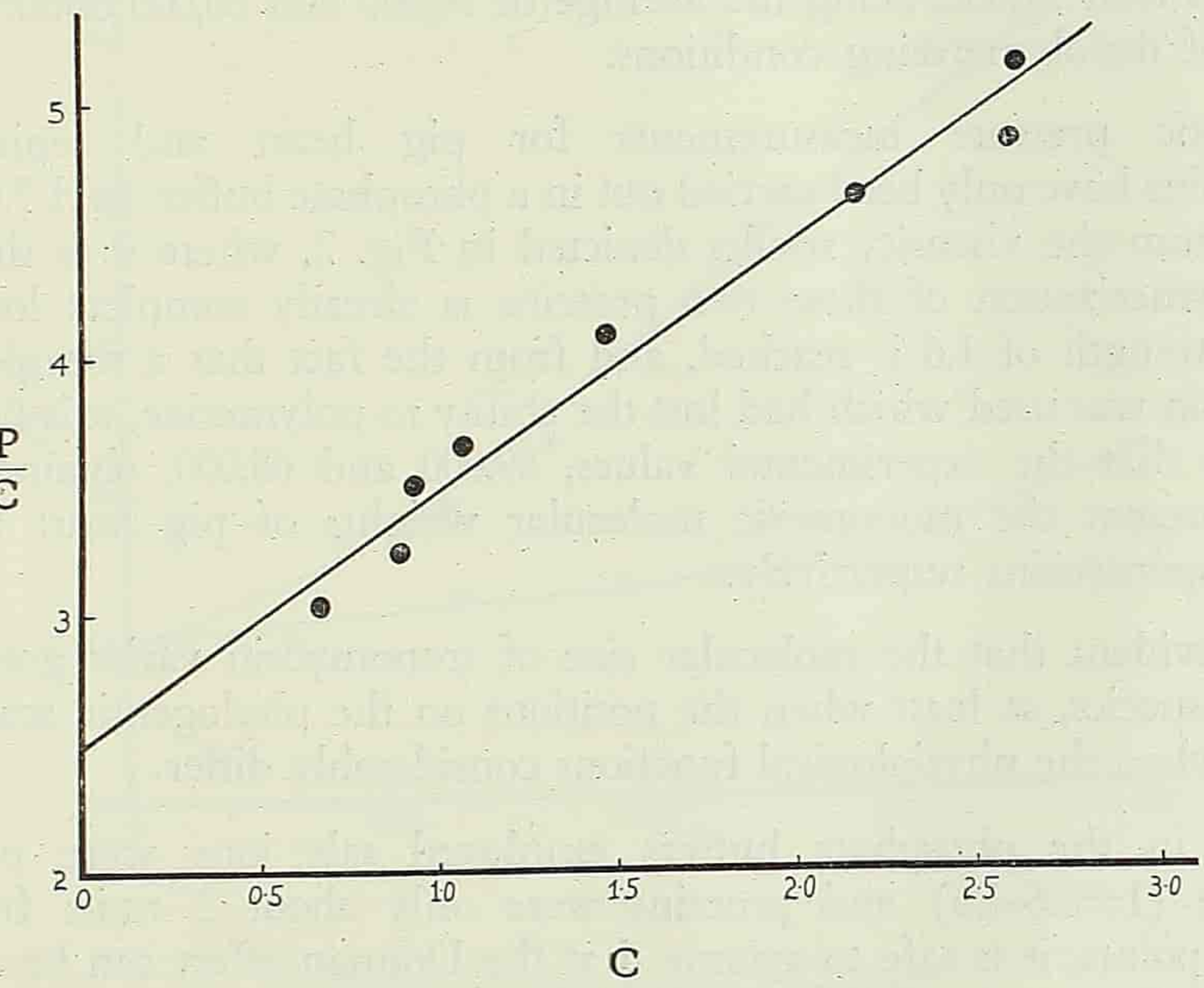

Fig. 8. Osmotic pressure of sepia tropomyosin. solvent—same as in Fig. 6. 0°C
$P/C = 0.983\ C + 2.50$, $M_0 = 68{,}000 \pm 2{,}000$.

The results are summarized in Table I.

Table 1. Molecular Weights of Tropomyosins from Different Sources.

Tropomyosin	pH 2 (I=0.1)	pH 7 (I=1.6)	Note
Rabbit striated muscle	52,700±1,800	~65,000*	(30)* pH 6.5 I=0.6-1.1 #I=0.2
Duck gizzard smooth muscle	147,000±4,000#	153,000±5,500	
Prawn striated muscle	74,000±5,000	80,000±3,000	
Sepia mantle smooth muscle		68,000±2,000	
Pig cardiac muscle		89,000±4,000	

It is seen from Table I that the particle weight of duck gizzard tropomyosin is about three times that of rabbit tropomyosin. The values obtained in a dilute acid at pH 2.1 and in a phosphate buffer (pH 7.0, I=0.6) agree well with each other. Considering also (Fig. 1) that at I=0.6 the curve η/η_0–I already flattens and that the value of η/η_0 is very high at this and even higher ionic strengths, we presume that salt ions alone at a sufficient concentration are capable of bringing about complete depolymerization of this protein. The experimental values, 147,000, or 153,000 (average 150,000), can therefore be regarded as the monomeric molecular weight of duck gizzard tropomyosin. Likewise, the molecular weight of prawn tropomyosin lies near 77,000, being the average of 74,000 and 80,000 obtained under two sets of depolymerizing conditions.

Osmotic pressure measurements for pig heart and sepia mantle tropomyosins have only been carried out in a phosphate buffer (pH 7.0, I=1.6). Judging from the viscosity results depicted in Fig. 2, where it is shown that the depolymerization of these two proteins is already complete long before an ionic strength of 1.6 is reached, and from the fact that a sample of sepia tropomyosin was used which had lost the ability to polymerize, it is permissible to assume that the experimental values, 89,000 and 68,000, obtained in this buffer represent the monomeric molecular weights of pig heart and sepia mantle tropomyosins respectively.

It is evident that the molecular size of tropomyosin varies greatly from species to species, at least when the positions on the phylogentic scale are far apart, or when the physiological functions considerably differ.

Since in the phosphate buffers employed salt ions were present in abundance (I=0.6–1.6) and proteins were only about 2 units from their isoelectric points, it is safe to assume that the Donnan effect can be neglected. An estimate was made of the molecular asymmetry of tropomyosin on the basis of Zimm and Onsager's theory (see Edsall[49]) from the the slope m and the

intercept $(P/C)_{c=0}$ The results of such calculations are given in Table 2.

Table 2. Shape of Tropomyosins from Osmotic Data.

Tropomyosin	m	(P/C) c=o	a/b	Note
Rabbit striated muscle	0.544	2.64	29	(30) pH 6.5 I=1.1
Duck gizzard smooth muscle	0.392	1.11	50	
Prawn striated muscle	0.337	2.12	22	
Pig cardiac muscle	0.493	1.92	36	
Sepia mantle smooth muscle	0,983	2.50	55	

3. *Viscosity and molecular asymmetry of tropomyosin*

The relative viscosity of tropomyosin was determined in the same depolymerizing solutions as those used in osmotic pressure measurements. The results are given in Figs. 9–12.

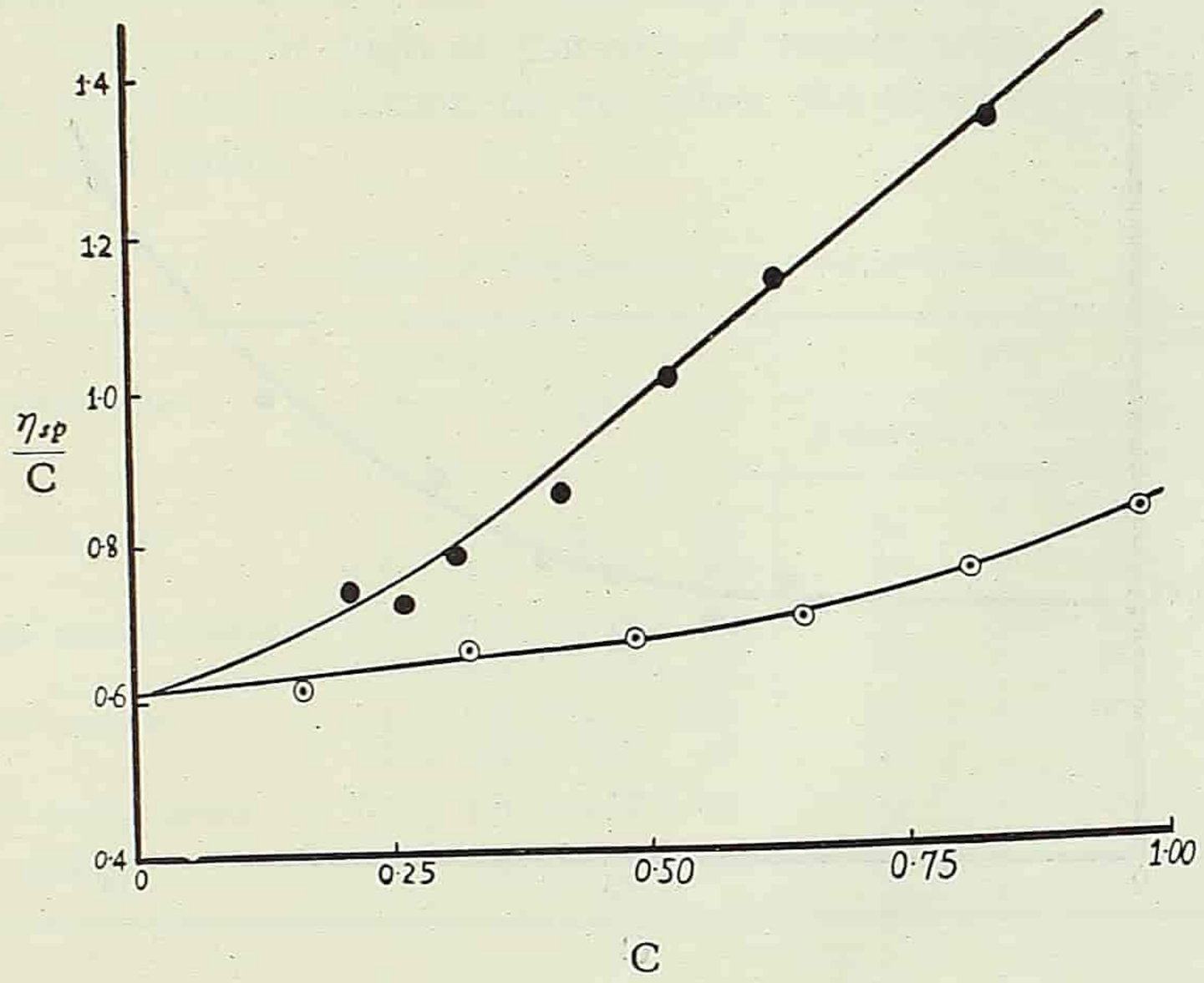

Fig. 9. Viscosity of duck gizzard tropomyosin.
20.5°C, ——⊙——⊙——pH 2.1, solvent same as in Fig. 3.
——●——●——pH 7.0, solvent same as in Fig. 4.

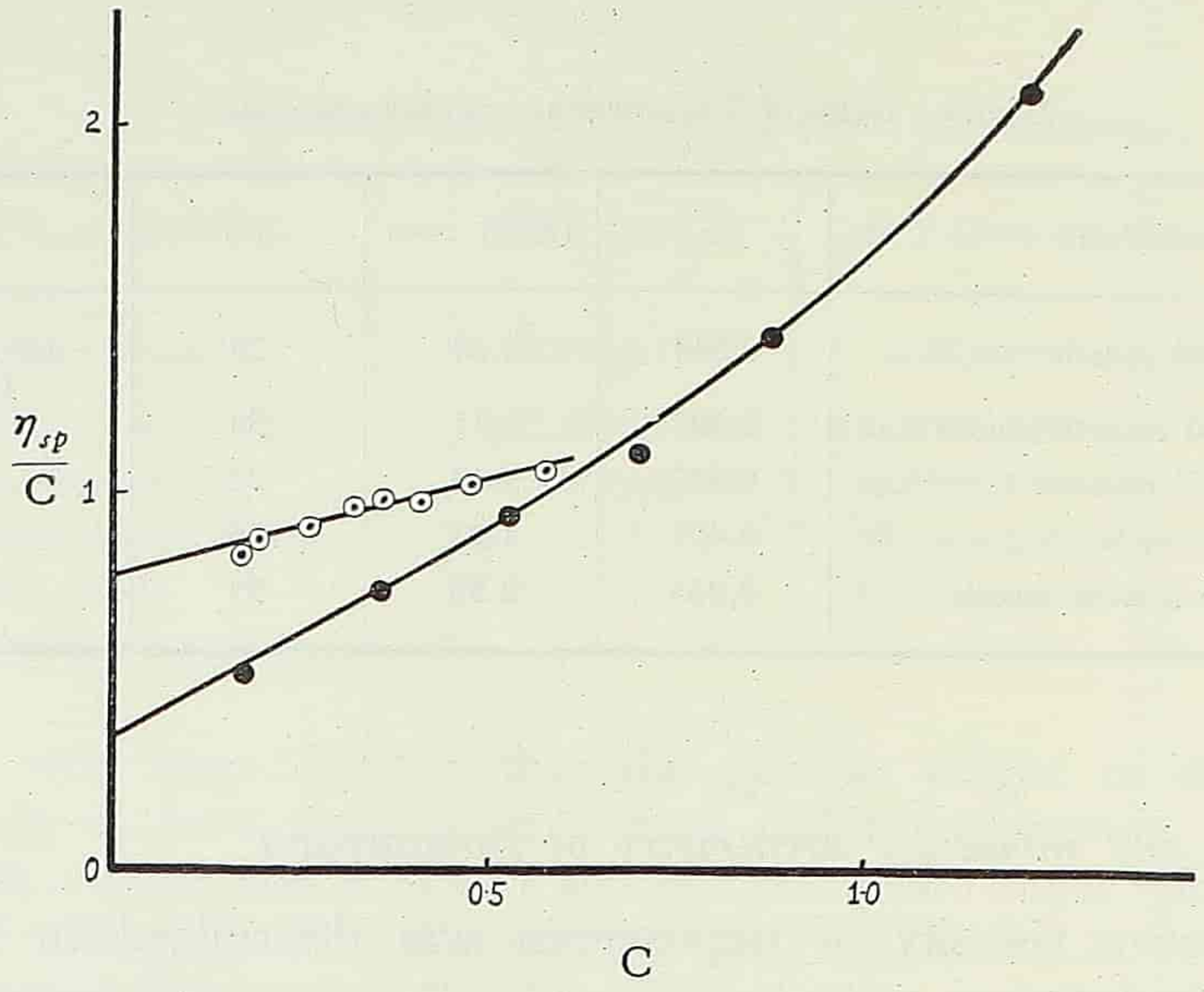

Fig. 10. Viscosity of prawn tropomyosin.
25°C, ——⊙——⊙—— solvent same as in Fig. 5.
——●——●——solvent same as in Fig. 6.

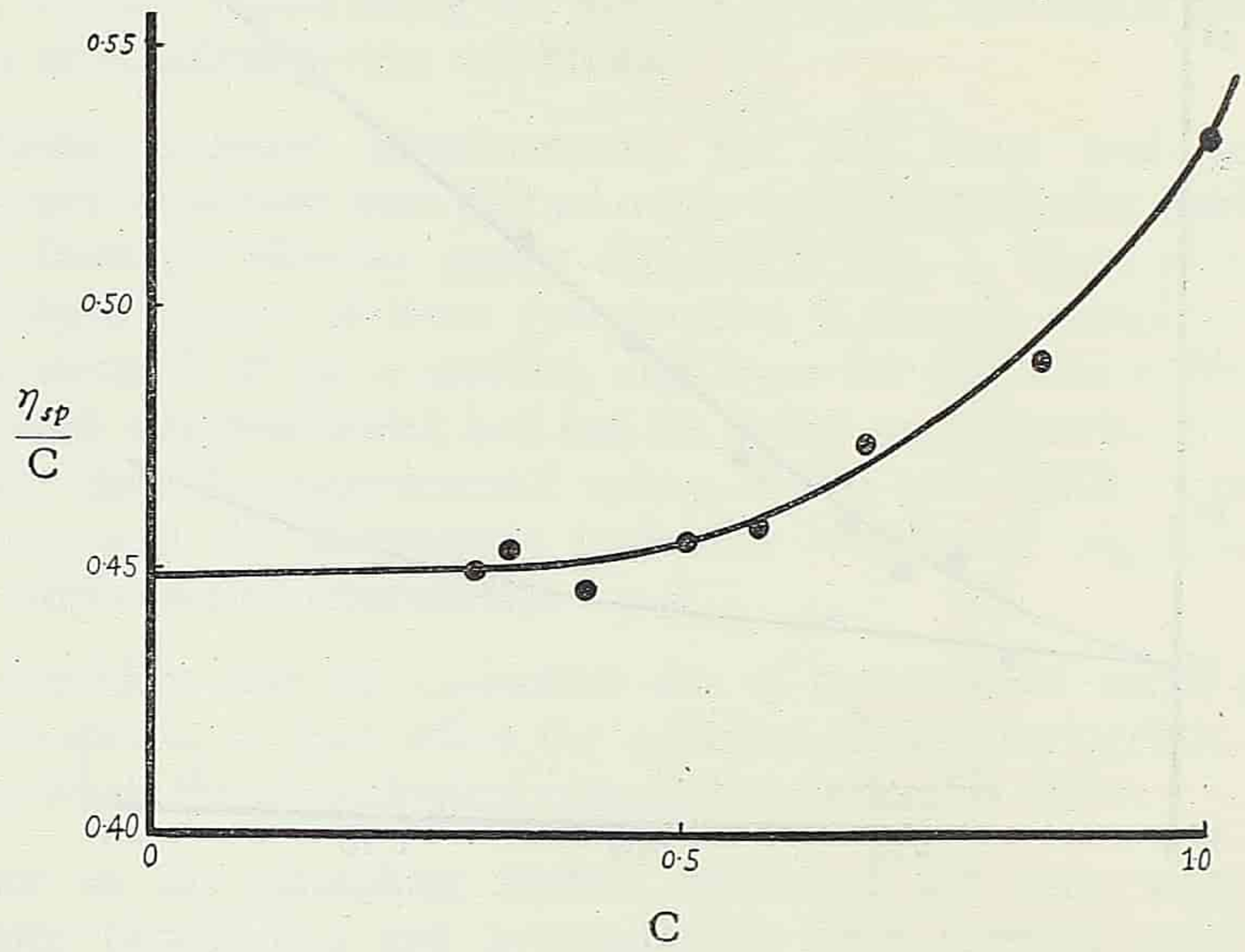

Fig. 11. Viscosity of pig heart tropomyosin.
25°C, solvent same as in Fig. 6.

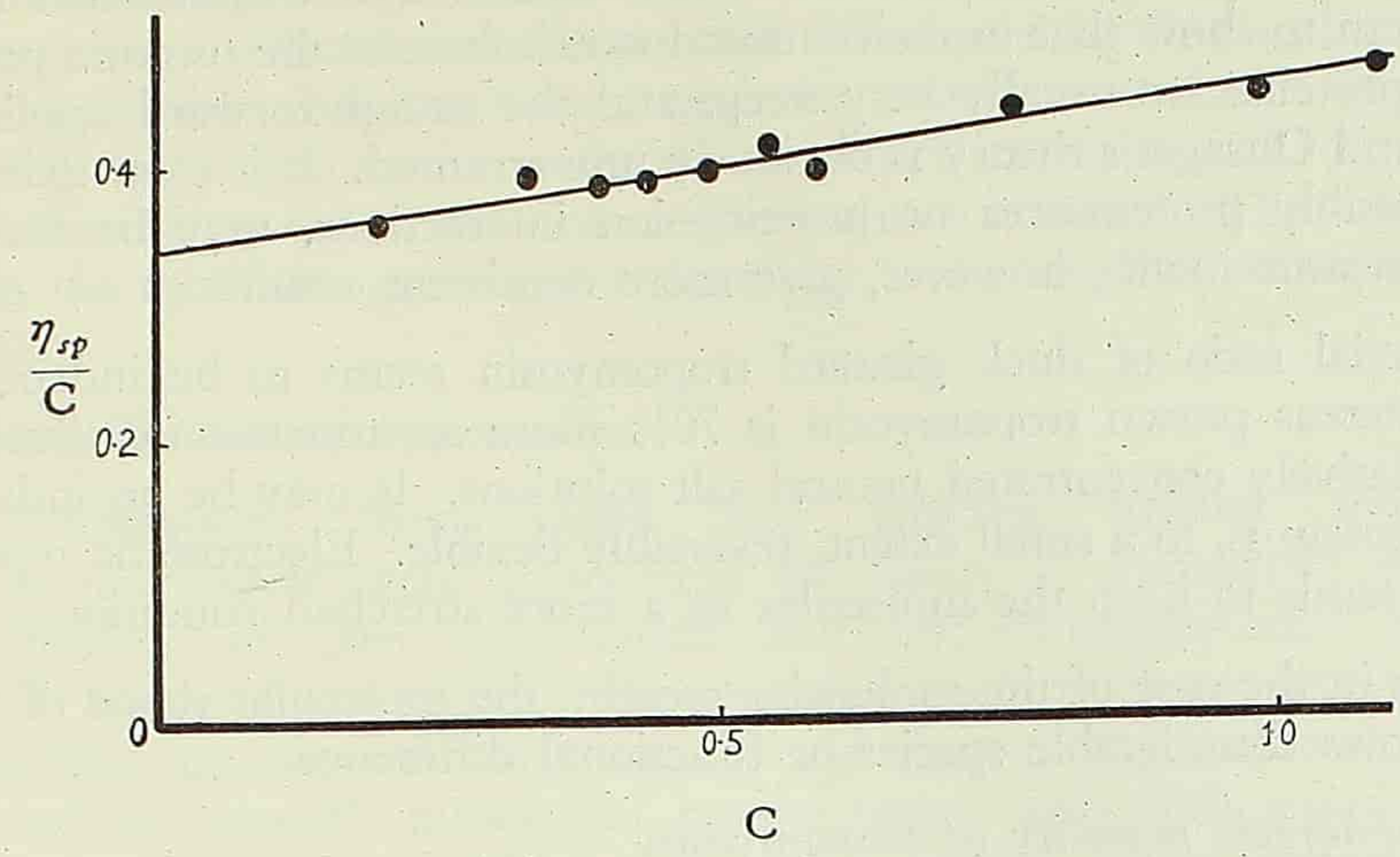

Fig. 12. Viscosity of sepia tropomyosin.
31 °C, solvent same as in Fig. 6.

The values for the intrinsic viscosity $[\eta]$ were obtained by graphical extrapolation. The viscosity increment $\nu = \frac{[\eta] \times 100}{\bar{v}}$ was calculated for each value of $[\eta]$ by employing the partial specific volume $\bar{v}=0.71$[48], and the hydration value 0.25 g/g[30] for rabbit tropomyosin. The axial ratio a/b was evaluated with the help of Simha's equation and the results are given in Table 3. Owing to the high asymmetry of tropomyosin, slight variations in the values for $\bar{v}$ and hydration do not affect the order of magnitude of the calculated axial ratios.

Table 3. Shape of Tropomyosins from Viscometric Data.

Tropomyosin	Solvent		$[\eta]$	ν	a/b		Note
	pH	I			Anhydrous	25% Hydration	
Rabbit striated muscle	2	0.3	0.52	74	30	25	(30)
	6.5	1.1	0.57	80	31	26	(30)
Duck gizzard smooth muscle	2.1	0.2	0.65	92	34	29	
	7.0	0.6	0.65	92	34	29	
Prawn striated muscle	2.1	0.1	0.77	109	38	32	
	7.0	1.6	0.35	49	23	19	
Sepia mantle smooth muscle	7.0	1.6	0.34	48	23	19	
Pig cardiac muscle	7.0	1.6	0.45	63	27	22	

By comparing Tables 2 and 3, it is seen that for rabbit and prawn tropomyosins the axial ratios from the osmotic and viscometric data agree well with each other; whereas for the other tropomyosins Zimm and Onsager's

theory leads to higher values for molecular asymmetry. Unpublished results of Tsao seem to show that in concentrated urea solutions the osmotic pressure curves of proteins are usually very steep, and the straightforward application of Zimm and Onsager's theory is obviously unwarranted. It is clear that other factors, possibly protein-urea or protein—ion interactions, may be involved. Viscosity measurements, however, give more consistent results.

The axial ratio of duck gizzard tropomyosin seems to be independent of pH, whereas prawn tropomyosin is 70% more asymmetric in dilute acid than in relatively concentrated neutral salt solutions. It may be an indication that this protein is, to a small extent, reversibly flexible. Electrostatic repulsion at pH 2.1 tends to keep the molecules in a more stretched condition.

Just as in the case of the molecular weight, the molecular shape of tropomyosin shows considerable species or functional difference.

4. *Electrophoretic mobility of tropomyosin*

In order to compare the distribution of charges in the different tropomyosin molecules, we have undertaken to measure the electrophoretic mobilities of the tropomyosins in a phosphate buffer of ionic strength 0.1, pH 6.5 at 0.5°C. The results are given in Table 4.

Table 4. Electrophoretic Mobilities of Tropomyosins.

Muscle Type	Animal or Tissue	Electrophoretic Mobility 10^{-5} cm^2 /V/ sec	
		Ascending	Descending
Striated	beef	−10	− 8
	rabbit	−11	−10
	rat	−11	− 8
	carp	− 9	− 8
	shell-carp	−13	− 9
	crab	− 9	− 9
	prawn	−10	− 8
Smooth	bovine uterus	−11	− 9
	duck gizzard	−12	−11
	bivalve foot	−14	−11
Mixed striated and smooth	bivalve adductor muscle	−11	− 9
Cardiac	pig heart	−12	− 8

It is seen from Table 4 that the different tropomyosins move in the electric field at about the same speed, the ascending and descending mobilities

lying respectively near -11×10^{-5} and -9×10^{-5} $cm^2/V/sec$. The slight fluctuation may be a reflection of the possible differences in chemical composition. It is conceivable that the nature and the relative abundance of polar and nonpolar side chains, the amount of amide nitrogen and of nonprotein constitutents may vary from one tropomyosin to another. The marked variation in the total nitrogen content described in section II–3 points to the same direction.

5. *Crystallization of tropomyosin*

Tropomyosins from rabbit and whiting striated muscles and pig cardiac muscle were crystallized by Bailey[31]. Hamoir[35] effected the crystallization of carp tropomyosin and nucleotropomyosin. Sheng and Tsao[38] obtained crystalline tropomyosins and nucleotropomyosins from the skeletal muscles of bovine adult and foetus, rat, shell-carp, toad and crab and the smooth muscles of bovine uterus and duck gizzard. In the present investigation we added five new members to the family of crystalline tropomyosins. These were derived from sepia mantle, the body muscle of prawn, the foot muscle of the bivalve Anodonta and the adductor muscles of the bivalves Anodonta and Cristaria. In general, tropomyosin crystals appear to be of two kinds: those derived from the skeletal and the cardiac muscles of the adult or foetus of higher animals possess straight edges (flat plates—squares, parallelograms; six-edged spindles; solid structures) and those from the smooth muscles of higher animals and from the smooth and striated muscles of lower invertebrates are elongated smooth spindles. The presence of ribonucleic acid seems to influence only the thickness but not the overall shape of the crystals.

IV. Discussion

Our present and previous[38] investigations have demonstrated that in respect of the molecular size, shape, solubility, crystalline form, polymerizability, electrophoretic mobility and the amount of associated ribonucleic acid, tropomyosins derived from all types of muscle (striated, smooth and cardiac) taken from different animals of the phylogentic scale (mammalia, aves, reptilia, amphibia, pisces, arthropoda and mollusca) exhibit delicate or marked species and functional differences. The physiological rôle of tropomyosin in muscle is as yet unknown. To differentiate tropomyosin from other structural proteins of muscle, it is necessary at this stage to forsake biological activity but to rely on physico-chemical characteristics. In view of the above-mentioned differences, some physico-chemical properties must necessarily be excluded or more stringently specified. As a class of protein, the salient characteristics of tropomyosins are: (1) the ability to polymerize in neutral solutions in the absence of salt and the reversible depolymerization by salt ions; (2) the ability to crystallize under favourable conditions; (3) the high asymmetry, with axial

ratios near or greater than 20; (4) the relative stability to organic solvents and to dilute acid; and (5) definite electrophoretic mobility.

The ratio of a/b and molecular weight differs slightly from one tropomyosin to another; this may be a reflection of minor differences in the polypeptide chain folding. Prawn tropomyosin seemed to suffer a change of configuration when the ionic environment was altered. However, it is difficult to agree with Wassermann[51] to the extent that rabbit tropomyosin molecules are flexible chains capable of marked changes in configuration. Such a concept, drawn from theories of simple synthetic polymers, is probably applicable to proteins in an unfolded, denatured condition, and is difficult to reconcile with the crystallizability and extraordinary stability[43] of the tropomyosin molecule.

Extensive, systematic and comparative studies of the molecular dimensions of any one kind of crystalline proteins are lacking. The few scattered investigations pertain to proteins isolated from sources which are very closely related in species.

Relatively more attention, however, has been paid to haemoglobin. There exists a definite integral relationship among different haemoglobins and their subunits, a situation well summarized by K. O. Pedersen[52] in his restatement of the Svedberg multiple concept: "...similar proteins, i.e., proteins that occur in the same way or have the same function, will either have about the same molecular weight or they will usually belong to the same multiple system." With the appearance of the extensive X-ray crystallographic work of Perutz[53] and Porter and Sanger's elegant terminal analysis of haemoglobin[54], the above-mentioned relationship becomes immediately understandable in terms of a limited number of polypeptide chains arranged in the forms of primitive laminae or rodlets in the larger globular protein molecules. The structural principles of asymmetric protein molecules are far less known. There appears to be no simple multiple relationship among the molecular weights of tropomyosins from different sources. It is conceivable that these different tropomyosins are structurally quite similar, but that they are elaborated to different lengths along the long axis.

According to Ellenbogen and Olson[14], the molecular weight of dog-heart myosin is 100,000. This is only about 1/8 of that of the same protein in rabbit skeletal muscle and is smaller than the subunit weight, 165,000, deduced by Tsao[55]. On the other hand, their value is identical with that of tryptic or chymotryptic L-meromyosin[56, 57] and is not far off from the molecular weight of pig-heart tropomyosin, 90,000, deduced in the present investigation. For rabbit skeletal muscle, the size of the myosin molecule is some 16 times that of tropomyosin monomer. It is this disparity in size and partial similarity in amino acid composition and physico-chemical properties that make it not illogical to think of tropomyosin as a possible subunit,

of which myosin is composed and elaborated. Although this original proposal of Bailey[3]1 could not be substantiated by the depolymerization studies of Tsao[38], and the comparative studies of Robinson[24] and of Sheng and Tsao[38], it has taken on a new form in the work of Kominz, Hough, Symond and Laki[32] who, on the basis of amino acid analysis, suggested that both tropomyosin and actin were structural components of myosin. Ellenbogen and Olson's finding and our own results indicate that in cardiac muscle systems, at any rate, molecules of myosin and tropomyosin may be of similar size. This fact alone seriously undermines the contention of Kominz *et al*[32]. Further comparative studies are evidently needed to settle the important points of the biogenesis of myosin and of the relationship of tropomyosin and myosin.

Cytological investigations, especially those carried out recently with the electron microscope[58], have thrown much light on the fine structures of the striated muscle. There are as yet no convincing indications as to how the various structural components—actin, myosin, tropomyosin, etc—are linked together in the A and I bands and what exactly are the molecular events when the bands undergo changes during muscle contraction. From a comparative point of view, the anatomically much simpler smooth muscle might be a more suitable material for biochemical investigation. In this respect, existing data[1, 7, 10, 11, 13, 22, 23, 29, 37] appear to be rather limited in scope; they are mainly concerned with the adenosinetriphosphatase activity and the behaviour of the ill-defined actomyosin system. The present study has been an attempt to cover only some aspects of the chemistry of tropomyosin. A comparative study of the size, shape, aggregation, mutual interaction and enzymic activities of other isolated, purified protein components of smooth muscle may prove to be of benefit to our understanding of the contractile mechanism of muscle.

V. Summary

1. Five new members have been added to the family of tropomyosins prepared from sources other than rabbit skeletal muscle. These were isolated from the mantle of the sepia (*Sepia esculenta*), the body muscle of the prawn (*Penaeus orientalis*), the foot muscle of the bivalve (*Anodonta pacifica*) and the adductor muscles of the bivalves (*Anodonta pacifica* and *Cristaria plicata*). All have been crystallized.

2. The size, shape, polymerizability and electrophoretic behaviour of tropomyosins of duck gizzard and sepia mantle smooth muscles, and pig cardiac and prawn striated muscles have been determined and compared with those of rabbit tropomyosin.

3. The polymerizability of duck gizzard tropomyosin is higher than that of either pig heart or rabbit muscle tropomyosin.

4. The molecular weights of gizzard, prawn, heart and sepia tropomyosins are respectively 150,000, 77,000, 89,000, and 68,000. These values are higher than that of rabbit tropomyosin (53,000). There appears to be no simple multiple relationship among the molecular weights of tropomyosins from different sources.

5. The axial ratios of gizzard, prawn, heart and sepia tropomyosins are respectively around 30, 20, 20, and 20. Like rabbit tropomyosin, these proteins are highly asymmetric.

6. All tropomyosins, including the above-mentioned four and those prepared from the skeletal muscles of cow, rabbit, rat, carp, shell carp and crab, from the smooth muscle of bovine uterus and from the adductor muscles of bivalves, are electrophoretically similar, with mobilities asc.–9 to -12×10^{-5} $cm^2/V/sec.$ and desc. –8 to -11×10^{-5} $cm^2/V/sec.$ in a phosphate buffer of pH 6.5 and ionic strength 0.1 at 0.5°C.

References

[1] Браун, А. Д., и Мирович, Н. И., 1955. Аденозинтрифосфатаза Матки. *Вопросы Мед. Химии*, **1**, 48.

[2] Иванов, И. И., и Касавина, Б. С., 1948. Сравнительное Биохимическое Изучение Контрактильных Белков Поперечнополосатых Мышц на Различных Ступенях Фило- и Онтогенеза. *ДАН СССР*, **60**, 417.

[3] Касавина, Б. С., 1949. Сократительные Белки Поперечнополосатых Мышц в Онтогенезе. *Вопросы Мед. Химии*, **1**, 298; 1950. **2**, 165; 1952. **3**, 189.

[4] Касавина, Б. С., и Кунеева, З. И. 1950 Биохимическое Изучение Сократительных Белков Скелетных Мышц Человека и Животных. *ДАН СССР*, **71**, 713.

[5] Фердман, Д. Л., 1953. *Биохимия Заболеваний Мышц*. изд. А. Н. Украинской ССР. Киев, 8-69.

[6] Bailey, K., 1937. Composition of the Myosins and Myogen of Skeletal Muscle. *Biochem. J.* **31**, 1406.

[7] Banga, I., and Nowotny, A., 1951. Comparative Studies about Adenosinetriphosphatase Activity of Human Muscles, Aorta and Arteria Femoralis. *Acta Physiol. Hung.* **2**, 317.

[8] Cornell, J. J., 1954. Studies on the Proteins of Fish Skeletal Muscle. *Biochem. J.* **58**, 360.

[9] Crepax, P., 1952. Étude électrophorétique d'extraits de muscles doués de différentes propertiétés morphologiques et fonctionnelles. *Biochim. Biophys, Acta,* **9**, 385.

[10] Csapó, Á., 1950. Actomyosin of the Uterus. *Am. J. Physiol.* **160**, 46.

[11] Csapó, Á., 1950. Studies on Adenosinetriphosphatase Activity of the Uterine Muscle. *Acta Physiol. Scand.*, **19**, 100.

[12] Csapó, Á., and Herrmann, H., 1951. Quantitative Changes in Contractile Proteins of Chick Skeletal Muscle during and after Embryonic Development. *Am. J. Physiol.*, **165**, 701.

[13] Dörr, D., and Portzehl, H., 1954. Der kontraktile Myosinfaden aus glatter muskulatur. *Zeit. f. Naturf.*, **9b**, 550.

[14] Ellenbogen, E., and Olson, R. E., 1955. The Contractile Proteins of Dog Heart. *Fed. Proc.*, **14**, 207.

[15] Gergely, J., and Gouvea, M. A., 1953. Combining Ratios of Cardiac Myosin and Actin. *Fed. Proc.*, **12**, 207.

[16] Gelotte, B., 1951. Myosin from Cardiac Muscle. *Biochim. Biophys. Acta*, **7**, 378.

[17] Gilmour, D., and Calaby, J. H., 1953. Physical and Enzymic Properties of Actomyosins from the Femoral and Thoracic Muscles of an Insect. *Enzymologia*, **16**, 23.

[18] Guba, F., 1943. Observations on Myosin and Actomyosin. *Studies Inst. Med. Chem. Szeged.*, **3**, 40.

[19] Herrmann, H., and Nicholas, J. S., 1948. Quantitative Changes in Muscle Protein Fractions during Rat Development. *J. Exp. Zool.*, **107**, 165.

[20] Humoller, F. L., Griswold, B., and McIntyre, A. R., 1950. Comparative and Chemical Studies in Skeletal Muscle following Neurotomy and Tenotomy. *Am. J. Physiol.*, **161**, 406.

[21] Kovâtos, J., 1949. Myosin and Actomyosin Content of the Heart-muscle. *Nature*, **163**, 606.

[22] Mehl, J. W., 1941. Studies on the Proteins of Smooth Muscle II. The Myosins of the Octupus, Snail, Sea Cucumber and Sea Anemone. *Biol. Bull.*, **79**, 488.

[23] Needham, D. M., 1954. Some Preliminary Observations on the Protein Fractions of the Uterus, and on the Adenosinetriphosphatase Activity of this Organ. *Acta Physiol. Hung.*, **6**, suppl. 61.

[24] Robinson, D. S., 1952. Changes in the Protein Composition of Chick Muscle during Development. *Biochem. J.*, **52**, 621.

[25] Snellman, O., and Gelotte, B., 1950. An Investigation of the Physical Chemistry of the Contractile Proteins. *Exp. Cell Res.*, **1**, 234.

[26] Wollenberger, A., 1954. Non-specificity of the Effect of Cardiac Glycosides on the Polymerisation of Actin. *Experientia*, **10**, 311.

[27] 丸山工作 1954. 昆蟲の筋肉の ATPase. 酵素化學シンポジウム **9**, 115.

[28] 丸山工作 1954. いろいろな 動物のアクトミオシンの ATPase 作用. 生化學 **26**, 595.

[29] 八木康一, 佐佐木昭雄, 松宮弘幸, 1955. 貝類ミオシン—B の酵素化學的及ぶ物理化學的性質に就いて, 生化學, **26**, 630; 1954. **26**, 359.

[30] Tsao, T. C., Bailey, K., and Adair, G. S., 1951. The Size, Shape and Aggregation of Tropomyosin Particles. *Biochem. J.*, **49**, 27.

[31] Bailey, K., 1948. Tropomyosin, a New Asymmetric Component of the Muscle Fibril. *Biochem. J.*, **43**, 271.

[32] Kominz, D. R., Hough, A., Symonds, P., and Laki, K., 1954. The Amino Acid Composition of Actin, Tropomyosin and Meromyosins. *Arch. Biochem. Biophys.*, **50**, 148.

[33] Bailey, K., 1951. End-group Assay in Some Proteins of the Keratin-myosin Group. *Biochem. J.*, **49**, 23.

[34] Locker, R. H., 1954. C-terminal Groups in Myosin, Tropomyosin and Actin. *Biochim. Biophys. Acta,* **14**, 533.

[35] Hamoir, G., 1951. Fish Tropomyosin and Fish Nucleotropomyosin. *Biochem. J.*, **48**, 146.

[36] Hamoir, G., 1951. Further Investigations on Fish Tropomyosin and Fish Nucleotropomyosin. *Biochem. J.*, **50**, 140.

[37] Snellman, O., and Tenow, M., 1954. A Contractile Element Containing Tropomyosin (actotropomyosin). *Biochim. Biophys. Acta,* **13**, 199.

[38] Sheng, P. K., and Tsao, T. C., 1954. A Comparative Study of Nucleotropomyosins from Different Sources. *Scientia Sinica,* 1955, **4**, 157; *Acta Physiologica Sinica,* **19**, 203.

[39] Chibnall, A. C., Rees, M. W., and Williams, E. F., 1943. The Total Nitrogen Content of Egg Albumin and Other Proteins. *Biochem. J.*, **37**, 354.

[40] Adair, G. S., 1949. Measurements of Osmotic Pressure of Haemoglobin. in Roughton, F.J.W. and Kendrew, J. C. *Haemoglobin,* 191, London, Butterworths Scientific Publications.

[41] Chi, C. W., and Tsao, T. C., 1954. The Interaction of Actin, Myosin and Adenosine Triphosphate in "Solutions". *Acta Physiologica Sinica,* **19**, 235.

[42] Tsuda, S., 1928. Zur Kenntnis der Strukturviskosität einiger sole polymerer Kohlenhydrate. *Koll. Z.*, **45**, 325.

[43] Tan, P. H., and Tsao, T. C., 1954. A Note on the Stability and Structure of the Tropomyosin Molecule. *Acta Physiologica Sinica,* **19**, 223.

[44] Simha, R., 1940. The Influence of Browian Movement on the Viscosity of Solutions. *J. Phys. Chem.*, **44**, 25.

[45] Mehl, J. W., Oncley, J. L., and Simha, R., 1940. Viscosity and the Shape of Molecules. *Science,* **92**, 132.

[46] Astbury, W. T., Reed, R., and Spark, L. C., 1948. An X-ray and Electron Microscope Study of Tropomyosin. *Biochem. J.*, **43**, 282.

[47] Doty, P., 1951. Private Communication.

[48] Bailey, K., Gutfreund, H., and Ogston, A. G., 1948. Molecular Weight of Tropomyosin from Rabbit Muscle. *Biochem. J.*, **43**, 279.

[49] Edsall, J. T., 1953. The Size, Shape, and Hydration of Protein Molecules. in Neurath, H. and Bailey, K. *The Proteins,* I. B. 595, N. Y. Academic Press.

[50] Oncley, J. L., 1941. Evidence from Physical Chemistry Regarding the Size and Shape of Protein Molecules from Ultracentrifugation, Diffusion, Viscosity, Dielectric Dispersion and Double Refraction of Flow. *Annals. N. Y. Acad. Sci.*, **41**, 121.

[51] Wassermann, A., 1954. Molecular Weight—Intrinsic Viscosity Relationships of the

Tropomyosins. *J. Polymer Sci.*, **14**, 512.

[52] Pedersen, K. O., 1950. Size Relationship among Similar Proteins, Association and Dissociation Reactions of Protein Units. *Cold Spring Harbour Symp. Quan. Biol.*,**14**, 140.

[53] Perutz, M. F., 1949. An X-ray Study of Horse Methaemoglobin. *Proc. Roy. Soc.*, A, **195**, 474.

[54] Porter, R. R., and Sanger, F., 1949. The Free Amino Groups of Haemoglobins. in Roughton, F. J. W. and Kendrew, J. C., *Haemoglobin*. 121, London, Butterworths Scientific Publications.

[55] Tsao, T. C., 1953. Fragmentation of the Myosin Molecule. *Biochim. Biophys. Acta.*, **11**, 368.

[56] Szent-Györgyi, A. G., 1953. Meromyosins, the Subunits of Myosin. *Arch. Biochem. Biophys.*,**42**, 305.

[57] Gergely, J., Gouvea, M. A., and Karibian, D., 1954. Effect of Proteolytic Enzymes on Myosin. *Fed. Proc.*,**13**, 216.

[58] Huxley, H. E., 1953. Electron Microscope Studies of the Organization of the Filaments in Striated Muscle. *Biochim. Biophys. Acta.*, **12**, 387.

EXPLANATION OF PLATE I

1. Prawn tropomyosin.
2. Prawn tropomyosin (after treatment at 0°C, pH 2 for 3 weeks.)

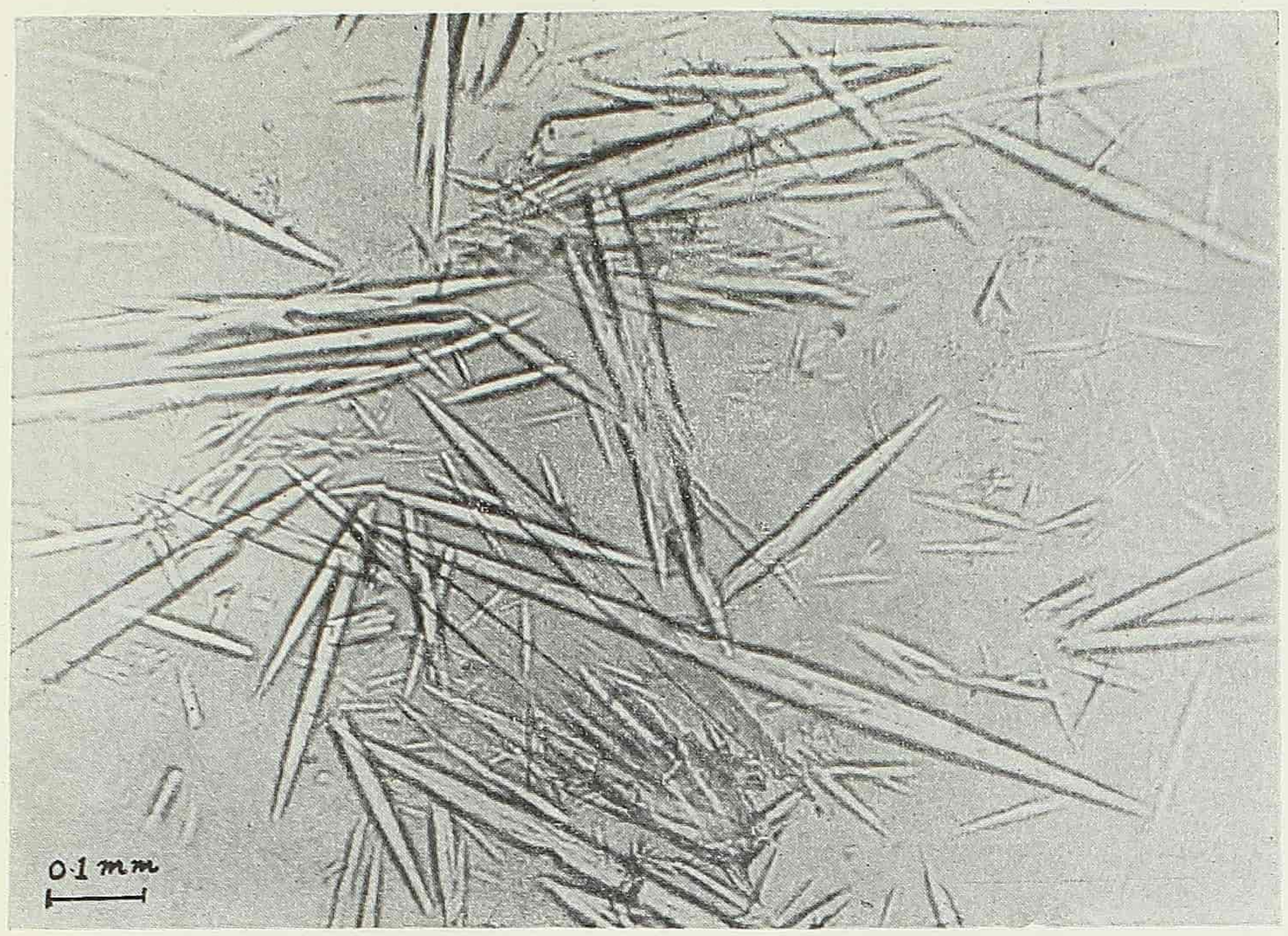

1

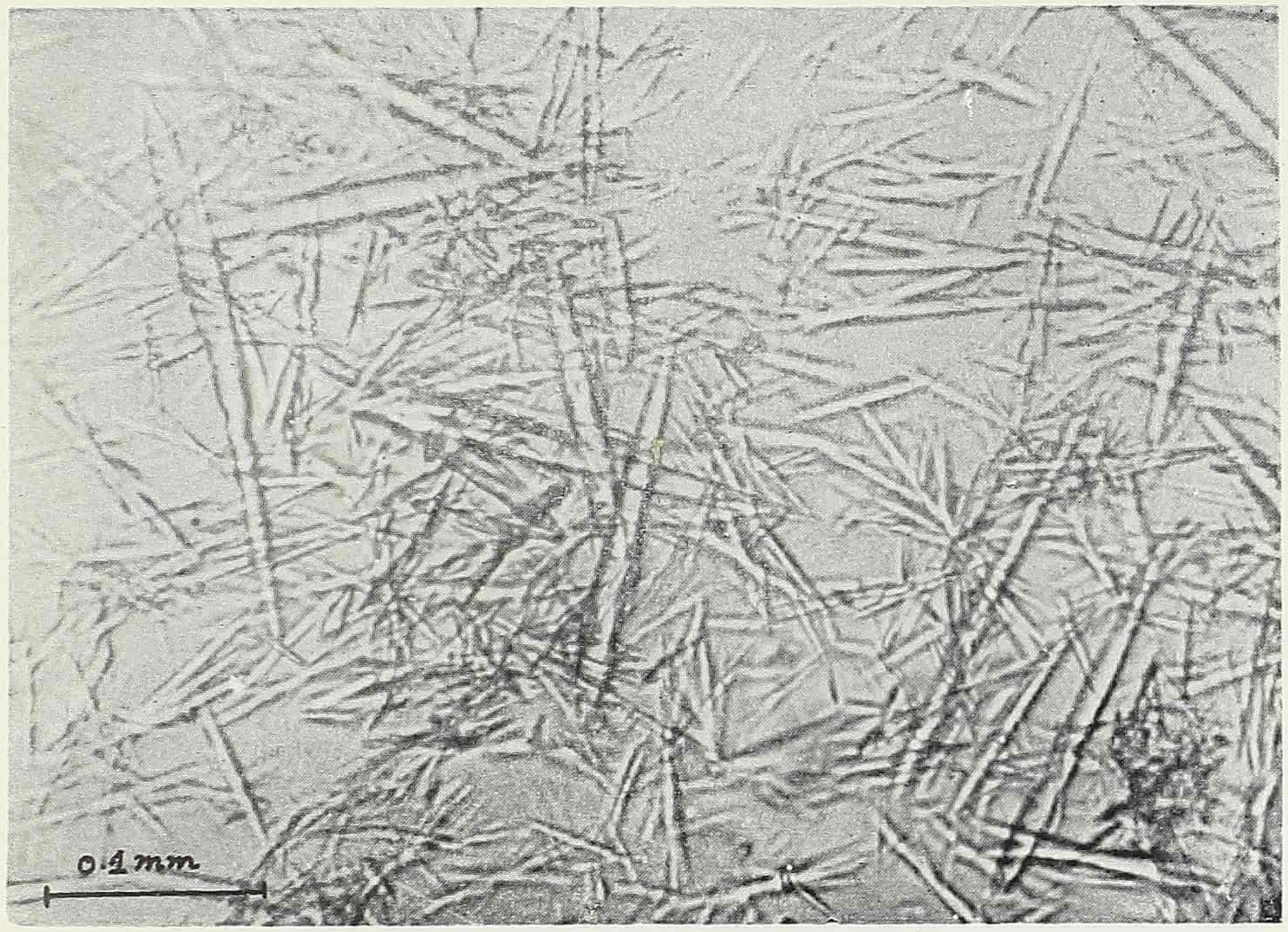

2

EXPLANATION OF PLATE II

1. Tropomyosin from adductor muscle of the bivalve *Cristaria plicata.*
2. Tropomyosin from adductor muscle of the bivalve *Anodonta Pacifica.*

1

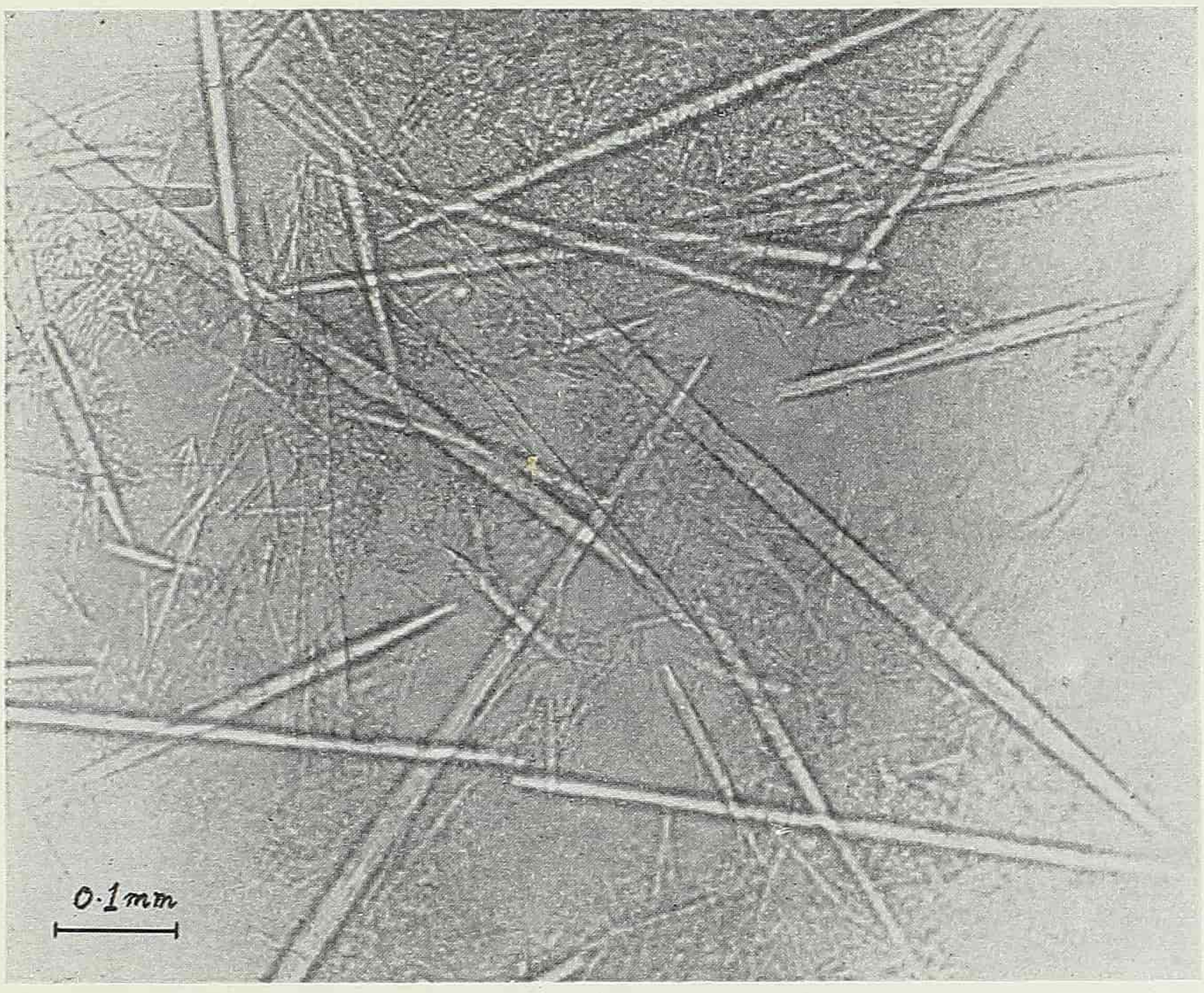

2

EXPLANATION OF PLATE III

1. Tropomyosin from foot muscle of the bivalve *Anodonta Pacifica*.
2. Tropomyosin from sepia mantle.

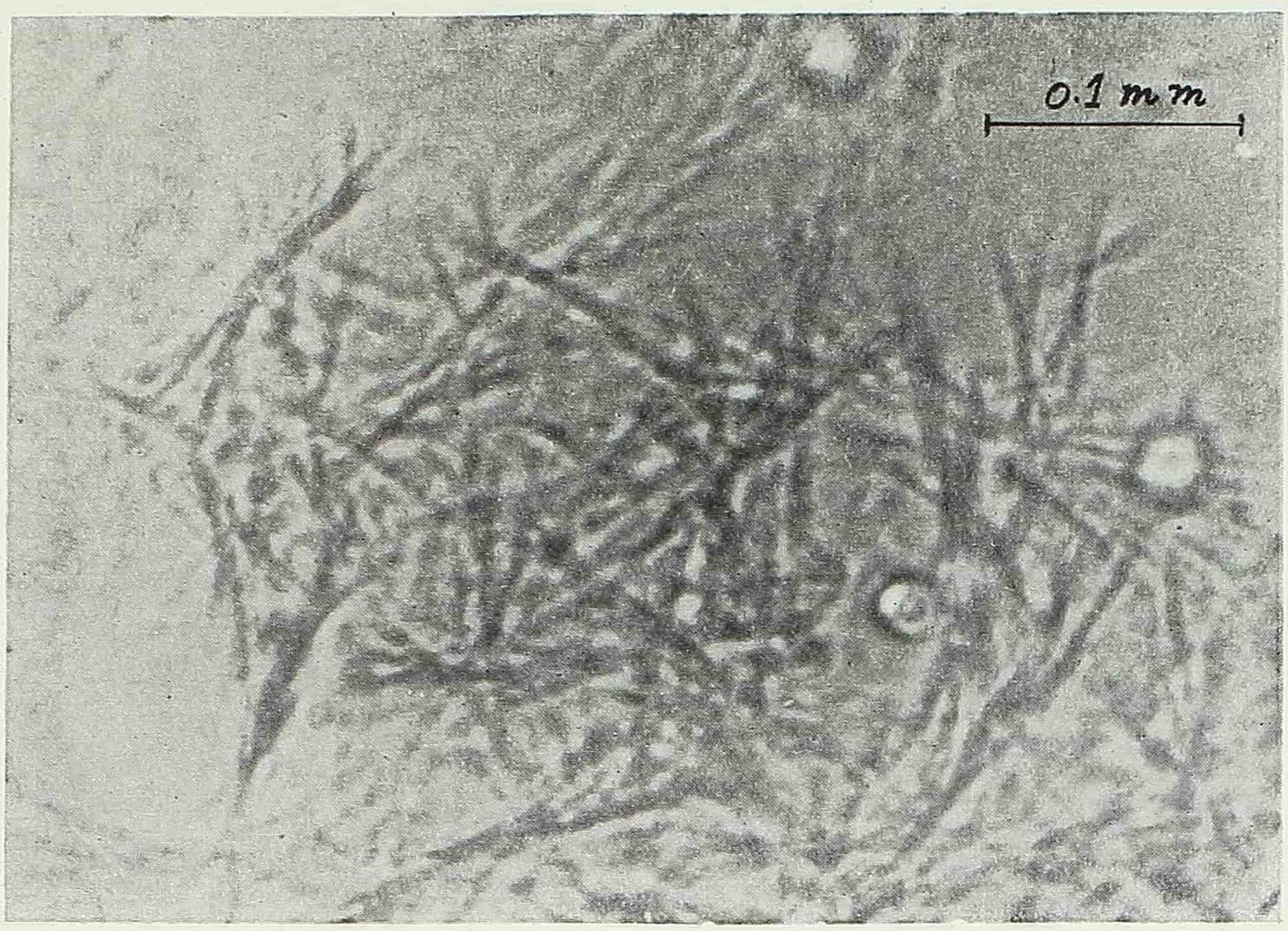

1

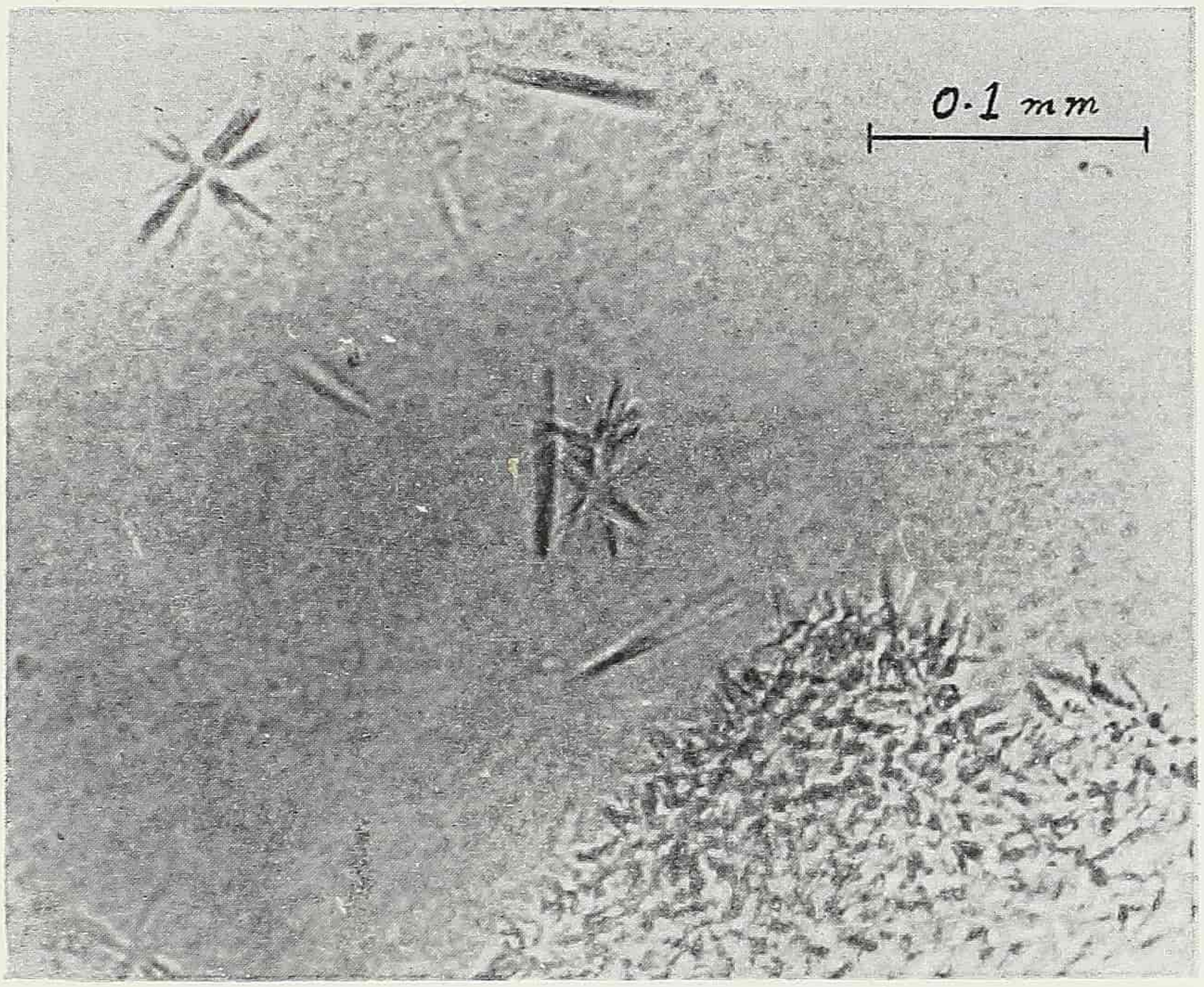

2

THE FORMATION OF NEW EPIDERMAL CELLS DURING THE PROCESS OF WOUND-HEALING ON THE RABBIT'S EAR*†

MA WEN-CHAO (馬文昭)

(Department of Anatomy, Peking Medical Institute)

There are ordinarily two theories regarding the origin of the newly formed epidermal cells during the process of wound-healing. One holds that they are derived from the pre-existing epidermis or remnants of hair follicles through mitotic or amitotic cell divisions, while the other stresses the migration of surrounding epidermal cells. Nevertheless, both the two theories are based on the same hypothesis that newly formed epidermal cells are derived from the pre-existing epidermal cells.

Academician O. B. Lepeshinskaya has already proved with facts the theory of the origin of cells from the living substance. "On the basis of these observations", she writes, "we finally come to the conclusion that the origin of the cells from the process of cell division is certainly undeniable, but as regards the origin of new cells, it is more correct to say that *all cells do not come from cells, but from protoplasm.*"[37] Thus we may expect to observe during the process of new formation of cells that some cells originate from protoplasm while others from other cells by means of cell division. At the very begining, cells would develop from protoplasm, but after these cells have already formed, mitotic division would follow.

During wound-healing, newly formed epidermal cells appear on the margin of the wound or in front of the pre-existing epidermis. In this region it would be possible to observe the whole process of the formation of new epidermal cells. On this assumption the present work is carried out by a series of observations and experiments on animal tissues.

MATERIAL AND METHOD

The skin of the ear and on the back of rabbits is served as experimental

---

*First published in Chinese in *Acta Anatomia Sinica,* Vol. I, No. 2, pp. 131–147, 1954.
Dr. Ho Chang-Nien and Dr. Fang Shih-Yuan assisted in the technical part of this work.
†Translated by Li Chao-Te.

material. Owing to the extreme thinness of its epidermis, usually of two to four layers of cells, it may be easy to find out any change to take place. The wound was produced by cutting off one stripe of tissue near the margin of the rabbit's ear; or a difinite area of skin was removed from the back with the subcutis remaining intact. No aseptic precaution was taken with the wounds, yet during the process of healing there has not been observed any sign of inflammation of pyogenic nature. The same experiment was also carried out on the guinea pig's ear.

Five cc of 1% aqueous solution of a vital dye, trypan blue, had been injected intravenously into some of the rabbits once the other day, for 5 times, before the wound was made. Under living conditions a large amount of the dye was taken up by the macrophages. Any change observed on the preparation made from these animals should have taken place while the animals were alive, and it is not due to any technical artefacts.

A series of successive observations was made with specimens from rabbits' ears, once per hour within 24 hours after wounds were made, and afterwards, every 4 hours, until the wounds healed (completed about 5 or 6 days). Further specimens were taken once every 12 hours until 180 hours when the subcutaneous tissues and cartilage were completely healed. Specimens were taken from 5 or 6 animals at every time interval.

Different fixatives, as formalin, Susa, Zenker-formalin, etc. were used for fixing the specimens taken from every stage. For differentiation of different tissue elements, different staining processes were employed: orcein for elastic fibres, Mallory's for collagenous fibres and matrix of cartilage, hæmatoxylin-eosin for tissue structures in general, Heidenhain's iron hæmatoxylin for nucleus and nucleolus. Specimens having been injected with trypan blue were fixed with Susa; they were stained with 0.25% acid fuchsin for ½ to 2 hours, and then counterstained with saturated aqueous solution of picric acid. Thereby, the tissues and cells taking trypan blue came out with clear contrast.

Specimens examined were made in serial sections of 5-micron in thickness. Sections were made in two kinds of planes both perpendicular to that of the wound. One series is perpendicular to the cartilage plate, while the other is parallel to it. Some of the sections from the latter go through the whole cartilage plate, hence a complete view of the changes taking place in the cartilageous tissue.

Observations

The results of observations are described as follows:

I. *The process of scab formation.*

The scab is already formed within 13 hours after the wound was made on the rabbit's ear (Plate I, fig. 1). On this specimen two parts can be dis-

tinguished: the upper is scab tissue, and the lower is normal tissue. The scab is again divided into two regions, with blood clot lying above and granulation tissue below. In the granulation tissue it can be observed that the collagenous fibres are arranged parallel to the surface of the cartilage, and are continuous with those from the normal tissue. Leucocytes, mostly neutrophils, migrating from the normal tissue below, fill in columns between the bundles of collagenous fibres in the scab to indicate the direction of their migration. At the same time their shape has changed from the original roundness into narrow and slender rectangles, as they go into the space between the bundles of collagenous fibres in the scab. They crowd here in a large number and in close contact; consequently they form a long column of leucocyte-chain between the longitudinally disposed collagenous fibres. The latter arrangement is of particular interest, for after the appearance of new epidermis their arrangement changes from the longitudinal direction into one of growth of new epidermal cells. The change of arrangement indicates that the migration of the leucocytes has changed its course.

2. *The process of formation of new epidermal cells under scab*

(1) A general survey of the regenerating epidermis. Around 24 hours after the cutting, new epidermis grows under the surface of the scab. The growth of the new epidermis is considerably rapid and as a result of it, sometimes the growing epidermis is much thicker than the original, but mitotic cell division has never been found in the region of the newly formed epidermis, save only a few mitotic figures observable in the basal and spinous layers of the pre-existing epidermis.

On the specimen taken off from the wound after 36 hours, (Plate IV, fig. 1), the newly formed epidermis grows from A and B towards the centre. Figure 2 on Plate IV is a highly magnified photomicrograph of area A in figure 1. It shows that the newly formed epidermis consists of more layers of cells than the original, and no mitotic figure can be observed. Serial sections have been traced forwards and backwards, giving, however, the same results.

Another unique event goes along with the advancement of the growing new epidermis, i.e., the transection of the longitudinally disposed collagenous fibres running from the scab to the normal tissues by the advancing new epidermis. The details of this change are described under (3).

(2) Changes due to the infiltration of leucocytes under the scab. Leucocytes undergo two kinds of changes in front of the growing epidermis, one being the change of direction of their arrangement and the other their disintegration. In the early stage (13 hours, Plate I, fig. 1) leucocytes migrate towards the wound and are arranged longitudinally, but later (32 hours, Plate IV, fig. 4), when the new epidermis, D, grows from right to left, the leucocytes in front of the newly-formed epidermis begin to appear, in the direction of

development of the growing epidermis, parallel to the level of the wound. The same picture is found in the case of guinea pig (Plate V, fig. 1, A), indicating that the tip of the new pigment epidermis is growing from lower right to upper left. In front of the new epidermis the leucocytes are arranged in a single column along the direction of advancement of the epidermis (from A to B), while in the upper region the leucocytes in the scab still remain in the original longitudinal orientation (Plate V, fig. 1 C). In specimens of the later stage, when the new epidermis has reached the cartilage, the leucocytes penetrate into the cartilage transversely along the direction of growth of the epidermis (Plate VI, figs. 3 and 4). It is plain that the direction of migration of leucocytes coincides with that of the advancement of the epidermis.

The second change of leucocytes in the wound is disintegration of cells. On the anterior and the inner sides of the new epidermis, there are deeply stained fragments of nuclei of leucocytes (Plate IV, fig. 4, in the marked rectangle). Among these nuclear fragments of leucocytes, some are solitary spheres surrounded with a layer of clear substance (Plate IV, fig. 4, A), resembling the clear cells; and some are aggregates of formless masses (same figure, B). At the same time, among the newly formed epidermal cells, there are fragments of nuclear substances (same figure, C), growing with the advancement of the new epidermis. This condition shifts forwards, and can only be observed in the region where the new epidermis has just formed. After the epidermis heals, their appearance is markly reduced or completely absent (Plate VI, fig. 2). This suggests that the leucocyte nuclei participate in the new formation of epidermis.

When these changes occur in the leucocyte nuclei, the specific granules of the leucocytes and the fragments of the nuclear substance mix together at the same time. Figure 2 of Plate I is a higher magnification of the rectangular area of fig. 2 of Plate V. This area is selected to indicate the anterior end of the growing epidermis which advances along the direction as indicated by the arrow point, A, in the latter figure. Under higher magnification the disintegrating leucocytes (which can be judged from the stainable red granules that they are the morphological modification of leucocytes), are in forms of granules, chains, and rods, which are mixtures of nuclei and special granules. Among the disintegrating leucocytes, there are lightly stained, newly formed young cells of different sizes and shapes (Plate I, fig. 2, AB). This again shows that after the disintegration of the leucocytes, their specific granules and nuclei mix together to participate in the formation of the new epidermis.

(3) Changes of the collagenous fibres in front of the newly formed epidermis. With Mallory's staining the collagenous fibres are coloured blue and can be distinguished from other tissues. Figure 1 of Plate I, and figure 2 of Plate IV, show the early changes of the collagenous fibres having been described above. In fig. 3 of plate II, the disintegration of collagenous fibres can be clearly shown. In this figure the upper right is the scab, under which

the new epidermis grows from lower right towards upper left. Along its course of growth many blue-coloured collagenous fibres pass through it, from the normal tissue into the scab. The parts of collagenous fibres, where the new growing epidermis passes through, show disintegration and fragmentation, while the parts above and below the epidermis still remain morphologically intact. In the region, where the collagenous fibres disintegrate, one may find the fragmentation of leucocytes and the mixing of the red and blue-coloured substances. This indicates the mixing together of the fragments of collagenous fibres and leucocytes. Besides, along the course of advancing epidermis there are immature cells which are stained faintly and have not yet acquired the distinctive form and shape (same figure, B).

In the H. E. stained specimens the mixing of the disintegrated collagenous fibres and leucocytes is not clearly shown, but on the better stained slides, as shown in fig. 4, Plate II, it is ready to observe. In the region where the photomicrograph was taken, the new epidermis has grown to considerable thickness. The direction of growth is from left to right. The scab is on the upper part, and under the scab on the right there are few new epidermal cells. The disintegrated collagenous fibres still can be identified in the newly formed epidermis (Plate II, fig. 4, A). Near the same place one may find the mixing together of the disintegrating leucocyte nuclei and fragments of collagenous fibres (same figure, B), and in its vicinity there is a deeply stained young cell nucleus still not acquiring a fully developed cytoplasm and a cell membrane (same figure, C). Moreover, there are also cases wherein a large, round-shaped fragment of disintegrated nucleus of a leucocyte would with the development of cytoplasm resemble the form of a lymphocyte (same figure D), and when the nucleus is well formed, the surrounding cytoplasm would become distinct (same figure, E). With the advancement of the growing epidermis, the immature cell nuclei are situated in the growing tip or along its margin, while cells with cytoplasm lie behind the tip. This indicates that the nucleus is formed first, and followed by the formation of cytoplasm and cell membrane. After the appearance of cytoplasm and cell membrane, it is then called a young cell.

The mixed debris from disintegrated collagenous fibres and leucocytes may develop into aggregates of different forms; some are larger and some smaller. The larger ones are shown in fig. 1, Plate II. In the same figure there are light-coloured swelling bodies formed of the aggregates and growing from right to left (as indicated by the arrow). Around the tip of its growth there are deep purple disintegrating tissues, composed of the fragments of collagenous fibres and leucocytes. Among the swelling bodies formed of the deep purple disintegrating tissues and light-stained aggregates, there are also deep-stained aggregates (Plate II, fig. 1, A). This again can be observed in the lightly-stained swelling bodies (same figure, B). The different shades of colour taken by the aggregates depend on the amount of disintegrating sub-

stances contained in them, more in the deep-stained ones, and fewer in the light ones. This picture indicates the development of the disintegrating tissues into deep-stained aggregates, which, in turn, into light-stained aggregates. During the development, the colour of the disintegrating tissues gradually faints, structures gradually make their appearance and young nuclei are formed (same figure, C). Afterwards, cytoplasm takes shape in the periphery, but the cell boundary is still indistinct; it now becomes a young cell (same figure, D).

At the tip of the growing epidermis the newly formed young nuclei are comparatively smaller. As indicated in fig. 3, Plate V, the upper part is the scab, and under the scab the new epidermis grows from left to right. At the tip of growth, there are very small young nuclei, which contain nuclear substance derived from disintegrating leucocytes.

At the tip of the growing epidermis, there are sometimes young cell nuclei and young cells. In fig. 2 of Plate II one may find, in the new epidermis growing from left to right, a large round young cell (Plate II, fig. 2, A) and a small spindle-shaped young cell nucleus. Their difference is striking.

These young nuclei and cells of different sizes could not be possibly derived from the pre-existing epidermal cells, instead, they are formed of the mixed disintegrating substances in the wound through very complex biochemical processes. Further histological evidences for this assumption are stated below:

(4) Changes of macrophages in the wound. Macrophages are shown in the specimens by vital staining method. They, too, first undergo disintegration in the wound under the scab, and mix together with the disintegrating collagenous fibres and leucocytes. Figure 3 of Plate I is a photomicrograph of lower magnification. The upper part is a deep-stained scab, under which and in front of the growing epidermis (A, B) there are many dark blue granules. When observed in a highly magnified photomicrograph (Plate I, fig. 4, A), they indicate the presence of macrophages. Many of these macrophages around the tip and the inner side of the epidermis have already been disintegrated, and the dark blue granules are released in masses, mixing together with the disintegrating leucocytes (same figure, D). A close examination of the new epidermis shows that at its tip residual trypan-blue granules are still contained in the two not yet well formed young nuclei (same figure, B). Tracing back along the growing tip against the direction of growth, one may find a well-formed young nucleus (same figure, C). The two young nuclei in the region B are still in the developing stage. Epidermal cells do not possess the ability of phagocytosizing the trypan-blue dye; consequently, the two young nuclei are developed from the disintegrating substances of macrophages and leucocytes.

(5) Changes of cartilageous tissue after the penetration of the growing epidermis. The growth of the new epidermis into the cartilage is very rapid.

The new epidermis can cross the whole cartilageous plate in no more than 30 hours and grow into considerable thickness. Figure 1 of Plate VI is a photomicrograph of a specimen taken after 90 hours, and figure 2 of Plate VI after 104 hours from the same animal. On both specimens not a single mitotic figure is found in the new epidermis, and so is the result on all serial sections. When the growing epidermis reaches the cartilage, leucocytes have already penetrated into the cartilage along the course of growth (Plate VI, figs. 3 and 4). The cartilage is destroyed at the place of penetration and the new epidermis is formed where the cartilage decomposes. The sequence of events is described as follows:

1. Leucocytes penetrate into the cartilage in the direction of the growing epidermis. Figure 3 of Plate VI is a photomicrograph of a complete view of the wound after 136 hours' and figure 4 on the same Plate is a higher magnification of the rectangular area in fig. 3. On both sides of the cartilage leucocytes accumulate at the tip of the advancing epidermis and infiltrate the cartilage, more on the right side and less on the left. The leucocytes after entering the cartilage show a tendency to cross it. This indicates that the direction of the migrating leucoytes is definite and along the same course, through which the epidermis is going to pass.

2. Leucocytes destroy the cartilageous tissue immediately after their penetration (Plate VII, figs. 1 and 2). At the same time they themselves disintegrate and mix together with the disintegrating cartilageous tissue. This is clearly shown in the second figure.

3. New epidermis is formed at the place where the cartilage is under destruction. For a complete view the following specimens were sectioned perpendicularly to the wound and parallelly to the cartilageous plate. Figure 1 of Plate III is a higher magnification of the rectangular area in fig. 4 of Plate V. The upper purple part is the new epidermis, and the lower blue part is the cartilage. Between the epidermis and the cartilage are the disintegrating cartilageous tissue (blue fragments) and the disintegrating leucocytes (purple) mixed together (Plate III, fig. 1, A). Among the fragments there are groups of young cell nuclei (same figure, B) which form a network with the remaining cartilageous matrix, and are in close connection with the new epidermis.

Young cell nuclei further develop into young cells, continuous with the pre-existing epidermal cells and adding to the thickness of the new epidermis. In the same way, the disintegrating substances in front of them continue to form young cell nuclei, which, in turn, further develop into cells. Thus the epidermis increases in thickness, sometimes even reaching the cartilage (Plate III, Figs. 3 & 4), or entering the destroyed cartilage lacunae (Plate III, fig. 5). Figure 4 of Plate III shows that the cartilageous tissue is disintegrating between the processes of new epidermal cells (Plate III, fig. 4, A). The cartilageous matrix has broken but still retains the normal stainability, and

mixes with the disintegrating substances of other tissues. Figure 5 of Plate III shows that the growth of new epidermis is very rapid—the young cell nuclei and the young cells are already formed before the cartilage is completely disintegrated, so that they fill in the lacunae of the cartilage.

When the new epidermis has reached a certain thickness, the disintegrating substances under the new epidermis cease to form epidermal cells and turn to the formation of connective tissue (Plate III, fig. 2). Under the new epidermis (A), fine bundles of blue collageous fibres are found intervening between the purple disintegrating substances, and later they develop into subcutaneous connective tissue.

(6) The process of the formation of new epidermal cells is summed up in the following sequence according to the time of stages of the specimens observed.

1. The disintegration of the tissues under the scab including all the damaged tissues, such as leucocytes, macrophages, etc.

2. The mixing up of the disintegrating tissues into formless masses. By appling different staining techniques, different tissues on the specimens show their specific colouration, and their mixture takes a more intense colour hue of different stains. Their colour depends on the stains used, and thus in fig. 1 of Plate II, it shows deep purple by Mallory's staining method, and when acid fuchsin and picric acid are used as in the case of specimens injected with trypan blue, the disintegrating substances appear in different colours, as red, yellow, blue and brown. (Plate I, fig. 4).

3. There are complex chemical and structural changes taking place in the mixture of the disintegrating substances, and through these changes they develop into aggregates of different sizes, and further into young cell nuclei.

4. Young cells are formed by the development of cytoplasm in the periphery of the cell nuclei. They further develop into normal cells.

5. When these cells reach maturity, they multiple by ordinary mitotic divisions. Ordinarily mitosis can only be found among the well-formed new epidermal cells, and is absent in the growing region.

Discussion

I. *Theories in relation to the origin of new epidermal cells.*

(1) In the past, under the influence of the traditional concept that all cells can only come from pre-existing cells, almost all authors have, with regard to the problem of the formation of new epidermal cells, accepted the saying that such new cells come from the pre-existing epidermal ones. Even up to now, it is so described still in all textbooks concerned. Take for examples,

Arey[1], Patten[2] Jordan and Kindred[3], etc. in embryology; Cowdry[4], Maximow and Bloom[5], Bailey[6], Bremer[7], Schafer[8], Jordan[9], Lamber[10], Ham[11], etc. in histology; Ormsley[12], Sutton and Sutton[13], etc. in dermatological pathology; McCarthy[14], Lewer[15], etc. in dermatological histo-pathology.

In a paper reveiwing the healing of wound, Arey in 1936, quoted from more than three hundred and sixty papers in literature. All those papers cited and his own review accept that the new epidermal cells come from original epidermis, or epithelium of the hair follicles.

Ham[17] writes in his new textbook of histology that during the healing of the burn the new epidermal cells come from hair follicles and sweat glands, but he does not mention how they are formed.

Gordon, Hall, Heggie and Horne[18] give the same description. They claim that chains of new cells come from the hair follicles and sweat glands to the surface, and as soon as they reach the surface of the wound they spread out into a thin layer of cellular membrane and later they develop into cells of stratified epidermis. They find no case of any cell in the conditions of mitosis, but arround the hair follicles they claim that they find cells in mitotic division. They describe isolated groups of epidermal cells as without any connection with the epidermis, but they consider that such groups come from cells of the hair follicles or sweat glands which do not undergo necrosis. They have not mentioned whether there is any mitotic figure in the non-necrotic hair follicles or sweat glands.

All the above-mentioned authors consider the new epidermal cells to be generated from the pre-existing epidermis or its appendages, hair follicles or sweat glands.

Investigators in the past, under the influence of the traditional cell theory, used to try various reasons to accommodate instead of questioning the soundness of the theory, whenever they came to any discrepancy in their research work. Those traditional concepts are hindrances to the progress of science. For instance, many investigators have found out in their experiments that the number of epidermal cells produced by means of mitosis is far below the number required to supply the loss of cells due to desquamation. But in order to suit the old theory, the following debatable explanations have been given.

(2) Thuringer[19] observed the scantiness of mitosis on the specimen of human epidermis. He concluded that new epidermal cells produced by mitosis could not replace the loss due to desquamation. He observed binucleated cells under the stratum granulosa, and considered that the supply of new epidermal cells was not only from mitosis but also from amitosis.

In his work on epidermis, Patzelt[20] argues that it is impossible to consider mitosis as the only source of new cells to replenish the desquamating cells, for the number lost far exceeds that produced from mitosis. Therefore,

he attributes the source of new cells chiefly to amitotic divisions, for under favourable dietary conditions cells under amitotic division can be observed around the margin of the growing epidermis.

(3) Holmes[21] considers that there is no mitosis in the early growing stage of epidermis. He has found cells in the growing epidermis migrating from the original epidermis. He mentions in his paper that he has directly observed amœboid movement in some of epidermal cells near the growing epidermis in larval and adult amphibians. This shows that the new epidermal cells are migrating from the pre-existing epidermal cells by cellular movement. Besides, many other authors give the same explanation, though they have never witnessed any amœboid movement of the cells.

The ability of cells to move was first described in 1875 by Kleb[22] and Peters[23], and later proved by Arey[24] and Herrick[25]. Others try to prove it with experiments. For instance, Poynter[26] made a wound on chick ectoderm. While healing, he observed cells along the margin of the wound changing to undifferentiated cells. He claimed that the undifferentiated cells were capable of making amœboid movement during the healing of the epidermis. He mentioned mitosis appearing in the later stage of wound-healing. Born[27] considered that in wound-healing on the epidermis of amphibians the number of the cells produced from mitosis could not reach that of the newly formed epidermal cells. The newly formed epidermis is a thin membrane of squamous cells which migrate from the pre-existing epidermal cells by amœboid movement. Hartwell[28] also mentions that the layer of squamous cells covering the surface of surgical wounds is formed by amœboid movement of cells from the spinous layer of the original epidermis. Mitosis can only be found after these cells have formed the new epithelium and further differentiated into epidermis.

(4) Besides, there is another school of investigators who are not satisfied with the evidences that the new epidermal cells come from the pre-existing epidermal cells and give other explanations.

In normal and irradiated epidermis of the frog, Cameron[29] has observed spindle-shaped mesodermal cells entering the epidermis and being converted into epidermal cells. MacCardle, Engman and Engman[30], in studying neurodermatitis, have discovered that during recovery, there are many clear cells in close relation with the new epidermal cells. When a wound just heals up, there are many poorly stained cells in the basal and spinous layers undergoing mitotic divisions. Many clear cells penetrate into the basal layer but they are also found in the dermis. They emphasize that the clear cells are rather related to the function of regeneration of the epidermis than the formation of pigment cells. Clear cells are derived from the dermis.

W. Andrew and N. V. Andrew[31] have examined the epidermis of men and rats. The results make them believe that mitosis can not make up the

loss of epidermis due to desquamation. And they have found migration of lymphocytes from dermis into epidermis and their convertion into epidermal cells.

These investigators, though hold a different concept from the former one, all agree that the new epidermal cells come from the cells in the dermis.

It is thus clear that as regards the formation of new epidermal cells, all the scientists mentioned about can not get rid of the traditional idea that "all cells come from the pre-existing cells", no matter what kind of cells is regarded by them as the source of the new epidermal cells.

2. *Further discussion on the aforesaid theories of the origin of newly formed epidermal cells.*

(1) New epidermal cells do not come from the pre-existing epidermal cells by means of mitosis.

Many investigators have discovered in their experiments that it is impossible for the epidermal cells to compensate the loss of cells due to desquamation by means of mitotic division.

Thuringer[19] examined the human epidermis, finding that the number of mitosis is scanty, and their ratios to the total number of cells are: epidermis of the ear, 1:268,275; that of the thigh, 1:378,325; that of the scalp, 1:2,414.

Ortiz-Picon[32] could not find any sign of mitosis in the epidermis of mice.

Arey[33] made a slight cut on the epidermis of the fish and amphibians, It healed after 3 hours. No cell under mitotic division was found and, in addition, he said that it was impossible to heal the wound in 3 hours by means of mitotic divisions even there were any. He performed another experiment and reached the same conclusion.

Harabath[34] made larger wounds on the epidermis of fish. They healed in 12-36 hours. From the results of his observation, he concluded that mitotic figures could not be found in the epidermis as well as in the dermis.

Both Oppel[35] and Holmes[21] got layers of epidermis in tissue culture. They found no mitosis in the early stage of the growth of the tissue, but in later stages.

Voit[36] made further chemical analysis of the weight of the epidermal cells desquamating every year. The result shows that there are 116.14 grams of epidermal cells to desquamate every year from a square metre of epidermis not including those from hair follicles.

Now return to our experiment. We have found that the growth of new epidermis is rather rapid. Within five days after a wound was made the new

epidermis has passed through tissues of different consistencies and healed to considerable thickness. In early stages, i.e., 32 hours after the wound-making (Plate IV, fig. 1), though the new epidermis is very thick and grows very rapidly, there is no mitosis. At the same time, the original epidermis does not change to any extent its thickness and the number of mitosis. In later stages, when the healed epidermis has increased in thickness, it remains in the same conditions. For instance, when the healed epidermis reaches 3 or 4 times its normal thickness 120 hours after the wound-making, the pre-existing epidermis remains in its normal thickness without any increase of the number of mitosis. In the new epidermis, mitosis is occasionally found along the margin of the early formed epidermis and its number is scanty. In the epidermis just formed, there is no mitosis.

To sum up the conclusions of the investigations of the previous workers and our own observations, it is questionable to say that the new epidermis is formed by means of mitosis of pre-existing epidermal cells. If the new epidermis of such thickness were formed in a short time interval from mitotic cell divisions, there would be much more mitotic figures in the original or newly formed epidermis. But this can not be proved on our specimens.

(2) New epidermal cells do not come from the pre-existing epidermal cells by means of amitosis.

Since the theory of mitosis as the source of supply of new epidermal cells has met with difficulty, many investigators try to explain their origin in the light of amitosis. But these explanations are not readily acceptable either.

Thuringer[19] concludes that the amitotic division of the cells below the granular layer is responsible for replacing the dead desquamated cells. This theory is not very sound, for these cells are approaching senility and death, have decreased their ability of multiplication, and are not capable of adding to the thickness of the spinous layer.

Patzelt's conclusion based on the amitotic division of cells along the margin of the newly formed epidermis does not fit to our observations. On our specimens there are many young cell nuclei in the periphery of the growing epidermis (Plate II, Figs. 1, 2, & 4). From these young nuclei, the epidermal cells are formed. These young nuclei usually accumulate in groups (Plate II, fig. 1, B). When cytoplasm develops around these nuclei and before they separate into individual cells, they appear as binucleated or multinucleated cells. Therefore these binucleated or multinucleated cells do not represent stages of amitosis, but rather stages of development from disintegrating tissues.

(3) Further discussion on the migration theory of the origin of the new epidermal cells.

Holmes gives witness to the migration of the epidermal cells around the new epidermis. This evidence is easily acceptable, if the original epidermal

cells are able to move, then they can migrate forward and become epidermal cells.

We have observed that the new epidermis is much thicker than the original, and the original epidermis has never changed its normal thickness and number of mitotic figures, and furthermore there is no sign of cellular movement in the epidermal cells. We can not agree with Holmes, because the evidences on which we formulate our theory, strongly prove against his explanation.

We consider that the cellular movements observed by Holmes are possible. The question is what kind of cells he observed is able to move. Holmes worked with fresh and living material, on which it is very difficult to distinguish whether these active cells are epidermal cells or cells of other categories. In our fixed and stained specimens various cells can be easily recognized. We have seen many leucocytes and macrophages in the vicinity of the new epidermis on our specimens. These cells are able to make active movements. The leucocytes are arranged longitudinally before the growth of new epidermis (Plate I, fig. 1), but when the new epidermis appears, the leucocytes change their arrangement, in front of the growing epidermis, along the direction of growth of the epidermis to the position where the future epidermis should be. And before the epidermis penetrates into the cartilage, along the course of the growing epidermis a layer of leucocytes is already present in the firm tissue of the cartilage. These evidences strongly suggest that the active moving cells in front of the growing epidermis are leucocytes. On our specimens we have also observed macrophages, labelled with trypan blue, penetrating into the cartilage before the epidermis. We believe that the cells showing movement in front of the growing epidermis are leucocytes and macrophages.

(4) On the formation of new epidermal cells from cells derived from mesoderm.

As we have already referred to, Cameron, MacCardle and Andrew in their papers claim that they have seen spindle-shaped cells, clear cells, or lymphocytes penetrating from dermis into epidermis and developing into epidermal cells there. They all believe that these cells penetrating from dermis are of mesodermal origin.

On our specimens we have seen conditions resembling their descriptions. But there is still another condition which should not be neglected and is of great importance. That is, in the process of wound-healing tissues in front of the growing epidermis change into disintegrating tissues. How and why these tissues disintegrate, and whether enzymes produced by the leucocyte fragments play a role in it, still remain as problems. But the fact is clear. These disintegrating tissues, as stated above, gradually develop into epidermal cells.

3. *On the basis of our observations, new epidermal cells are formed from the development of the living substance.*

(1) Material basis for the formation of new epidermis.

Academician Lepeshinskaya in the theory relating to the possibility of protoplasm developing into cells, writes, "In the protoplasm there should be all the components, necessary for the construction of the cell and its nucleus"[37]. On the specimens we have clearly observed substances formed of different kinds of disintegrating tissues. These substances undoubtedly containing a large quantity of proteins, nuclear substance, lipoids etc. serve as the material basis for the formation of living substance and its subsequent development into cells.

On the specimens we have observed that there are formless masses of aggregates containing remnants of leucocytes, collagenous fibres, and macrophages not yet completely decomposed. These formless masses are developed from the accumulation of the disintegrating substances; in other words, they are substances from the disintegrated tissues in the region of the wound and capable of development, hence the living substance.

These substances, as described by Academician Lepeshinskaya in her book, *Life and Origin of the Cell,* " . . . . are protoplasm isolated from the cells of organism by mechanical destruction; under favorable conditions it acquires characters foreign to its own organization, and develops into another form, the cell."[38] Again she writes in the *Life Process in the Pre-cell Stage:* "The multiplication of cells in the process of wound-healing is not only by means of cell division or migration of cells along the blood vessels, but also by means of neo-formation from living substance, in form of small granules observed during destruction and disintegration of cells."[39]

(2) The developmental process of the epidermal cells.

On the basis of the facts observed from specimens, the process of new formation of epidermal cells can be summed up into the following stages:

1. In the wound the connective tissue elements, such as leucocytes, collagenous fibres, macrophages, cartilage, etc., are under destruction and disintegration and form the living substance.

2. The living substance develops along the margin of the epidermis. Morphologically it passes through different stages of development, such as the stages of formless masses aggregates, young cell nuclei, and young cells. Needless to say, there are complicated bio-chemical processes and physiological regulations from the organism taking place at the same time with the morphological changes, but they are beyond the scope of the present investigation.

3. Finally, it develops into newly formed epidermal cells. After the epidermal cells formed through the development from the living substance,

they are able to divide mitotically. Occassionally we find larger cells on the specimen showing mitotic division (Plate VII, fig. 3, A), which probably represents that young cells are in the process of changing into normal epidermal cells through mitosis.

According to the theory of V. N. Michin[39], cells mutiply not only by means of mitosis, amitosis, and budding, but also from a large amount of nuclear substance released from cells, and new cells are developed therefrom.

E. E. Malovitchko and T. N. Rupasova in studying wound-healing have discovered that the living substance released from leucocytes (pus) is the source of newly formed cells. They described the process of formation and said: "Nuclei are formed by condensation of the fragments resulting from the segmentation and the breaking down of the nuclei of the neutrophil leucocytes. Probably this is not a degenerative process, but a special type of mitosis. These fragments gather into a deep-stained spherical body resembling the nucleus of a lymphocyte. It is then isolated from the destroyed neutrophil leucocyte and becomes the central part, surrounding which accumulate small cytoplasmic granules from the decomposing products of the cytoplasm of the neutrophil."

Our results agree with the statement made by the above mentioned Soviet workers.

From the aforesaid experiment naturally arise two other questions: Does the development of tissues follow a certain rule? What role does the living substance play in cell production of normal organism?

1. During the process of wound-healing there is a certain rule observed from the development of the living substance into different kinds of tissues.

For example, when the living substance develops into epidermal cells, it is not that the cells grow diffusely from anywhere on the surface of the wound at random, but that they always develop gradually along the margins of the epidermis of the wound or on the cut surfaces of the hair follicles and sweat glands. The direction of growth of the new epidermis is toward the centre of the wound from the two sides.

There is another example. After the wound heals and the epidermis reaches a certain thickness, the development of the disintegrating tissues directs chiefly not to the formation of epidermis, but to the development of other tissues. On the specimen taken 144 hours after a wound was made (Plate III, fig. 2), the epidermis has grown to a considerable thickness, and under the new epidermis at A in this figure there is one kind of mesenchyma-like tissue consisting of young cell nuclei and branched advantitious cells. At the same time there are collageous fibres between them. This specimen is fixed with Susa and stained with Mallory's the collageous fibres taking the blue colour. This picture shows that the development has turned to the connective tissues. In the lower region the cartilageous tissue is still in the process

of disintegration. Another specimen taken 181 hours after the wound-making (Plate VII, fig. 4), shows that the wound has healed to a certain extent, the new epidermis is extraordinarily thick, there is a thick layer of connective tissue under the spidermis, the number of leucocytes in it has decreased to the normal extent, and the cartilage has ceased to disintegrate. This speaks that 144 hours after the formation of new epidermis is completed, disintegration of the connective tissue is still going on under it, and simultaneously new connective tissue is formed. When the process reaches a certain extent, as shown in the case of 181 hours after the wound-making, the disintegrating substances not only continue to form connective tissue, but also begin to form new cartilage. The living substance first forms epidermal cells, then connective tissues. This process follows a definite sequence.

The auther in his study of the tissues of lymph node in 1937[41] found one kind of small bodies in the connective tissue of the lymph node. These bodies can develop into undifferentiated cells, which, in turn, form various kinds of leucocytes. Under normal conditions there is a certain percentage of leucocytes developing from the small bodies.

The facts cited above show that there is a definite rule followed by the development of tissues. Of what mechanism is underlying this sequence and rule we are still ignorant. It should be investigated in future in the light of Pavlov's theory. As proved by the experiment of Professor Zazipin, "in the organism, not only the cells but all the non-cellular living substance is controlled by the nervous system." The sequence and rule of development of the disintegrating tissues and of the formation of cells in the organism is of vital importance; without this rule, a pathological state will arise.

The literature relating to the development of living substance into tissues of organism, and the facts the author has observed in his own experiments, such as the role of living substance in wound-healing, and the development of small bodies in the development of leucocytes, make him consider in a broader sense the formation of cells from the living substance in the organism. *In the organism, the tissues under disintegration and destruction are not all going to die, while they may develop into new tissues and cells under favourable conditions.*

Summary

I. Different stages of growth of new epidermis were examined during wound-healing on the rabbit's ear.

II. Disintegrating tissues, including fragments of leucocytes, macrophages, collagenous fibres, and cartilage, were discovered in front of and along the margin of the growing epidermis.

III. A large quantity of nuclear substance was released by the disintegrating tissues, able to develop into nuclei of young cells in the growing epidermis, and further into young cells with cytoplasm and cell membrane.

IV. In addition to epidermal cells, the disintegrating tissues were able to develop into connective tissues.

V. Mitosis took place after the young cells had been formed in the new epidermis, but the number was rather limited.

VI. New epidermal cells chiefly developed from the disintegrating tissues, while a small number of them resulted from mitotic divisions.

References

[1] Arey, L. E., 1947. Developmental Anatomy, Philadelphia, W. B. Saunders Company.

[2] Patten, B. M., 1947. Human Embryology, Philadelphia, The Blakiston Company.

[3] Jordan, H. E., and Kindred, J. E., 1937. A Text-book of Embryology. 3rd. Ed. New York. D. Appleton-Century Company.

[4] Cowdry, E. V., A Text-book of Histology. 4th Ed., London, Henry Kimpton, 25 Bloomsbury Way. W.C.I.

[5] Maximow, A. A., and Bloom, W., 1943. Text-book of Histology, 4th Ed. Philedelphia and London, W. B. Saunders Company.

[6] Bailey, 1944. Text-book of Histology, 8th Ed., A William Wood Book, The Williams and Wilkins Company. Baltimore. MD, U.S.A.

[7] Bremer, J. L., 1944. A Text-book of Histology, 6th Ed. The Blakiston Company, Philadelphia, U.S.A.

[8] Schafer, 1950. Essentials of Histology, Edited by H. M. Carleton, M. A., B. Sc., D. Phil. and E. H. Leach, M. A., B. Sc., 15th Ed. Printed in Great Britain Spottiswoode, Ballautyne and Co. Ltd. London and Colchester.

[9] Jordon, H. E., 1947. A Text-book of Histology, 8th Ed. Appleton-Century-Crofts, Inc. New York.

[10] Lambert, 1948. Histology, revised by Helen L. Dawson, Ph. D., 2nd Ed. Blakiston Company, America.

[11] Ham, A. W., 1950. Histology, 3rd Impression, America, By J. B. Lippincott Company.

[12] Ormsley, O. S., 1937. Practical Treaties on Disease of the Skin for the Use of Students and Practitioners. 5th Ed. Philedelphia, Lea and Fibiger.

[13] Sutton, R. L., and Sutton, R. C. Jr., 1939. Disease of the Skin, St. Louis, C. V. Mosby Company.

[14] McCarthy, L., 1931. Histopathology of Skin Disease, St. Louis, C. V. Mosby Co.

[15] Lewer, W. F., 1949. Histopathology of the Skin, Philadelphia, J. B. Lippincott Co.

[16] Arey, L. B., 1936. Wound Healing. *Physiological Reviews,* **16** (3), 327—406.

[17] Ham, A. W., 1950. Histology, J. B. Lippincott Company, London, Philadelphia. Montreal.

[18] Gordon, J. O., 1946. Hall, R. A., Heggie, R. M., and Horne, E. A., A Histological and Bacteriological Study of Healing Burns with an Enquiry into the Significance of Local Infection. *Jour. Path. and Bact.* **58** (1), 51—61.

[19] Thuringer, J. M., 1928. Studies on Cell Division in the Human Epidermis. II. A. Rate of Cell Division in the Prepuce. B. Influence of Various Factors on Cell Division. *Anat. Rec.,* **40,** 1—13.

[20] Palzelt, V., Bau und verhornung der menschlichen Epidermis. *Wien med. Wchnschr.,* **78**, 663—665.

[21] Holmes, S. J., 1914. The Behavior of the Epidermis of Amphibians when Cultivated Outside the Body. *J. Exp. Zool.,* **17**, 281.

[22] Klebs, E., 1875. (cited from Leslie B. Arey, 1936) *Arch. f. exp. path. u. pharm.,* **3**, 124.

[23] Peters, A., 1885. Inaug. Diss. Zu Boun. 32, pp. C. Georgi. Bonn.

[24] Arey, L. B., 1932a. Certain Basic Principles of Wound Healing. *Anat. Rec.,* **51**, 299—313.

[25] Herrick, E. H., 1932. (cited from Leslie B. Arey, 1936) *Biol. Bull.,* **63**, 271.

[26] Poynter, C.W.M., 1919. Some Observations on Wound Healing in Early Embryo. *Anat. Rec.,* **16**, 1.

[27] Born, G., 1896. Über verwachsungsversuche mit Amphibienlarven. *Arch. f. Entwickl-mech. d. Org.,* **4**, 349.

[28] Hartwell, S. W., 1928. The Various Parietal Tissue in Healing of Surgical Wound. 1. The Healing of the Epithelium *Proc. Stoffmeet, Mayo Clin.,* **3**, 344.

[29] Cameron, J. H., The Origin of New Epidermal Cells in the Skin of Normal and X-rayed Frogs. *J. Morph.,* **59**, 327—350.

[30] MacCardle, R. C., M. F. Engman, Jr., and M. F. Engman, Sr., 1943. Histology of Neurodermatitis from Studies on Neurodermatis, American Medical Association, 1—29.

[31] Andrew, W., and Andrew, N. V., 1921. Lymphocytes in the Normal Epidermis of the Rat and of Man. *Anat. Rec.,* **33**, 463.

[32] Ortiz-Picon, J. M., 1934. Über Zellteilungsfrequenz und Zellteilungsrhythmms in der Epidermis der Maus. *Ztschr. f. Zellforsch. u. mikr. Anat.,* **19**, 488—509.

[33] Arey, L. B., 1921. An Experimental Study on Glochidia and the Factors Underlying Encystment. *J. Exp. Zool.,* **33**, 463.

[34] Harabath, R., 1928. (cited from Leslie B. Arey, 1936) *Arch. f. path. Anat. u. Physiol.,* **268**, 794.

[35] Oppel, A., 1912. Causal-morphologische Zellenstudien. V. Mitteilung: Die aktive Epithelbewegung, ein Faktor beim Gestaltungs– und Erhaltungsgescheh. *Arch. f. Entwickl-mech. d. Org.,* **35**, 371.

[36] Voit, E., Über die Grösse der Erneurung der Horngebilde beim Menschen III. Mitteilung. Die Oberhaut. *Ztschr. f. Biol.,* **90**, 549—533.

[37] Лепешинская, О. Б., 1950. Происхождение клеток из живого вещества и роль живого вещества в организме. Глава XVII, 116; Глава III, 33.

[38] Лепешинская, О. Б., 1952. Клетка его жизнь и Происхождение Бивкуль, Москва.

[39] Лепешинская, О. Б., Совещание по пробпеме живого вещества и расвития клеток, стр. 32.

[40] Маловичко Е. Е., и Рупасова Т. Н., 1953. Материалы к вопросу о роли живого вещества в процессе заживления ожогов (Предварительное сообащение). *Архие Анатомии Гистологии и Эмбриологии*, **29**(3), 23–27.

[41] Ma, W. C., 1937. Blood Changes during Intoxication and Detoxication in the Chronically Morphinized Rat. IV. Changes in the Lymph Mode. *Chinese J. Physiol.*, **12**, 429—484.

EXPLANATION OF PLATE I

1. Photomicrograph of specimen taken after 13 hours, showing the formation of the scab. Scab in purple, normal tissues in blue. In the scab the upper is the blood clot and the lower is injured tissue with blood cells. The central blue column is the longitudinal section of the elastic cartilage. Fixative: Susa, Staining: Mallory's. Eyepiece: × 18, Objective: × 10. Photo: Leica colour film, enlarged × 5.7.
2. Mignified photomicrograph of the rectangle in fig. 2 of Plate V, showing disintegration of the leucocytes at the tip of the growing epidermis. A and B, newly formed young cells.
   Fixative: Formalin, Staining: H. E. Eyepiece: × 8, Objective: × 100. Photo: as Fig. 1.
   Formalin, Staining: H. E. Eyepiece: × 8, Objective: × 100. Photo: as Fig. 1.
3. Photomicrograph of trypan-blue-injected specimen. A and B show the new epidermis growing toward the centre. The pale blue granules under and in front of the new epidermis show the macrophages undergoing changes in the place.
   Fixative: Susa. Staining: 0.25% acid fuchsin and 1% picric acid. Eyepiece: × 8, Objective: × 10. Photo: as above.
4. Magnified photomicrograph of the rectangle in the above figure. A, trypan blue granules in the macrophages; B, trypan blue granules in the mucleus of the newly formed young cells; C, newly formed young cell; D, a mass of mixing trypan blue granules and disintegrated leucocytes. Eyepiece: × 8, Objective: × 100, Photo: as above.


2
A
B

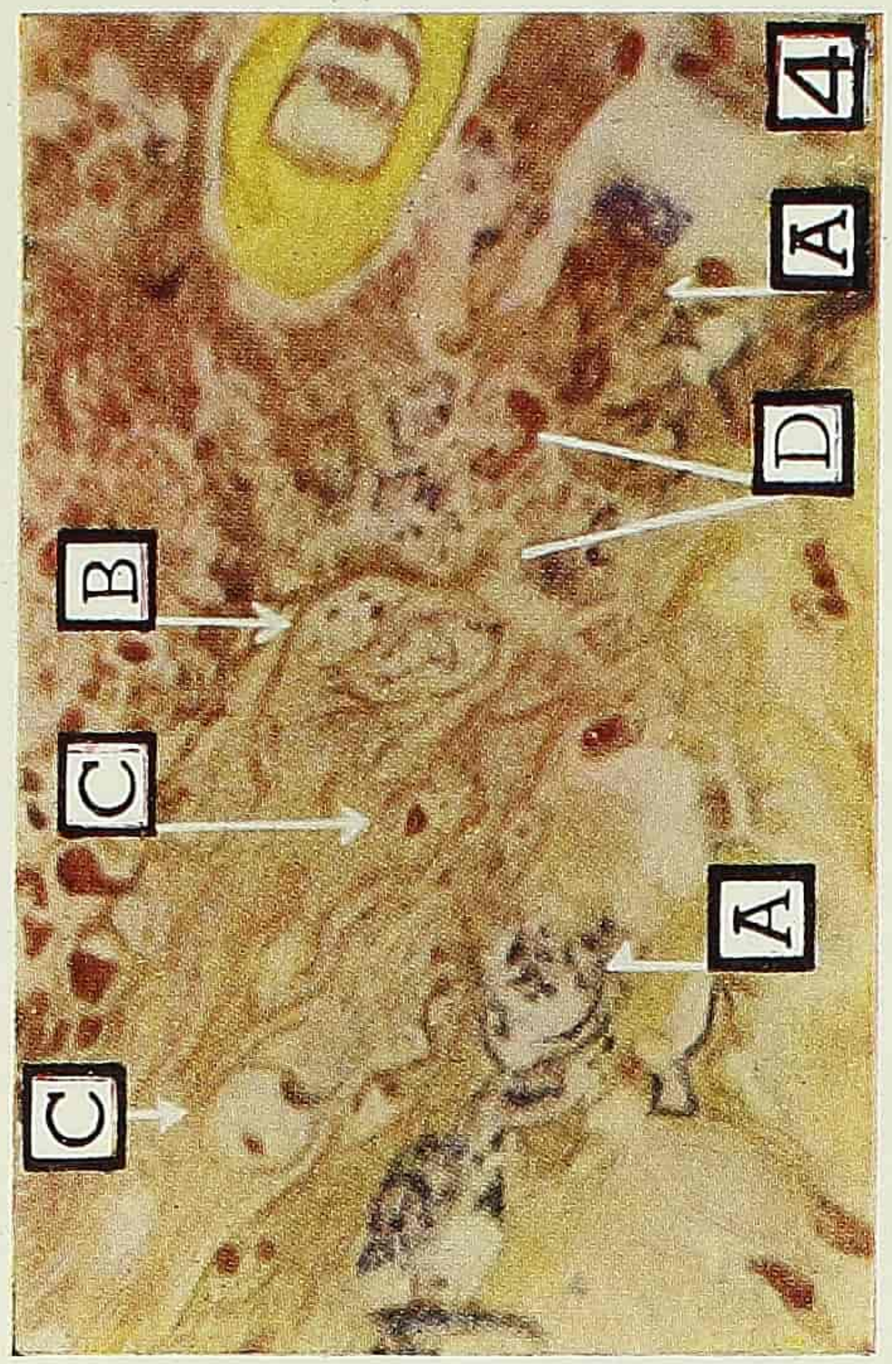
4
A
D
B
C
C
A


1

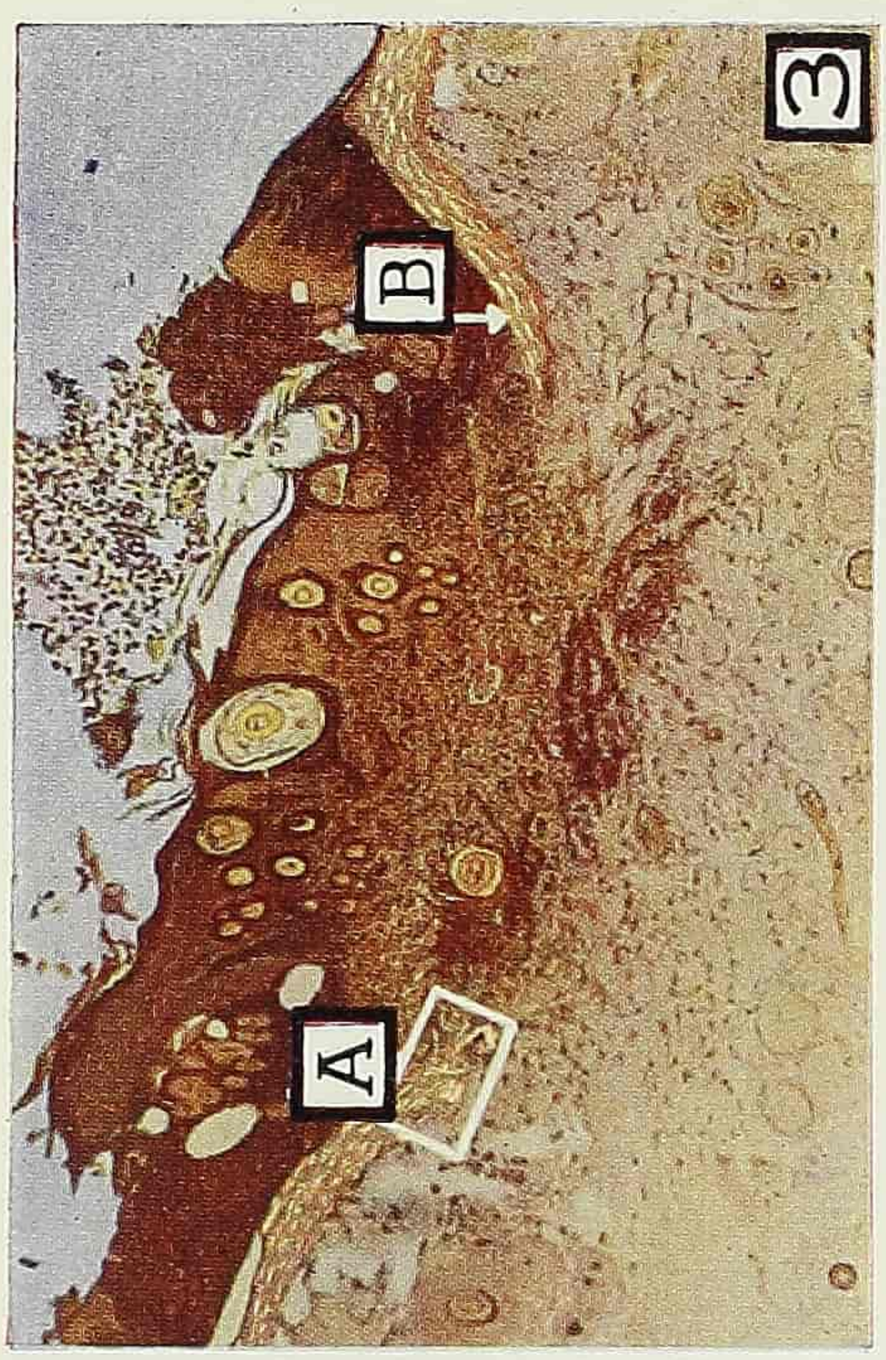
3
B
A

EXPLANATION OF PLATE II

1. Photomicrograph showing stages of the development of disintegrating tissues into young cells. The arrow head shows the direction of growth of the new epidermis; at the tip of growth there is a swelling body surrounded by disintegrating tissues stained in dark blue and purple. A and B, aggregates; C, a newly formed young cell nucleus; D, a young cell.
   Fixative: Susa, Staining: Mallory's, Eyepiece: × 8, Objective: × 100, Photo: Leica colour film, × 5.7.
2. A, a larger, spherical young cell; B, a smaller spindle-shaped newly-formed young cell nucleus; C, cartilage.
   Fixative: Susa, Staining: Mallory's Eyepiece: × 8, Objective: × 45, Photo: as above.
3. Photomicrograph showing the disintegration of the connective tissue. The new epidermis grows under the scab from lower right to upper left. Along the course of growth there are disintegrating collageous fibres. A, the mixing of disintegrating collageous fibres and disintegrating leucocytes; B, newly-formed young cell nucleus.
   Fixative, staining, magnification, and photo as above.
4. Photomicrograph showing disintegration of the connective tissue. The new epidermis grows under the scab from lower right to upon left. Along the course of growth there are disintegrating fibres. A, Disintegrating collagenous fibres; B, the mixing of disintegrating collagenous and disintegrating leucocytes; C, newly-formed young cell nucleus; D, a newly-formed young cell nucleus resembling a lymphocyte; E, a young cell.
   Fixative: Zenker-formalin, Staining: H. E. The rest as above.

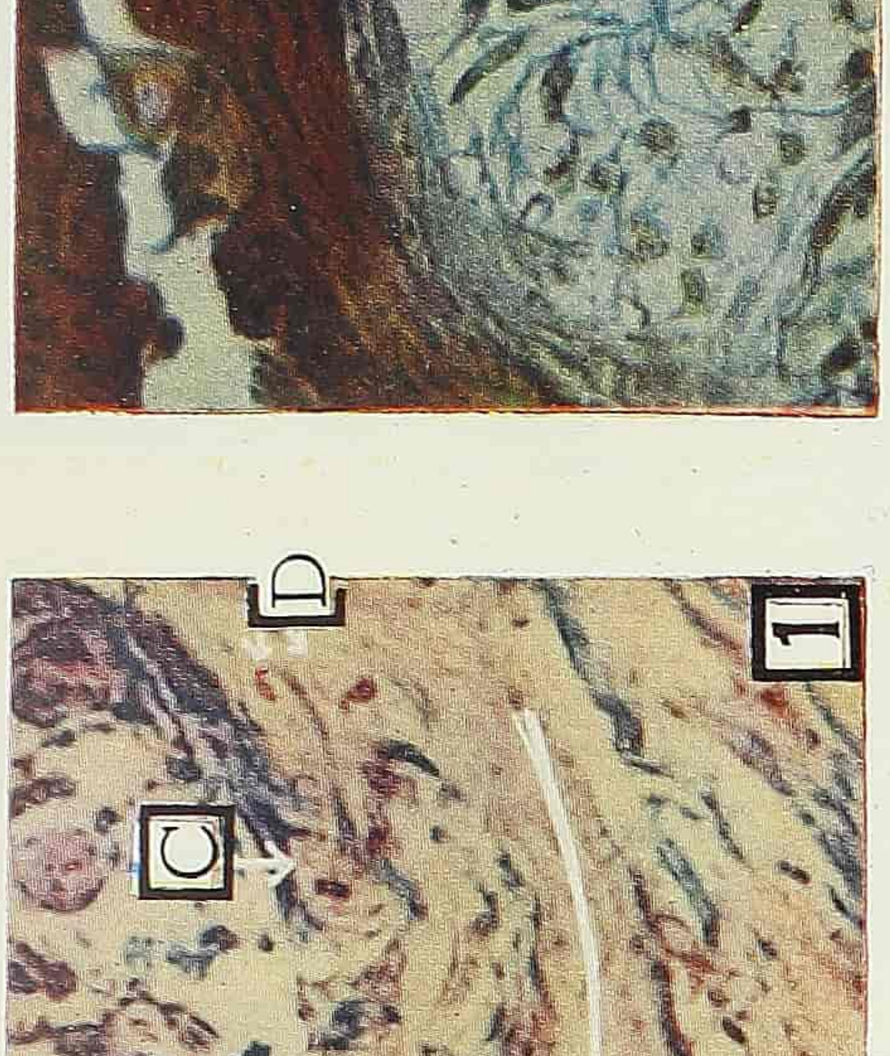
2
A
B
C

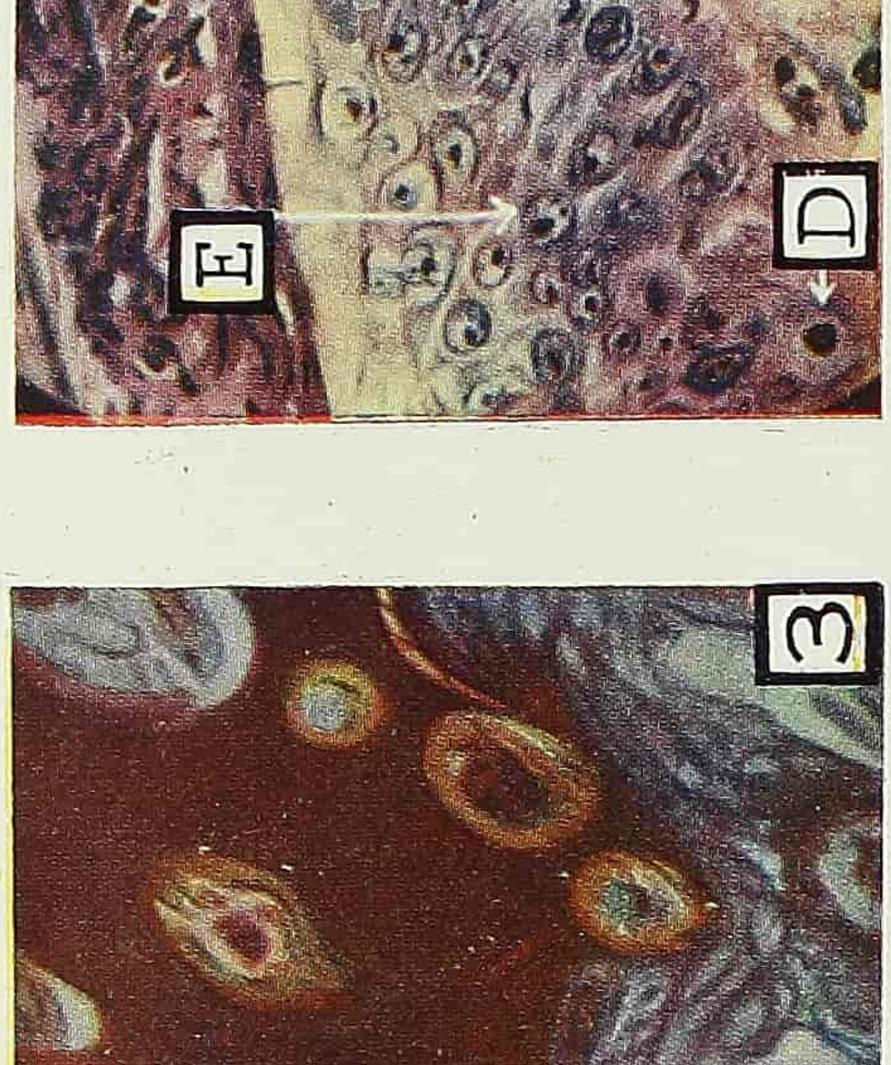
4
C
B
A
E
D


1
D
C
A
A
B


3
A
B

EXPLANATION OF PLATE III

1. Magnified photomicrograph of figure 4 of Plate V, showing disintegration of elastic cartilage. The new epidermis grows from upper right downward. The connective tissue is continuous with the cartilage. A, the mixing of the disintegrating cartilage and disintegrating leucocytes; B, the accumulation of a few newly-formed young cell nuclei.
   Fixative: Susa, Staining: Mallory's, Eyepiece: × 8, Objective: × 45. Photo: Leica colour film, × 5.7.
2. Photomicrograph showing that, after the new epidermis has grown to a certain extent, the disintegiating tissues cease to develop into epidermis and turn to the formation of the connective tissue. A, the tip of the growing epidermis. In the middle part of the figure there are newly-formed young cell nuclei and young cells. Among them there are blue collagenous fibres. In the lower region of the figure the cartilage is disintegrating.
   Fixative: Susa, Staining: Mallory's sections parallel to the cartilage plate. The rest as above.
3. Photomicrograph of a section parallel to the cartilage plate. The upper 1/3, dead cartilage; the lower 1/3, living cartilage; the middle 1/3, the growing epidermis with its papillae.
   Fixative: Susa, Staining: Mallory's, Eyepiece: × 8, Objective: × 10. Photo: as above.
4. Magnified photomicrograph of the rectangle in the above figure, showing the relation of the new-formed young cell nuclei and young cells with the disintegrating cartilage. A, disintegration of the cartilage.
   Eyepiece: × 8, Objective: × 45.
5. Photomicrograph showing the penetration of the growing epidermis into the cartilage. Fixative, etc. as above.

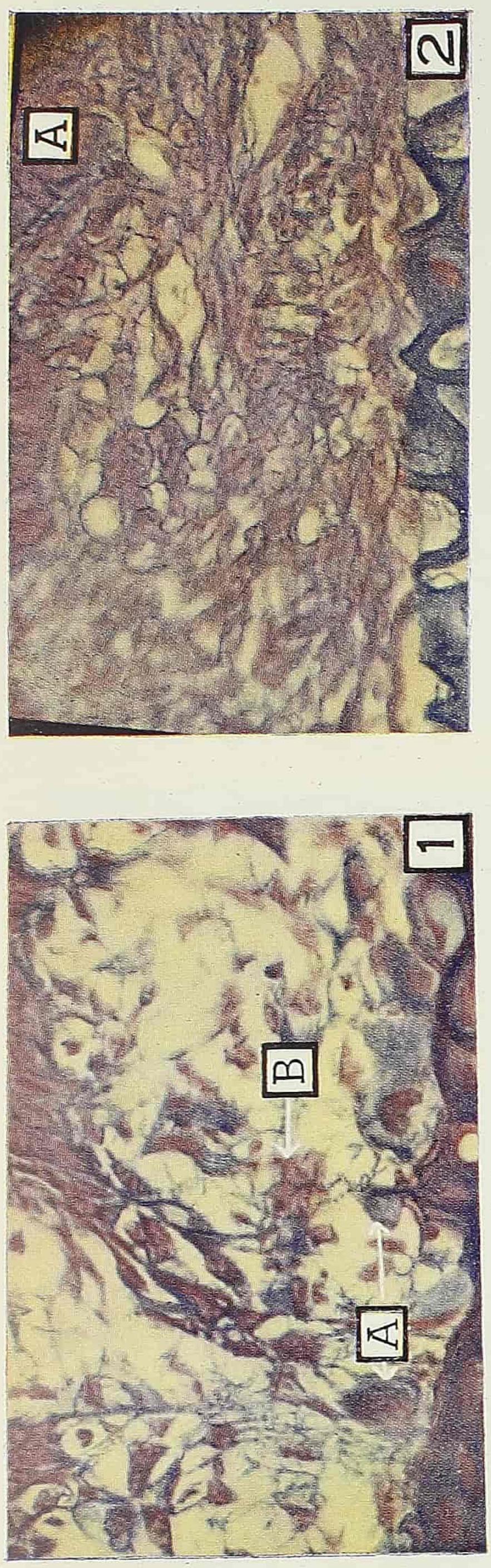
A
2

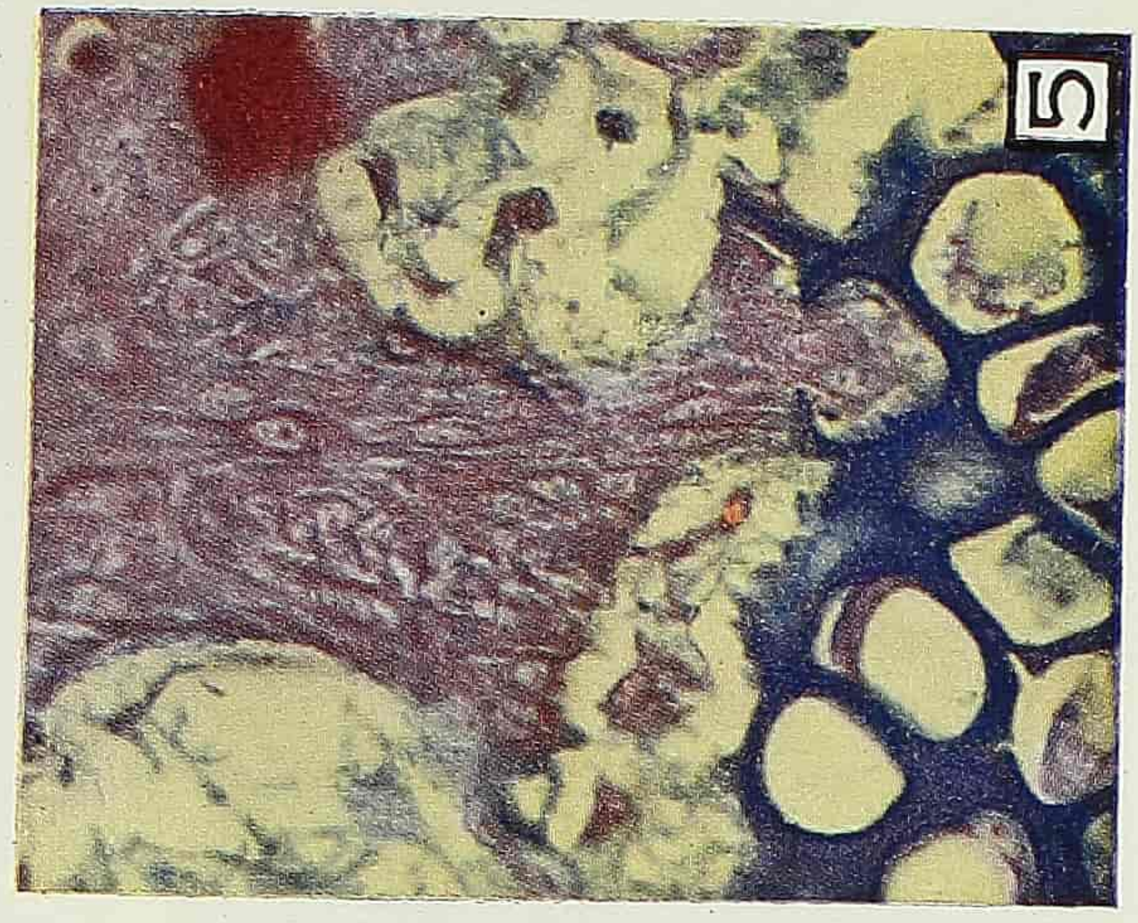
5

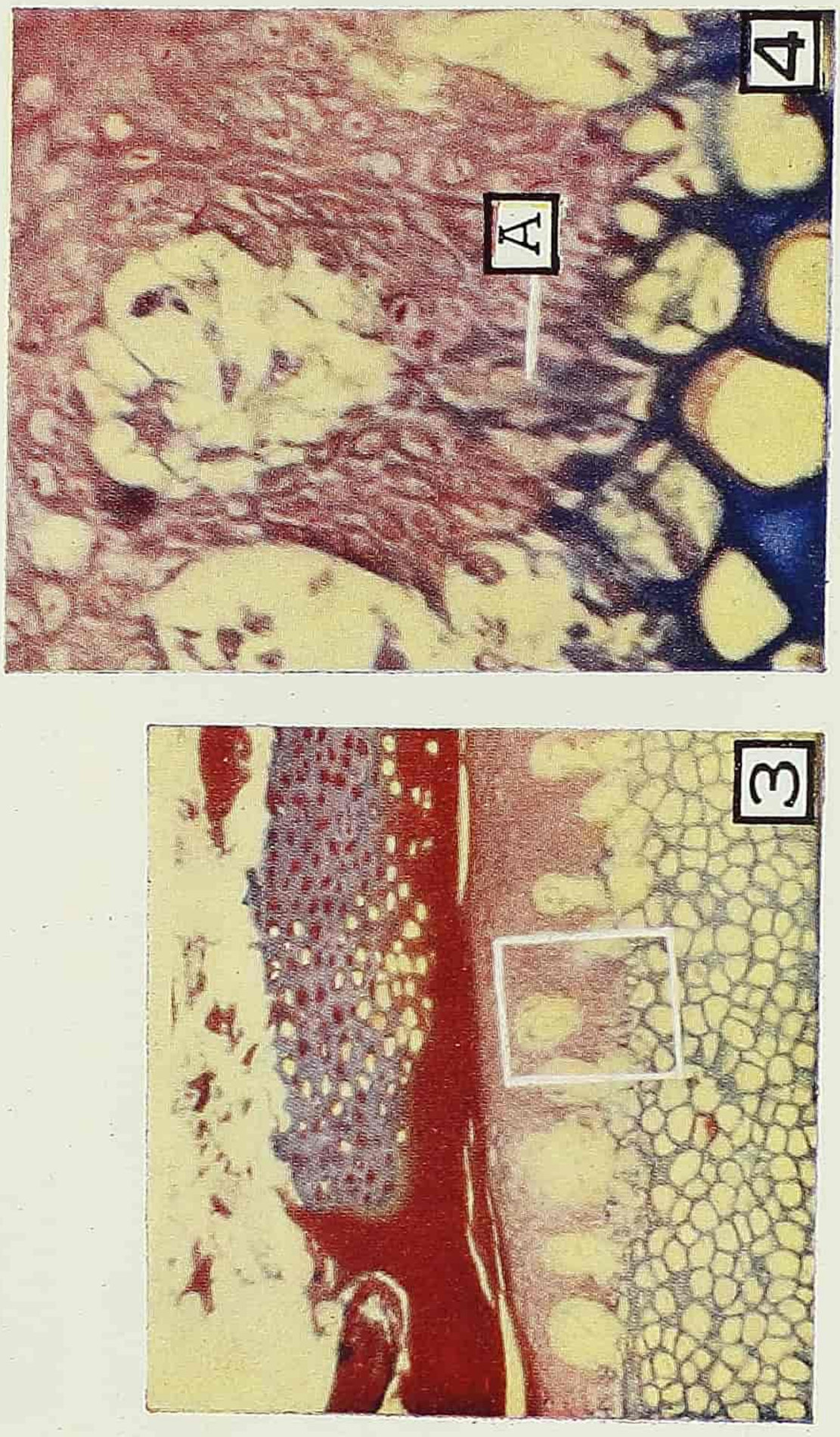
4
A
2

1
B
A

3

EXPLANATION OF PLATE IV

1. Photomicrograph of a specimen taken 32 hours after a wound was made. A and B, showing the boundary between the original and the new epidermis.
   Fixative: Susa, Staining: H. E., Eyepiece: × 8, Objective: × 10.
2. Photomicrograph of A in the above figure, showing that the new epidermis is thicker than the original, mitotic figures in the new epidermis, and the transection of the collagenous fibres.
   Eyepiece: × 8, Objective: × 45.
3. Photomicrograph showing that the healed new epidermis is thicker than the original.
   Fixative: Susa, Staining: H. E., Eyepiece: × 8, Objective: × 10.
4. Photomicrograph showing that the new epidermis is thicker than the original. In the rectangle the orientation of the disintegrating leucocytes is along the direction of the growth of the new epidermis.
   Fixative: Susa, Staining: H. E., Eyepiece: × 8, Objective: × 45.


2

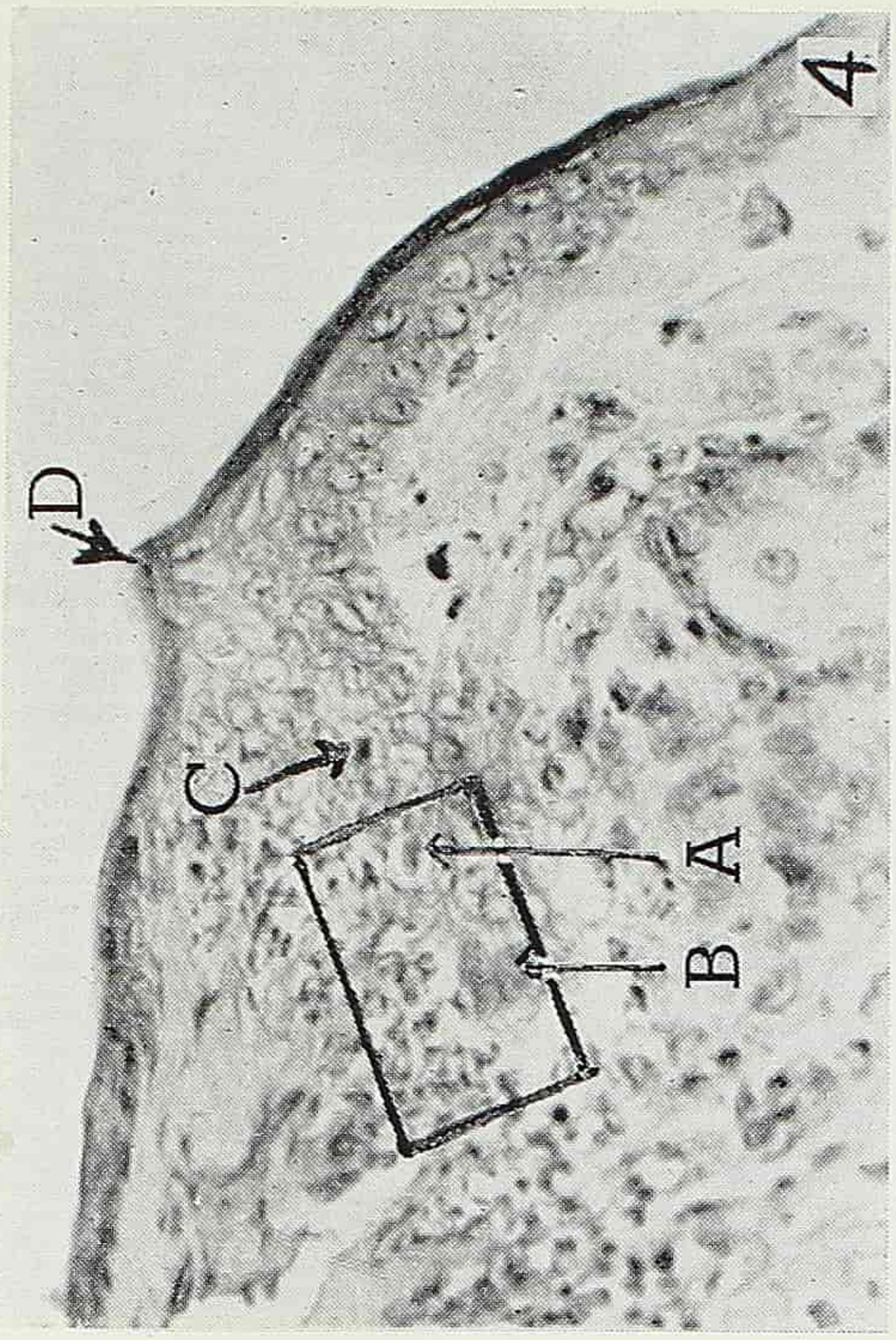
4
D
C
B
A

1
B
A

3

EXPLANATION OF PLATE V

1. Photomicrograph of a section of a wound on the guinea pig's ear. The black masses in the lower right corner are the newly-formed pigmented epidermis. In front of it, from A to B, leucocytes are arranged along the direction of the growing epidermis and at right angle of C, the original longitudinally arranged leucocytes.
   Fixative: Susa, Staining: H. E., Eyepiece: × 8, Objective: × 45.
2. Photomicrograph showing the formation of cells in front of the growing epidermis.
   Fixative: Formalin, Staining: H. E., Eyepiece: × 8, Objective: × 30.
3. Photomicrograph showing newly-formed young cell nuclei at the tip of the growing epidermis.
   Eyepiece: × 8, Objective: × 45.
4. Photomicrograph of a section parallel to the cartilage plate.
   Fixative: Susa, Staining: Mallory's, Eyepiece: × 8, Objective: × 10.

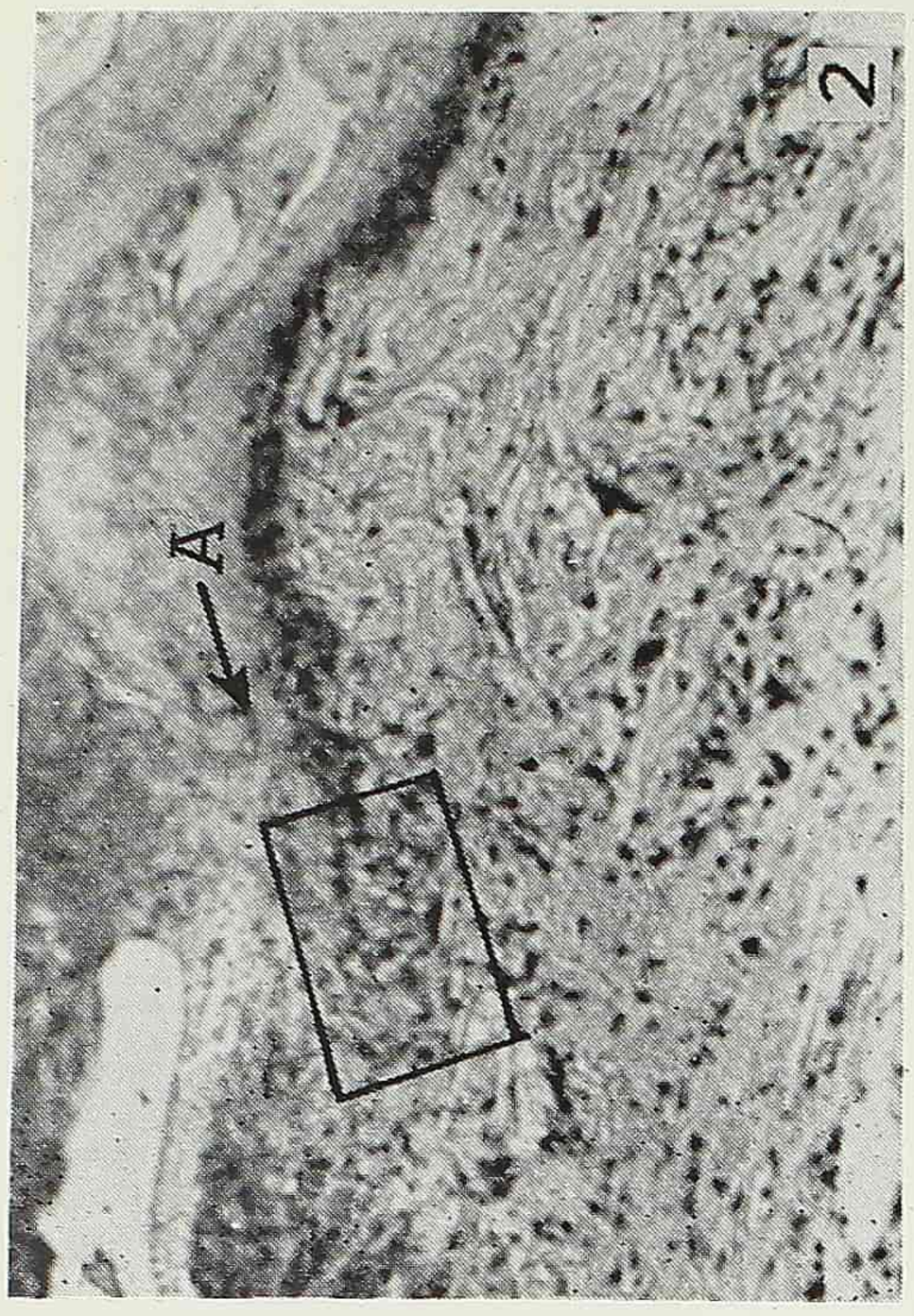
2
A

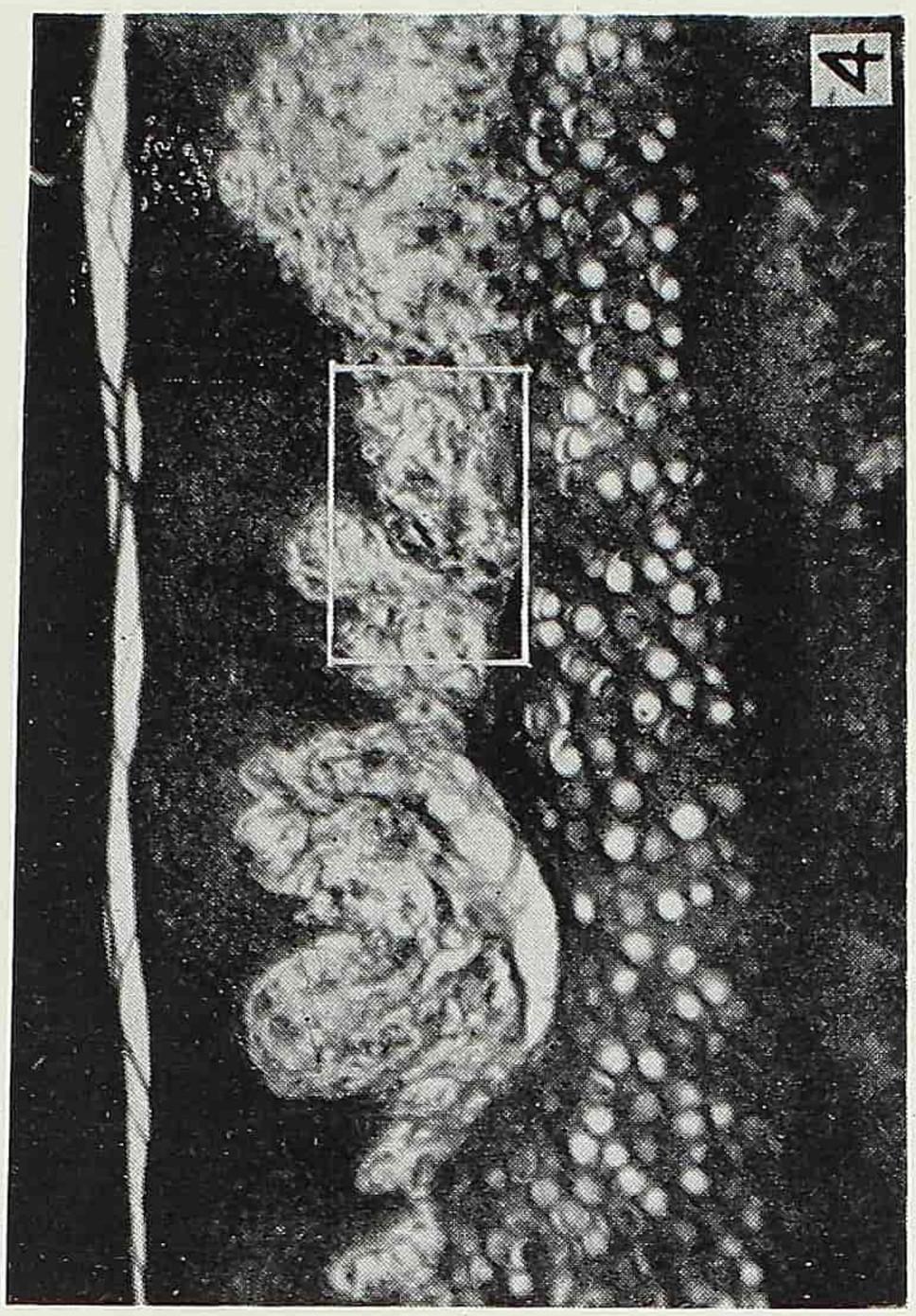
4

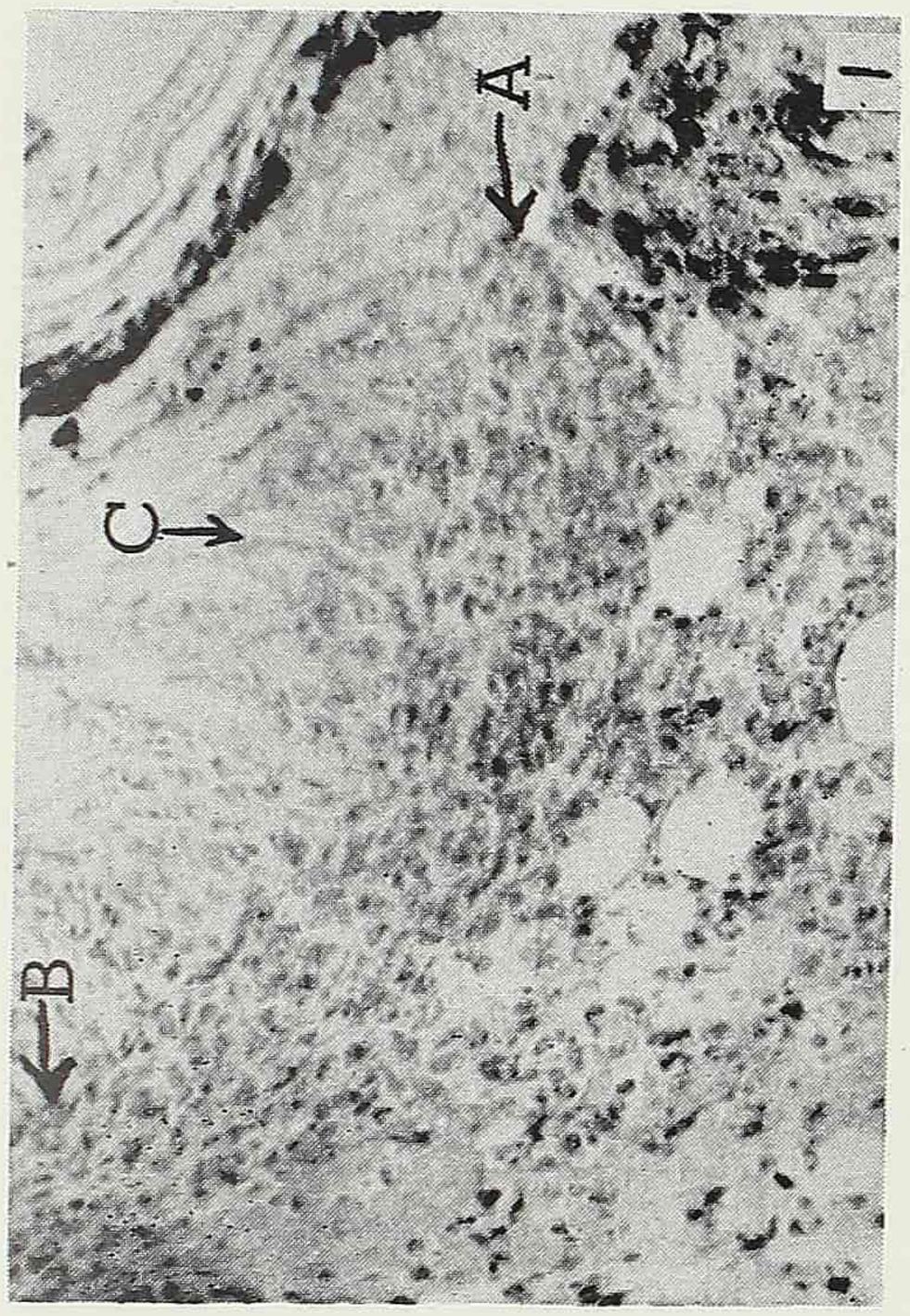
1
A
C
B


3

EXPLANATION OF PLATE VI

1. Photomicrograph showing the growing epidermis cut through the cartilage and increasing in thickness. The rectangular area, A, shows the thickening of the epidermis and the disintegration of the cartilage.
   Fixative: Susa, Staining: H. E., Eyepiece: × 8, Objective: × 10.
2. Photomicrograph showing the growth of new epidermis in thickness and density in passing through the cartilage, and the disintegration of the cartilage.
   Fixative, staining, and magnification as above.
3. Photomicrograph showing the penetration of the leucocytes into the cartilage along the direction of the growth of the new epidermis.
   Fixative, staining, and magnification as above.
4. Magnified photomicrograph of the rectangle in the above figure.
   Eyepiece: × 8, Objective: × 45.

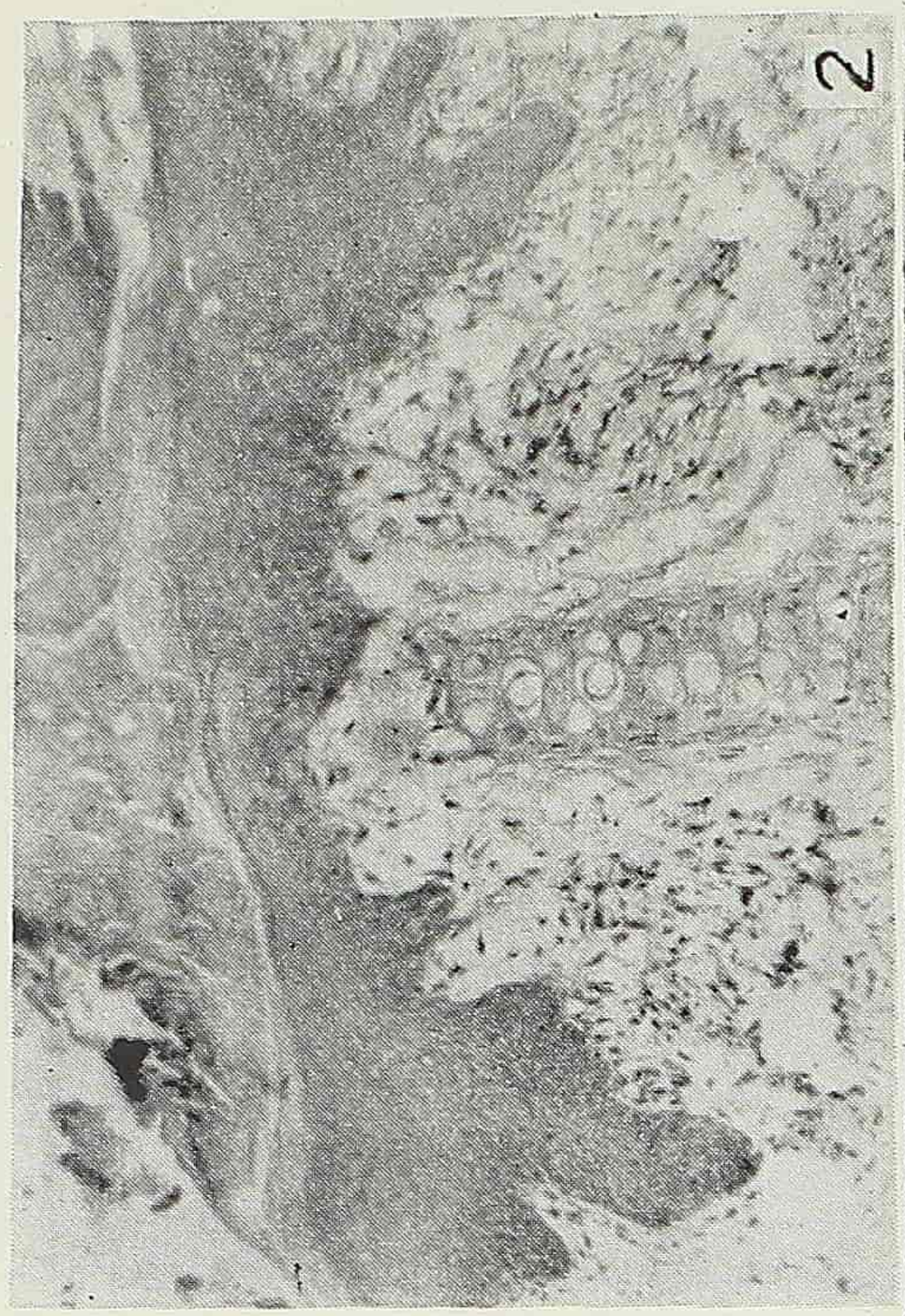
2


4

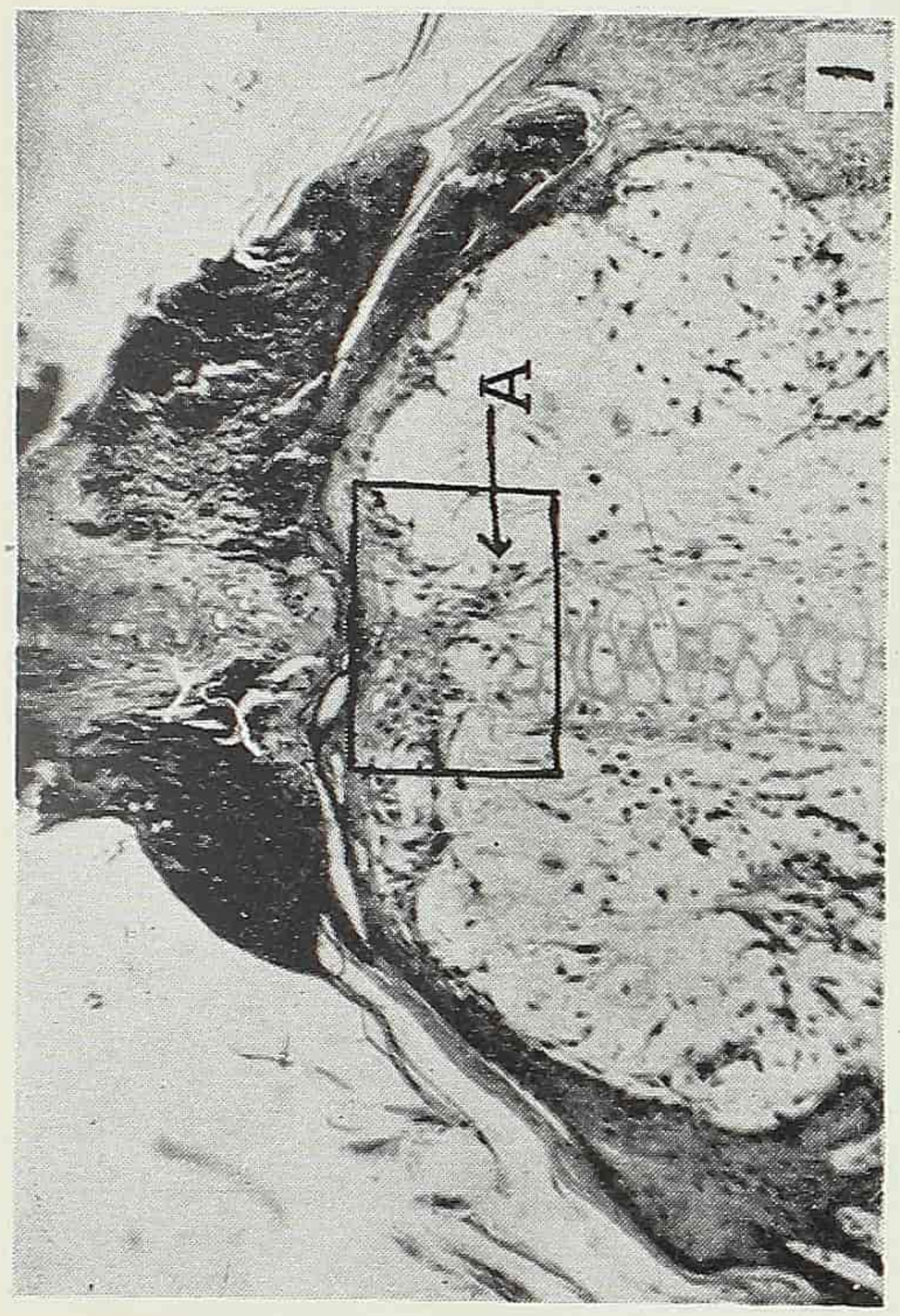
1
A

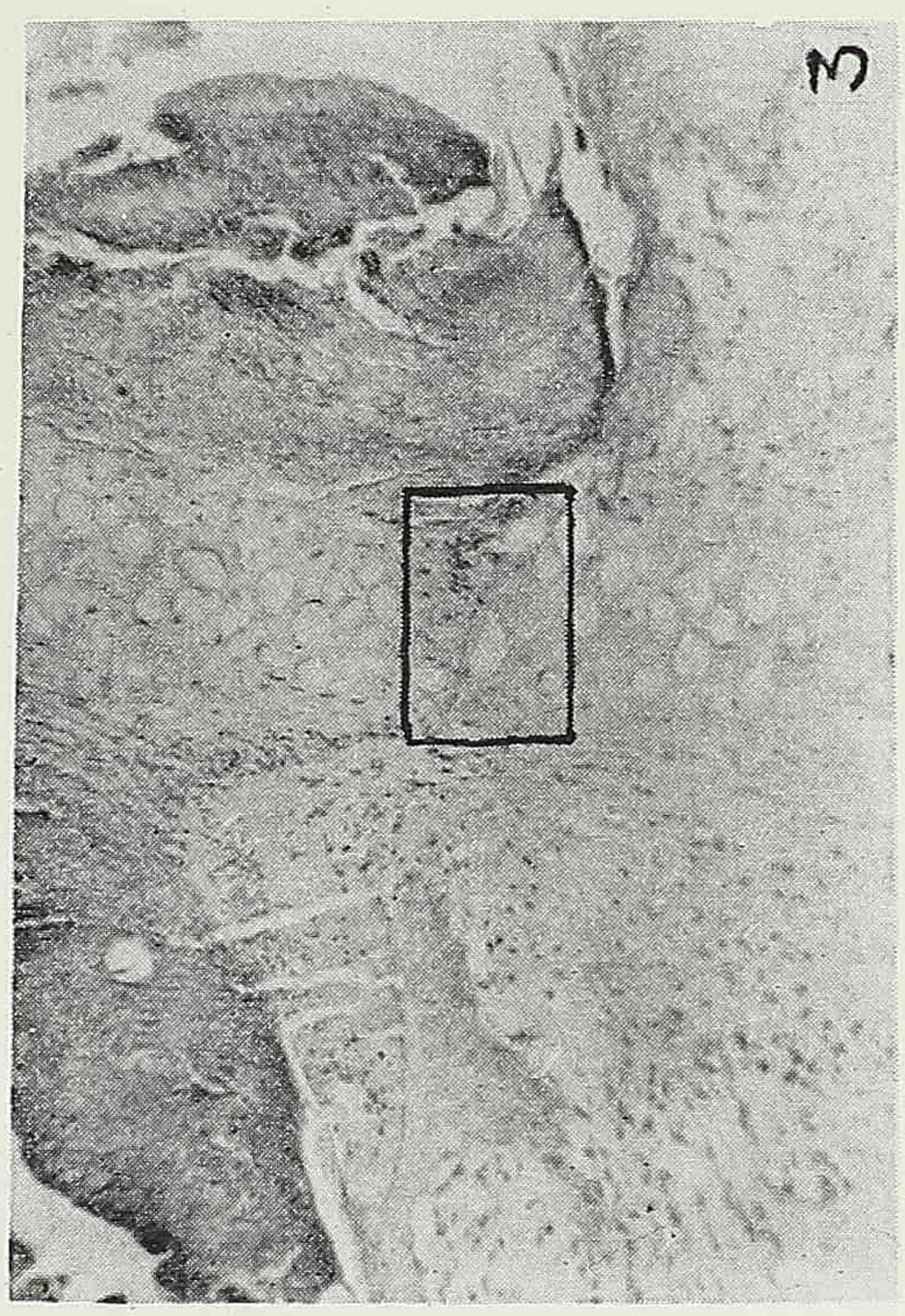
3

EXPLANATION OF PLATE VII

1. Photomicrograph showing how the leucocytes pass through the cartilage.
   Fixative: Susa, Staining: Mallory's, Eyepiece: × 8, Objective: × 10.
2. Magnified photomicrograph of a portion of the above figure.
   Eyepiece: × 8, Objective: × 45.
3. Photomicrograph of a specimen taken 72 hours after a wound was made. A, a large cell undergoing mitosis ocassionally found in the early stage of the growing epidermis.
   Eyepiece: × 8, Objective: × 30.
4. Photomicrograph of a specimen taken 181 hours after a wound was made, showing the development of the connective tissues after the epidermis has healed.
   Eyepiece: × 8, Objective: × 10.


2

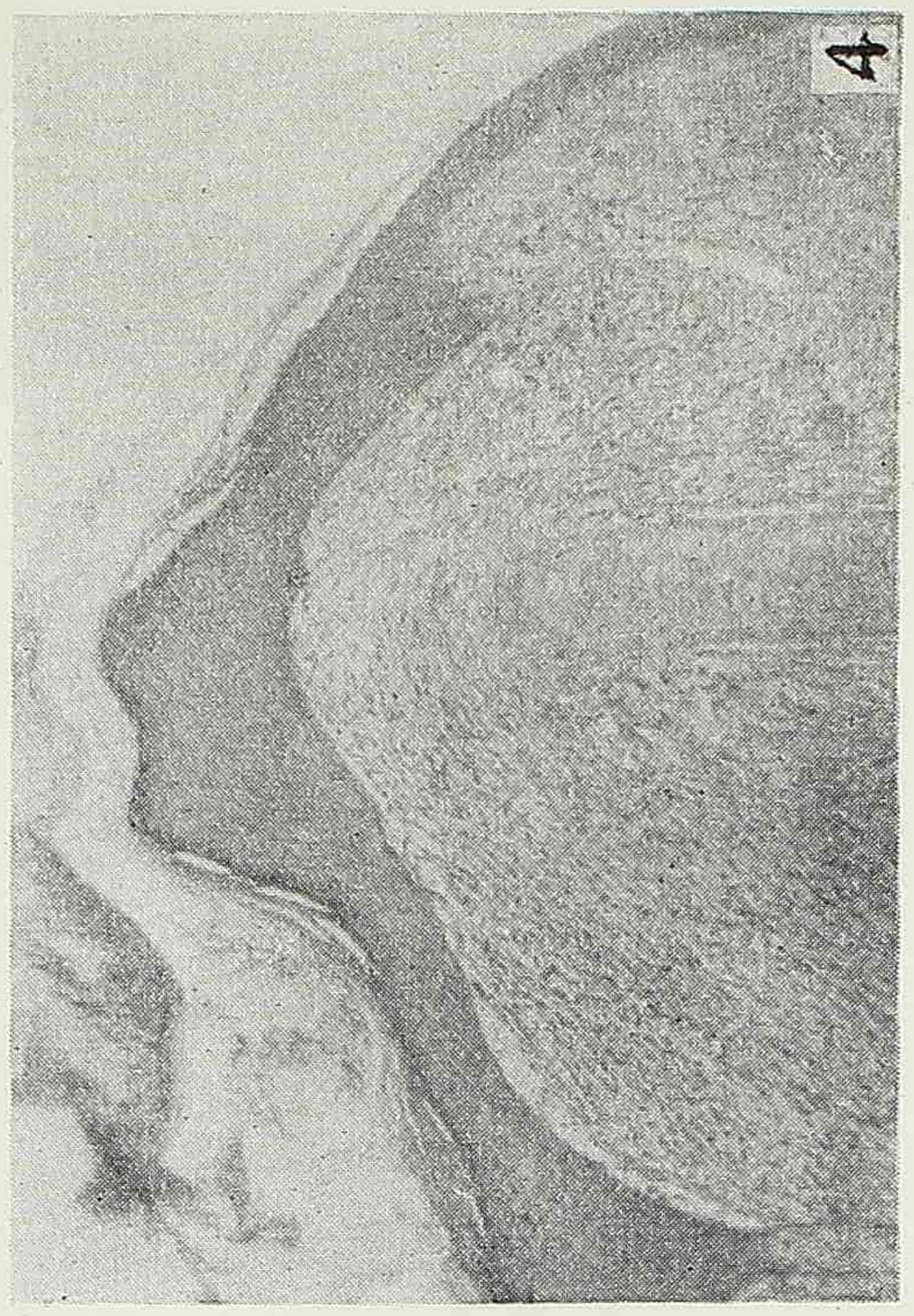
4

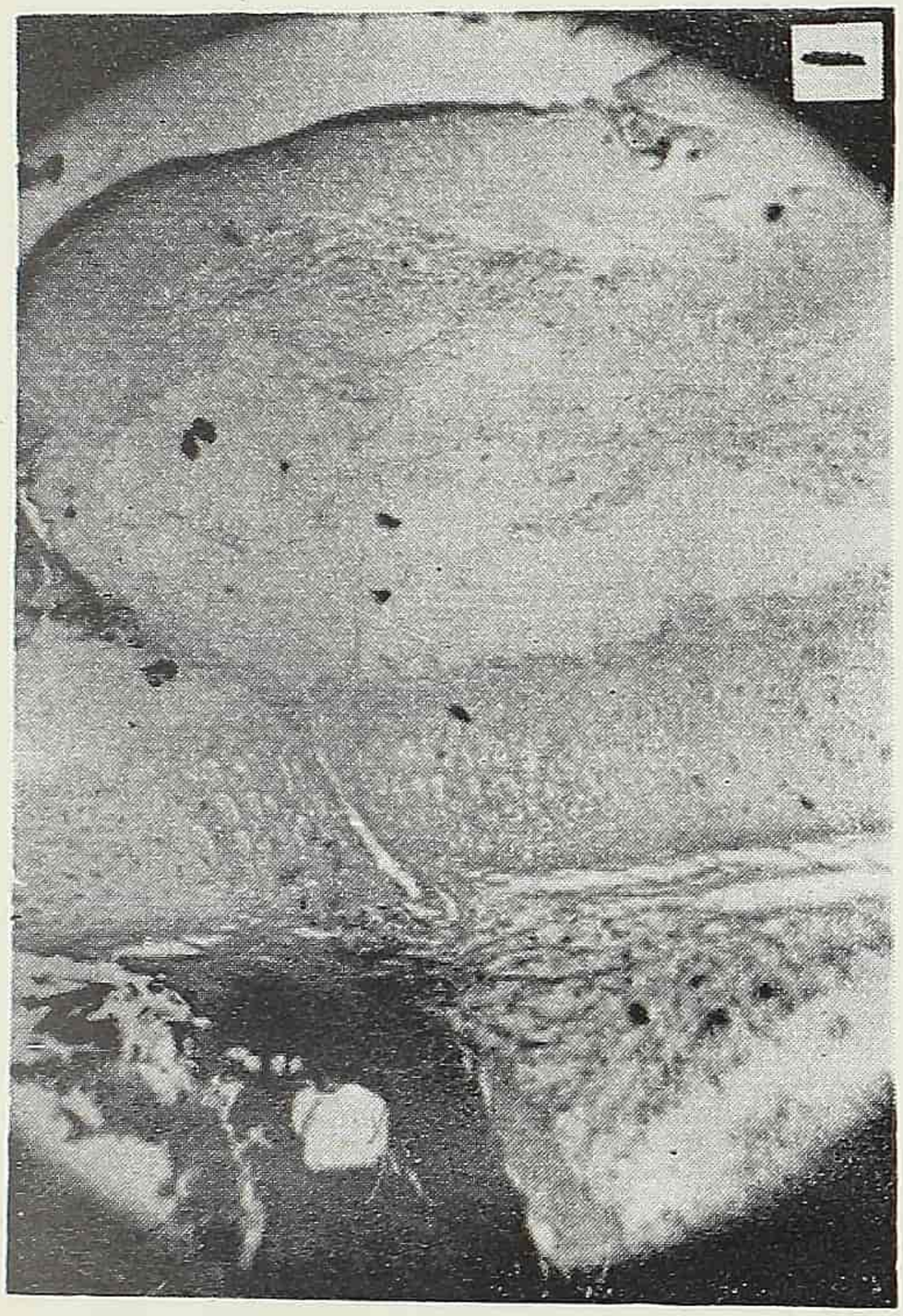
1

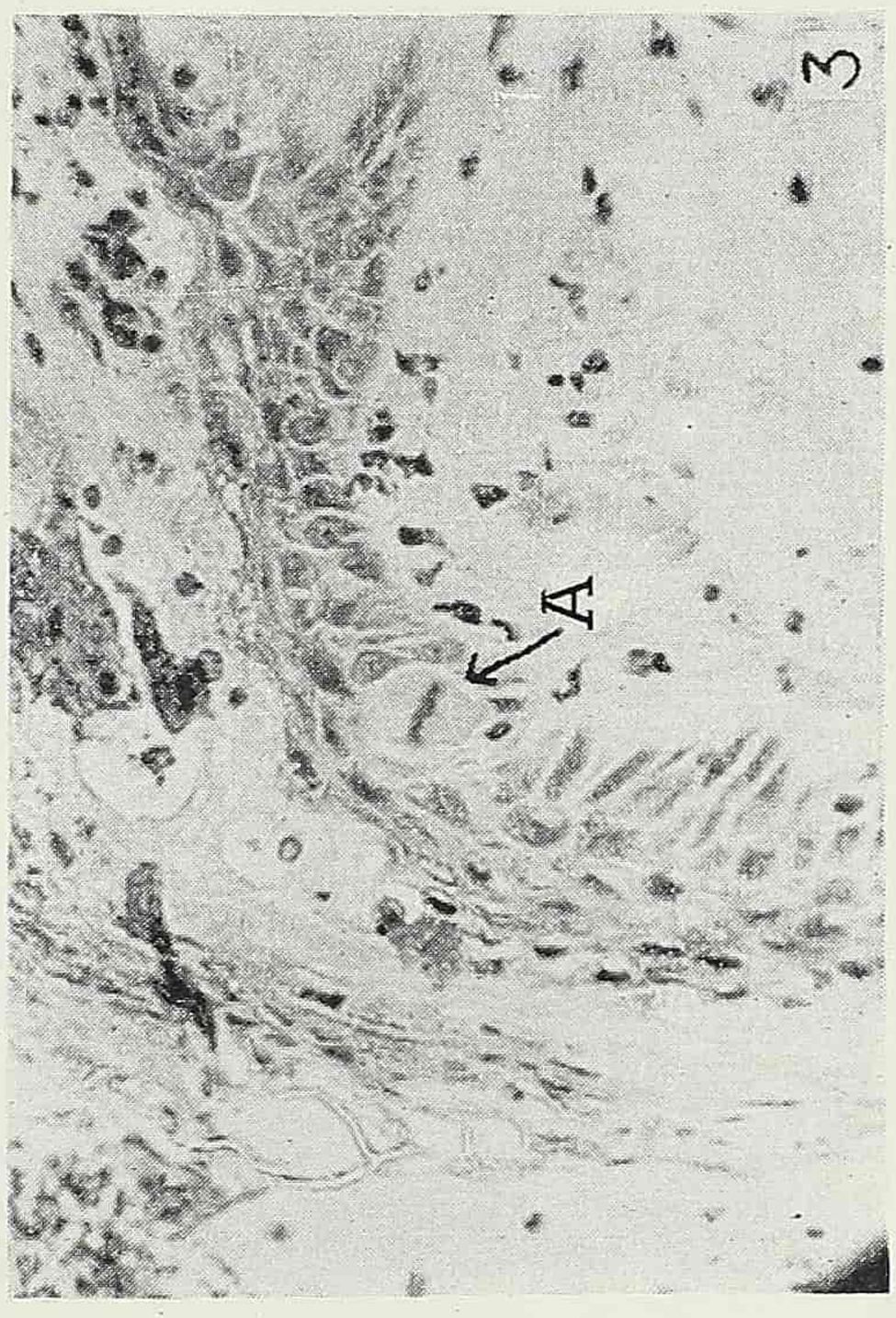
3
A

NOTES ON THE OSSIFICATION AND GROWTH OF THE HUMAN ZYGOMATIC BONE*

Woo Ju-Kang (吳汝康)

(Department of Anatomy, Dairen Medical Institute)

Studies on the ossification of different bones of man have been carried on for almost a century, but still not all questions are settled. One of the unsettled problems is the number of ossification centres of the zygomatic bone.

As early as 1864 Rambaud and Renault[9] described 3 ossification centres for the zygomatic bone which appeared in the 8th week in an embryo and fused into one in the 5th month. According to Mall[5], however, the bone is ossified from one centre. In view of the fact that the zygomatic bone in adult skull is sometimes split transversely into 2 or 3 pieces, many anatomists thus believe that it is developed from 3 centres. This state is reflected in the popular textbooks on human anatomy in the United States of America. Morris' Anatomy[6] states that the zygomatic bone is ossified from 3 centres and Gray's Anatomy[2] cites both theories. Thus this problem remains to be solved.

As to the growth of the zygomatic bone after the appearance of the ossification centre, no detailed description is available so far as the present author knows.

This paper deals with these problems regarding the zygomatic bone.

Material and Method

The material of this study includes 84 human embryos and fetuses ranging in age from 5 weeks to full term. The age of embryos and fetuses was determined by the C-R or crown-rump length according to Patten[8]. In measuring the older fetuses, the C-H or crown-heel dimension was also determined for the estimation of age.

The method used for clearing and staining embryos and fetuses generally followed the procedures suggested by Noback[7] with minor modifications as stated in the previous paper of the present author[12].

---

*First published in Chinese in the *Collections of Dairen Medical Institute* for the first Conference on Medical Science of the Northeastern Provinces in August, 1951, pp. 14—17.

Results and Discussion

The ossification centre of the zygomatic bone first appears in a fetus of 34 mm C-R length, aged 59 days according to estimate (fig. 1). Mall[5] described the centre of the zygomatic bone appearing in a fetus of 32 mm C-R length, estimated at 57 days. Thus the date of appearance of the ossification centre in the present study seems to be two days later than that given by Mall. However, the age of Mall's specimen was estimated in days by multiplying the square root of the C-R length in millimetres by 10 or $\sqrt{\text{C-R(mm)}} \times 10$. In the present study, the age was determined according to Patten's table. Mall's specimen of 32 mm C-R length in Patten's table gives an age of about 58 days. Thus the actual difference in the dates of appearance of the ossification centre of the zygomatic bone in both studies is only one day. No second centre of ossification was seen in all our specimens.

The zygomatic bone in adult skull is sometimes seen to be divided transversely into 2 or even 3 bones. The possible explanation is that in rare cases the zygomatic bone may be developed from 2 or 3 centres of ossification, but, in general, it is ossified from a single centre only.

The time of appearance of the ossification centre and the differentiation of the different processes of the zygomatic bone are given in Table 1.

Table 1. Time of Appearance of Ossification Centre and Different Processes of the Zygomatic Bone

No.	C—R length	Age	Appearance of Ossification Centre and Processes
80	10	5	None
26	12	6	,,
52	12	6	,,
44	15	6	,,
51	15.5	6	,,
55	16	6	,,
31	18	6	,,
49	21	7	,,
53	27	7	,,
18	29	8	,,
20	31	8	,,
48	31	8	,,
17	34	8	Ossification centre
54	37	8	Inf. & zygo. proc.
46	42	9	Fron. proc.
5	45	9	,, ,,
25	53	10	Orbit. proc.

The ossification centre of the zygomatic bone appears first as a small angular point located in the lower outer side of the orbit. In a fetus of 37 mm C-R length, estimated at about 61 days, the anterior or infra-orbital and posterior or zygomatic processes are seen to be formed. In a fetus of 42 mm C-R length, estimated at 64 days, the infra-orbital and zygomatic processes are more marked and the fronto-sphenoidal process begins to appear (fig. 2). The orbital process appears in a fetus of 53 mm C-R length, estimated at 71 days (fig. 3). Then the zygomatic bone possesses all its characteristic features.

Summary

1. The zygomatic bone of man is ossified from one centre only which appears in a fetus of eight and a half weeks old.

2. The infra-orbital and zygomatic processes appear at the end of the 8th week of the fetus.

3. The infra-orbital and zygomatic processes are more marked and the fronto-sphenoidal process begins to be differentiated in the 9th week of the fetus.

4. The orbital process appears in the 10th week of the fetus and then the form of the zygomatic bone is completed.

References

[1] Dawson, A., 1926. A Note on the Staining of the Skeleton of Cleared Specimens with Alizarin Red S. *Stain Techn.*, **1**, 123—124.

[2] Gray, 1948. *Anatomy of the Human Body.* Twenty-fifth ed., edited by Charles Mayo Goss, Lea & Febiger, Philadelphia, 168—170.

[3] Hollister, G., 1934. Clearing and Dyeing Fish for Bone Study. *Zoologica,* **12**, 89—101.

[4] Lundvall, H., 1905. Weiteres ueber Demonstration embryonaler Skelette. *Anat. Anz.,* **27**, 520—523.

[5] Mall, F. P., 1906. On Ossification Centres in Human Embryos Less than 100 Days Old. *Am. J. Anat.,* **5**, 433—458.

[6] Morris, 1942. *Human Anatomy,* Tenth ed., edited by J. Parsons Schaeffer, The Blakiston Co., Philadelphia, 164—165.

[7] Noback, Charles R., and Eleanor Noback, 1944. Demonstrating the Osseous Skeleton of Human Embryos and Fetuses, *Stain Techn.,* **19**, 51—54.

[8] Patten, B. M., 1946. *Human Embryology,* The Blakiston Co., Philadelphia.

[9] Rambaud, A., and Renault, Ch., 1864. *Origine et développement des os.* Paris.

[10] Schultze, O., 1897. Ueber Herstellung und Conservirung durchsichtiger Embryonen zum Studium der Skeletbildung. *Verh. Anat. Ges.,* 11 Versam., 3—5.

[11] Spalteholz, W., 1914. *Ueber das Durchsichtigmachen von menschlichen und tierischen Praeparaten.* 2. Auf., Leipzig.

[12] Woo, Ju-Kang, 1949. Ossification and Growth of the Human Maxilla, Premaxilla and Palate Bone, *Anat. Rec.,* **105**, 737—761.

EXPLANATION OF PLATE I

Fig. 1. From a fetus of 34 mm C-R length, estimated at 59 days, showing the beginning of appearance of the ossification centre of the zygomatic bone. Right side view. × 10.

Fig. 2. From a fetus of 42 mm C-R length, estimated at 64 days, showing the appearance of the fronto-sphenoidal process. Left side view. × 10.

Fig. 3. From a fetus of 53 mm C-R length, estimated at 71 days, showing the appearance of the orbital process. Right side view. × 10.

Cz., centre of ossification of zygomatic bone; F.p., fronto-sphenoidal process; In., incisive bone; Inf. p., infra-orbital process; Mx., maxilla; O.p., orbital process; Tem., temporal bone; Z.p., zygomatic process.

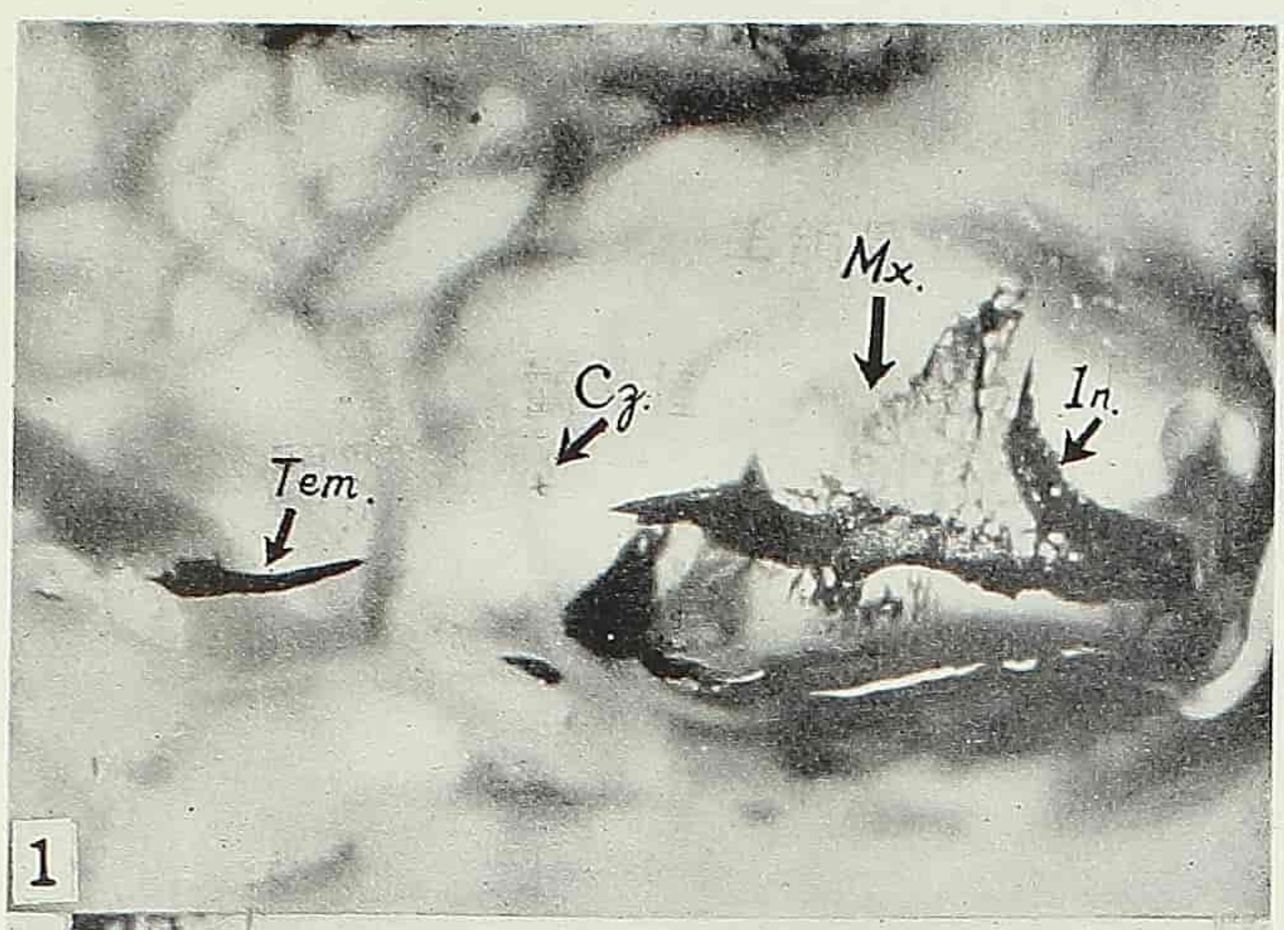

1

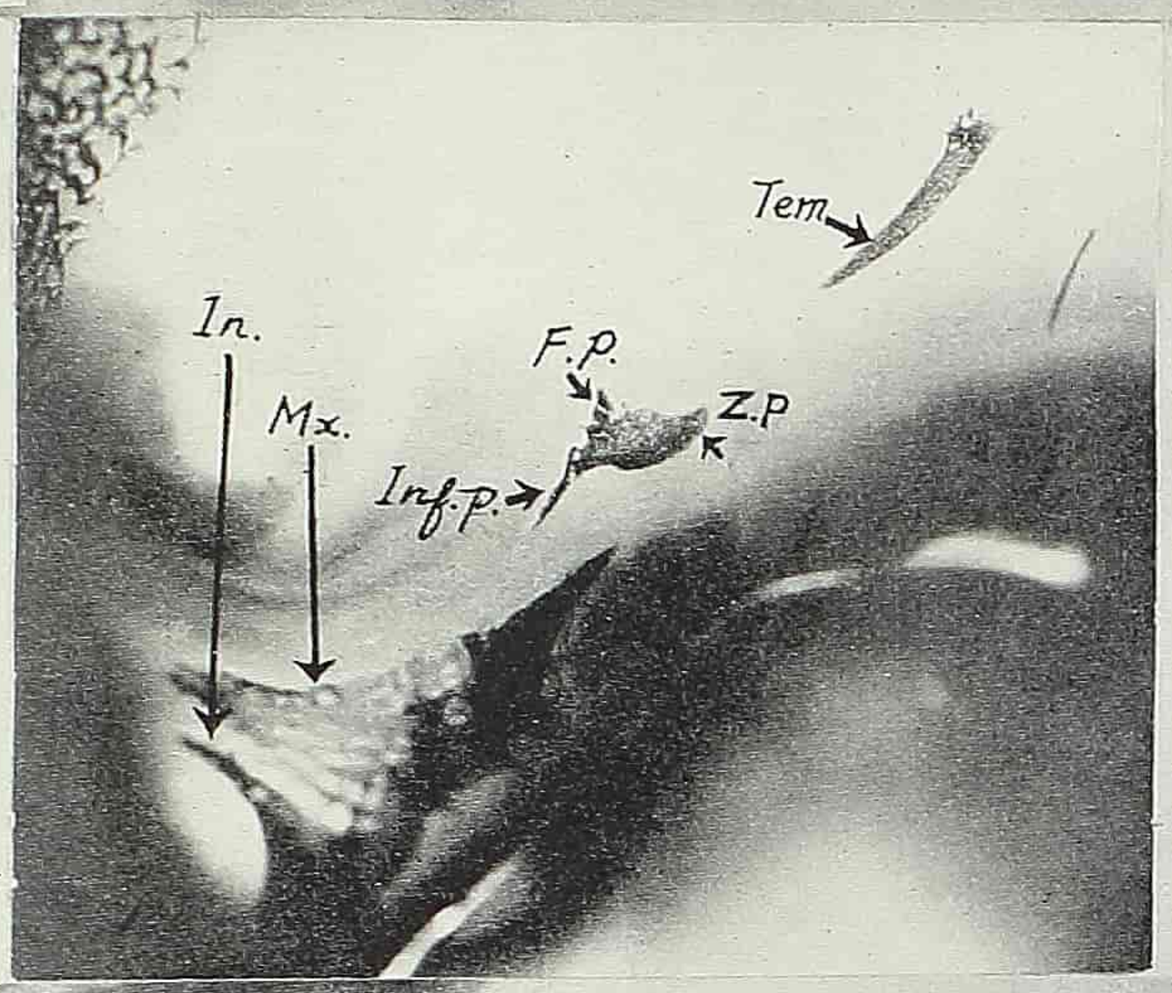

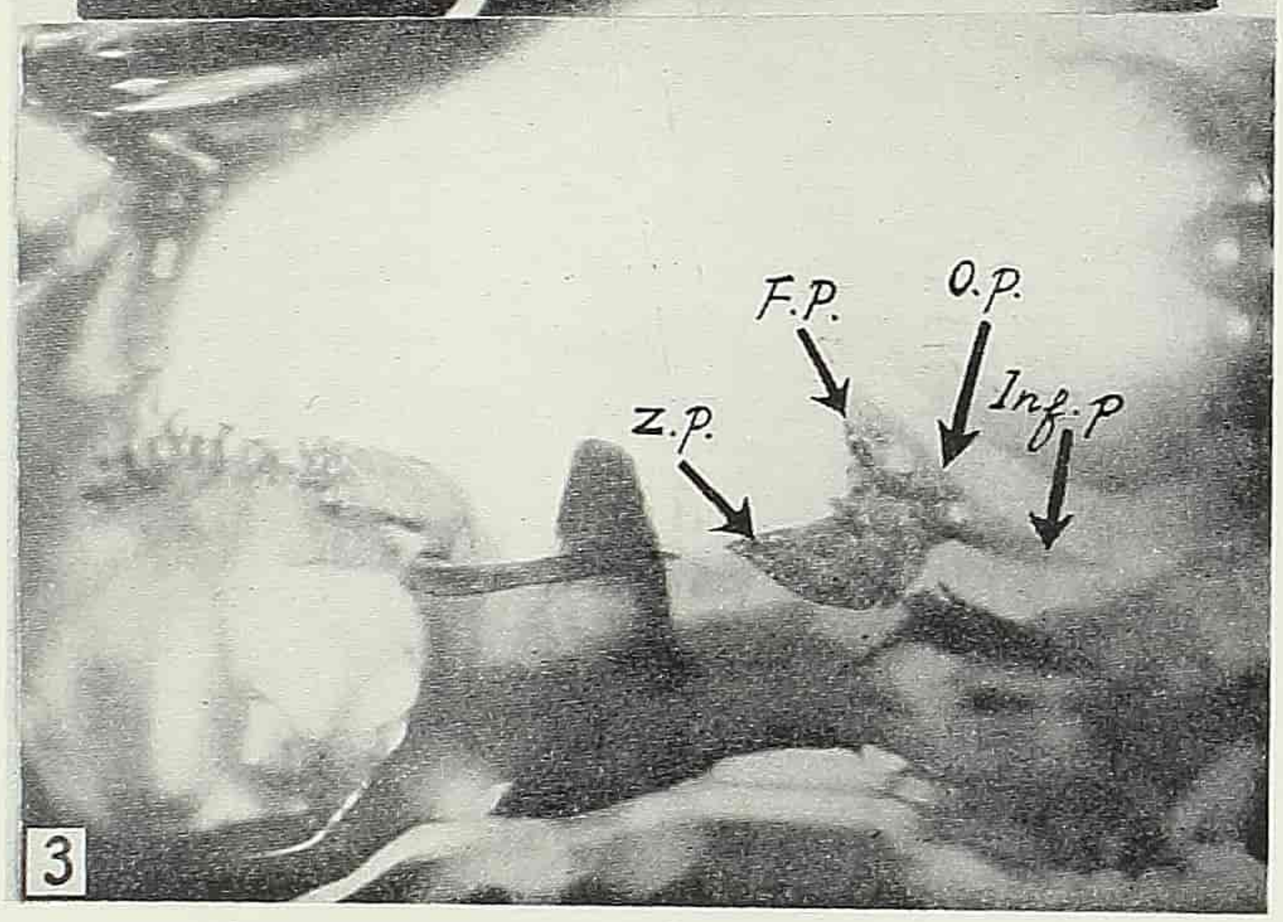

3

ON SOME SPECIMENS OF *LEPIDODENDROPSIS HIRMERI* LUTZ FROM THE WUTUNG SERIES OF KIANGSU*

H. C. Sze (斯行健)

(*Institute of Palæontology, Academia Sinica*)

The flora of the Wutung Series in Eastern China was held by Gothan and Sze[1, 2a] to be the oldest Lower Carboniferous. According to Sze[3a], this series is equivalent more or less in age to the Etroeungtian in Europe. In view of the fact that the fossil plants of the Lower Carboniferous in middle Europe belong mostly to the Viséan and that the plant beds of the Etroeungtian and Tournaisian in Europe contain only very few plant-remains, I proposed in 1943[3b] the name Wutungian, which represents in China a formation of continental sedimentation with a special flora in the oldest Lower Carboniferous time. A complete list of the flora found from this formation was given in a paper published in 1943[3c]. Particular interest in the subject was aroused by Mr. K. P'an's recent finding of several well preserved and almost complete specimens of the Devonian fishes of the *Bothriolepis* type from the Wutung Series in Lungt'an, some 20 km southeast of Nanking. The evidence of fossil faunas especially in China has often been and will always be considered as carrying much more weight than that of fossil floras. Many geologists are thus inclined to believe that the age of the Wutung Series may represent the passage from the Devonian to the Carboniferous. Some palæozoologists and geologists, on the other hand, persist in regarding the Wutung Series as Devonian, chiefly because of the discovery of the important evidence of fossil fishes. The relation of the evidence of the fossil fishes and fossil plants in the Wutung Series becomes now a most fascinating problem. If I am right in supposing that the Wutungian of China is more or less equivalent to the Etroeungtian of Europe, the discrepancies between the chronological testimony of fossil fishes and fossil plants of the Wutung Series would be materially lessened, since the European Etroeungtian has been placed to the uppermost Devonian by many Carbon-geologists[3, 4] in the Heerlen Congresses (1927, 1935, 1951) based on the evidence of the *Goniatites*. The important point is that the Wutung Series consists of a flora with *Sublepidodendron*

---

*First published in Chinese in *Acta Palæontologica Sinica*, Vol. IV, No. 1, pp. 45—52, 1956.

mirable, Sphenopteris taihuensis, Sphenophyllum pseudotenerrimum, Sphenophyllum lungtanense, etc. The composition of the flora is quite different from that of the *Archaeopteris-Cyclostigma* flora of the Etroeungtian of Europe. The assignment of such forms of the Wutung Series to a formation older than the Lower Carboniferous is indeed impossible. Prof. Jongmans[6] expressed his view that these forms might possibly belong to the Lowermost Namurian. He says for instance (1942, p. 35): "Eine weitere altkarbonische Flora beschrieb Sze, welche wohl zum tiefsten Namur gehört." It seems to have escaped his notice that the Wutung Series of Eastern China is overlain by the Tournaisian Kinling Limestone and the uppermost Tournaisian Kaolishan Series which, in turn, is overlain by the Hochow Limestone of the Viséan age[3d, 7]. One of the most impressive fossil plants discovered from the Wutung Series in recent years is a typical *Lepidodendropsis* preserved often on the same slabs with the Devonian fishes in the Lungt'an area. A best preserved specimen was figured by me[8a] in another paper published in the summer of 1954 (Sze 1954, pl. 1, figs. 21, 21a) dealing with the age of the basal part of the Wutung Series. I have already pointed out[8b] that this specimen is identical almost in all respects with the genotype *Lepidodendropsis hirmeri,* originally described by Lutz[9a] in 1933 from the Lower Carboniferous of Geigen, near Hof, Bavaria, and that it also agrees fairly well with the specimens described by Jongmans[10], Gothan and Darrah as *Lepidodendropsis hirmeri* from the Lower Carboniferous Pocono Formation of North America. The specimens found from the Wutung Series at Lungt'an may be briefly described below.

Genus Lepidodendropsis Lutz

Lepidodendropsis hirmeri Lutz

Pl. I, figs. 1-3.

The species is represented by a few stem-fragments. They are covered with cushions very similar to those of *Lepidodendropsis*. The most typical specimen is figured on Pl. 1, figs. 1, 1a, 1b. The impression of the flattened stem is measured 4 mm in breadth and about 18 cm in length. The cushions are much crowded, narrowly rhombic to fusiform, their prolonged upper and lower portions being little prominent. The length of the whole cushion is about 2–2.5 mm and its maximum breadth about 1 mm. The arrangement of the cushions appears to be verticillate with the members of successive whorls alternating. Judging from the members of cushions exposed on the impressions, each verticil might have probably consisted of 14 or 15 leaves. The margin of the cushions being contiguous, only a very narrow part of the surface of of the stem is exposed between them. At its apex and base each cushion passes gradually into the opposed cushion in the second verticil above and

below, and the cushions thus form fairly marked longitudinal rows. No real leaf-scar is visible.

Our knowledge of this important genus is derived from Lutz's description of the type species *Lepidodendropsis hirmeri* from the Lower Carboniferous of Geigen, near Hof, Bavaria. The diagnosis of the genus may be cited below[9b].

"Gattungsdiagnose: *Lepidodendron*ähnliche Pflanzenreste mit länglich-rechteckigen bis undeutlich-spindelförmigen, schmalen Blattpolstern vom Typ des *Sublepidodendron* Nathorst, die aus grobem Haupt– und kleinem Nebenpolster bestehen. Blattnarben undeutlich, ohne Ligule und Parichnosmale. Anordnung der Polster in Schraubenwirteln. Mehr oder weniger ausgeprägte Längslinien zwischen den Polstern. Meist pfriemliche Blätter." Dr. Lutz believed at that time that there was only one species known in this genus, i.e. *Lepidodendropsis hirmeri* Lutz.*

It seems to me that the most important features of this genus are the indistinct leaf scars, the verticillate arrangement of the crowded and almost contiguous leaf cushions (see also Lutz 1933, p. 130, " . . . . und noch mehr durch ihre fast wirtelige Anordnung . . . . . ") and the undivided narrow, linear and almost filiform leaves. In many recent publications, Prof. Jongmans[11, 12a, 13a, 21] has placed in the genus *Lepidodendropsis* numerous known species from the Devonian to the Lower Carboniferous all over the world described by numerous previous authors as *Protolepidodendron, Protolepidodendropsis, Sublepidodendron, Porodendron, Helenia, Heleniella, Utaria, Lepidodendron etc.* It is outside the scope of the present account to deal at length with all these occurrences. It seems to me that Prof. Jongmans has included a very heterogeneous material in this genus as a result of his very strong subjective interpretations, and I firmly believe that many authors, including Lutz himself, will not agree with these determinations. I shall discuss here only the related Chinese specimens at some length. A great number of the species which Jongmans has transferred to *Lepidodendropsis* are characterized by the not crowded and almost spiral arrangement of the cushions. Some of the species even show a distinct apical bifurcation of leaves, e.g. the specimens described by Prof. Halle[14a] from the Middle Devonian of Yunnan Province. I am in complete accord with Prof. Halle[14b] that the verticillate arrangement of the leaves of the Yunnan specimens may perhaps be said to some extent to recall the Articulatales and that the features of the apical bifurcation of the leaves and the probable occurrence of two veins in the lower part of the lamina might be regarded as possibly indicating some slight relationship to the Sphenophyllales. From a botanical point of view, therefore, the species described by Halle as *Protolepidodendron scharyanum*

---

*Dr. Lutz said in his paper of 1933 (p. 118): "Es ist nur eine einzige Art bekannt."

Krejci can not appropriately be placed in the genus *Lepidodendropsis.*

Passing now to the question of the generic identity of the species described as *Protolepidodendron? arborescens* Sze[15a] from the Middle Devonian of Central Hunan to the genus *Lepidodendropsis,* I deem it necessary to state that, although I have already placed this species with a query to this genus[16, 17a], I am in complete agreement with Prof. Kräusel[18] that these specimens must be placed in the group of the "Lepidophyten unklarer Verwandtschaft" for the present (see Kräusel 1937, p. 533). Despite the fact that some specimens from the Middle Devonian of Central Hunan bear a superficial resemblance to the genus *Lepidodendropsis*[15b, 17b], the relation of these specimens to this genus seems to require further elucidations. The same can be said for the specimens found from the Upper Devonian of Hupeh Province[19a]. I am not quite prepared to agree with Prof. Jongmans[13b] that this species "almost certainly belongs to *Lepidodendropsis.*"

Let us now turn to the species *Lepidodendron* aff. *leeianum* G. et S. (?n. sp.) from the Wutung Series of Wusih District, Kiangsu Province. This species was described by me[2b] in 1936. In one of my later publications[3e], it was regarded as a separate new species of *Lepidodendron* and I had named it: *Lepidodendron wusihense* Sze sp. nov. This species differs from the young branches of *Sublep. mirabile* (i.e. *Lep. leeianum*) in having a more distinctly preserved leaf scar in the cushions. The cushions are marked with an obtusely rounded upper end and with a distinct keel in the lower field. Prof. Jongmans[13b] stated that these specimens "very much resemble *Lepidodendropsis*", yet it seems to me that the species *Lep. wusihense* Sze is much more related to *Sublepidodendron* than to *Lepidodendropsis,* because the cushions of the species are not crowded and contiguous and are in a typically spiral arrangement (see Pl. 1, fig. 4 in this paper), i.e. the cushions of this species are absolutely not in verticillate arrangement as in the genus *Lepidodendropsis.* I do agree with Prof. Jongmans that there is no true *Lepidodendron* from the uppermost Devonian and the lowermost Carboniferous. He[12b] said for instance: "As far as I have been able to study specimens and literature, I am convinced that no true *Lepidodendron* is known from this horizon." On the other hand, however, I do not agree with him that my *Lepidodendron wusihense* is a *Lepidodendropsis.* This is a species much more related to *Sublepidodendron,* and I would prefer to propose here the name: *Sublepidodendron wusihence* (Sze) Sze n. comb.

Regarding the true relationship of *Lep. leeianum* G. & S. with *Sublepidodendron mirabile* from the Wutung Series of Kiangsu, I have in fact changed my views several times[2c, 3e, 19b] and now I am rather inclined to the view, as I have said before[3f], that *Lep. leeianum* and *Sublep. mirabile* should probably be combined into one species as Gothan[20] advocated. This is also a species much more related to *Sublepidodendron* than to *Lepidodendropsis* on account of the distinctly spiral arrangement of the leaf-cushions. Whether

or not it represents young branches of *Sublep. mirabile,* it is a species probably not a *Lepidodendropsis.*

Judging from the conclusion of the present study, I am disposed to believe that there is so far in China only one occurrence of *Lepidodendropsis* known, i.e. the specimens described in the present paper from the Wutung Series of Lungt'an. In this connection, it is of interest to point out that in the map of distribution of *Lepidodendropsis* given by Prof. Jongmans[12c], the small point indicating the presence of this genus in the Wutung Series near Nanking has been wrongly placed in a region north of the Yangtze River. This point should be situated at a place south of the river. The other two points indicating the presence of *Lepidodendropsis* in Central Hunan and Eastern Yunnan in Jongmans' map must, based on the present study, be discarded. The composition of the Middle Devonian floras in Eastern Yunnan and Central Hunan is consistent with the conclusions based on stratigraphical and palæozoological evidences.

There remains the question whether the age of the Wutung Series could be assigned to the Upper Devonian. In a recent account[8c], I have pointed out that until the characteristic elements of the Upper Devonian *Leptophloeum* floras of Hupeh, Kiangsi and Kwangtung have been found in the Wutung Series, the assignment of this series to an Upper Devonian age must be accepted with reserve. As stated above, the assignment of such forms as *Sphenophyllum lungtanense, Sph. pseudotenerrimum, Sphenopteris taihuensis, Sublepidodendron mirabile* etc. of the Wutung Series to a formation older than the Lower Carboniferous is impossible. The discovery of a typical lower Carboniferous species *Lepidodendropsis hirmeri* Lutz in the Wutung Series confirms also this view. The former conjecture that the age of the Wutungian of China is more or less equivalent to the Etroeungtian of Europe could probably be ruled out, since the Etroeungtian in Europe has been placed, as stated above, by many Carbon-geologists to the Uppermost Devonian in the Heerlen Congress. The composition of the Wutung Flora is also quite different from that of the Etroeungtian in Europe. The relation between a few Devonian fishes and the Wutung flora, however, remains to be a most fascinating problem; we may hope that more evidences will soon be forthcoming to show whether the occurrence of a few Devenian fishes in the Wutung Series could be regarded as residual remains of the Devonian forms in the lowermost Carboniferous time. There is no adequate reason for supposing that this group of fishes which played a prominent part in the Devonian faunas was no longer in existence during the Lowermost Carboniferous era. Caution is, therefore, necessary in assigning a geological age to any beds solely on the ground of the presence of a few residual remains.

References

[1] Gothan, W., et Sze, H. C. 1933. Ueber die Palæozoische Flora der Provinz Kiangsu. *Mem. Nat. Res. Inst. Geol.,* No. 13. Acad. Sin.

[2a] Sze, H. C., 1936. Ueber die altkarbonische Flora der Prov. Kiangsu mit besonderer Beruecksichtigung des Alters des Wutung quartzites. *Bull. Geol. Soc. China,* **15** (2), 135—164.

[2b] ————, *Ibid.* p. 141, pl. II, figs. 1-6; pl. III, figs. 1, 2; pl. V, figs. 1, 2.

[2c] ————, *Ibid.* p. 142.

[3a] ————, 1943. On the Occurrence of *Sublepidodendron,* a Lepidodenroid Plant from the Wutung Formation. *Bull. Geol. Soc. China,* **23** (1-2), 66.

[3b] ————, *Ibid.,* 66.

[3c] ————, *Ibid.,* 66—67.

[3d] ————, *Ibid.,* 67.

[3e] ————, *Ibid.,* 63.

[3f] ————, *Ibid.,* 63.

[4] Paeckelmann, W., et Schindewolf, O. H., 1937. Die Devon-Karbon Grenze, Compte Rendu Deuxième Congrès. L'avancement études stratigr. Carbonifère Heerlen, II. p. 704.

[5] Gothan, W., et Weyland, H., 1954. Lehrbuch der Palæobotanik. Akademie-Verlag. Berlin, 438, 446.

[6] Jongmans, W. J., 1942. Das alter des Karbon und Perm-floren von Ost-Europa bis Ost-Asien *Palaeont. Abt.,* B. **87**, 35.

[7] Lee, J. S., 1937. Geology of China, 469.

[8a] Sze, H. C., 1954. On the Age of the Basal Part of Wutung Series (written in Chinese). *Acta Palæont. Sin.,* **2** (3), pl. I, figs. 21, 21a.

[8b] ————, *Ibid.,* 312.

[8c] ————, *Ibid.,* 310.

[9a] Lutz, J., 1933. Zur Kulmflora von Geigen bei Hof. *Palæontgraphica Abt. B,* **78**, 118, pl. XV, figs. 1-12; pl. XVI, figs. 1-10.

[9b] ————, *Ibid.,* 118.

[10] Jongmans, W. J., Gothan, W., et Darrah, W. C., 1937. Beiträge zur Kenntnis der Flora der Pocono-Schichten aus Pennsylvanien und Virginia. Compte Rendu Deuxième Congrès, L'avancement études stratigr. Carbonifère Heerlen. Tom 1, p. 431, pls. 48—49, figs. 21-25.

[11] Jongmans, W. J., 1951. Some Problems on Carboniferous Stratigraphy. Extrait Compte Rendu 3ième Congrès Strat. et de Géol. du Carbonifère Heerlen, 299—300.

[12a] ————, 1952. Coal Research in Europe (Reprinted from 2nd Conference on the Origin and Constitution of Coal), Crystal Cliffs, Nova Scotia, 18.

[12b] ————, *Ibid.,* 18.

[12c] ————, *Ibid.,* 19.

[13a] ————, 1954. The Carboniferous Flora of Peru. *Bull. British Mus. (Nat. Hist.) Geol.,* **2** (5), 215—220.

[13b] ————, *Ibid.,* 220.

[14a] Halle, T. G., 1936. On *Drepanophycus, Protolepidodendron* and *Protopteridium* with notes on the Palæozoic Flora of Yunnan. *Pal. Sin., Ser. A,* I, Fasc. 4.

[14b] ————————, *Ibid.,* 15.

[15a] Sze, H. C., 1936. Ueber einen baumfoermiegen Lepidophyten-Rest. in der Tiaomachien Serie in Hunan, *Bull. Geol. Soc. China,* Vol. 15, No. 1.

[15b] ————————, *Ibid.,* Pl. I, figs. 1, 2.

[16] Sze, H. C., 1944. On the Age of the *Protolepidodendron* and *Bothriolepis* bearing Formations in Southwestern China, *Bull. Geol. Soc. China,* **24** (3-4), 214.

[17a] ————————, 1953. Atlas to Palæozoic Plants from China (written in Chinese), 64. Published by Academia Sinica.

[17b] ————————, *Ibid.,* pl. 17, figs. 3-4.

[18] Kräusel, R., 1937. Die Verbreitung der Devonfloren. Deuxième Congrès pour L'avancement des Études de Stratigr. Carbonifère Heerlen, 1935. *Compte Rendu,* Tom. II, 533.

[19a] Sze, H. C., 1952. Upper Devonian Plants from China, *Acta Sci. Sin.,* **1** (2), 175—177, pl. VI, figs. 1, 1a; pl. V, figs. 1-2.

[19b] ————————, *Ibid.,* 178.

[20] Gothan, W., 1933. Ueber neue *Lepidodendron* funde aus dem Unter Karbon von Lungtan, China. *Mem. Res. Inst. Geol.,* No. 13, Acad. Sin.

[21] Jongmans, W. J., & Van der Heide, S., 1955. Flore et Faune du Carbonifère Inférieur de L'Égypte. Mededelingen van de Geologische Stichting Nieuwe Serie, No. 8, 65—72.

EXPLANATION OF PLATE I

All the illustrations are photographs by Mr. L. H. Liu, reproduced without any retouch. If not otherwise stated, the figures are in natural size. All the specimens are kept in the Institute of Palæontology, Academia Sinica.

Figs. 1-3. *Lepidodendropsis hirmeri* Lutz.

Fig. 1a. The greater part of the same specimen shown in Fig. 1. × 3.

Fig. 2a. The greater part of the same specimen shown in Fig. 2. × 4.

Fig. 3a. The greater part of the same specimen shown in Fig. 3. × 3, showing the crowded, almost contiguous and verticillately arranged leaf-cushions and the narrow, linear and almost filiform leaves (on the margin).
Formation and Locality: The Wutung Series of Lungt'an, near Nanking. The specimens have been found in close association with fossil fishes of the *Bothriolepis* type. The two forms are often preserved on the same slabs.

Fig. 4. *Sublepidodendron wusihense* (Sze) Sze n. comb.
Impression of a stem-fragment showing the rather distantly and spirally arranged leaf-cushions.
Formation and Locality: The Wutung Series of Wusih District, Kiangsu.

1

2

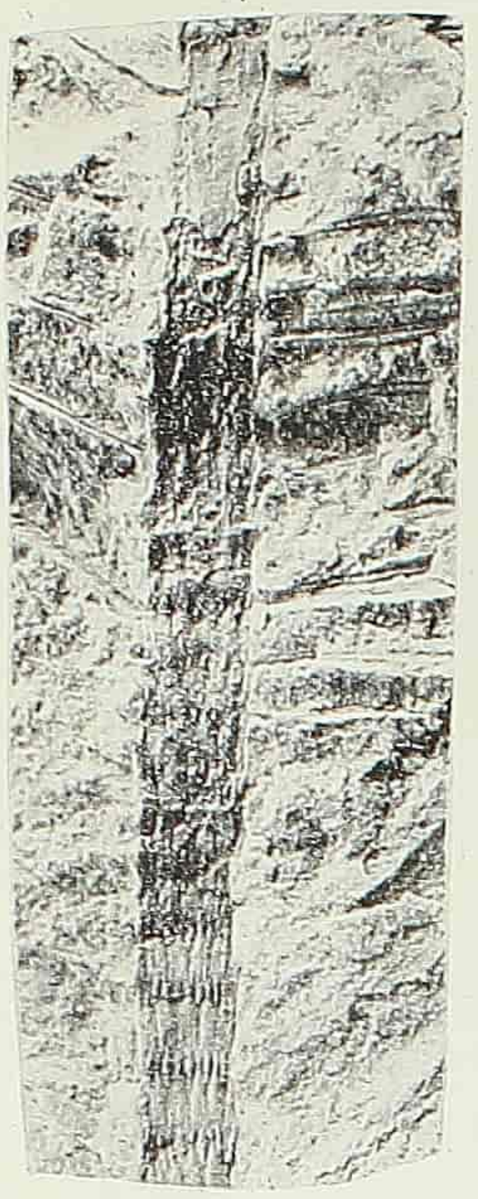

×3 3a

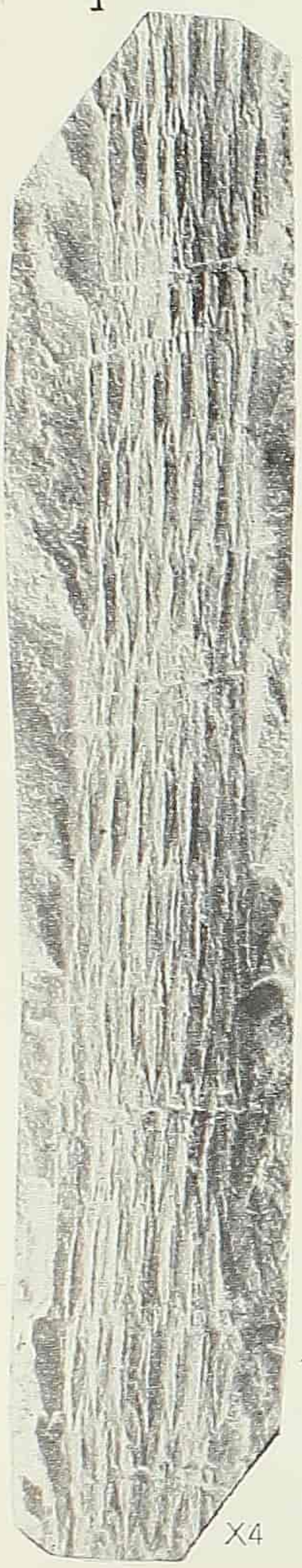

×4 2a

×3 1a

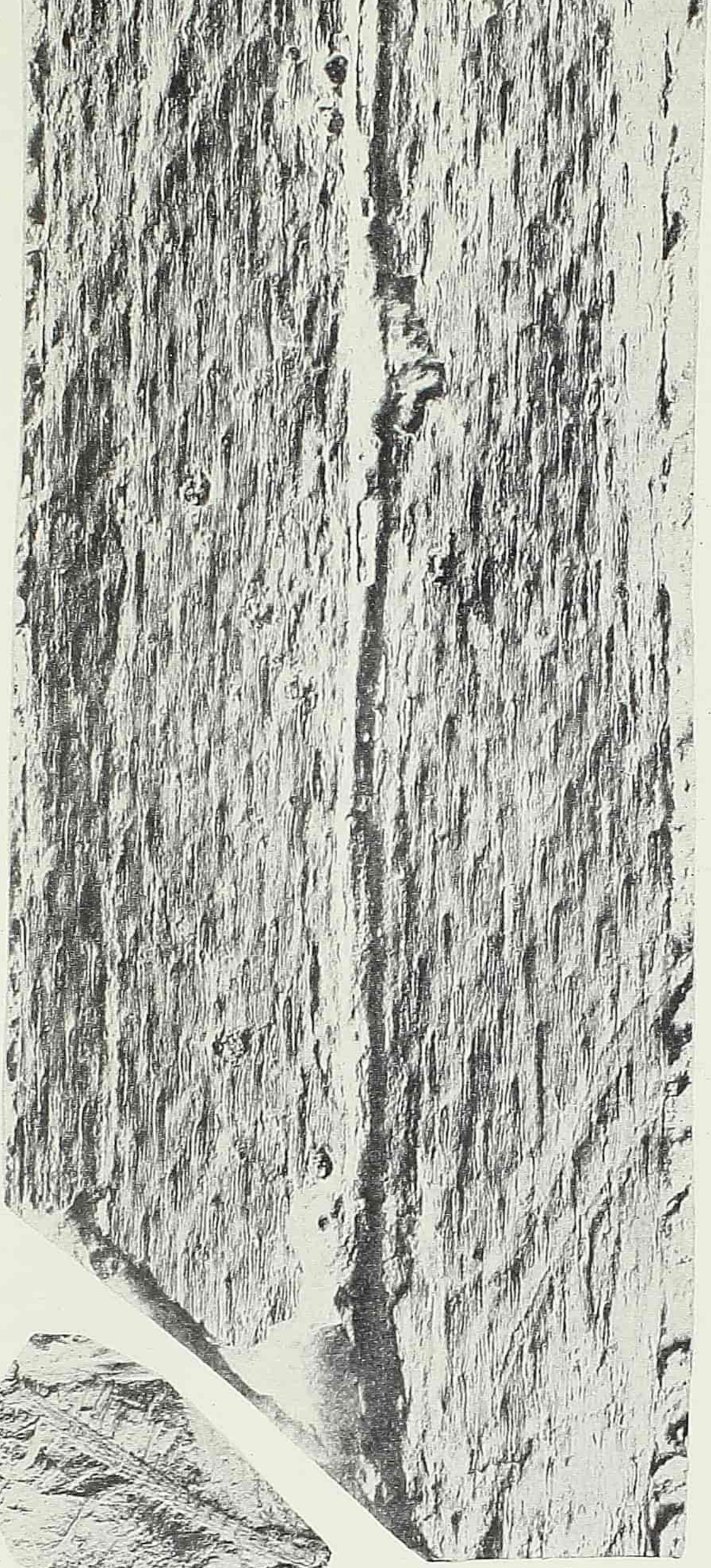

4

3

THE CORRELATION AND THE AGE OF THE YENCHANG FLORA, NORTHERN SHENSI*

H. C. Sze (斯行健)

(*Institute of Palæontology, Academia Sinica*)

From what has been said about the botanical character of the Yenchang flora in a paper published in *Scientia Sinica* Vol. IV, No. 4 (1955)[1], it is evident that the composition of this flora is quite different from the commonly known Rhaeto-Liassic and the Middle Jurassic floras in Eastern Asia and the whole world as well. The Yenchang flora is characterized by a dominant assemblage of *Bernoullia zeilleri* and *Danaeopsis fecunda* which occur throughout the whole complex of the formation and in the majority of its fossil localities. This flora is apparently older than the Tonking flora of Indo-China[2] and the Pinghsiang flora[3, 4] of Southern China, which is characterized by a dominant assemblage of *Dictyophyllum, Clathropteris,* etc. The writer is quite prepared to agree with Dr. C. H. P'an[52] that the Yenchang flora of Northern Shensi cannot be younger than the Rhaetic or older than the Keuper and that it is, most probably, mainly of Keuper—perhaps Middle and Upper Keuper—and the uppermost part of it is possibly Rhaetic. Dr. P'an concluded that the Yenchang formation in Northern Shensi might be tentatively designated as Keuper-Rhaetic in age, and with this view the present writer is in complete accord.

As far as the present knowledge goes, the Yenchang flora is more or less equivalent to the floras of the Lunzer Keuper of Austria[6] and the Basler Keuper[7, 8a] of Neuewelt, Switzerland. Both are characterized by a dominant assemblage of *Bernoullia, Danaeopsis, Glossophyllum,* etc. and both belong to the Middle Keuper. The other new species of the Yenchang flora which show a close relationship with the characteristic forms of the Lunz and Basel floras may be mentioned: *Cladophlebis shensiensis* P'an. It is closely related to *Cl. rütimeyeri* Heer[8b] of Basel in regard to the shape of the pinnules and the pattern of the venation. The only difference between these two forms is that the shape of the pinnules of the former is much more varied than that of the pinnules of the latter. There are considerable variations of the form and size

---

*First published in Chinese in *Acta Palæontologica Sinica,* Vol. IV., No. 1, pp. 25—44, 1956.

of the pinnules displayed in *Cl. shensiensis* obtained from the Yenchang formation of Northern Shensi. But apart from minor differences, these two species might be classed under one morphological type. The specimen of *?Sphenobaiera furcata* (Heer) Florin of the Yenchang flora bears a strong resemblance to the species of Basel which was first described by Heer (1865)[9] as *Sclerophyllina furcata* and later transferred by the same author (1877)[10a] to *Baiera*. In 1936, Prof. Florin[11] referred this species to *Sphenobaiera*. In 1943, Prof. Kräusel[12a] described many better preserved specimens from Basel, finding that the epidermal and stomatal structure of this species belongs evidently to the *Sphenobaiera*-type. It is of interest to point out that the epidermal structure of our specimen can also be compared more or less with that of the Basel species. The species *Ginkgoites chowi* sp. nov. agrees fairly well with *Ginkgoites lunzensis* (Stur) Florin[12b] from Lunz, Austria, in regard to the size of the leaf with coarse venation. It is highly possible that future investigations of our localities may reveal similar specimens of Lunz with the characteristic truncate segments[12c]. The species *Cladophlebis szeiana* P'an in the present material, though no doubt a distinct one, is closely comparable with *Merianopteris angusta*[10b, 8c] of Basel. This species was also described by Krasser[6a] in the Lunz flora. He changed its specific name to *Asterotheca meriani* (Brongniart) Stur and placed the species *Asterocarpus virginiensis* Fontaine in the same Synonym-list. All geologists and palæobotanists now generally agree that the age of the Virginia-Keuper of North America is equivalent more or less to the Basler Keuper and Lunzer Keuper in Europe and that all these three formations belong definitely to the Middle Keuper age. If the species *Asterocarpus virginiensis* Fontaine from the Virginia-Keuper[13] is really identical with *Asterotheca meriani* (Brongn.) Stur (=*Merianopteris angusta* Heer) from the Basler Keuper and Lunzer Keuper in Europe, our species *Cl. szeiana* can also be compared with *Asterocarpus virginiensis* of North America and its fructification may also belong to the *Asterotheca* type. According to P'an[5b], our species is more closely comparable with the form *Asterocarpus virginiensis* var. *obtusilobus* of Virginia[13b]. It seems to the present writer that not only do the sterile but also the fertile pinnae of our species remind us of those of the American species. *Cl. szeiana* is also similar to *Asterocarpus platyrachis* Fontaine[13c] of North America, which, according to Krasser[6b], is also identical with *Merianopteris angusta* Heer of Europe, and can also be placed in the same synonym with *Asterotheca meriani* (Brongn.) Stur. The other species of the Yenchang Formation which show a relationship to the Virginia flora of North America need also be mentioned. *Cladophlebis graciles* Sze recalls *Cladophlebis microphylla* Fontaine from the Virginia Keuper[13d], and it is also comparable with *Cl. pseudowhitbiensis* Fontaine from the same locality[13e]. In regard to the size of the pinnae, our *Sphenozamites changi* Sze is perhaps more closely related to *Sphenozamites rogersianus* Fontaine[13f] than to any other known fossil plants, in spite of the fact that the shape of the pinnae of the American

species is somewhat different and that there are numerous globular prominences or dots between the nerves of this species. As explained by Fontaine, these dots do not seem to be anything but a fine granulation of the epidermis; sometimes, owing to distortion from pressure, these dot-like elevations are drawn out into little bars which extend from nerve to nerve and look like transverse nerves. It is interesting that in regard to the size of the leaf, there are no known species of *Sphenozamites* which could be compared with *Sph. rogersianus* from the Virginia-Keuper and with *Sph. changi* from the Yenchang Formation. The form *Equisetites*? sp. (cf. *E. rogersi* Schimper), resembles also *E. rogersi*[13g] from Virginia in regard to the shape and the size of the teeth of the leaf-sheath, though the evidence is not conclusive; it should probably be referred to the same genus. According to P'an[5c], the specimens of *Danaeopsis* in the Yenchang flora bear a close resemblance to *Pseudodanaeopsis obliqua* (Emmons) Fontaine[13h] and *Pseudodanaeopsis plana* (Emmons) Fontaine[13i], but in our species, the secondary veins are not so frequently anastomosed and furthermore the pinnae are broader as compared with those of Fontaine's species. Dr. Lundblad[14] is of the opinion that, in the light of the evidence brought forward in the last decades, even the filicinean affinities of the type of Fontaine's genus seem very doubtful, on account of the features of the rather thick and coriaceous leaf-substances. Lundblad believes that the North American plant might, in reality, be a gymnosperm, and with this view, one can well agree[15]. Finally, the species *Sphenobaiera crassinervis* sp. nov. bears also a certain resemblance to the American species *Sphenobaiera multifida* (Fontaine) Florin[13j]. In any case, the points of resemblance between the Basel, the Lunz and the Virginia floras of Europe and America on the one side and the Yenchang flora of Northern and Northwestern China on the other as expressed in the number of related forms are quite significant.

In addition to the species closely similar to the characteristic species of Basel, Lunz and Virginia, there are some other forms which tend to give the Yenchang flora an aspect typical of the Keuper. All the new species of *Equisetites,* such as *E. sthenodon, E. deltodon,* etc., are closely comparable to *Equisetites platyodon* Brongniart[8d, 16], an index fossil of the Schilfsandstein (Middle Keuper) of Southern Germany and Northern Switzerland in regard to the size of the stem and the shape of the teeth of the leaf-sheath. In the large size of the stem, the species *Equisetites arenaceous* Jäger, one of the most abundant plants of the Keuper formations (Lettenkohle and Schilfsandstein) in Europe can also be compared with the present new species of the Yenchang Formation. The occurrence of the new species of *Neocalamites, Neocalamites rugosus* Sze sp. nov. in the collection is of special importance, since it bears an aspect of an older age of the Yenchang Formation. This species agrees, in the marked zig-zag lines of the outer surface of the cortex, fairly well with the species described by Jongmans as *Calamites rugosus* of the Westphalian age[17, 29]. The presence of many specimens of this peculiar

form in the Yenchang flora is of interest, and may afford evidence of considerable weight to the Older Mesozoic age of this formation.

The composition of the Yenchang flora bears, moreover, a striking resemblance to the two Upper Triasic or Keuper floras described recently by Brick[18a] from Western Kazakstan. The lower plant-bearing series is named the Курашасайская Series with a thickness of about 250-300 metres. It contains the following forms:

Danaeopsis marantacea (Presl) Heer
Danaeopsis emarginata Brick
Danaeopsis bipinnata Brick
Danaeopsis angustipinnata Brick
Bernoullia aktiubensis Brick
Todites roesserti Zeiller
Polypodites cladophleboides Brick
Cladophlebis simplicinervis Brick
Cladophlebis tripinnata Tur-Ket ex Ms.
Equisetites arenaceus (Jaeger) Schenk
Lepidopteris ottonis (Goepp.) Schimper
Callipteridium remotum Brick
Aipteris nerviconfluens Brick
Thinnfeldia sp.
Taeniopteris angustifolia Schenk
Sphenozamites surakaicus Prynada ex Ms.
Yuccites spathulatus Prynada ex Ms.
Yuccites uralensis Prynada ex Ms.
Araucarites convexus Brick
Sagenopteris ilekensis Brick
Ixostrobus sp. cf. *I. groenlandicus* Harris
Swedenborgia cryptomerioides Nathorst

The upper series is called the Курайлинская Series with a thickness of about 40-45 metres. This formation has been regarded as a transitional horizon between the Upper Triassic and the Lower Jurassic. According to Dr. Brick, it belongs also to the Upper Triassic. It contains the following forms:

Xylomites zamites Geopp.
Danaeopsis hughesi Feistm.
Bernoullia aktiubensis Brick
Todites roesserti Zeiller
Diplozites kazachstanicus Brick
Cladophlebis szeiana P'an
Cladophlebis aktiubensis Tur.-Ket. ex Ms.
Rhacophyllum pachyrhachis (Schenk) Schimper
Lepidopteris ottonis (Goepp.) Schimper

Taeniopteris ensis (Oldh.) Zeiller
Yuccites uralensis Prynada

From the foregoing lists, it appears evident that the Upper Triassic flora of two horizons of Kazakstan is likewise characterized by a dominant assemblage of *Danaeopsis, Bernoullia* and *Glossophyllum* (=Brick's *Yuccites*) and also contains *Cladophlebis szeiana, Cl. shensiensis* (=Brick's *Todites roesserti*), ?*Protoblechnum hughesi* (=Brick's *Danaeopsis hughesi*), *Swedenborgia cryptomerioides* and *Sagenopteris, Thinnfeldia, Sphenozamites, Ixostrobus, Equisetites,* etc. The two horizons of Kazakstan can therefore be undoubtedly correlated with the Yenchang Formation, N. Shensi. It should be pointed out, however, that some determinations of Dr. Brick can not be accepted as correct. From the examination of the published figures[18b], the writer is convinced that her *Todites roesserti* Zeiller is undoubtedly identical with our *Cladophlebis shensiensis*. There are also considerable variations of the pinnules of the Kazakstan specimens. In regard to the pattern of the venation, the species of Kazakstan agrees fairly well with *Cl. shensiensis* and with *Todites roesserti* Presl described by Zeiller from the Tonking Coal Field. The writer has already pointed out that Zeiller identified his Tonking specimens with *Cl. roesserti* Presl, but Presl's type specimen of this species is an indeterminable fragment. Harris referred Zeiller's specimens to the species *Todites goeppertianus* (Münster) Krasser. It seems that both the specimens of Tonking and Northern Shensi are not identical with *Todites goeppertianus*. The specimens described by Brick[18c] as *Yuccites uralensis* Presl, etc. are all but indistinguishable from *Glossophyllum? shensiense* and her specimens of *Danaeopsis hughesi*[18d] are all indeterminable fragments similar to those found from the Yenchang Formation. It is evident that the specimens of Kazakstan can also be determined under the name of ?*Protoblechnum hughesi* (Feistm.) Halle. The species described by Brick as *Danaeopsis emarginata*[18e] is very difficult to distinguish from our *Danaeopsis fecunda* and it is possible that her *D. marantacea*[18f] belongs to this species too. There are also many specimens of a typical *Bernoullia* in the Kazakstan flora. In regard to the size and shape of the pinnae and especially in regard to the pattern of venation, the specimens described by Brick under the name of *Danaeopsis bipinnata* and *D. angustipinnata*[18g] agree well with our *Bernoullia zeilleri* and it is highly possible that these specimens of Kazakstan belong to this species. The determination is all the more certain, when we found a few fertile specimens of this genus presented also in the Kazakstan flora[1][8h]. The sterile specimens described as *Bernoullia aktiubensis* in the Kazakstan flora are, however, indeterminable and the same can be said for the specimens of *Callipteridium* and *Lepidopteris*. The determinations of all these forms are apparently doubtful. Finally, it should be pointed out that the species *Cladophlebis aktiubensis*[18] in Kazakstan is very closely allied to our *Cl. ichünensis*.

There can, at any rate, be no doubt that the Upper Triassic Kazakstan

flora is roughly contemporaneous with our Yenchang flora of Northern Shensi. In this connection, it is of interest to point out that in Western Kazakstan, the Upper Triassic formation is overlain unconformably by a coal series (the so-called дженишке Series with a thickness of about 100 metres) which is undoubtedly the equivalent of the Lower and Middle Jurassic coal series in North China, and is also characterized by a dominant assemblage of *Coniopteris hymenophylloides, Cladophlebis denticulata, Cl. whitbyensis, Cl. lobifolia, Phoenicopsis speciosa, Pityophyllum nordenskiöldi,* etc. This coal series has been regarded by Brick as belonging to the Middle Jurassic. The present writer is not quite prepared to regard it as proved; this coal series in Kazakstan, as has been stated above, is characterized by a dominant assemblage of the *Coniopteris-Phoenicopsis* elements and its geological age must be from the Lower to Middle Jurassic. It can be roughly correlated with the Wayaopu Coal Series (the upper part of which has now been called the Ishihtsun Coal Series) of Northern Shensi, the Tatung Coal Series in Northern Shansi and the Mentoukou Coal Series of Peking, which it resembles in making the maximum of coal formation of the Jurassic period. The flora of this coal series of Kazakstan cannot be said to contradict this parallelization. For the purpose of comparison, the composition of this Jurassic flora in Kazakstan may be mentioned below:

Gleichenites sphenopteroides Brick
Coniopteris hymenophylloides (Brongn.) Sew.
C. porcina Brick ex Ms.
C. sp. cf. *C. fursenkoi* Pryn.
Dictyophyllum sp.
Cladophlebis haiburnensis (L. et H.) Brongn.
Cl. whitbiensis Brongn. var. *punctata* Brick
Cl. sp. ex. gr. *C. denticulata* (Brongn.) Font.
Cladophlebis lobifolia (Phill.) Brongn.
Equisetites ferganensis Sew. sensu lato
E. hallei Thomas
Ptilophyllum cutchense Morris
Nilssonia vittaeformis Pryn.
N. compta (Phillips) Bronn
Phoenicopsis speciosa Heer
Ginkgoites sp.
Feildenia sp.
Pagiophyllum peregrinum (L. et H.)
P. setosum (Phillips)
Pityophyllum angustifolium (Nath.) Möller
Podozamites sp.
Conites sp. a.
Conites sp. b.

It should be remarked that there are no typical elements of the Upper Jurassic and Lower Cretaceous *Ruffordia-Onychiopsis* flora of Eastern Asia in this Kazakstan coal series. This coal series cannot, therefore, be younger than the Middle Jurassic.

The Yenchang flora of Northern Shensi may also be roughly equivalent to the Upper Triassic flora of Arizona, North America. The percentage of species common to the two regions is not high, but the close relationship of the two floras is apparent. This Arizona Upper Triassic flora contains, likewise, the following genera: *Equisetites, Neocalamites, Cladophlebis, Danaeopsis* (Daugherty wrongly determined as *Ctenis arizonicus*), *Phlebopteris* (=Daugherty's *Laccopteris*), *Sphenopteris, Podozamites,* etc. It appears that the species *Equisetites bradyi* of Arizona[19a] is hardly distinguishable from our *Equisetites sarrani* and the species *Cladophlebis microphylla* is very similar to our *Cladophlebis graciles*. *Sphenopteris arizonicus* agrees well with our *Sphenopteris* sp. and *Laccopteris smithii* is closely related to our *Phlebopteris linearifolia*. In addition, the specimen *Yuccites poleonsis* Daugherty[19b] may belong to a species of *Neocalamites* and the specimen *Ctenis neuropteroides* Daugherty[19c] may possibly be a *Danaeopsis* of the *Danaeopsis fecunda* type. This specimen should be determined under the name of *Danaeopsis*? sp. The specimens described by Daugherty[19d] as *Podozamites arizonicus* are apparently not a new species and in regard to the size and the shape of the leaves, they are almost indistinguishable from certain forms of *Podozamites lanceolatus* (L. & H.) Braun. It is surprising to find in the list of species from the Arizona flora a species of *Coniopteris* which is one of the most typical European and cosmopolitan Jurassic forms. Daugherty stated: "The sterile fronds or sterile parts of the fronds of this species closely resemble *Sphenopteris nystroemii* described by Halle from the Permian of China, but the fertile fronds more closely resemble *Coniopteris hymenophylloides* Brongniart from the Jurassic." Judging solely from the illustrations[19e], the present writer cannot express definite opinions, but it seems to him that the species of the Upper Triassic formation of Arizona is quite distinct from the Jurassic species *Coniopteris hymenophylloides* Brongn. and that these specimens might more appropriately be referred to the genus *Sphenopteris*. The Arizona flora contains also a typical Middle Keuper species of Virginia, that is, *Lonchopteris virginiensis* Fontaine[19f]. In habit, the frond of this American Keuper species agrees with *Cladophlebis whitbyensis,* but the lateral veins form an anastomosing system like that in the Palæozoic genus *Lonchopteris*. Regarding the systematic position of this American Keuper species, Prof. Seward[20] pointed out: "Seeing that *Lonchopteris* is a designation of a purely provisional kind, it would be convenient to institute a new generic name for Triassic species having the *Lonchopteris* venation, which there are good reasons for regarding as Osmundaceous ferns." A more or less similar form was described by Leuthardt[8e] as *Pecopteris* (*Lonchopteris*) *reticulata* from the Middle Keuper flora of Basel, Switzerland.

The composition of the Upper Triassic or Rhaetic flora of the Molteno beds, South Africa[21, 22] is somewhat different from that of the Yenchang flora. There are only two species in common, i.e. *Neocalamites carrerei* Zeiller and *Ginkgoites magnifolia* (Fontaine). Other closely comparable forms may be mentioned: *Cl.* (*Todites*) *roesserti, Cl.* (*Todites*) *goeppertiana* and *Cl. nebbensis*. The first two forms may be compared with our *Cl. shensiensis,* and the last one recalls more or less our *Cl. ichünensis*. The specimen described as *Stenopteris elongata* is also more or less comparable to one of ours described under the name of *?Sphenobaiera furcata*. It is interesting to note that in the Molteno beds of South Africa, there are also four or five species of *Thinnfeldia,* but most of the specimens might belong to the genus *Dicrodium* in the sense of Prof. Gothan.

Our Yenchang flora seems, moreover, to have some species in common with the Scoresby Sound flora in Eastern Greenland. They are *Equisetites sarrani, Neocalamites carcinoides, Swedenborgia cryptomerioides,* etc. It is striking that all these forms are found in the Lower Jurassic *Thaumatopteris* zone in Eastern Greenland, and only *S. cryptomerioides* is obtainable also in the *Lepidopteris* zone, or in the transitional beds between the *Lepidopteris* zone and the *Thaumatopteris* zone. Other related or closely comparable forms between the Yenchang and Scoresby Sound floras are *Neocalamites hoerensis, Todites goeppertianus, Drepanozamites nilssoni,* etc. Only *T. goeppertianus* is found in the transitional beds between the *Lepidopteris* zone and *Thaumatopteris* zone, while the other two forms are confined to the *Lepidopteris* zone. *N. hoerensis* is all but indistinguishable from our *N. carrerei; Todites goeppertianus* is a closely related species of *Cl.* (*Todites*) *shensiensis; Drepanozamites nilssoni* is somewhat distinct from *D.? p'ani* from the Yenchang Formation, because the latter has a more or less distinct midrib in the segments. There are many *Podozamites* forms in the Scoresby Sound flora, most of which are found in the *Lepidopteris* zone. The majority of these forms belong to the type of *Podozamites lanceolatus* and are closely comparable to the specimens found in the Yenchang Formation. In conclusion, the composition of the Yenchang flora is not exactly comparable to that of the Scoresby Sound flora. It is, however, highly probable that the uppermost part of the Yenchang Formation corresponds to the *Lepidopteris* zone of Eastern Greenland.

There are some common species, too, between the Yenchang flora and the Mesozoic floras in Sweden[23, 24]. All these forms seem to occur in the higher horizon, i.e. Lower Jurassic in Sweden. They are *Neocalamites carcinoides* (found from Scania), *Thinnfeldia nordenskioldi* (known in Pålsjor), *Swedenborgia cryptomerioides* (known in Hör and Pålsjor), *Danaeopsis fecunda* (known in Scania)[25], etc. Other closely related forms may also be mentioned, e.g. *Neocalamites hoerensis, Todites goeppertianus, Drepanozamites nilssoni,* the species of *Sagenopteris, Phlebopteris* and

Podozamites, etc. It is evident that only the upper part of the Yenchang Formation can be possibly correlated with the Rhaetic horizons of Sweden.

The Tonking Coal Series in Indo-China, which is nearly equivalent to the Anyuan Coal Series in Pinghsiang, Kiangsi Province, and which is also characterized by a dominant assemblage of the *Dictyophyllum-Clathropteris* flora, comprises many important elements of the Yenchang flora, namely, *Equisetites sarrani, Neocalamites carrerei, Cladophlebis raciborskii, Bernoullia zeilleri, Ctenopteris sarrani,* etc. It is also highly possible that Zeiller's *Noeggerathiopsis hislopi* is identical with *Glossophyllum? shensiense* in the Yenchang flora and his *Cladophlebis* (*Todites*) *roesserti* is identical with our *Cl.* (*Todites*) *shensiensis.* In addition, Zeiller's *Podozamites distans* recalls *Podozamites lanceolatus* from the Yenchang Formation. It is striking that the Yenchang flora has eight species in common with the Rhaeto-Liassic flora of Tonking. This surprising result may suggest the view that the upper part of the *Danaeopsis-Bernoullia* flora is probably equivalent in age to the lower part of the *Dictyophyllum-Clathropteris* flora. The species *Bernoullia zeilleri* is represented in the Tonking flora by very few small fragments which were described by Zeiller as *Bernoullia* sp. In Northern Shensi, this species occurs also very rarely in the basal part of the Lower Jurassic Wayaopu Coal Series which seems to overlie conformably the Yenchang Formation. The deposition of these two formations in Northern Shensi appears to be continuous without interruption.

The plant remains from Nariwa District in Japan were first described by Yokoyama[26] in 1891. In 1932, the late Prof. Ôishi[27] described more than 80 species systematically and again in 1938, Ôishi and Huzioka added to the Nariwa flora a certain number of new species. The Rhaeto-Liassic aspect of the Nariwa flora in Japan is, on the whole, very strong as is shown in the analysis of the flora in comparison with the *Lepidopteris* and *Thaumatopteris* zones of Eastern Greenland[28]. According to the present writer, the Nariwa flora is nearly equivalent in geological age to the Tonking flora of Indo-China as well as to the Pinghsiang flora of Southern China. It is also characterized by a dominant assemblage of the *Dictyophyllum-Clathropteris* flora. The writer is in complete agreement with Prof. Ôishi that the lower part of the Nariwa flora is of the Rhaetic age and that the upper part of it may belong to the Liassic. It should be pointed out that our Yenchang flora has also five or six species in common with the Nariwa flora, they are: *Cladophlebis gigantea, Cl. raciborskii, Neocalamites carrerei, Swedenborgia cryptomerioides, Podozamites lanceolatus* and probably also *Stenorachis* (*Ixostrobus?*) *konianus.* All these identical forms are confined to the upper part of the Yenchang Formation.

Finally, it is of special interest to point out that the Yenchang flora in Northern Shensi comprises also a few identical forms of the Hsiangchi flora of western Hupeh which is evidently of the Lower Jurassic age. The identical

species of the two floras are: *Equisetites sarrani, Neocalamites carrerei, Ginkgoites magnifolia, Podozamites lanceolatus* and *Swedenborgia cryptomerioides.* Except the species *Ginkgoites magnifolia,* all other identical forms are found only in the upper part of the Yenchang Formation. From the Hsiangchi Coal Series of Szechwan, there has been found another important identical species, *Cladophlebis raciborskii.*

Taken as a whole, the Yenchang flora of Northern and Northwestern China is most closely related to the Middle Keuper floras of Europe and Northern America, corresponding to the Lunzer Keuper of Austria, the Basler Keuper of Switzerland and the Virginia-Keuper of North America. Palæobotanical evidence points generally to the conclusion that the fossil flora at present known from the Yenchang Formation is of the Upper Triassic age. It might indeed be classed as Keuper-Rhaetic, as Dr. P'an advocated.

References

[1] Sze, H. C., 1955. On the Botanical Character of the Yenchang Flora, Northern Shensi. *Scientia Sinica,* **4** (4), 599—607.

[2] Zeiller, R., 1903. Flora fossile des gîtes de charbon du Tonkin, Paris. Études des gîtes minéraux de la France.

[3] Sze, H. C., 1931. Beiträge zur Liassischen Flora von China. *Mem. Nat. Res. Inst. Geol.* (Academia Sinica), No. 12.

[4] ————, 1933. Beiträge zur Mesozoischen Flora von China. *Palæont. Sinica,* Ser. A, Vol. IV, Fasc. 1.

[5a] P'an, C. H., 1936. Older Mesozoic Plants from North Shensi. *Palæont. Sinica,* Ser. A, Vol. 4, Fasc. 2, p. 36.

[5b] ————, *Ibid.* pp. 35, 36.

[5c] ————, *Ibid.* p. 25.

[6a] Krasser, F., 1909-1910. Zur Kenntnis der fossilen Flora der Lunzer Schichten. *Jahrbuch der Kaiserlich-Königlichen geologischen Reichsanstalt.* Bd. 59, Heft I, p. 108.

[6b] ————, *Ibid.* p. 108.

[7] Leuthardt, F., 1903. Die Keuperflora von Neueselt bei Basel. Teil. I. Phanerogamen. *Abhandl. d. Schweiz. Palæont. Gestll.,* Bd. 30.

[8a] ————, 1904. Die Keuperflora von Neuewelt bei Basel. Teil. 2. Kryptogamen. *Abhandl. d. Schweiz. Palæont. Gestll.,* Bd. 31.

[8b] ————, *Ibid.* p. 34; pl. 15, figs. 1, 2.

[8c] ————, *Ibid,* p. 32, pl. 18, figs. 1, 1a.

[8d] ————, *Ibid.* pl. XXI, figs. 1, 2.

[8e] ————, *Ibid.* pl. XVIII, figs. 2, 2a.

[9] Heer, O., 1864-1865. Die Urwelt der Schweiz. Zürich.

[10a] Heer, O., 1877. Flora fossilis Helvetiae, Nachtrag z. Triasflora.

[10b] ———, *Ibid*. p. 69, pl. 24, figs. 7-12, etc.

[11] Florin, R., 1936. Die fossilien Ginkgophyten von Franz-Joseph-Land nebst Erörterungen über vermeintliche Cordaitales mesozoischen Alters. I. Spezieller Teil. *Palæontographica,* Bd. 81, Abt. B, Stuttgart.

[12a] Kräusel, R., 1943. Die Ginkgophyten der Trias von Lunz in Nieder-österreich und von Neue Welt bei Basel. Untersuchungen zur mesozoischen Florengeschichte des alpinen und süddeutschen Raumes II. *Palæontographica,* Bd. LXXVII, Abt. B, Lief. 2.

[12b] ———, *Ibid*. p. 72; pl. 1, figs. 1-8; pl. II, figs. 1-8; pl. III, figs. 1-5; textfigs. 6-7.

[12c] ———, *Ibid*. p. 75, textfig. 1.

[13a] Fontaine, W. M., 1863. Contributions to the Knowledge of the Older Mesozoic Flora of Virginia. *U. S. Geol. Surv. Monographs,* Vol. 6, Washington.

[13b] ———, *Ibid*. p. 45, pl. XXI, figs. 3, 4; pl. XXIV, figs. 3-5; pl. XXV, fig. 1.

[13c] ———, *Ibid*. p. 46, p. 49, fig. 2.

[13d] ———, *Ibid*. p. 51, pl. XXVII, figs. 2, 2a.

[13e] ———, *Ibid*. p. 52, pl. XXVII, fig. 4.

[13f] ———, *Ibid*. p. 80, pl. 43, fig. 1; pl. 44, figs. 1, 2; pl. 45, figs. 1, 2:

[13g] ———, *Ibid*. pl. 11, figs. 1-3.

[13h] ———, *Ibid*. p. 61, 116; pl. XXXI, figs. 1, 2; pl. LIV, fig. 8.

[13i] ———, *Ibid*. p. 59, 116; pl. XXX, figs. 1, 2, 2a, 4, 4a; pl. LIV, fig. 8.

[13j] ———, *Ibid*. p. 87, pl. 46, 47, fig. 1.

[14] Lundblad, A. B., 1950. Studies in the Rhaeto-Liassic Floras of Sweden. I. Pteridophyta, Pteridospermae & Cycadophyta from the Mining District of New Scania. *K. Svenska Vet. Akad. Handl.,* Fjärde Serien. Bd. I, No. 8, Stockholm.

[15] Sze, H. C., & Lee, H. H., 1951. Notes on a Rhaetic Species *Danaeopsis fecunda* Halle from the Yenchang Formation of Kansu. *Sci. Rec.,* Vol. 4, No. 1.

[16] Frentzen, K., 1933. Equisetaceen des germanischen Keupers. *Palæontolog. Zeitschrift,* Bd. 15.

[17] Jongmans, W. J., 1915. A Monograph of the *Calamites* of Western Europe. Mededeelingen van de Rijksopsporing van Delfstoffen, No. 7, Vol. I.

[18a] Брик, М. И. 1952. Ископаемая флора и стратиграфия нижнемезозойских отложений бассейна среднего течения р. илек в западном казахстане. Госгеолиздат.

[18b] ———, *Ibid*. pl. VII, figs. 1-7, fig. 106.

[18c] ———, *Ibid*. pl. XV.

[18d] ———, *Ibid*. Pl. IV, figs. 1-6.

[18e] ———, *Ibid*. Pl. 1, figs. 1-5.

[18f] Брик, М. И., *Ibid*. Pl. 1, fig. 6.

[18g] ————, *Ibid*. Pl. II, figs. 3, 4; Pl. III, figs. 1-11.

[18h] ————, *Ibid*. Pl. V, figs. 9-11.

[18i] ————, *Ibid*. pl. IX, fig. 4.

[19a] Daugherty, L. H., 1941. The Upper Triassic Flora of Arizona. *Carnegie Inst. Washington,* Publication 526.

[19b] ————, *Ibid*. pl.13, fig. 1.

[19c] ————, *Ibid*. pl. 14, fig. 3.

[19d] ————, *Ibid*. pl. 14, figs. 1, 2.

[19e] ————, *Ibid*. pl. 9, figs. 3-5.

[19f] ————, *Ibid*. p. 49, pl. 5, figs. 4, 5; pl. 6, figs. 1, 2.

[20] Seward, A. C., 1910. Fossil Plants, Vol. 2.

[21] Du Toit, A. L., 1927. The Fossil Flora of the Upper Karoo Beds. *Ann. S. African Museum,* Vol. XXII, Pt. 2.

[22] ————, 1939. The Geology of South Africa. p. 317.

[23] Nathorst, A. G., 1876. Bidrag till Sveriges Fossila Flora, I. Växter fran rätiska formationen vid Pålsjö i Skane. *Kgl. Svensk. Vet.-Akad. Handl.,* Bd. XIV, No. 3.

[24] ————, 1878. Bidrag till Sveriges Fossila Flora. Floren vid Höganäs och Helsingborg. *Kgl. Sv. Vet. Ak. Handl.,* Bd. 16, Nr. 7.

[25] Yokoyama, M., 1891. On Some Fossil Plants from the Coal-bearing Series of Nagato. *Journ. Coll. Sci. Imp. Univ. Tokyo,* Vol. 4, Art. 2.

[26] Ôishi, S., 1932. The Rhaetic Plants from the Nariwa District, Prov. Bitchu (Okayama Prefecture). *Japan. Journ. Fac. Sci. Hokkaido Imp. Univ.,* Series 4, Vol. 1, Nos. 3-4.

[27] Ôishi, S., et Huzioka, K., 1938. Fossil Plants from Nariwa, A Supplement. *Journ. Fac. Sci. Hokkaido Imp. Univ.,* Ser. 4, Vol. 4, Nos. 1-2.

[28] Jongmans, W. J., 1951. Les Bassins Houillers du Sud-Oranais. *Bull. du service de la carte geologique de L'Algerie,* No. 13.

NEW SPECIES OF BRACHIOPODS [I]*

WANG YÜ (王 鈺)

(*Institute of Palæontology, Academia Sinica*)

In preparing the brachiopod chapter for the "Index Fossils of China", the writer encountered a difficulty in selecting sufficient materials from the published literature for such a comprehensive compilation. Inasmuch as the "Index" will be in constant use by field geologists, its contents should include extensive illustrations to meet the requirements. With this conception in mind, the writer has made a thorough examination of the specimens kept in the museum of his institute, and has accepted many of them in the "Index". It is evident that a number of new specific names should be proposed for several materials hitherto not adequately studied. The purpose of this paper is to describe these new species.

A paper dealing with eleven new genera of Brachiopods also contained in the "Index Fossils of China" was published in *Scientia Sinica* Vol. IV, No. 2.

Genus *Palæobolus* Matthew 1899

Palæobolus discus Wang (sp. nov.)

(Pl. 1, A; Fig. 1)

Represented by a single dorsal valve.

Outline subcircular to roundly oval, greatest width a little anterior to the middle of the valve, gradually acuminate toward the posterior end; anterior margin broadly rounded. Surface of shell marked by sharp, fine, elevated concentric ridges. These ridges run wavily in the median part and merge each other in the postero-lateral regions of the shell.

Dimensions (mm): Length 5.3; width 5.6.

Figured specimen, I.P.A.S. 7981.

Horizon and Locality: Chiushukou Bed, Uppermost Cambrian; limestone quarry, south of Huolianchai Station, Penhsi District, Liaoning Province.

Collectors: Members of the Taitzeho Party, 1950.

---

*First published in Chinese in *Acta Palæontologica Sinica*, Vol. IV, No. 1, pp. 1—24, 1956.

Discussion: There are no *Palæobolus* known in China. This new species distinguishes itself from *Palæobolus bretonensis* (Matthew)[1] by its small size and by the closeness of the surface ridges.

Palæobolus rotulus Wang (sp. nov.)

(Pl. 1, B; Fig. 1)

Represented by a single ventral valve.

Size small; general form broadly ovate; lateral margins gradually acuminate toward the posterior end; anterior margin rounded; lateral profile evenly and moderately convex. Surface marked by fine, elevated concentric lines.

Dimensions (mm): Length 5.2; width 5.4.

Figured specimen, I.P.A.S. 7982.

Horizon and Locality: Kushan Formation, Upper Cambrian; summit of Nanchimao Hill, Pangchiawa, southwest of Chiawang Colliery, Kiangsu Province.

Collector: J. C. Sheng.

Discussion: This species differs from *Palæobolus discus* (sp. nov.) in its smaller size and in its more delicate ornamentations.

Genus *Westonia* Walcott 1901

Westonia obovata Wang (sp. nov.)

(Pl. 1, C; Figs. 1-2)

Represented by several ventral valves.

General outline subrounded, greatest width near the anterior margin; posterior extremity gradually acuminate, anterior margin broadly rounded; evenly and gently convex in lateral profile, with the greatest convexity about at the middle of the valve. Surface marked by fine concentric growth lamellae; semi-imbricate, ripply lines well developed in whole surface.

Dimensions (mm): Length 11.7; width 11.2.

Figured specimens, I.P.A.S. 7983, 7984.

Horizon and locality: Kushan Formation, Upper Cambrian; limestone quarry near Changshan, Chiawang Coal Field, Kiangsu Province.

Collector: J. C. Sheng.

Discussion: This species differs from the hitherto known members of the genus *Westonia* by its subrounded outline and by its greatest width of the valve near the anterior margin.

Westonia shengi Wang (sp. nov.)

(Pl. 1, D; Fig. 1)

Represented by two ventral valves.

General form elongately oval, with the width about two-thirds the length; lateral profile moderately convex; anterior margin subtruncated, narrower than the greatest width in the middle of the valve; posterior extremity obtusely acuminate; concentric growth lamellae well developed, whole surface ornamented by fine, ripply lines.

Dimensions (mm): Length 8.7; width 6.4.

Figured specimen, I.P.A.S. 7985.

Horizon and locality: Fengshan Formation, Upper Cambrian; west of Hsiatsun Village, Chiawang Coal Field, Kiangsu Province.

Collector: J. C. Sheng.

Discussion: *Westonia shengi* strongly recalls *W. blackwelderi* Walcott[2] found in the Middle Cambrian, Shantung Province, but differs from it in the possession of more convex postero-lateral margins and a subtruncated anterior end.

Genus *Lingulepis* Hall 1863

Lingulepis nanchuanensis Wang (sp. nov.)

(Pl. 1, E; Fig. 1)

General form elongately oval; posterior margin bluntly acuminate, anterior margin broadly rounded; proportion between length and width about 3:2, with the widest part near the anterior margin. Surface ornamented by concentric growth lines and fine radiating striae.

Dimensions (mm): Length 12.3; width 7.7.

Figured specimen, I.P.A.S. 7986.

Horizon and locality: Panho Series, Lower Ordovician; Hot Spring, east of Nanchuan City, Szechwan Province.

Collector: The author.

Discussion: This species is represented by a single flattened specimen. In general outline, this species agrees with *Lingulepis* cf. *acuminata* (Conrad)[3] found in Patzelao, I-Tu District, Hupeh Province, but differs from it in the possession of more convex lateral margins and less acuminate posterior extremity.

Genus *Lingula* Bruguiere 1792

Lingula kwani Wang (sp. nov.)

(Pl. 1, F; Figs. 1-4)

Shell large, attaining 40 mm in mature specimen; narrowly elliptical to sub-oblong in outline; anterior end rounded to subtruncated; posterior margin gradually acuminated; lateral profile equally convex, lenticular. Surface ornamented by strong, coarse, undulated lines.

Dimensions (mm): Length 21.8; width 12.3; thickness 5.6.

Holotype, I.P.A.S. 7987, paratype, I.P.A.S. 7988.

Horizon and locality: Kelimoli Limestone, Lower Ordovician; Latsatsung, south of Chotzeshan, Ordos, Inner Mongolia.

Collectors: S. C. Kwan and Y. H. Lu.

Discussion: This new species can be recognized by its large size and narrowly elongate form. In size and outline, this species suggests relationship with *Ectenoglossa nympha* (Billings)[4] from the Middle Ordovician of North America. But no trace of "teeth" can be observed in the internal mold of our specimen.

Genus Paterina Beecher 1891

Paterina talingensis Wang (sp. nov.)

(Pl. 1, I; Figs. 1-2)

Shell minute; outline broadly ovate; ventral valve depressed subconical; beak highly arched, marginal, curving abruptly backward and downward to form a steep false area. Dorsal valve slightly convex, with the posterior margin nearly straight and a little narrower than the greatest width of the valve. Surface marked by fine concentric irregular lines.

Syntypes: I.P.A.S. 7989, 7990.

Horizon and locality: Mant'o Shale, Lower Cambrian; Taling, east of Kaochiatsui Station, Penhsi District, Liaoning Province.

Collectors: Members of the Taitzeho Party, 1950.

Discussion: This species differs from *Paterina lucina* Walcott[5], a Middle Cambrian species known from China, in its less convex ventral valve and more rounded outline.

Genus *Apheoorthis* Ulrich and Cooper 1936

Apheoorthis costalis Wang (sp. nov.)

(Pl. 1, G; Figs. 1-3)

Shell of medium size for the genus; width greater than length, with the hinge-line forming the greatest width of the shell. Cardinal extremities acute; lateral margins broadly rounded.

Ventral valve gently convex; umbo swollen; beak small, a little arched.

Dorsal valve flatly convex, with most convexity in the umbonal region; beak low, inconspicuous; sulcus wide and angular, extending a little anterior from the beak and deepening toward the front.

The median part of the shell is marked by three strong, subangular plications extending from the beak to the anterior margin. On each side of the median part there are usually two similar plications, the outer one being much weaker. The postero-lateral flanks are unplicated but are marked by very fine, subequal costellae. The anterior half of each strong plication is obscurely fasciculate.

Measurements (mm)

	Length	Width	Hinge-width
Ventral valve 7991	5.2	9.4	7.6
Dorsal valve 7992	5.6	9.4	10.2

Syntypes: I.P.A.S. 7991, 7992, 7993.

Horizon and locality: Upper Cambrian; Wanchiachai, east of the Yellow River, 25 miles north of Piankwan, Shansi Province.

Collector: F. H. Chia.

Discussion: Owing to the poor preservation, the characters of the specimens are not entirely clear. It is tentatively placed to the genus *Apheoorthis* on account of its fasciculate surface plications. *Apheoorthis costalis* recalls *A. meeki*[6] and *A. oklahomensis*[7], both occurring in the Upper Cambrian of North America, but differs from the two species in the possession of a very broad and deep sulcus in the dorsal valve. The surface ornamentation of this new species can be recognized by the few strong and prominent plications which tend to flatten and bifurcate toward the front.

Genus *Glyptorthis* Foerste 1914

Glyptorthis simplex Wang (sp. nov.)

(Pl. 1, H; Figs. 1-5)

Exterior: Shell moderately large for the genus; subquadrate in outline; hinge-line straight, as wide as or a little narrower than the greatest width; cardinal extremities square or nearly so; valves subequally biconvex, the ventral valve having greater convexity; ornamentation multicostate; costæ angular, strong, increasing by bifurcation and implantation; imbrications delicate, only developed in the anterior part of the shell.

Ventral valve evenly and gently convex in lateral profile, the medial portion of the valve being most convex; lateral regions flatly convex; front of the valve slightly flattened; umbo less swollen; beak pointed; interarea apsacline, moderately curved.

Dorsal valve flatly convex in lateral profile; unevenly convex in the anterior half of the valve; the median region being flattened or depressed into a well marked sulcus; median sulcus moderately deep, originating from the beak of the valve and widely extended toward the anterior margin; beak small; interarea short, anacline.

Interior: Teeth strong, ponderous; dental plates low, obsolete; muscular field subcordate, adductor and diductor scars not clearly separated; a short and weak median ridge extends from the anterior of the adductors.

Cardinalia strong; brachiophores thick, ventrally carinate; cardinal process moderately high, expanded in front; notothyrial platform thickened, produced anteriorly as a broad median ridge about to the middle of the valve.

Measurements (mm)

	Length	Width	Hinge-width	Thickness
Complete specimen 7994	13.8	15.9	14.6	9.7
Ventral valve 7995a	16.2	18.5	15.8	5.7
Dorsal valve 7995b	16.2	18.5	15.8	3.9

Holotype, I.P.A.S. 7994, paratypes, I.P.A.S. 7995a-b.

Horizon and locality: Shitzepu Formation, Middle Ordovician; north of Tungkungtze Village, Tsunyi District, Kweichow Province.

Collector: V. K. Ting.

Discussion: This species is based on two complete specimens which are coarsely silicified to retain the delicate structures of the shell. One of the complete specimens was opened in the hope of obtaining a good internal mold. However, the matrix was proved to be too coarse and porous to preserve the pallial and ovarian markings.

This species approaches *Glyptorthis balclatchiensis* (Davidson)[8] in its size and outline but differs in having a much shallower ventral valve, a broader hinge-line, and a more incurved beak. The surface ornamentation of *G. simplex* differs from that of *G. balclatchiensis* in being somewhat angular and less uniform, and in the imbricate lamellae developed only in the anterior of the shell.

Genus *Finkelnburgia* Walcott 1905

Finkelnburgia meitanensis Wang (sp. nov.)

(Pl. 1, J; Figs. 1-4)

Exterior: Shell large for the genus; outline subcircular, width a bit larger than length; hinge-line narrower than the greatest width at the middle; cardinal extremities rounded to obtusely angular; lateral and front margins rounded. Surface ornamented by costellae, increasing by intercalations. There are 11 to 12 costellae in 5 millimetres at the front margin of the valve. Concentric growth lamellae crowdly developed.

Ventral valve somewhat subquadrate in outline; flatly convex in lateral profile, with the greater convexity along the median line. Interarea long, apsacline; delthyrium wide.

Dorsal valve strongly and evenly convex in lateral profile, with the greatest convexity at the middle of the valve; lateral slopes steep and gently convex. Beak low, inconspicuous as usually in the genus. No sulcus.

Ventral interior: Pseudospondylium prominent, wide, extended anteriorly into a broad and low ridge; adductor track elongately oval, elevated above the adductor scars.

Dorsal interior: Brachiophore supporting plates low, recumbent; cardinal process a low, simple ridge; pallial trunks strongly developed.

Syntypes: I.P.A.S. 7996, 7997, 7998.

Horizon and locality: Upper-most part of Loushankuan Limestone, Upper Cambrian; east side of Tuanchiakou Valley, about one mile north of Meitan City, Kweichow Province.

Collector: The author.

Discussion: The available specimens of this species are coarsely silicified, and details of the internal characters are difficult to be observed. The surface ornamentations and dorsal interior, on the other hand, are fairly well preserved. These shells are the only fossil so far known from the barren Upper Cambrian limestone distributed widely in southwestern China.

This species differs from the other members of *Finkelnburgia* in its subcircular ventral valve, wide and shallow pseudospondylium and flat and high convexity of the dorsal valve.

Genus *Mimella* Cooper 1930

Mimella formosa Wang (sp. nov.)

(Pl. II, B; Figs. 1-8)

Shell large for the genus; roundly subquadrate in outline; hinge-line equal to about two-thirds the width of the valve; cardinal extremities and antero-

lateral angles rounded; lateral profile equally biconvex. Surface multicostellate, costellae being curved and increasing by repeated bifurcation. At the front margin of the shell there are about 10 costellae in 5 millimetres.

Ventral exterior: Strongly and evenly convex in lateral profile, with the greatest convexity a little posterior to the middle; umbo swollen, separated from the flanks of the shell by a concave area just in front of the posterior margin; beak prominent, incurved; interarea short, apsacline.

Dorsal exterior: Gently and evenly convex, the greatest convexity being around the middle; umbo flatly convex, slightly swollen; beak not prominent; interarea almost in the same height as the ventral one, orthocline.

Ventral interior: Teeth stout, triangular; dental plates low, receding; umbonal cavities indistinct; muscular area large, trilobate; adductor track broad and prominent, highly elevated by callus at the front; diductor tracks triangular, divergent, much shorter than the adductors; adjustor scars small, located at the base of the dental plates. Pallial markings conspicuously developed.

Dorsal interior: Cardinalia confined; brachiophores short and blunt; supporting plates largely obscured by callus, converging toward each other to form a cruralium; sockets shallow; cardinal process a thin linear ridge; adductor scars subquadrate, deeply impressed, the anterior pair the larger; median ridge strong, extending not beyond the anterior margin of the muscle field. Pallial markings strongly developed.

Measurements (mm)

	Length	Width	Thickness	Hinge-width
Complete specimen 7999	20.5	23.8	12.4	16.5
Ventral valve 8000	20.3	23.8	5.3	15.2
Dorsal valve 8001	22.2	25.0	5.6	18.1

Holotype, I.P.A.S. 7999, paratypes, I.P.A.S. 8000, 8001, 8002.

Horizon and localities: Neichia Series, Middle Ordovician; Pankuchai, west of Tangtishuya Village, north Ichang District, Hupeh Province; half a mile east of Yingwuhsi, Ssunan District, Kweichow Province.

Collectors: T. Y. Hsu and the author.

Discussion: This species is represented in our collection by abundant fine specimens. The Kweichow materials include several excellent internal molds from which all the details of the pallial markings could be determined.

The distribution of *Mimella* is chiefly in the Appalachian region of North

America. There can be no doubt that *Mimella formosa* is the first record of this genus in China and Eastern Asia.

Important differences between *Mimella formosa* and all other species of the genus are to be found both inside and outside. Externally, our form is characterized by its short, normally apsacline ventral interarea, swollen umbonal region and strongly incurved beak, with the greatest convexity of the shell around the middle and a very narrow fissure between the interareas. The American species, on the other hand, is distinct by virture of its highly erect ventral umbo and much higher interarea. Internally, the diductor scars of *Mimella formosa* are conspicuously shorter than those of the American species.

Genus *Martellia* Wirth 1936

Martellia ichangensis Wang (sp. nov.)

(Pl. II, C; Figs. 1-5)

1936 *Martellia giraldii,* Wirth: Palæont. Zeit., B. 18, T. 20, Figs. 1-19.

Shell medium in size; anterior margin extended; subpentagonal in outline; hinge-line straight, usually less than the greatest width at the middle; unequally biconvex in lateral profile; the ventral valve deeper than the dorsal valve, hemipyramidal; cardinal extremities rectangular or obtusely acute; lateral margins rounded; anterior commissure slightly uniplicate. Ventral interarea conspicuously long, strongly apsacline; delthyrium narrow and long, covered by a highly arched pseudodeltidium, without apical perforation. Surface multicostellate, costellae fine and even, about 20 costellae in 5 millimetres at front of the shell; surface undulated by variations of growth.

Ventral exterior: Strongly convex in lateral profile, with the greatest convexity at the postero-median part of the valve, anterior profile broadly and evenly convex; interarea flat, strongly apsacline, ornamented by horizontal striations; umbo flattened; beak minute, obtuse, apical angle being of about 130 degrees; front half of the valve marked by a faint, shallow sulcus.

Dorsal exterior: Lateral profile flatly and moderately convex; umbo depressed; a narrow and low fold originating from the middle of the valve and extending to the anterior margin; beak minute, inconspicuous; interarea short, strongly anacline; notothyrium wide, closed completely by a horizontal chilidial plate.

Dimensions (mm): Length 12.2; width 13.0; thickness 5.4; hinge-width 11.8.

Holotype, I.P.A.S. 8003.

Horizon and locality: Neichia Series, Middle Ordovician; about one mile

west of Tangtishuya and Fenhsiang Villages, North-Ichang District, Hupeh Province.

Collectors: Y. S. Chi, T. Y. Hsu and the author.

Discussion: This pretty small species is quite abundant in the weathering slopes formed by the Neichia Series in the Gorge Region of Central China. The material consists mainly of complete individuals with well-preserved external characters. Separated valves are very scarce. It is associated with *Yangtzeella poloi* and *Mimella formosa* (sp. nov.).

This species resembles in several respects *Martellia giraldi* (Martelli)[19] from the Middle Ordovician, Shensi Province, but differs in having a less convexity of the valves and in possessing exceedingly faint, weak fold and sulcus. It is also recognized by its small size, never reaching more than 15 millimetres in width as exhibited by about 30 specimens in our collection.

Genus *Hemipronites* Pander 1830

?*Hemipronites hupeihensis* Wang (sp. nov.)

(Pl. II, D; Figs. 1-4)

Shell rotund, outline subquadrate to subcircular; hinge-line shorter than the greatest width of the shell; cardinal extremities obtusely angular; beaks closely oppressed; lateral profile strongly and subequally biconvex; anterior commissure rectimarginate. Surface finely multicostellate, with about 3 costellae in 5 millimetres at the front of the shell; interspaces marked by radiating rows of minute pits.

Ventral valve strongly and evenly convex in lateral profile, with the greatest convexity at the middle; lateral and anterior margins rounded; anterior profile flatly convex; umbo swollen; beak incurved; interarea short, apsacline, slightly curved.

Dorsal valve very strongly and evenly convex, the greatest convexity being at the middle; anterior profile gently convex; umbo flatly convex, slightly swollen; beak inconspicuous; interarea moderately long, orthocline.

The umbonal regions of both valves in this specimen have externally worn out, the dental plates and brachiophore supports exhibited as dark lines which are short and widely divergent.

Dimensions (mm): Length 27.5; width 31.2; thickness 21.1; hinge-width 21.2.

Holotype, I.P.A.S. 8004.

Horizon and locality: Neichia Series, Middle Ordovician; Pankuchai, one mile west of Tangtishuya Village, Ichange District, Hupeh Province.

Collectors: T. Y. Hsu and the author.

Discussion: This species is represented by a single complete specimen which was collected from the same bed with *Yangtzeella poloi* and *Martellia ichangensis* (sp. nov.). Because of the scarcity of material, the details of the interior of this species are impossible to be ascertained. The surface ornamentation of this species resembles *Porambonites* more than *Hemipronites.* But in regard to the characters of the rotund form, the strongly biconvex lateral profile and the rectimarginate anterior commissure, the present specimen is Hemipronitoid. Inside the dorsal valve, the brachiophore supporting plates are widely divergent and short, unlike *Porambonites,* of which the brachiophore lamellae are subparallel and extend forward about to the middle of the valve. The generic assignment of the present specimen is tentative.

Genus *Palæostrophia* Ulrich and Cooper 1936

Palæostrophia recta Wang (sp. nov.)

(Pl. II, A; Figs. 1-3)

Shell small; subrectangular in outline; lateral profile subequally biconvex, dorsal valve having greater convexity; hinge-line straight, about equal to the width of the shell; cardinal extremities obtusely angular; anterior commissure strongly uniplicate. Surface smooth, only ornamented by few concentric lines.

Ventral valve gently convex, highest in the umbonal region; lateral margins sharply subangular; sulcus deep and wide, originating from the beak; beak minute.

Dorsal valve strongly convex, greatest convexity anterior to the middle of the valve; fold highly elevated, short, rounded, widening anteriorly and originating a little behind the middle of the valve; lateral flanks broadly convex, giving the shell a trilobate appearance in anterior view.

Syntypes, I.P.A.S. 8005, 8006, 8007.

Horizon and locality: Upper Cambrian; a small hill behind Tsingshantsun Village, west of Chiawang Colliery, Kiangsu Province.

Collector: J. C. Sheng.

Discussion: All specimens of this species available for study are crowded in a slab of white limestone with the shells badly exfoliated. This species is characterized by the rectangular general contour, the wide hinge-line and the high, rounded fold confined to the anterior half of the shell. These features and its small size serve to differentiate it from *Palæostrophia orthia* (Walcott)[10], a well-known species from the Upper Cambrian limestone of Shantung Province.

Genus *Pentamerus* Sowerby 1813

Pentamerus dorsoplanus Wang (sp. nov.)

(Pl. III, B; Figs. 1-5; Pl. IV, B; Figs. 1-3)

1911, *P. borealis,* Fresh: von Richthofen's China, Vol. 5, p. 15, pl. 4, fig. 3.

1922, *P. borealis,* Hayasaka: *Sci. Rep. Tohoku Imp. Univ.,* Vol. VI, No. 1, pp. 28-29, pl. 1, figs. 9a-c.

1925, *P. borealis,* Grabau: *Bull. Geol. Surv. China,* No. 7, p. 80.

Shell very large; elongate-subovate in outline, anteriorly widened; lateral profile plano-convex; lateral commissures almost straight; anterior commissure broadly unisulcate; hinge-line relatively short, commonly equal to only one-third the maximum width of the shell.

Ventral valve very strongly convex in lateral profile, highest region a little posterior to middle of the valve, whence sloping first smoothly and then rapidly toward the anterior margin; shell posterior to the umbo bending abruptly dorsoward; anterior profile rather evenly and broadly convex; lateral slopes bending abruptly downward; lateral margins straight or slightly re-entrans; umbo narrow, elongate, extending far back over the hinge; beak prominent, pointed, strongly incurved like a hook.

Dorsal valve very shallow, attaining less than one-fourth the thickness of the ventral valve; outline subpentagonal, with the greatest width distinctly in front of the mid-length; moderately or gently convex in lateral profile; medially depressed to form a broad shallow sulcus in the anterior region of the valve; umbo widely swollen; beak small, concealed.

Measurements (mm)

	Length	Width	Thickness	Hinge-width
Mature specimen 8008	63.6	40.9	34.3	13.5
Immature specimen 8010	31.6	21.6	18.1	12.2

Holotype, I.P.A.S. 8008, paratypes, I.P.A.S. 8009, 8010.

Horizon and locality: Lojoping Village, Ichang District, Hupeh Province.

Collectors: Y. S. Chi, T. Y. Hsu and the author.

Discussion: This species is abundantly distributed in the Middle Silurian Lojoping Series of the Gorge District, west Hupeh Province. It has originally been identified with the European species *P. borealis* Eichwald by Fresh and Hayasaka. The differences between these two species are apparent. In the Lojoping specimens, most of the mature shells are quite large, ranging from 60 to 65 millimetres in length, therefore, it attains over one-third the size of the typical *Pentamerus borealis*. *Pentamerus dorsoplanus* differs from *P. borealis* further in having an exceedingly shallower and less convex dorsal valve, and a pronounced and broadly depressed sulcus. In dorsal view, its general outline is subpentagonal rather than elongate-ovate, and the maximum

width of the shell is near the anterior margin. Moreover, the lateral commissure of our form is commonly not flexed as in *P. borealis,* and the dorsal valve is nearly flat.

Pentamerus muchuanensis Wang (sp. nov.)

(Pl. IV, C; Figs. 1-4)

Shell moderately large, typically sub-globose; outline suboval, greatest width distinctly in front of the mid-length; subequally biconvex in lateral profile, with the ventral valve deeper; anterior margin broadly rounded, anterior commissure rectimarginate; hinge-line exceedingly narrow, usually equal to only one-fourth the greatest width of the shell.

Ventral valve broadly convex, highest region a little posterior to the middle of the valve, curving sharply and steeply toward lateral margins, gradually and smoothly toward the anterior margin, and bending abruptly and vertically toward the umbo; umbo very prominent, globose; beak small, closely incurved against the dorsal valve.

Dorsal valve subtriangular in general outline; more strongly convex longitudinally than transversely, greatest convexity a little anterior to the umbo, sloping steeply posteroward but gently to the anterior margin; umbo somewhat tumid; beak strongly incurved, concealed under the delthyrium of the ventral valve.

Dimensions (mm): Length 45.4; width 41.2; thickness 32.5, hinge-width 11.5.

Holotype, I.P.A.S. 8011.

Horizon and locality: Lojoping Series, Middle Silurian; Muchuan District, Kweichow Province.

Collector: I. Huang.

Discussion: This species is represented by two specimens. The shell is considerably exfoliated with the umbonal region partially broken so that its internal structures are clearly exhibited. This species differs from *Pentamerus dorsoplanus* (sp. nov.) in having a relatively shorter shell length, in being subtriangular instead of subpentagonal in outline and in having a strong convex dorsal valve with no trace of sulcus.

Genus *Clorinda* Barrande 1879

Clorinda subaequata Wang (sp. nov.)

(Pl. III, A; Figs. 1-5)

Shell medium size; transversely suboval in outline, greatest width about in mid-length; lateral and anterior margins rounded; subequally biconvex in lateral profile; anterior commissure strongly uniplicate.

Ventral valve moderately convex, curving gradually toward the anterior margin and steeply toward the lateral and the cardinal margins; sulcus narrow and well defined, originating from the beak and widening rapidly anteroward, equal to about one-third the width of the valve in the front margin; beak small, incurved.

Dorsal valve flatly convex, greatest convexity near the umbo; median fold prominent and sharply defined, originating from the beak and increasing in width anteriorly until it occupies about one-third the width of the valve, top rounded and highly elevated at the front; beak minute, incurved.

Dimensions (mm): Length 13.0; width 14.6; thickness 13.0.

Holotype, I.P.A.S. 8012.

Horizon and locality: Upper Silurian; Hueichenkou, near Changning City, southwestern Szechwan Province.

Collector: L. T. Yeh.

Discussion: This species can be recognized readily by its transversely oval outline and less convexity in both valves. Generally, this species resembles *Clorinda linguifera* (Sowerby)[11] in having a transversely oval outline, but differs from that species in its smaller size, more sharply defined fold and sulcus, and less convexity in lateral profile.

Genus *Camarotoechia* Hall and Clarke 1893

Carmarotoechia fengkangensis Wang (sp. nov.)

(Pl. V, B; Figs. 1-5)

Anastrophia fengkangensis, Wang: Index Fossils of China (Invertebrate), pt. II, p. 129, pl. 68, figs. 25, 26.

Shell medium size; subquadrate to subpentagonal in outline, lateral margins broadly rounded; subequally biconvex in lateral profile; anterior commissure strongly uniplicate. Surface covered by simple plications, fine on the beak and strongly subangular toward the anterior margin, five on fold and four in sulcus, with 12-13 on each lateral slope, two additional plications extend beside the fold and sulcus and die out a little anterior to the middle of the valve.

Ventral valve gently convex, highest region posterior to the middle of the valve, elongately elevated in umbonal region, sloping steeply to the anterior and lateral margins; median portion depressed anteriorly to form a very broad and deep sulcus, about equal to one-third the width of the valve, continued anteriorly into a short tongue-shaped prolongation; umbo narrowly convex; beak prominent, pointed, erected and incurved.

Dorsal valve broadly and evenly convex, highest at mid-point whence surface descends gradually to lateral margins; umbo broadly convex; beak

minute, incurved; fold moderately high, short, appearing about at the middle of the valve.

Dimensions (mm): Length 18.5; width 18.5; thickness 11.4.

Holotype, I.P.A.S. 8013.

Horizon and locality: Lojoping Series, Middle Silurian; Changshengkou, Chahuaping Village, Fengkang District, Kweichow Province.

Collector: The author.

Discussion: In regard to its surface ornamentation, this specimen is erroneously identified with *Anastrophia* by the author in his previous work. A careful study of some serial sections leads the author to believe that this specimen may belong to the genus *Camarotoechia*. It has no ventral spondylium and has a median septum in the dorsal valve.

This species resembles *Camarotoechia bieniaszi* Kozlowski[12] in general outline but has a larger size and strong surface plications.

Genus *Paurorhyncha* Cooper 1942

Paurorhyncha squamosa Wang (sp. nov.)

(Pl. IV, D; Figs. 1-5)

Shell large; much wider than long, transversely sub-oval to subrectangular in outline; hinge-line narrow, equal to about half the width of the shell; cardinal extremities and lateral margins broadly rounded; anterior commissure strongly uniplicate; lateral profile subequally biconvex, the dorsal valve having a little more convexity; lateral commissures flexed ventrally. Surface ornamented by even, subrounded plications, except the sides of the sulcus and fold.

Ventral valve moderately convex, highest around the middle, curving rapidly anteroward and gradually to the cardinal and lateral margins; sulcus wide, with flat bottom, originating about from middle of the valve; tongue subquadrate, extending far beyond the anterior commissure; beak obtuse, slightly incurved.

Dorsal valve strongly convex, with the greatest convexity a little posterior to the middle; anterior profile strongly convex, posterior slope steep; fold moderately high, top flat, lateral sides abrupt, originating about in the vicinity of the middle of the valve, anterior end truncated; umbo broadly swollen; beak incurved and concealed by the ventral beak.

Dimensions (mm): Length 33.2; width 42.6; thickness 25.6; hinge-width 21.3.

Holotype, I.P.A.S. 8014.

Horizon and locality: Upper Devonian; Itate, Pohsi, Huaning District, Yunnan Province.

Collectors: Students of Chungshan University.

Discussion: *Paurorhyncha squamosa* appears to be closely related to *P.* sp., figured in plate 119 of the Index Fossils of North America, from which it differs in the subrectangular outline instead of subtriangular, the most convex umbonal region of the dorsal valve, the narrower and shorter median fold, and the wide lateral flanks of both valves.

Paurorhyncha depressa Wang (sp. nov.)

(Pl. V, D; Figs. 1-5)

Shell large; typically rectangular in outline; cardinal and antero-lateral angles broadly rounded; lateral profile lenticular, subequally biconvex, the dorsal valve having a little greater convexity; anterior commissure uniplicate.

Ventral valve moderately convex around the umbonal region, but flattened in lateral flanks; sulcus broad, bottom flat, originating as a shallow depression about in middle of the valve, becoming deeper and bending abruptly at the front to form a short and sharp tongue, extremity of the tongue being truncated; beak small, incurved.

Dorsal valve gently convex in lateral profile and most convex along the medial region of the valve; fold low and broad, equal to about one-third the shell width; umbo tumid; beak incurved.

Dimensions (mm): Length 31.4; width 48.0; thickness 15.0; hinge-width 22.6.

Holotype, I.P.A.S. 8015.

Horizon and locality: Upper Devonian; Itate, Pohsi, Huaning District, Yunnan Province.

Collectors: Students of Chungshan University.

Discussion: This species is associated with *Paurorhyncha squamosa* (sp. nov.). It differs from the latter in the general outline and the lateral profile. In the first place, the general outline of this species is rectangular rather than oval, and the maximum length is about only two-thirds the width of the valve. It differs from *P. squamosa,* moreover, in having a much less convexity of both valves.

Genus *Hypothyridina* Buckman 1906

Hypothyridina hunanensis Wang (sp. nov.)

(Pl. V, C; Figs. 1-5)

Shell of medium size; subpentagonal in outline, shape subcuboidal; width a little greater than length, with the greatest width about along the cardinal

line; cardinal extremities obtuse; very unequally biconvex in lateral profile, greatest thickness in the anterior margin; anterior commissure strongly uniplicate.

Ventral valve very shallow, flatly convex, postero-lateral margins sloping abruptly toward the cardinal line; lateral flanks moderately convex; median portion depressed anteriorly to form a broad and shallow sulcus with a flat bottom, and geniculated in right angle to meet the dorsal fold; lingual extension quadrate and long; umbo narrowly and gently arched; beak small, incurved against that of the dorsal valve.

Dorsal valve very strongly convex, more than four times the thickness of the ventral valve; surface curving from median portion rapidly to the beak and flattening thence toward the anterior margin; flanks sloping abruptly from borders of the fold to lateral margins, almost making a right angle with the plane of commissure; fold low, narrower than the sulcus, gently convex, developed only in the anterior part of the valve; umbo narrowly convex; beak minute, incurved, hidden under the ventral beak.

External surface ornamented with simple, low, rounded plications, 9 in sulcus, 8 on fold, and 16 or more on each lateral flank; interspace about as wide as the plication.

Dimensions (mm): Length 27.3; width 28.8; thickness 27.0.

Holotype, I.P.A.S. 8016.

Horizon and locality: Lungkouchung Bed, Middle Devonian; Lungkouchung Village, Hsianghsiang District, Hunan Province.

Collector: K. K. Chao.

Discussion: This species is distinguished by its large size, its sharp and obvious surface ornamentations with its prominent sulcus extending dorsoward into a long quadrate prolongation, the greatest thickness of the shell being thus in the anterior margin.

In regard to the large size and cuboidal outline, this new species appears to be allied to *Hypothyridina obesa* Grabau[13] from northern Szechwan Province. It differs, however, in having a width greater than length, in having a less convexity in the posterior portion of the dorsal valve, and in having a much narrower fold and sulcus with a relatively longer lingual extension.

Furthermore, the flattened rather than rounded surface plications and the linear interspaces of *Hypothyridina obesa* also serve to distinguish it from the present form.

Hypothyridina linglingensis Wang (sp. nov.)

(Pl. III, C; Figs. 1-5)

Size small for the genus; subcuboidal in shape, rectangular in outline,

having a width greater than length, greatest width about near the mid-length; anterior margin truncated; lateral margins broadly rounded; lateral profile very unequally biconvex; anterior commissure strongly uniplicate.

Ventral valve flatly convex; postero-lateral margins slightly depressed; median portion moderately elevated; umbonal region narrow, highly arched; beak small, slightly incurved; sulcus very broad, shallow, equal to more than half the width of the valve; tongue exceedingly long, bottom flat, bending almost in right angle or a little recumbent posteriorly.

Dorsal valve strongly convex and most convex in the anterior margin; posterior and lateral slopes curving abruptly and steeply toward the plane of the commissure; fold low, broad, defined only in the anterior half of the valve; umbo widely swollen; beak concealed under the ventral beak.

Surface marked by broad flat plications, separated by much narrow and shallow furrows; number of plication 7 in sulcus, 6 on fold and about 11 or more on each lateral slope.

Dimensions (mm): Length 18.3; width 20.4; thickness 15.2.

Holotype, I.P.A.S. 8017.

Horizon and locality: Upper Devonian; one mile west of Yenmuchiao, Lingling District, Hunan Province.

Collector: K. K. Chao.

Discussion: This species is represented by a single well preserved specimen and is the first known species of *Hypothyridina* from the Upper Devonian in China.

This species resembles *Hypothyridina cuboides* (Sowerby)[14] in its general shape and outline, but differs in being comparatively smaller in size, in having more surface plications and a much longer sulcus. It resembles also *Hypothyridina emmonsi* (Hall and Whitfield)[15] from the Independence Shale of North America in proportion and outline but differs from it in the number of plication both in sulcus and lateral slopes. As described by Strainbrook, in mature specimen of *H. emmonsi,* there are 14 plications in sulcus, 15 on fold and 18 or more on each lateral slope.

Genus *Wellerella* Dunbar and Condra 1932

Wellerella subdekalbensis Wang (sp. nov.)

(Pl. V, A; Figs. 1-5)

Shell substance very thin; size small; outline subtriangular to subpentagonal, having a considerably greater width than length and a bit greater length than thickness, greatest width near anterior margin; antero-lateral angles broadly rounded; very inequivalved; anterior margin truncated; anterior commissure widely uniplicate.

Ventral valve shallow, gently and flatly convex; elevated a little in umbonal region, depressed anteriorly by very broad shallow sulcus, equal to about three-fourths the width of the valve; anterior half of the sulcus strongly geniculate at right angle and continued forward as a short lingual prolongation; beak narrow and acutely pointed; foramen minute, circular.

Dorsal valve strongly convex, with the greatest convexity near the anterior margin whence the surface descends steeply and abruptly toward the lateral margins and slopes gradually toward the beak; fold short, equal to only one-third the length of the valve, bending abruptly to meet the sulcus; beak concealed.

Posterior portion of the shell smooth; anterior margin marked by strong, short, angular plications, the number averaging 6 on the fold, 5 in the sulcus and 2 or more obsolete ones on each lateral slope.

Dimensions (mm): Length 6.7; width 7.9; thickness 5.6.

Holotype, I.P.A.S. 8018.

Horizon and locality: Penhsi Series, Middle Carboniferous; south of the second tunnel, Tsuichiakou, Yentai Colliery, Liaoning Province.

Collectors: Y. H. Lu, S. W. Tang, and the author.

Discussion: This species agrees both in size and number of surface plications with *Wellerella dekalbensis* Dunbar and Condra[16] but differs strikingly from the latter in having a width greater than its length and in having a less pointed ventral beak. Externally, it is easy to separate the present form from *W. dekalbensis* by its much shorter surface plications which originate farther anterior to the middle of the valve.

Genus *Zygospira* Hall 1862

Zygospira kueichowensis Wang (sp. nov.)

(Pl. IV, A; Figs. 1-5)

Size small; valves subequal in depth, biconvex; outline subcircular; hinge-line narrow, curved; cardinal extremities and antero-lateral angles rounded. Surface marked by sixteen or more subrounded, sharp costae; all costae originate from the beaks with few secondary costae added in the antero-median parts of the shell.

Ventral valve moderately convex, with the greatest convexity along the postero-median region, thence it slopes gradually toward the lateral and anterior margins; beak elongate, strongly incurved.

Dorsal valve evenly and broadly convex, lateral flanks fairly swollen; umbonal region a little sulcate; beak concealed by the ventral one.

Dimensions (mm): Length 6.8; width 6.8; thickness 3.6.

Holotype, I.P.A.S. 8019.

Horizon and locality: Lojoping Series, Middle Silurian; east of Tashutze, Yingwuhsi, Ssunan District, Kweichow Province.

Collector: The author.

Discussion: The assignment of the present shell to *Zygospira* is based only on its external similarity of the genus. It is characterized by the sub-circular outline, non-appearance of a fold and sulcus in the median part of the valve.

(*To be continued*)

References

[1] Walcott, Charles, D., 1912. Cambrian Brachiopoda. *Monog. United States Geol. Surv.*, **51**, 426—427, pl. 32, figs. 5, 5a-g.

[2] ———————, 1913. The Cambrian Faunas of China. *Research in China,* **3**, 68—69, pl. 2, figs. 5, 5a-c.

[3] Hsu, Singwu, C., 1948. The I-Chang Formation and the Ichangian Fauna. *Contr. Inst. Geol., Acad. Sinica,* **8**, 43—44, pl. 9, figs. 16-18.

[4] Sinclair, Winston, G., 1945. Some Ordovician Lingulid Brachiopods. *Trans. Roy. Soc. Canada,* Ser. 3, sect. 4, **39**, 63, pl. 2, figs. 3-6.

[5] Walcott, Charles, D., 1913. *Ibid.,* 62—63, pl. 1, figs. 7, 7a.

[6] Ulrich, E. O. and Cooper, G. A., 1938. Ozarkian and Canadian Brachiopoda. *Geol. Soc. Amer. Spec. Papers,* **13**, 83—84, pl. 11D, figs. 9-15.

[7] ———————, 1938. *Ibid.,* 85—86, pl. 9C, figs. 5-7.

[8] Reed, F. R. C., 1917. The Ordovician and Silurian Brachiopoda of the Girvan District. *Journ. Roy. Soc. Edinburgh,* **51** (4), 840—841, pl. 7, figs. 13-20.

[9] Martelli, Alessandro, 1901. Fossili del Siluriano inferiore dello Schensi. *Bull. Soc. Geol. Italiana,* **20**, 305—307, pl. 4, figs. 7-12.

[10] Walcott, Charles, D., 1913. *Ibid.,* 85—86, pl. 5, figs. 1, 1a-b.

[11] Barrande, Joachim, 1879. *Systeme silurien du centre de la Bohême,* **5**, pl. 24, III, figs. 1c-9b; pl. 119, figs. 10a-c.

[12] Kozlowski, Roman, 1929. Les Brachiopodes Gothlandiens de la Podolie Polonaise. *Palaeont. Polonica,* **1**, 158—159, pl. 5, figs. 12-14.

[13] Grabau, Amadeus, W., 1931. Devonian Brachiopoda of China. *Palæont. Sinica,* Ser. B, **3** (3), 121—122, pl. 23, figs. 7a-e, 8a-e.

[14] Gürich, G., 1908. *Leitfossilien (Devon)*, 145, pl. 45, figs. 5a-c.

[15] Stainbrook, Merrill, A., 1945. Brachiopoda of the Independence Shale of Iowa. *Geol. Soc. Amer. Mem.,* **14**, 42—43, pl. 4, figs. 10-14.

[16] Dunbar, Carl, O. and Condra, G. E., 1932. Brachiopoda of the Pennsylvanian System in Nebraska. *Bull. Neb. Geol. Surv.,* **5**, 294—295, pl. 37, figs. 22a-c.

EXPLANATION OF PLATES

EXPLANATION OF PLATE I

(No figures retouched)

A. *Palæobolus discus* Wang (sp. nov.) ..... p. 157
1: Exterior of dorsal valve showing ornamentation, × 6, figured specimen, I.P.A.S. 7981.
Chiushukou Bed, Upper-most Cambrian; limestone quarry, south of Huolianchai Station, Penhsi District, Liaoning Province.

B. *Palæobolus rotulus* Wang (sp. nov.) ..... p. 158
1: Exterior of ventral valve showing ornamentation, × 3, figured specimen, I.P.A.S. 7982.
Kushan Formation, Upper Cambrian; summit of Nanchimao Hill, Pangchiawa, southwest of Chiawang Colliery, Kiangsu Province.

C. *Westonia obovata* Wang (sp. nov.) ..... p. 158
1: Ventral valve showing subrounded outline of the species, × 2, figured specimen, I.P.A.S. 7983; 2: Portion of exterior enlarged to show ripply surface sculpture, × 10, figured specimen, I.P.A.S. 7984.
Kushan Formation, Upper Cambrian; limestone quarry near Changshan, Chiawang Coal Field, Kiangsu Province.

D. *Westonia shengi* Wang (sp. nov.) ..... p. 159
1: Exterior of ventral valve showing general outline, × 3, figured specimen, I.P.A.S. 7985.
Fengshan Formation, Upper Cambrian; west of Hsiatsun Village, Chiawang Coal Field, Kiangsu Province.

E. *Lingulepis nanchuanensis* Wang (sp. nov.) ..... p. 159
1: Poorly preserved ventral valve showing general outline of the species, × 2, figured specimen, I.P.A.S. 7986.
Panho Series, Lower Ordovician; Hot Spring, east of Nanchuan City, Szechwan Province.

F. *Lingula kwani* Wang (sp. nov.) ..... p. 159
1, 2, 3: Respectively, ventral, dorsal and lateral views of complete immature individual showing general form of the species, × 1, syntype, I.P.A.S. 7987; 4: Exterior of ventral valve showing surface sculpture, × 1, syntype, I.P.A.S. 7988.
Kelimoli Limestone, Lower Ordovician; Latsatsung, south of Chotzeshan, Ordos, Inner Mongolia.

G. *Apheoorthis costalis* Wang (sp. nov.) ..... p. 160
1: Partially exfoliated ventral valve showing ornamentation, × 2, syntype, I.P.A.S. 7991; 2: exterior of poorly preserved dorsal valve showing broad sulcus, × 2, syntype, I.P.A.S. 7992; 3: impression of exterior of ventral valve showing strong angular costae in median part and fine costellae in postero-lateral flanks of the valve, × 2, syntype, I.P.A.S. 7993.
Upper Cambrian: Wanchiachai, east of Yellow River, 25 miles north of Piankwan, Shansi Province.

H. *Glyptorthis simplex* Wang (sp. nov.) ..... p. 161
1, 2, 3: Ventral, dorsal and lateral views of complete specimen showing ornamentation and strongly biconvex valves, × 1.5, holotype, I.P.A.S. 7994; 4, 5: ventral and dorsal interiors of complete individual showing ventral musculature and dorsal cardinalia, × 1.5, paratypes, I.P.A.S. 7995a-b.
Shitzepu Formation, Middle Ordovician; north of Tungkungtze Village, Tsunyi District, Kweichow Province.

I. *Paterina talingensis* Wang (sp. nov.) ..... p. 160
1: Exterior of ventral valve, × 5, syntype, I.P.A.S. 7989: 2: exterior of dorsal valve, × 5, syntype, I.P.A.S. 7990.
Mant'o Shale. Lower Cambrian; Taling, east of Kaochiatsui Station, Penhsi District, Liaoning Province.

J. *Finkelnburgia meitanensis* Wang (sp. nov.) ..... p. 163
1: Exterior of ventral valve showing delicate costellae and subrounded general outline, × 1.5, syntype, I.P.A.S. 7996; 2, 4: exterior and interior of dorsal value, × 1.5, syntype, I.P.A.S. 7997: 3; interior of poorly preserved ventral valve showing pseudospondylium and pallial markings, × 1.5, syntype, I.P.A.S. 7998.
Upper part of Loushankuan Limestone, Upper Cambrian; east side of Tuanchiakou Valley, about one mile north of Meitan City, Kweichow Province.

A

1

B

1

C

1

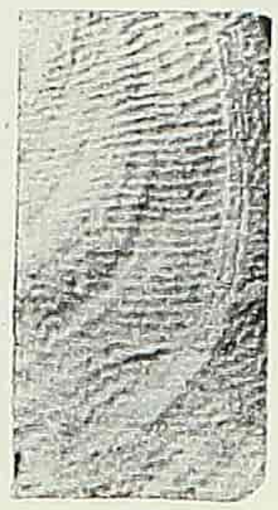

2

D

1

E

1

F

1

2

3

4

G

2

1

H

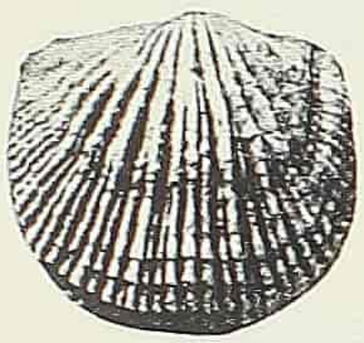

1

3

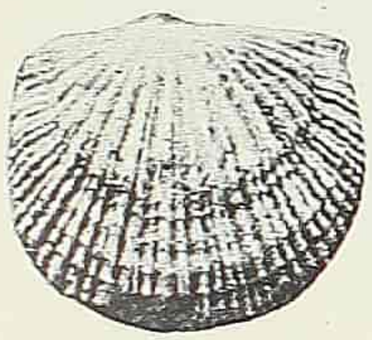

2

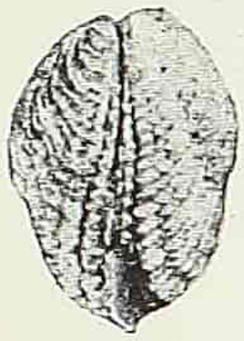

3

4

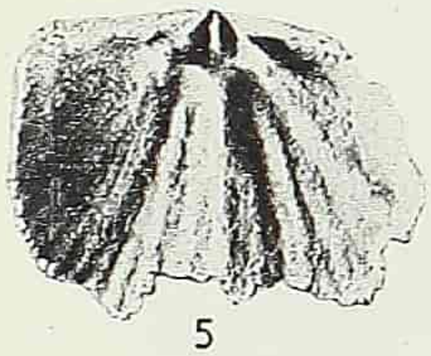

5

I

1

2

J

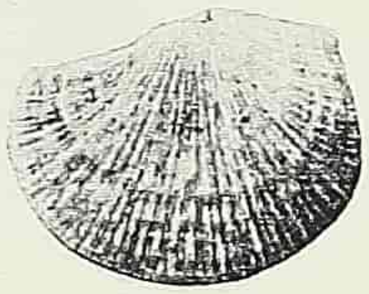

1

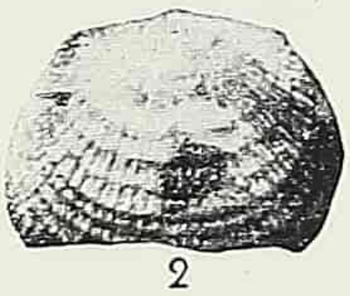

2

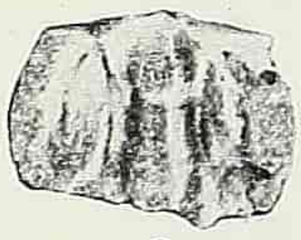

3

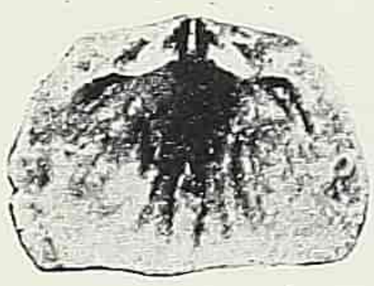

4

EXPLANATION OF PLATE II

A. *Palæostrophia recta* Wang (sp. nov.) ..... p. 167
1: Exfoliated ventral valve showing pallial marks, × 2, syntype, I.P.A.S. 8007; 2: exterior of imperfect ventral valve showing sulcus, × 2, syntype, I.P.A.S. 8005; 3: exterior of imperfect dorsal valve showing broad and short fold, × 2, syntype, I.P.A.S. 8006.
Upper Cambrian; a small hill behind Tsingshantsum Village, west of Chiawang Colliery, Kiangsu Province.

B. *Mimella formosa* Wang (sp. nov.) ..... p. 163
1, 2, 3, 4: Respectively, ventral, dorsal, posterior and lateral views of complete specimen, × 1.5, holotype, I.P.A.S. 7999; 5: interior of ventral valve showing highly elevated adductor tracks, × 1.5, paratype, I.P.A.S. 8000; 6: interior of dorsal valve showing brachiophores, cardinal process and deeply impressed muscle area, × 1.5, syntype, I.P.A.S. 8001; 7,8: ventral and dorsal views of well preserved internal mold showing ovarian impressions and pallial trunks, × 1.5, syntype, I.P.A.S. 8002.
Neichia Series, Middle Ordovician; Pankuchai, west of Tangtishuya Village, north of Ichang District, Hupeh Province; half a mile east of Yingwushi, Ssunan District, Kweichow Province.

C. *Martellia ichangensis* Wang (sp. nov.) ..... p. 165
1, 2, 3, 4, 5: Respectively, ventral, dorsal, lateral, posterior and anterior views of mature individual showing ornamentation and faint sulcus and fold, × 2, holotype, I.P.A.S. 8003.
Neichia Series, Middle Ordovician; about one mile west of Tangtishuya and Fenhsiang Villages, north of Ichang District, Hupeh Province.

D. ?*Hemipronites hupeihensis* Wang (sp. nov.) ..... p. 166
1, 2, 3: Ventral, dorsal and lateral views of complete specimen, × 1, holotype, I.P.A.S. 8004; 4: same, portion of exterior enlarged to show small pits along the radiating interspaces, × 2.5.
Neichia Series, Middle Ordovician; Pankuchai, one mile west of Tangtishuya Village, Ichang District, Hupeh Province.

A

1

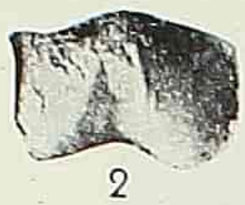

2

3

C

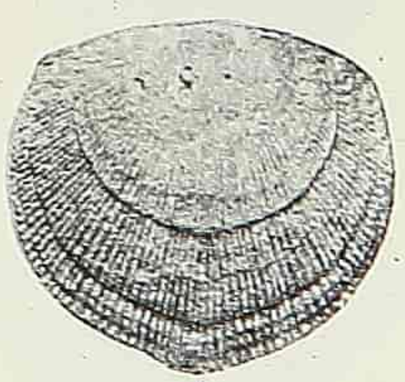

1

3

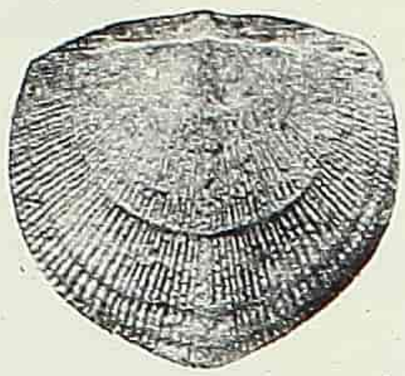

2

4

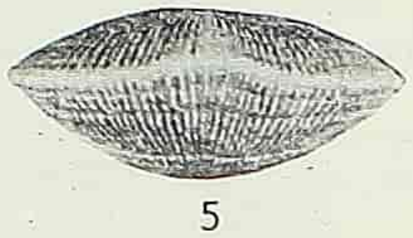

5

B

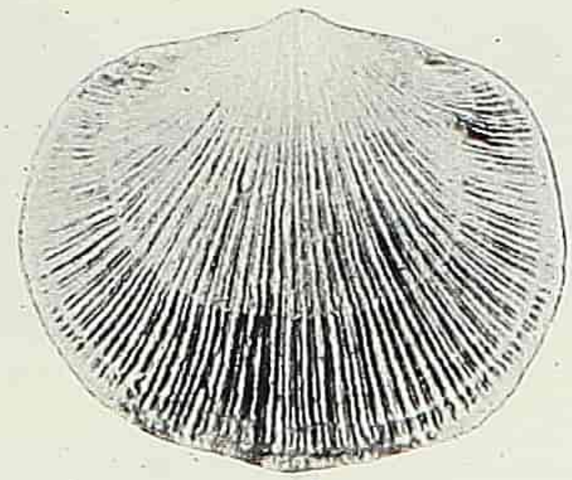

1

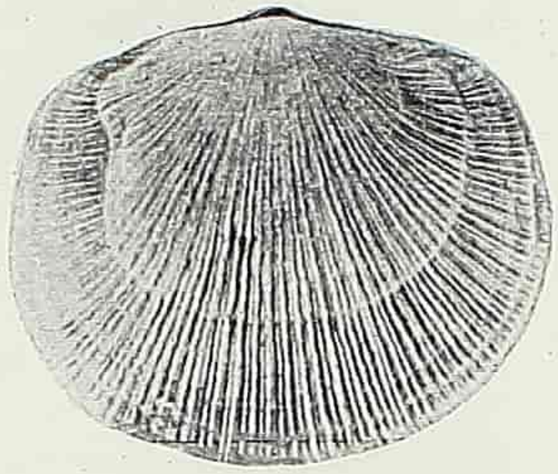

2

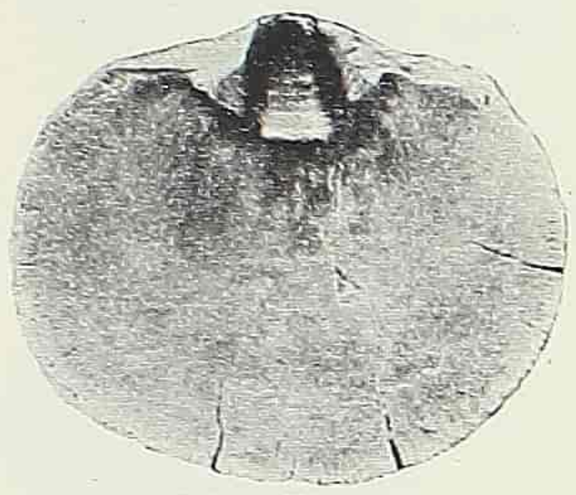

5

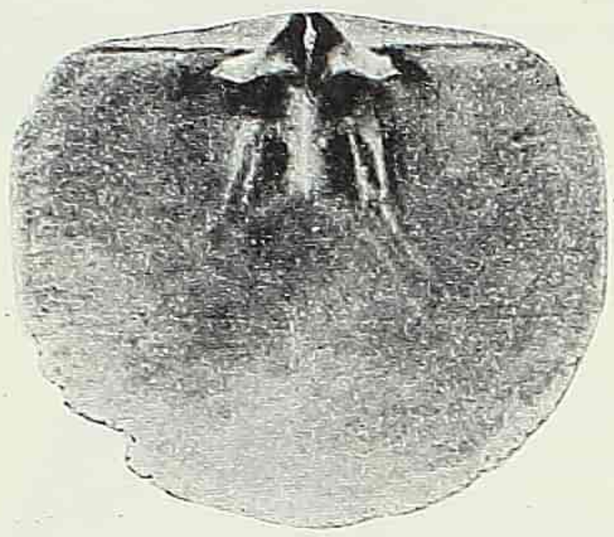

6

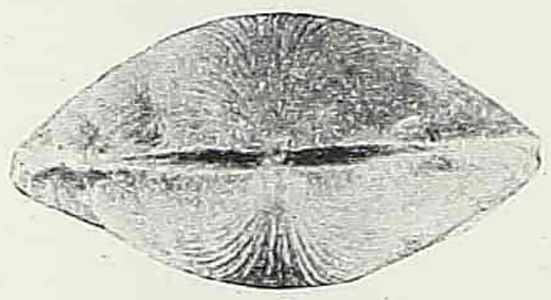

3

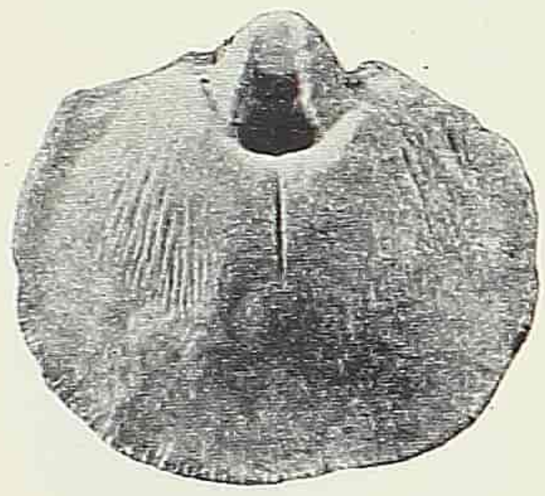

7

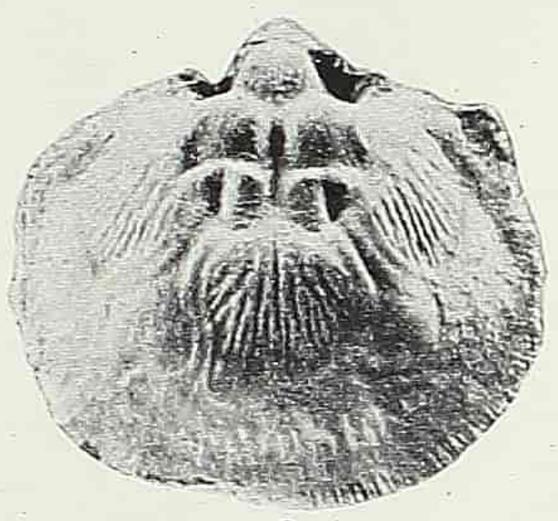

8

4

D

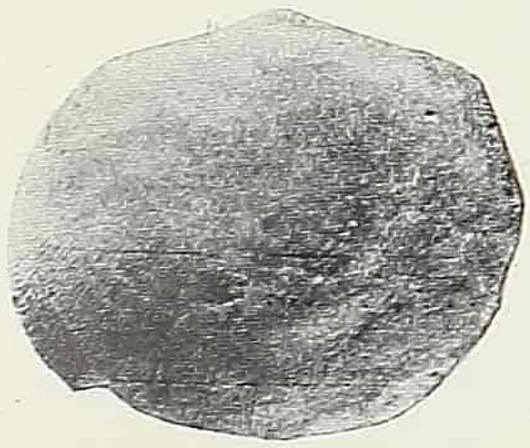

1

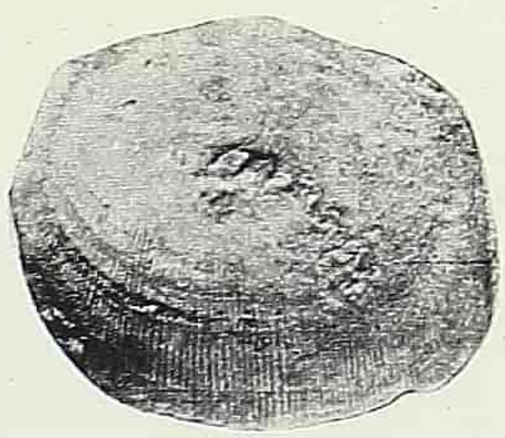

2

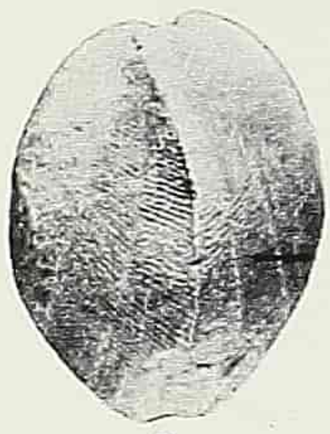

3

4

EXPLANATION OF PLATE III

A. *Clorinda subaequata* Wang (sp. nov.) ..... p. 169
1, 2, 3, 4, 5: Respectively, ventral, dorsal, posterior, lateral and anterior views of complete specimen, × 2, holotype, I.P.A.S. 8012.
Upper Siiurian; Hueichenkou, near Changning City, southwestern Szechuan Province.

B. *Pentamerus dorsoplanus* Wang (sp. nov.) ..... p. 167
1, 2, 3, 5: Respectively, ventral, dorsal, lateral and anterior views of mature individual showing subpentagonal general outline and dorsal broad sulcus, × 1, holotype, I.P.A.S. 8008; 4: specimen broken along median line showing internal septa, × 1, paratype, I.P.A.S. 8009.
Lojoping Series, Middle Silurian, west of Wulungkuan Hill, north of Lojoping Village, Ichang District, Hupeh Province.

C. *Hypothyridina linglingensis* Wang (sp. nov.) ..... p. 173
1,2,3,4,5: Respectively, ventral, dorsal, lateral, posterior and anterior views of complete specimen, × 1.5, holotype, I.P.A.S. 8017.
Upper Devonian; one mile west of Yenmuchiao, Lingling District, Hunan Province.

A

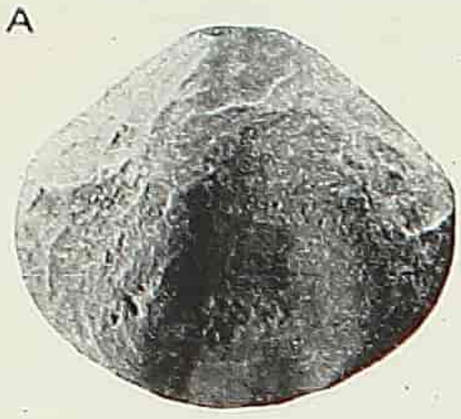

1

2

3

4

5

B

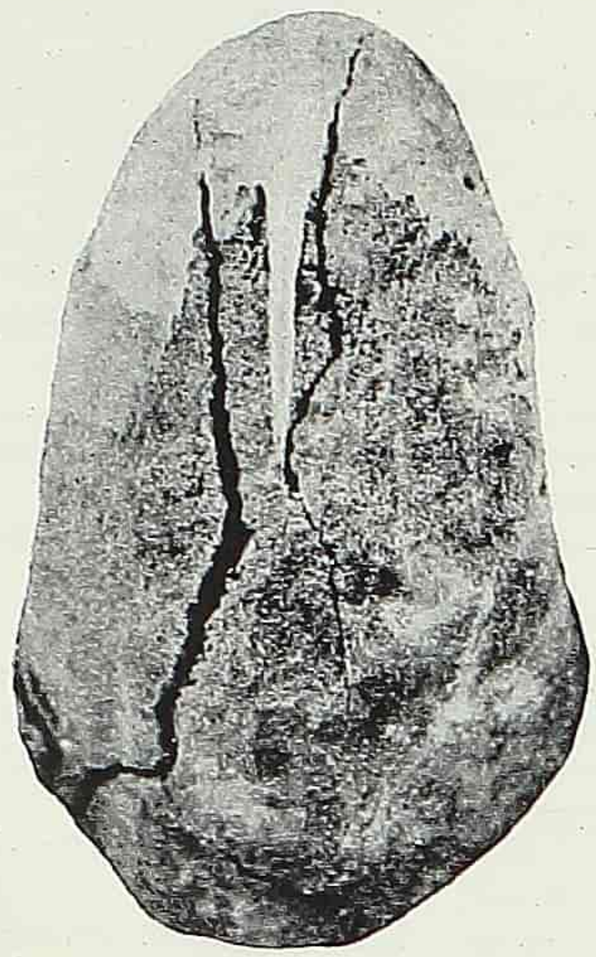

1

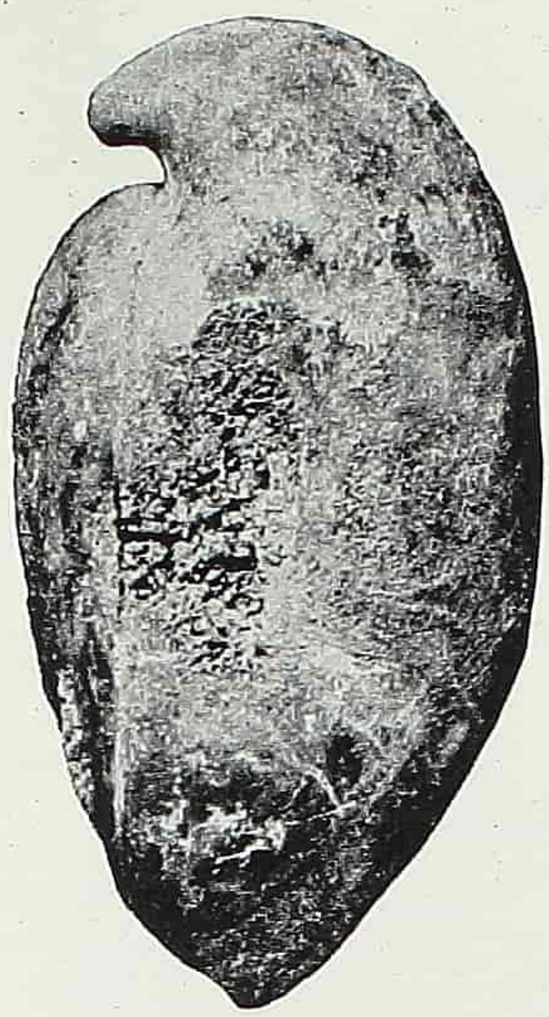

3

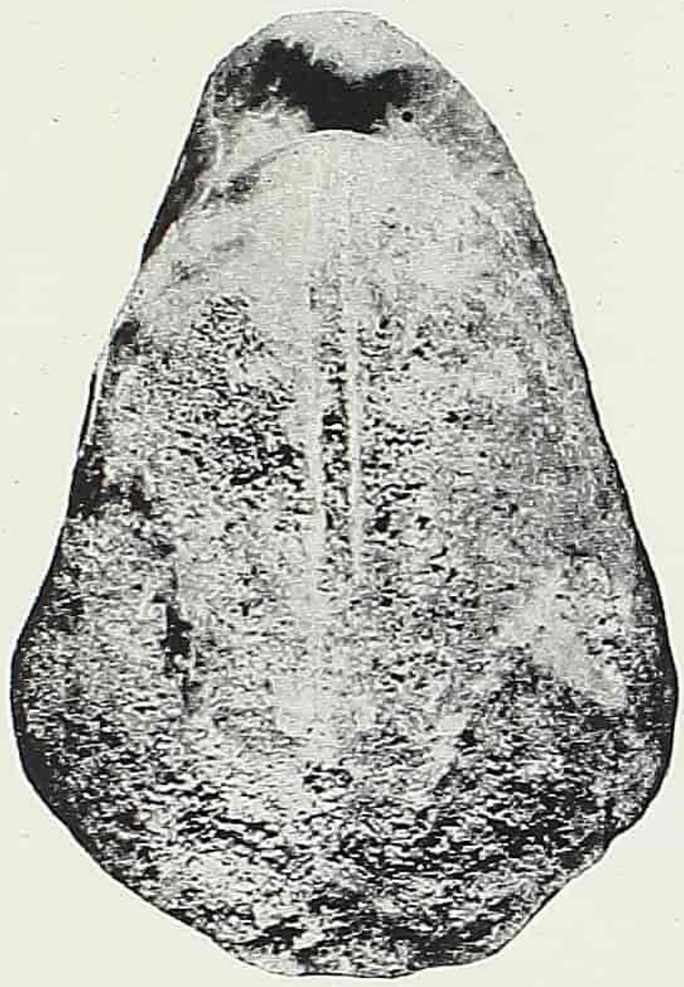

2

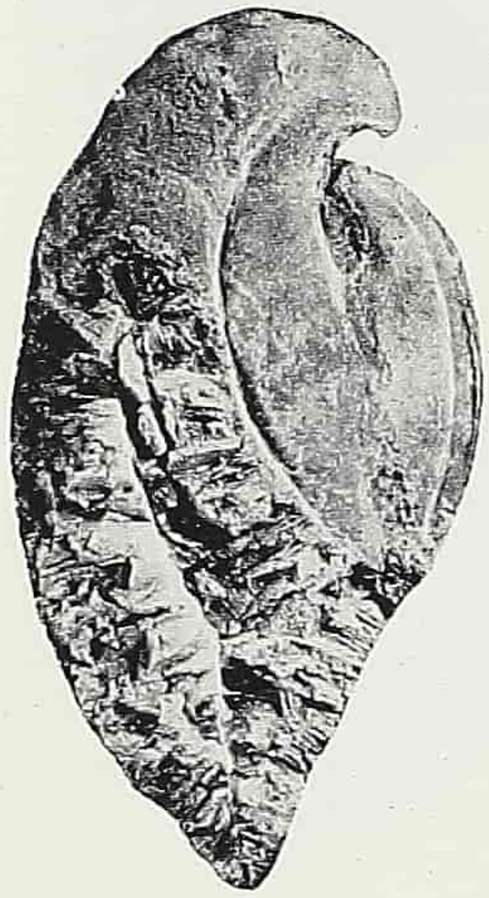

4

C

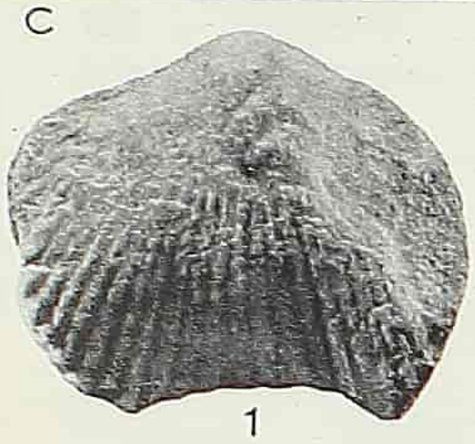

1

2

3

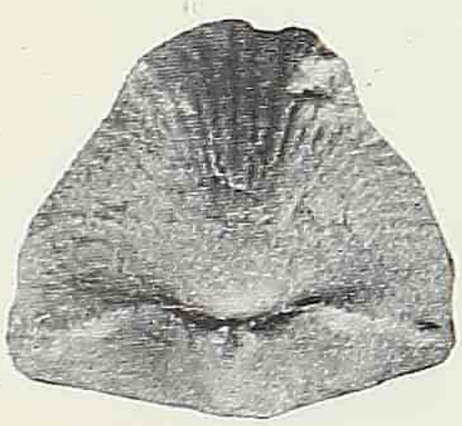

4

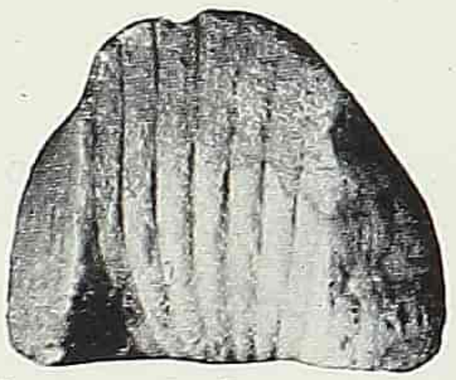

5

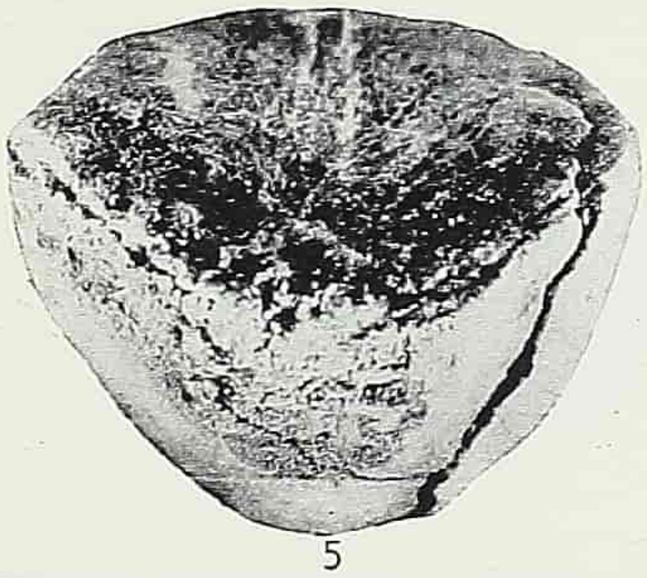

5

EXPLANATION OF PLATE IV

A. *Zygospira kueichowensis* Wang (sp. nov.) ..... p. 175
1, 2, 3, 4, 5: Respectively, ventral, dorsal, posterior, anterior and lateral views of complete specimen showing general form and ornamentation, × 3, holotype, I.P.A.S. 8019.
Lojoping Series. Middle Silurian; east of Tashutze, Yingwuhsi, Ssunan District, Kweichow Province.

B. *Pentamerus dorsoplanus* Wang (sp. nov.) ..... p. 167
1, 2, 3: Ventral, dorsal and lateral views of immature specimen, note more convex dorsal valve and elongately oval outline, × 1, paratype, I.P.A.S. 8010.
Lojoping Series, Middle Silurian; west slope of Wulungkuan Hill, north of Lojoping Village, Ichange District, Hupeh Province.

C. *Pentamerus muchuanensis* Wang (sp. nov.) ..... p. 169
1, 2, 3, 4: Dorsal, lateral, ventral and posterior views of complete specimen, note strongly biconvex lateral profile and broadly oval outline, × 1, holotype, I.P.A.S. 8011.
Lojoping Series, Middle Silurian; Muchuan District, Kweichow Province.

D. *Paurorhyncha squamosa* Wang (sp. nov.) ..... p. 171
1, 2, 3, 4, 5: Ventral, dorsal, anterior, lateral, and posterior views of complete specimen, note appearance of fold and sulcus, × 1, holotype, I.P.A.S. 8014.
Upper Devonian; Itate, Pohsi, Huaning District, Yunnan Province.

A


1


2


3


4

B


1


2


3


5

C

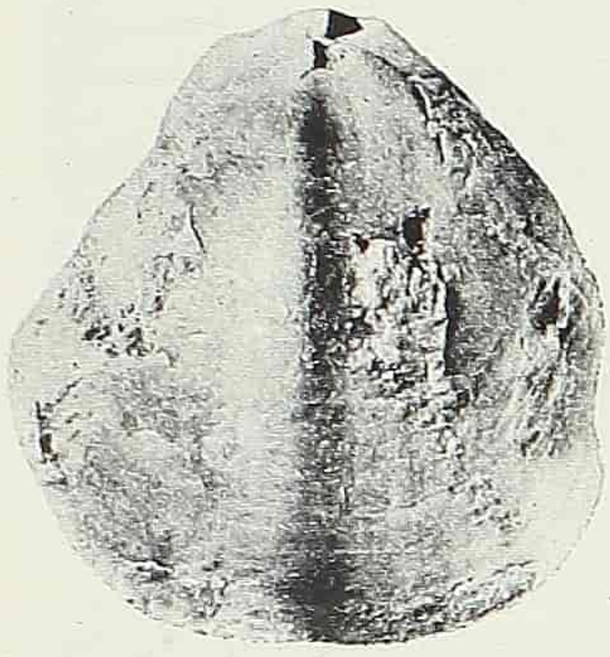
1

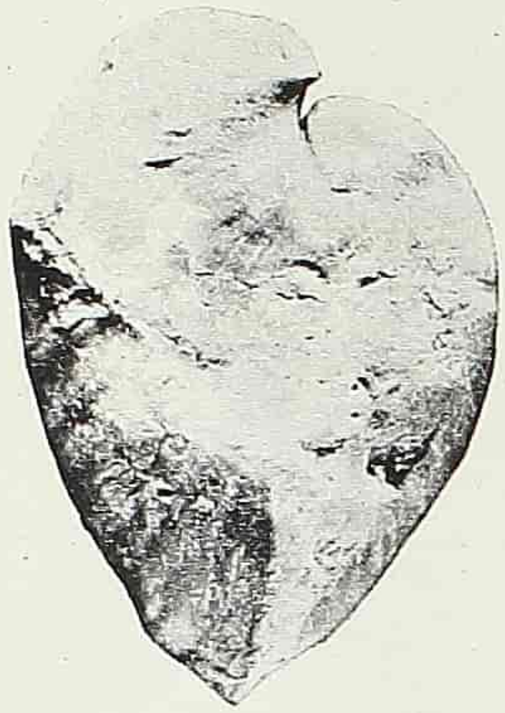
2

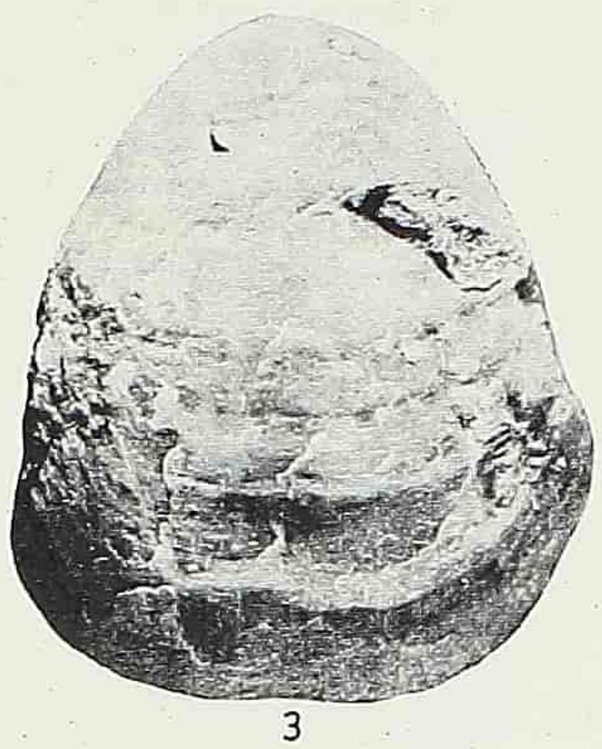
3

D

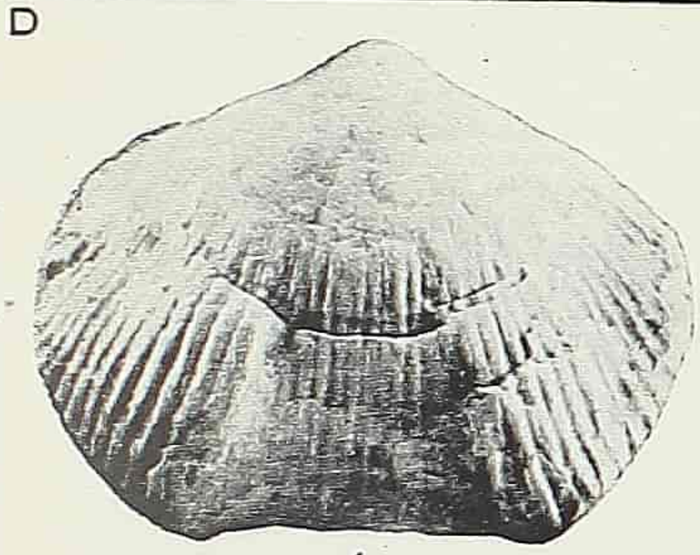
1

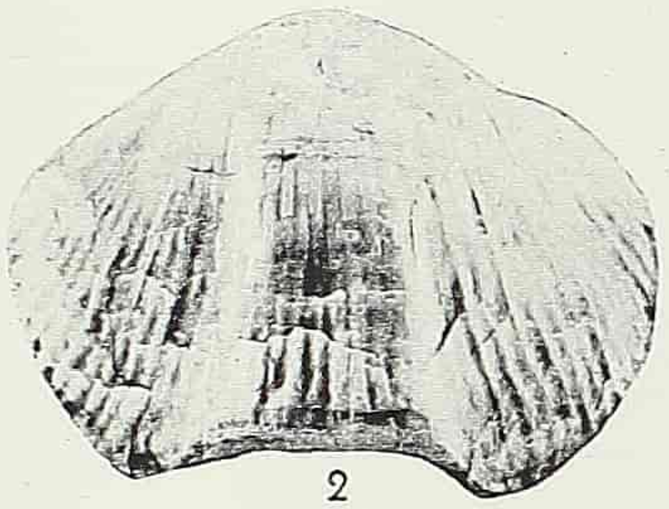
2

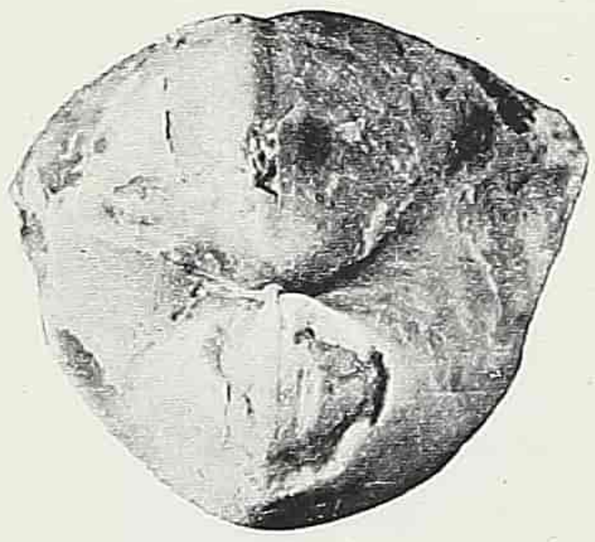
4

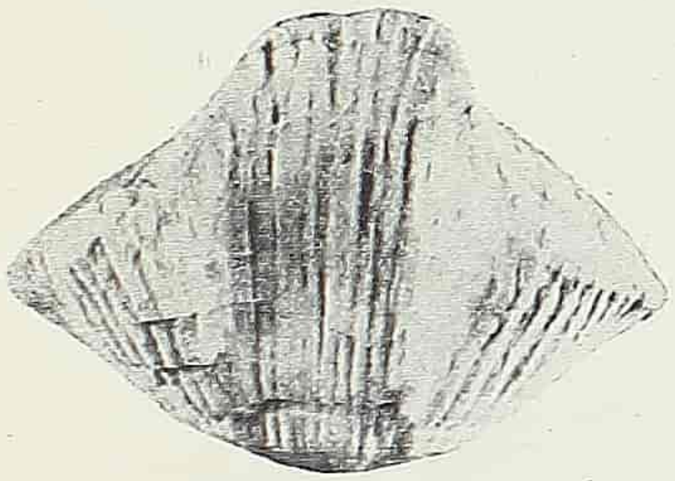
3

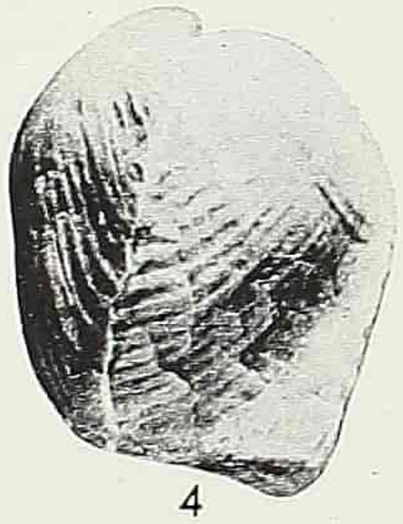
4

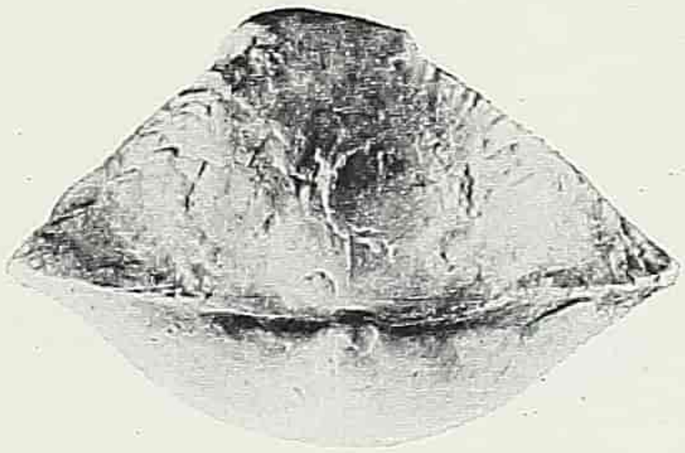
5

EXPLANATION OF PLATE V

A. *Welierella subdekalbensis* Wang (sp. nov.) ..... p. 174
1, 2, 3, 4, 5: Ventral, dorsal, lateral, anterior and posterior views of complete specimen, note short and strong plications, × 3, holotype, I.P.A.S. 8018.
Penhsi Series, Middle Carboniferous; south of the second tunnel, Tsuichiakou, Yentai Colliery, Liaoning Province.

B. *Camarotoechia fengkangensis* Wang (sp. nov.) ..... p. 170
1, 2, 3, 4, 5: Ventral, dorsal, posterior, lateral and anterior views of complete specimen showing ornamentation, × 1.5, holotype, I.P.A.S. 8013.
Lojoping Series, Middle Silurian; Changshengkou, Chahuaping Village, Fengkang District, Kweichow Province.

C. *Hypothyridina hunanensis* Wang (sp. nov.) ..... p. 172
1, 2, 3, 4, 5: Ventral, dorsal, lateral, posterior and anterior views of complete specimen showing general form and ornamentation, × 1.5, holotype, I.P.A.S. 8016.
Lungkouchung Bed, Middle Devonian; Lungkouchung Village, Hsiang-hsiang District, Hunan Province.

D. *Paurorhyncha depressa* Wang (sp. nov.) ..... p. 172
1, 2, 3, 4, 5: Ventral, dorsal, lateral, anterior and posterior views of complete specimen showing lenticular lateral profile and short lingual prolongation, × 1, holotype, I.P.A.S. 8015.
Upper Devonian; Itate, Pohsi, Huaning District, Yunnan Province.

A


1

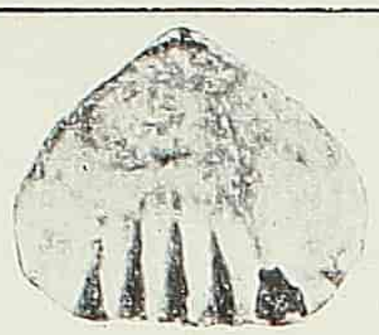
2


3


4

B

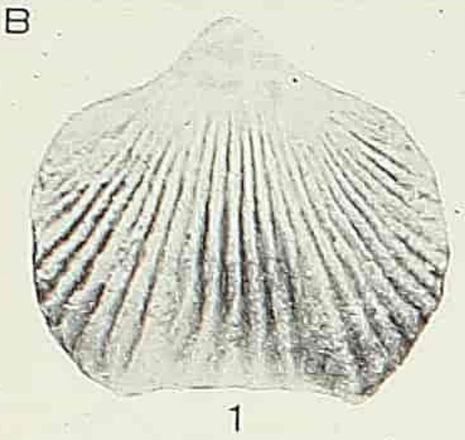
1

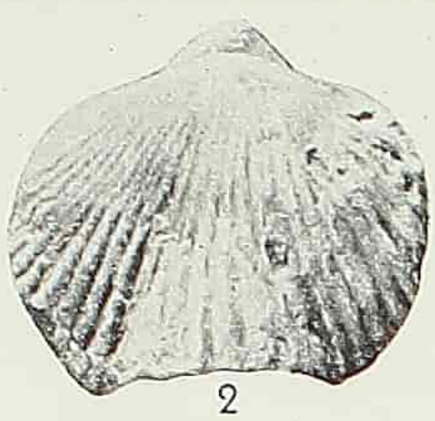
2


3

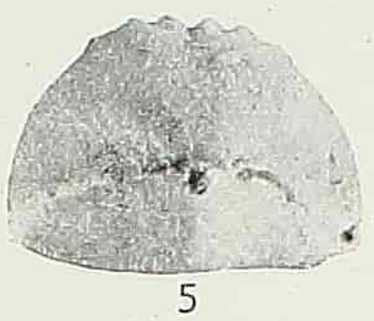
5


4

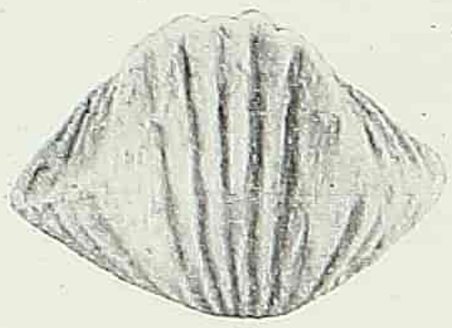
5

C

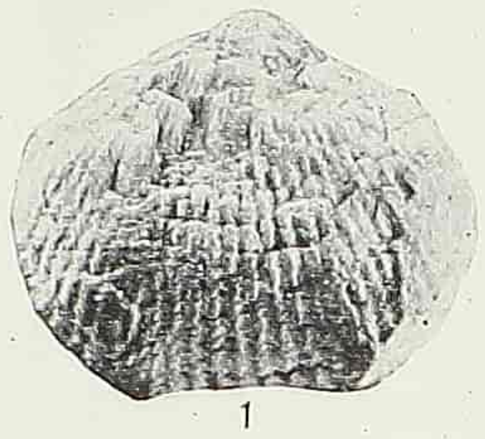
1

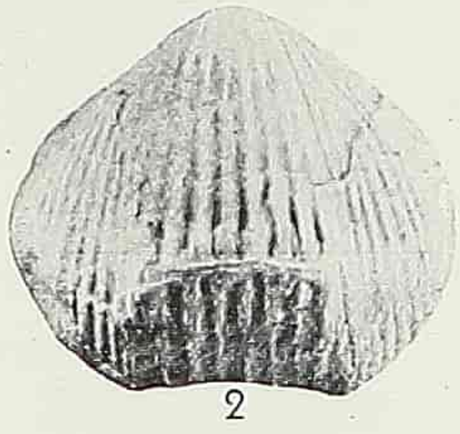
2


3

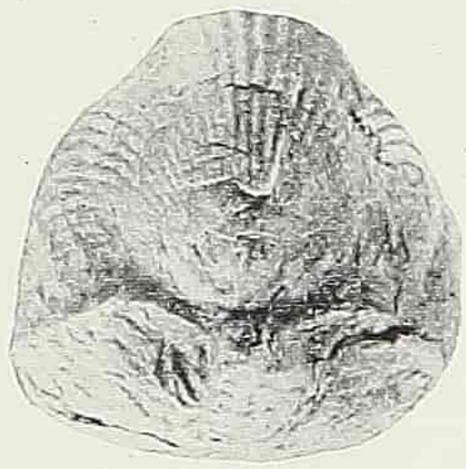
4

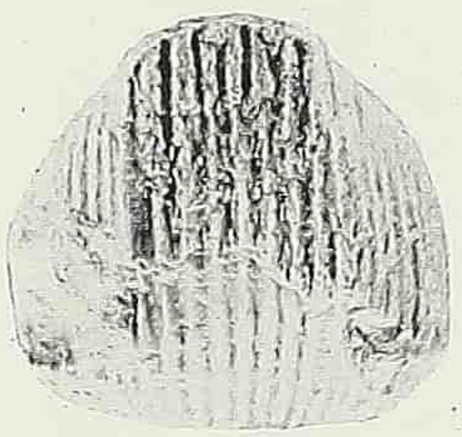
5

D

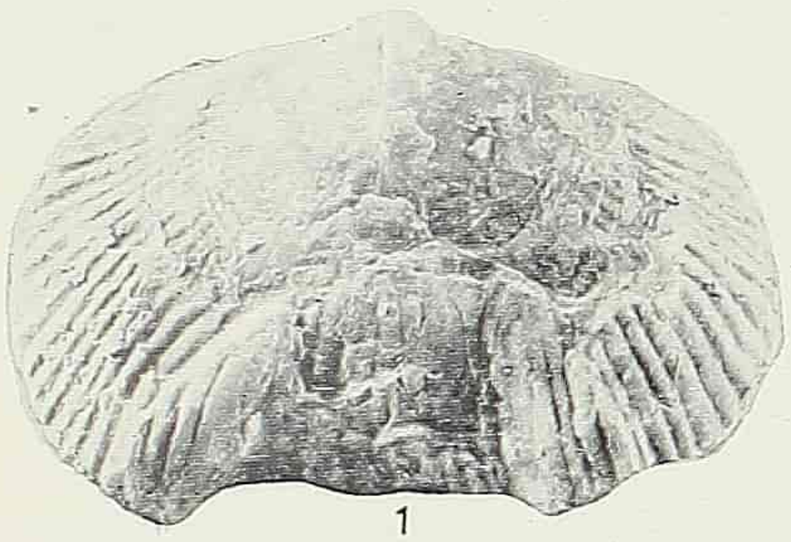
1

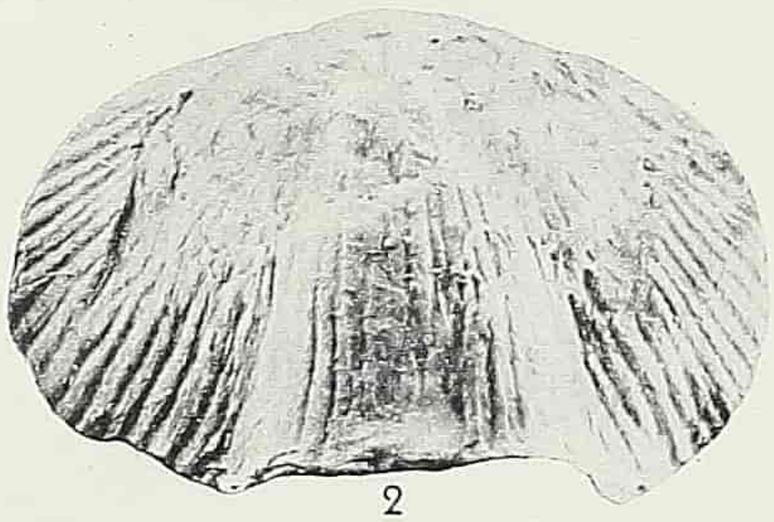
2


3

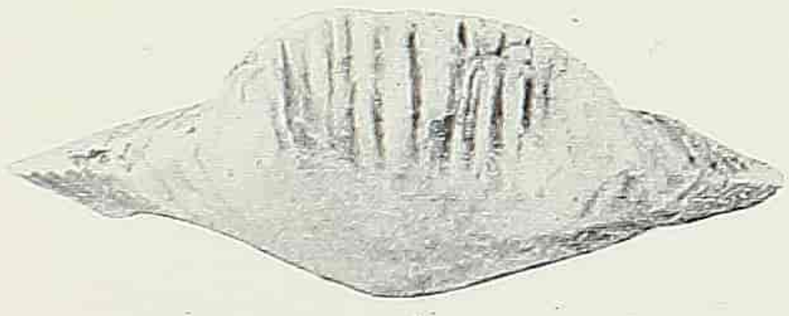
4


5

PRELIMINARY RESULTS ON THE HYDROTHERMAL SYNTHESIS OF BRITTLE MICAS*

Tu Kwang-Chih (涂光熾)

(*Institute of Geology, Academia Sinica*)

Introduction

There have been controversies among geologists as to the role played by the shearing stress in mineral formation. Micas, chlorites and brittle micas are listed by Harker[12] as stress minerals, whose stability field on the temperature-pressure diagram is extended by the introduction of stress. Larsen[13] expresses doubts as to the importance attributed to stress by Harker, while Read[20] states that "all stress minerals can be formed under no stress condition."

In the past two decades, it has been shown experimentally that various members of the mica group can be made under high vapour pressure in the absence of stress[3, 8, 9, 10, 16, 17,18, 21, 22]. The synthesis of Mg-chlorite in bombs free from stress was also reported[23]. It remains to be proved whether brittle micas could be prepared without applying any differential stress, and if they could be synthesized at all to investigate their stability range with respect to temperature, pressure, and concentration. With this view in mind, the author conducted a series of experiments in the attempt to prepare brittle micas under hydrostatic pressure. The results of experiments and their geologic interpretations are given below. It is necessary to point out that no brittle micas have ever been successfully synthesized, though a doubtful artificial margarite was reported to have been observed by Chroustchoff[4] in his work on mica synthesis.

Methods of Investigation

About 30 experiments were performed, in which a stainless steel bomb was used, similar to that described by Morey and Ingerson[15]. The temper-

*To be published in Chinese in *Acta Geologica Sinica,* Vol. XXXVI, No. 2, 1956.

ature range of the experiments was 250–550°C. Pressure was calculated from the initial degree of filling and temperature. The initial charge consisted of a mixture of simple chemical compounds. It was well mixed and the solution was tested for its pH value both before and after each run. Most runs lasted for two or three days, during which period equilibrium was thought to have been reached.

Since chloritoid, the more widespread member of brittle micas, contains ferrous iron, an attempt was made to introduce the latter into the initial charge. Iron was present in the form of carbonate or oxalate. However, after each run it invaribly formed magnetite and thus did not take part in the crystal structures of the synthetic products. The condition within the bomb could not

Table I. Synthesis of Brittle Micas (Degree of Filling 0.2)

Expt. No.	Temp. in C°	Time in hrs.	Pressure in kg/cm²	Ingredients SiO_2 : Al_2O_3 : CaO	Other Alkalies Added	pH before run	pH after run	Products
1	420	63	305	2 : 2 : 1		8.5	7	Margarite & boehmite
2	420	68	305	2 : 2 : 1 ($CaCl_2$)		5.5	5	Boehmite & Margarite
3	410	67	290	2 : 2 : 1 ($CaCO_3$)		6	6	Boehmite & Margarite
4	420	85	340*	2 : 2 : 1	$NaCO_3$	12	11.5	Cancrinite
5	410	66	290	2 : 2 : 1	Na OH	10	9	Cancrinite
6	370	71	220	2 : 2 : 1	Na OH	12.5	10.5	Cancrinite
7	475	70	390	2 : 2 : 1	Na OH	13	11.5	Cancrinite & Unknown A
8	420	68	305	2 : 2 : 1	NaCl	8.5		Boehmite & margarite
9	420	90	305	2 : 2 : 5 ($CaCl_2$)		5	4.5	Margarite
10	420	95	305	2 : 2 : 5 ($CaCO_3$)			7.5	Calcite & margarite
11	420	62	305	2 : 2 : 5		9	7	Unknown A
12	415	46	295	2 : 2 :	$5Na_2O$ as NaCl	6.5	6	Boehmite & Paragonite
13	420	67	305	2 : 1 : 5 ($CaCl_2$)	3 Mg O	6.5	5	Serpentine
14	420	67	305	2 : 1 : 4 ($CaCl_2$)		5	5	Margarite-like
15	320	70	120	2 : 2 : 5 ($CaCl_2$)		5	5	Boehmite
16	485	47	395	2 : 2 : 5 ($CaCl_2$)		5	5	Margarite
17	350	96	170	2 : 2 : 5 ($CaCl_2$)		5	5	Boehmite
18	370	16 days	220	2 : 2 : 5 ($CaCl_2$)		5	5	Boehmite & trace of margarite
19	540	44	460	2 : 2 : 5 ($CaCl_2$)		5	5	margarite

*Degree of filling=0.4.

be controlled as far as the oxidation state of iron went. As a result, iron had to be discarded.

The identification of the products was made primarily by x-ray diffraction method. Powder photographs were taken in precision cameras of 57.3 mm radius. Due to the very fine crystalline nature of the product, optical identification was impossible except for a rough determination of the refractive indices.

The results of the more representative runs are listed in Table 1.

Discussion of Experiments

Margarite, the Ca brittle mica, has the theoretical formula: $CaAl_2(Al_2Si_2O_{10})(OH)_2$. The simplest equation of its formation from oxides may be expressed as follows:

$$CaO + 2Al_2O_3 + 2SiO_2 + H_2O \rightarrow CaAl_2(Al_2Si_2O_{10})(OH)_2$$

Therefore, as shown in Table 1, the $Al_2O_3 : SiO_2$ ratio was kept at 1:1. The starting substance consisted of $Al(OH)_3$, "Acid Silicic," and various amounts of Ca salts. When attempts were made to synthesize members of Fe-free brittle micas other than margarite, the $Al_2O_3 : SiO_2$ ratio was changed to that called for by the desired product.

It was realized at the beginning that because of the large proportion of $Al(OH)_3$ present in the initial charge, much of it probably would crystallize out as boehmite unless solutions used were rather basic or acidic, or, unless excessive Ca salt was added, which might retard this tendency. This was exactly shown to be the case; earlier experiments (Expts. 1, 2 and 3) gave much boehmite and some margarite when the ingredients were in the molecular proportion of margarite.

Therefore, in Expts. 4-7, NaOH or Na_2CO_3 was added to the initial charge in the hope that it might serve as an agent to give a relatively strong alkalinity. The results, however, were discouraging, as invariably cancrinite $Na_6Ca_2(Al_6Si_6O_{24})(CO_3, SO_4) \cdot 3H_2O$ formed. According to Betechtin[2], cancrinite may contain as little as 0.3% of CO_2.. NaOH used in our experiments contains 1.5% of Na_2CO_3. Apparently, even the presence of a very small quantity of $CO_3^=$ tends to shift the reaction in favour of cancrinite[1].

A comparison of x-ray patterns of these synthetic cancrinites with the natural mineral reveals an interesting phenomenon. Lower temperature cancrinite (Expt. 6, 370°C) corresponds very well in both spacings and intensities with cancrinite from Renfrew Co., Ont., Canada. Expts. 4 and 5, at

---

1) Cancrinite has been identified a number of times in hydrothermal mineral synthesie[6, 7, 14] and also recently in boiler deposits[5].

420° and 410°C respectively, yielded a product that differs from natural cancrinite somewhat in intensities but not in spacings. The higher temperature product (Expt. 7, 475°C), however, showed a slightly but distinctly expanded lattice.

When NaCl solution was tried, much margarite and some boehmite appeared in the final product (Expt. 8).

In later experiments (Expts. 9, 10, 11) an excess of Ca salts was added. Five times as much Ca equivalent as would be required by the formula of margarite was introduced into the charge. With $CaCl_2$, the final product consisted solely of margarite. When $CaCO_3$ was used, much of it recrystallized as calcite and only part of it went into margarite formation. If CaO was added, margarite would not form at all; an unknown compound "A", which resembles sodalite in x-ray pattern, was the only product.

Unknown "A" appeared in both Expts. 7 and 11. As shown in Table 1, the chemical composition of the initial charge should make the product more like hauynite than sodalite, if the final product would be feldspathoid at all. However, x-ray analysis showed the reverse to be true. Barth[1] gives the a-dimension of the unit cell of sodalite as 8.89 Å, and that of hauynite, 9.11 Å. The synthetic product gives 8.84 Å, showing a slight shrinkage as compared with sodalite, and may have the composition of a Ca-sodalite. As far as we know, no pure Ca-sodalite has ever been reported in nature. However, Barth states that "the essential constitution in the hauynite system are noselite silicates: $Na_8Al_6Si_6O_{24} \cdot SO_4$ and Silicate III: $Ca_4Al_6Si_6O_{24} \cdot SO_4$". It is probable that unknown "A" chemically resembles Barth's Silicate III.

So far the experimental results show that in the presence of $CaCl_2$ margarite formed more readily than otherwise. Therefore, in further experiments (Expts. 15, 16, 17, and 18) with different temperatures, $CaCl_2$ was added in large excess. The results indicate that below 350°C the products consisted solely of boehmite. At 370°C in 16 days, boehmite plus a little margarite formed. It appears likely that the lower temperature boundary of margarite formation in slightly acid solutions lies in the range 350–370°C. The upper temperature limit of margarite formation was not determined. It must be much higher than 500°C (Expt. 19).

Expt. 12 (415°C) was tried to see if a Na-margarite, in which Ca is replaced by Na, could be synthesized. The initial charge consisted of $Al(OH)_3$, "Acid Silicie", and NaCl. Only boehmite and paragonite showed in the product. Runs at other temperatures gave essentially the same result.

Expt. 13 was an attempt to prepare clintonite ($H_2CaMg_3Al_2Si_2O_{12}$). It is a brittle mica with Mg replacing part of the Al in the margarite structure. The initial charge had an Al:Si:Mg ratio of 2:2:3 as called for by the formula, but with an excess of Ca. The product gave an x-ray pattern of serpentine.

In Table 2 are listed the spacings and intensities of the synthetic margarite, together with those of a natural margarite. The average index of refraction of artificial margarite is 1.615, which is slightly lower than that of the natural mineral. This may be due to the extremely fine size of the synthetic product.

Table II. Powder Diagrams of the Synthetic Margarite and the Natural Magarite from Chester, Mass., U.S.A. (Radius of Camera 57.3 mm, FeK_α 1.932.)

Synthetic Margarite			Margarite, Chester, Mass.	
No.	d	Observed I	d	Observed I
1	Indistinct		9.47	VW
2	4.82	VW	4.71	VW
3	4.422	S	4.388	W
4	3.566	VW	3.645	S
5	3.203	S	3.186	VS
6	2.974	W	2.898	W
7	2.808	S	2.777	S
8	2.681	W	2.683	W
9	2.533	VS	2.529	S
10	2.425	S	2.408	S
11	2.094	S	2.078	Br
12	1.916	W	1.913	VS
13	1.780	VW	1.757	W
14	1.684	W	1.673	W
15	1.601	W	1.592	S
16	1.483	VS	1.486	W
17			1.465	S

VS=very strong, S=strong,
W=weak, VW=very weak,
Br=broad

Geological Considerations

That margarite, the Ca brittle mica, was hydrothermally prepared in our experiments tends to indicate that brittle micas might have formed at least partly in nature under non-stress conditions. Betechtin[2] in his "Mineralogy"

states that xanthophyllite (or clintonite), the Mg-Ca brittle mica, does occur in contact-metamorphic deposits in schists on the Western Urals, while chloritoid is found, although only in small amounts, in contact-metamorphic deposits in the marble. Gustavson[11] also concludes, that chloritoid, the Fe brittle mica, could occur as a distinctly hydrothermal mineral. It is to be noted that in the cases described by Betechtin brittle micas formed most likely in the process of thermal metamorphism rather than regional metamorphism. This of course, is in accord with the findings of our experiments.

In the Western Hills of Peking, China, chloritoid is a widespread rock-forming mineral, occurring in beds ranging in age from the Sinian up to the Jurassic. It is interesting to note that while much of the chloritoid probably formed as a result of low-grade regional metamorphism, part of it occurs distinctly in veins.[1)]

However, the occurrence of brittle micas as a hydrothermal alteration product or in hydrothermal veins is much rarer than their occurrence as a product of regional metamorphism. In addition, brittle micas are considerably less abundant than ordinary micas in nature. All this may be partly due to the comparably narrow range of stability of brittle micas with respect to temperature, concentration, and the presence of radicals, such as $CO_3^=$. Our experimental results indicate that phlogopite can be hydrothermally synthesized at temperatures as low as 250°C[2)], while the lowest temperature limit at which margarite could be made lies much higher (350–370°C). The change of acidity might more seriouly effect the stability range of brittle micas than that of ordinary K-micas. In the case of margarite high basicity probably renders it unstable and tends to form feldspathoids (cancrinite and others). This tendency is likely to be strengthened if $CO_3^=$ and other radicals are present in even small amounts. This does not seem to have occurred with the synthesis of the ordinary K-micas. All this may partly explain the comparative rarety of margarite as compared with K-micas. In addition, the factor of unfavourable ionic size of Ca in the margarite structure might render it less stable than a K-mica. Similar reason was pointed out by Gruner[9] to explain partly the rare occurrence of paragonite in nature.

Our experimental findings show that while margarite was readily synthesized, we had failed to prepare other members of the Fe-free brittle micas (Na-margarite, clintonite). The explaination may lie in the following facts. No "pure" Na-margarite has ever been recorded in geological literature. The most sodic margarite ever reported appears to be the mineral ephesite from the Postmasburg district, S. Africa, containing as much as 8.65% Na_2O and 1.4% CaO[19]. The other sodic margarites contain considerably less Na. In

---

1) Oral communication by K. Yang and T. L. Ho.

2) Results of synthesis of phlogopite will be published in a separate paper.

addition, they are very rare in nature. The meager occurrences of margarite high in Na manifest that they formed under unusual conditions.

With the introduction of Mg salts into the initial charge, aluminous serpentine was yielded, instead of clintonite, as would have been desired (Expt. 13). This indicates that Ca ions stayed in solution and did not participate in the crystal structure of serpentine.

Our experimental findings are in accord with the geological facts in that serpentine is far more widespread than the Mg-Ca brittle micas. In nature the formation of serpentine is frequently accompanied by carbonatization, indicating that the Ca ions likewise stayed out of the serpentine structure. Apparently, the chemical reaction in nature tends to favour the formation of serpentine, talc, carbonate (the so-called process of listwanitization) rather than the Mg-Ca brittle mica, when the reaction involves the same chemical elements in similar proportions.

There is reason to suspect that the presence of Fe might conceivably widen the stability range of brittle micas, especially toward the low temperature side. According to Betechtin[2], chloritiod forms in the earlier stages of regional metamorphism; in more intensively metamorphosed rocks chloritoid is not observed. This means that a low temperature condition would probably favour the formation of the Fe brittle mica. The author noticed a similar situation in his work on the synthesis of chlorite[23].

In conclusion, it should be noted that the fact that members of the brittle mica group occur mainly in metamorphic rocks likewise indicates that the presence of stress might extend their stability field. Further research work is to be done before this can be proved.

References

[1] Barth, T. F. W., 1932. The Structures of the Minerals of the Sodalite Family. *Zeits. Krist.*, **83**, 405—414.

[2] Betechtin, A. G., 1950. Mineralogy (in Russian), pp. 823—825.

[3] Caillere, S., and Henin. S., 1949. Transformation of Minerals of the Montmorillonite Family into 10 Å Micas. *Mineral Mag.*, **28**, 606—611.

[4] von Chroustschoff, K., 1888. Über Künstlichen Magnesia-Glimmer. *Tsch. Min. Petrog. Mitt.*, **9**, 55—60.

[5] Clark, L. M., 1948. The Identification of Minerals in Boiler Deposit; Examples of Hydrothermal Synthesis in Boiler. *Mineral Mag.*, **28**, 359—366.

[6] Friedel, G., 1896. Sur un nouveau silicate artificiel. *Soc. Francais Mineralogie, Bull.*, **19**, 5—14.

[7] Friedel, G., 1896. Sur un nouveau silicate artificiel. *Soc. Francaise Mineralogie, Bull.*, **24**, 141—159.

[8] Gruner, J. W., 1939. Formation and Stability of Muscovite in Acid Solutions at Elevated Temperatures. *Am. Mineralogist,* **24**, 624—628.

[9] ————, 1942. Conditions for the Formation of Paragonite. *Am. Mineralogist,* **27**, 131—134.

[10] ————, 1944. The Hydrothermal Alteration of Feldspars in Acid Solutions between 300 and 400°C. *Econ. Geol.,* **39**, 578—589.

[11] Gustavson, J. K., 1946. Two Occurrences of Chloritoid as a Hydrothermal Mineral in Igneous Rocks. *Am. Mineralogist,* **31**, 313—316.

[12] Harker, A., 1950. Metamorphism, 3rd ed., 148—151.

[13] Laren, E. S., 1941. Geochemistry. *Geol. Soc. Am.,* 50th Anniversary Vol., Geol. 1888-1938, 391—413.

[14] Lemberg, J., 1887. Zur Kenntnis der Bildung und Umbildung von Silicaten. *Zeits. Deut. Geol. Ges.,* **39**, 559—600.

[15] Morey, G. W., and Ingerson, E., 1937. A Bomb for Use in Hydrothermal Experimentation. *Am. Mineralogist,* **22**, 1121—1122.

[16] Noll, W., 1932. Hydrothermale Synthese des Muscovits. Nach. Gesell. Wiss. Göttingen, Math.-Physik. Kl., 122—134.

[17] Norton, F. H., 1939. Hydrothermal Formation of Clay Minerals in the Laboratory. *Am. Mineralogist,* **24**, 1—17.

[18] O'Neill, J. F., 1948. The Hydrothermal Alteration of Feldspars at 250–400°C. *Econ. Geol.,* **43**, 167—180.

[19] Phillips, F. C., 1931. Ephesite (soda-margarite) from the Postmasburg District, S. Africa. *Mineral. Mag.,* **22**, 482—485.

[20] Read, H. H., 1948. A Commentary on Place in Plutonism. *Quar. Jour. Geol. Soc. London,* **54**, 155—205.

[21] Roedder, E. W., 1948. System K_2O-MgO-SiO_2. *Geol. Soc. Am. Bull.,* **59**, 1347. (in abstract form).

[22] Roy, R., 1949. Decomposition and Re-synthesis of the Micas. *Jour. Am. Ceramic Soc.,* **32**, 202—209.

[23] Tu, K. C., 1951. The Hydrothermal Synthesis of the Mg-clorite, *Science Record,* **4** (2), 157—162.

CORRIGENDA

SCIENTIA SINICA, Vol. IV, No. 4

Page	Line	Reads	To Read
538	1	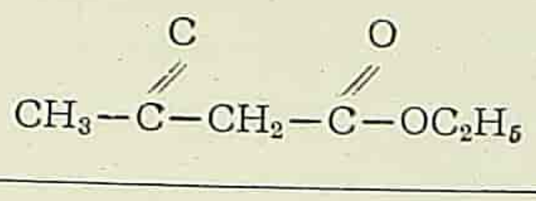	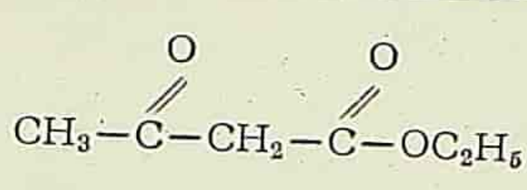
538	2	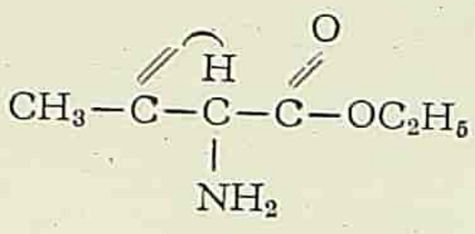	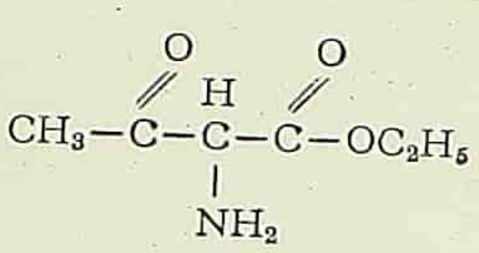
538	2	50% Pd-c	5% Pd-c
538	6	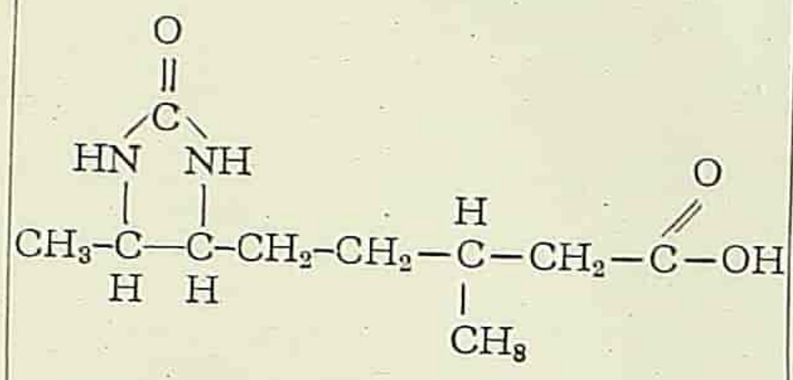	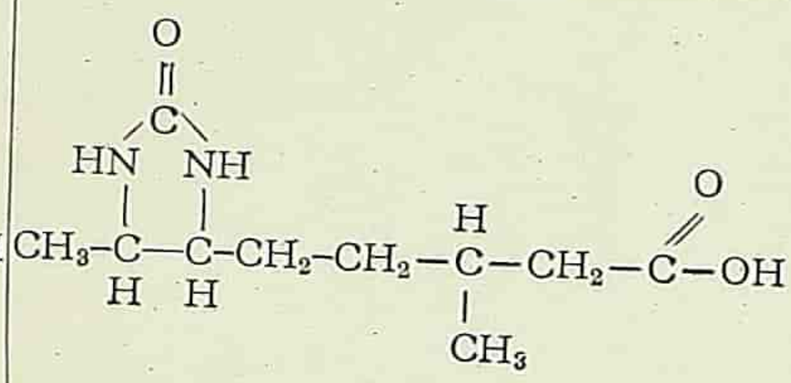
544	35	at a reduced pressure	at reduced pressure
546	17	ω, ω—	ω, ω'—
548	3	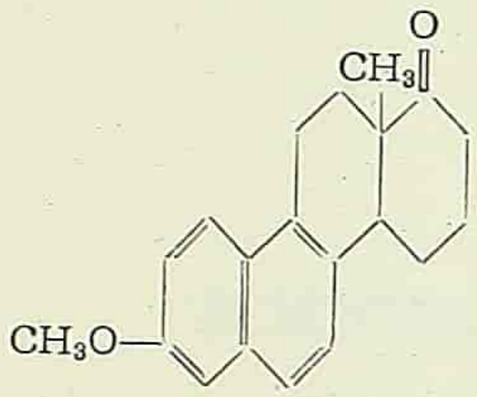	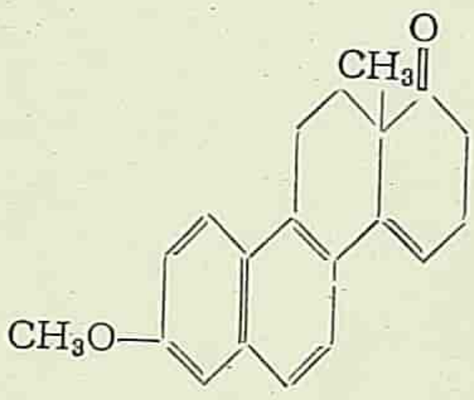
549	2	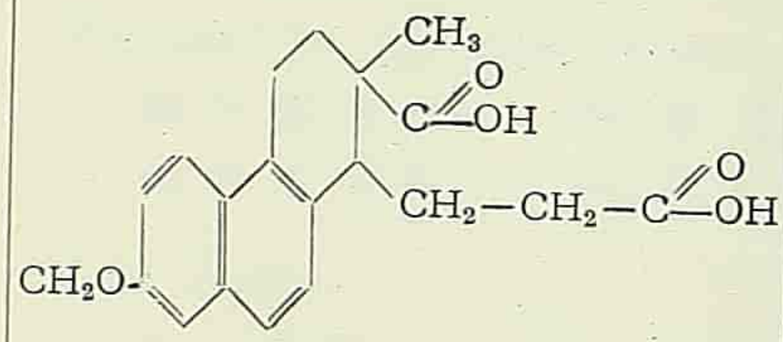	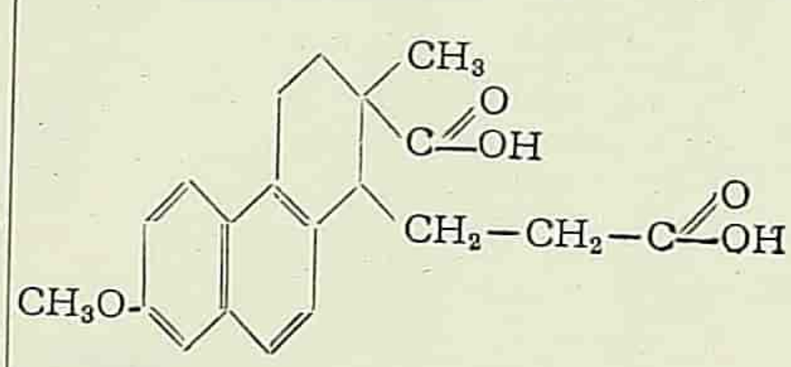
550	31	Simple	Sample
579	24	law	low
601	30	number	numbers

SCIENTIA SINICA

Vol. V, No. 1

Published by Academia Sinica

國外發行者：　國際書店

國內發行者：　北京郵局

Sales Agent:

Guozi Shudian, 38 Suchou Hutung, Peking.

Гоцзй Шудянь КНР, Пекин, Сучжоухутун 38.

Printers：　The Graphic Art Book Co., Shanghai.

S. S., V, 1—2,400　　March, 1956